Control of Parameter-Dependent Mechanical Systems

Giles David Wood

St Johns College
Cambridge

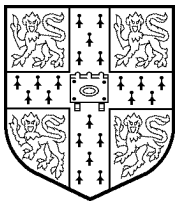

A dissertation submitted for
the degree of Doctor of Philosophy

16 November 1995

Abstract

This dissertation considers the application of recent robust control techniques to parameter-dependent mechanical systems. Particular emphasis is placed on the study of flexible dynamic systems that possess lightly-damped, parameter-dependent, resonances at frequencies that are within the bandwidth of the controller. A detailed examination of an example system, highlighting the complexities associated with the control of these systems, is motivated. The applicability of robust control techniques that are based on stabilising unstructured neighbourhoods characterised by the gap and ν-gap metrics is examined. Particular difficulties arising when these techniques are applied to the chosen class of systems are highlighted, and it is shown how the frequency-response interpretation permitted by the ν-gap metric can be used to overcome them.

For systems that undergo large parameter variations, it is shown how controllers can be designed for each of the sets in a finite cover of the parameter space. Switching techniques based on real-time parameter measurements are used to switch between the controllers. The issues of bumpless transfer and reference signal injection are addressed through the use of appropriate coprime factorisations of the controllers.

An experimental facility is developed to evaluate the applicability of these control techniques on a real system. The importance of the tradeoff between robustness and performance is demonstrated, as is the effectiveness of the switching methodology at achieving bumpless transfer. It is shown that the chosen robust control approach can be used to obtain controllers that achieve a high level of performance while still being robust to time-varying parametric perturbations.

New model-reduction techniques are developed, allowing balanced truncation to be extended to bounded-rate, linear, parameter-varying systems. These are based on the solutions of various parameter-dependent Lyapunov and Riccati differential inequalities, the latter allowing both stable and unstable systems to be factorised, enabling the symbol of the system's graph can be approximated. Generalisations of known error bounds for balanced truncation of time-invariant systems are examined. Techniques for solving the differential inequalities are considered, and procedures for computing the balancing transformation developed.

Analytical techniques for synthesising gain-scheduled controllers for parameter-varying systems are extended by allowing explicit rate-bounds to be incorporated into the synthesis, thus reducing conservatism. A specific four-block synthesis setup is considered in some detail and shown to result in a particularly transparent solution. Direct connections are made between this four-block setup and the model-reduction techniques. An efficient procedure for the synthesis of reduced-order controllers in the four-block setup is developed. The techniques are successfully demonstrated on a missile autopilot design.

Acknowledgements

I am particularly indebted to my supervisor Dr Jim Woodhouse for the encouragement and support he has given me over the last three years. His enthusiasm, expert knowledge of dynamics, and willingness to allow me to pursue my own interests have been much appreciated. I am also very grateful to Professor Keith Glover, Dr Malcolm Smith and Dr Glenn Vinnicombe from whom I have learned much about control theory. They have all given freely of their time and advice. Glenn, in particular, has had a very strong influence on my view of control theory and I shall miss the many and varied discussions we have had on control and related topics. I would also like to thank Professor David Newland for the advise and help he gave me when I first arrived in Cambridge and my former lecturer Dr Charles Constancon for getting me interested in dynamics and control in the first place.

My contemporaries from College, those in the Dynamics Group, and those in Control Group have made my time in Cambridge very enjoyable, in particular: Adam, Brian, Gavin, Haig, Jie, Kristian, Michael, Paul, Phil, Richard, Rob, and Sanjay. Special thanks to Phil Goddard and Rick Hyde who, while at British Aerospace and Cambridge Control respectively, motivated the missile autopilot study.

On a more personal note I would like to thank my family for everything they have given me over the years, particularly the encouragement and support given to me while I have been in Cambridge.

Finally, I would like to thank Rebecca for her love, support and understanding, had it not been for her I would never have completed this thesis.

While at Cambridge I have been supported by the Emanuel Bradlow Foundation, their support is gratefully acknowledged.

As required by University Statute, I hereby declare that this dissertation is not substantially the same as any that I have submitted for a degree at any other University, is the result of my own work, and includes nothing which is the outcome of work done in collaboration.

Giles Wood
St Johns College
Cambridge

Contents

Notation

Symbols

$\in$	is an element of
$\forall$	for all
$\exists$	there exists
$\triangleq$	equal to by definition
$\Longrightarrow$	implies
$\Longleftrightarrow$	implies and is implied by
$\blacksquare$	end of proof
$\mathbb{R}$	field of real numbers
$\mathbb{C}$	field of complex numbers
$\Re(\bullet)$	real part of $\bullet$
$\mathbb{R}^{n\times m}$	real matrix with n rows and m columns
$\mathbb{C}^{n\times m}$	complex matrix with n rows and m columns
M^T	transpose of M
M^*	complex conjugate transpose of M
$\sigma_i(M)$	i'th singular value of the matrix M
$\bar{\sigma}(M)$	maximum singular value of the matrix M
$\underline{\sigma}(M)$	minimum singular value of the matrix M
$\lambda_i(M)$	i'th eigenvalue of a square matrix M
$\bar{\lambda}(M)$	maximum eigenvalue of a square matrix $M = M^*$
$\underline{\lambda}(M)$	minimum eigenvalue of a square matrix $M = M^*$
$M > 0$	$M = M^*$ is positive definite ($\underline{\lambda}(M) > 0$)
F_ρ	class of feasible parameter trajectories
$\|x\|$	standard Euclidean norm $\|x\| = \sqrt{x^*x}$
$G^*(s)$	conjugate transpose of $G(s)$
wno $g(s)$	winding number of $g(s)$ taken about the origin
$\delta_g(P_1, P_2)$	gap metric between systems P_1 and P_2
$\delta_\nu(P_1, P_2)$	ν-gap metric between systems P_1 and P_2

Acronyms

SISO	Single Input-Single Output
MISO	Multiple Input-Single Output
MIMO	Multiple Input-Multiple Output
LTI	Linear Time Invariant
LTV	Linear Time Varying
LPV	Linear Parameter Varying
LQG	Linear Quadratic Gaussian
LFT	Linear Fractional Transformation
LMI	Linear Matrix Inequality
RCF	Right Coprime Factor/Factorisation
LCF	Left Coprime Factor/Factorisation
GCRI	Generalised Differential Control Riccati Inequality
GFRI	Generalised Differential Filtering Riccati Inequality

1

Introduction

1.1 Motivation

The work presented in this thesis has arisen out of a desire to understand the control issues that arise in violin bowing. By way of motivation, consider what occurs when a violinist bows an instrument. The player moves the bow across the violin string while keeping a number of parameters within desired limits. These include bow-bridge distance, bow-speed, and of particular interest to us, bow-pressure. The bow-pressure is the normal force developed between the bow-hair and the violin string and this has a strong influence on the nonlinear oscillation of the string. Whilst it is possible to set up a number of different steady oscillation patterns in the violin string (most of which are highly undesirable), there is one particular oscillation pattern that is of interest. This is known as the Helmholtz oscillation and it results in what we, as listeners, perceive to be a desirable note. Recent theoretical work ([90],[91]) indicates that the attainment of a Helmholtz oscillation is strongly influenced by bowing transients, that is, the Helmholtz oscillation does not depend solely on the steady bow pressure, but also depends to a large extent upon the chosen path whereby the steady pressure is attained. Extensive simulations indicate that certain transients give rise to a Helmholtz oscillation, whereas others do not. It is believed that the range of allowable transients permitted by any given instrument is intimately related to what players refer to as the "playability" of an instrument.

A natural extension of this theoretical work involves obtaining experimental evidence to either validate or invalidate these claims. Herein lies a dilemma, and the motivation for this thesis. It is not possible for a violinist to control the bow-pressure to within the required tolerances necessary to make such an experimental investigation meaningful. Even if it were, the number of experimental transients that would be required makes such an approach totally implausible. Instead, what is needed is a high-performance bowing machine capable of controlling the bow-pressure to within strict tolerances over a sufficiently high bandwidth to follow specified force/time variations. This is a control problem, and examination of the control issues that arise in this problem, and in problems involving systems which exhibit similar dynamical characteristics, make up a major part of this work.

On a more prosaic level, a violin bow is similar to any elastic continuum, exhibiting numerous lightly damped vibration modes which can easily interact with a control system. This type of interaction has traditionally been avoided by placing sufficient limitations on the bandwidth of the controller. Unfortunately, in high-performance applications the performance limitations that result from this approach are not acceptable, and this necessitates the design of control systems that allow for the appearance of flexible dynamics within the control bandwidth. This is certainly true of the bowing problem, and to an increasing extent is also the case with control systems designed for the highly flexible structures that find application in astronautical systems and robotics.

An unusual and interesting feature of the bowing problem is that the dynamics also exhibit strong parameter dependence. That is, the dynamics depend causally, but not predictably, on some measurable parameter (in this case the contact position of string on bow). Parameter-dependent systems are by no means new to control engineers, more common examples include tactical aircraft and missiles, but it is unusual to encounter lightly-damped parameter-dependent flexible dynamics within the control bandwidth. This said, the constant improvements being made in technological industries requires a commensurate increase in the performance of control systems, and it is expected that the structural dynamics of parameter-dependent systems will become increasingly important. For example, performance specifications for modern missiles require the autopilot to operate at frequencies that are close to the first bending mode of the airframe. As these specifications are tightened to meet improvements in aircraft technology it will be necessary to design controllers which account for the flexible dynamics of the airframe. Other examples that by their very nature involve parameter-dependent flexible dynamics include vibration suppression systems used on helicopter rotor blades, and positioning control systems for deployable structures used in astronautical applications. The development of control techniques which are capable of dealing with these systems is therefore seen as being of some importance.

1.2 Historical background

Central to the development of feedback control theory has been the notion of uncertainty. This arises in two distinct forms, unpredictable disturbances which act on the physical plant, and mismatches between the behaviour of the physical plant and the behaviour of the mathematical model used to design the controller. Feedback can be used to significantly reduce the effects of the former class of uncertainty, but can easily result in closed-loop instability if due consideration is not given to the latter class of uncertainty.

Classical control techniques were developed with both classes of uncertainty in mind. Graphical techniques capable of dealing with single-input single-output plants were the primary tool and quickly found wide use in practice. These allowed performance specifications to be met using loop-shaping concepts, and when used in conjunction with gain and phase margins, allowed the designer to account for uncertainties in an intuitive manner. Unfortunately, these techniques are somewhat ad-hoc and often require a lot of iteration and much intuition on the part of the designer. Also, they do not provide easy answers to such questions as achievable performance,

and are difficult to apply to plants having multiple unity-gain crossover frequencies. Furthermore, they are not easily extended to multivariable plants. The classical control period gave way to the so-called Modern Control era which saw the development of optimisation techniques which were better able to deal with performance and existence issues. Of these, the Linear Quadratic Gaussian ([2],[45],[103]) technique proved to be very popular as it dealt with multivariable plants in a systematic manner. This synthesis technique involves finding a controller which internally stabilises the feedback interconnection and which minimises the variance of a chosen set of output signals when noise, of known statistical properties (usually assumed to be white noise), acts on the plant. Under reasonable assumptions Kalman's elegant separation principle provides a unique optimal controller which achieves this objective. These techniques also found application to linear time-varying systems and appeared to offer a systematic, single-step approach to the design of control systems.

During this period overemphasis on performance objectives at the expense of uncertainty considerations (and to an extent uncertainty about the disturbance spectra) quickly led to a schism between practitioners and theoreticians. This was primarily because the controllers computed using these techniques would often perform inadequately in practise. Not surprisingly, tremendous research effort subsequently went into the development of design techniques which were based on optimisation principles, but which allowed robustness properties to be built into the controller directly. The result of this effort is a comprehensive theory ([45],[60],[103]), which has its origins in the seminal paper of Zames [99] and which has come to be known as H_∞ control theory. Central to this approach is the interconnection structure shown in Figure 1.1, which shows the interconnection of a finite-dimensional linear time-invariant plant P, with a finite-dimensional linear time-invariant controller C. The plant P is usually referred to as the generalised plant in the control literature, and the interconnection structure is an example of a Linear Fractional Transformation (LFT). Conformally partitioning the plant P with the dimensions of its inputs and its outputs it is possible to write the transfer function from w to z, $\mathcal{F}_l(P,C) : w \mapsto z$ as $\mathcal{F}_l(P,C) = P_{11} + P_{12}C(I - P_{22}C)^{-1}P_{21}$. Here z is the vector of controlled outputs, w contains all disturbance and reference signals, y is the vector of measured outputs, and u the vector of manipulated inputs.

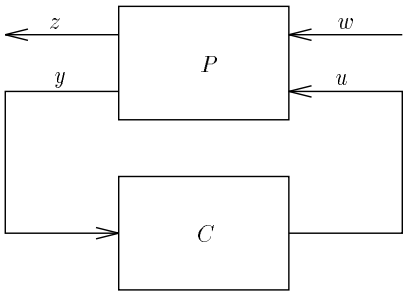

Figure 1.1 *Linear fractional transformation of a generalised plant P with a controller C.*

The suboptimal H_∞ control problem involves finding a controller C which internally stabilises

the feedback interconnection in Figure 1.1 and which bounds the induced L_2 gain from w to z. This has direct robustness interpretations in terms of the small gain theorem [98] and also satisfies the performance objective of minimising the energy in the output z for the worst-case bounded-energy input w. There now exist a number of elegant solutions to this problem using a wide variety of mathematical techniques [24]. These range from the early operator-theoretic approaches [32] to the more recent state-space procedures [24].

Techniques for dealing with plants that exhibit some form of parameter dependence are still under development. In this case the plant, while still linear, is often more accurately modelled as a causal time-varying operator. This leads to a substantial complication in terms of analysis, controller synthesis, and ultimately, implementation. The work presented in this thesis can be broadly divided into two different approaches to the problem of synthesising adequate controllers for these systems. The first half makes use of linear time-invariant approximations of the parameter-dependent plant dynamics in order to synthesise controllers which perform adequately for a range of parameter values. The issue of incorporating knowledge about the predictable parameter variations in the plant dynamics into the controller, whilst still maintaining robustness to modelling uncertainty, is given special attention. Particular care is taken to formulate this problem in the correct framework where the effect of uncertainty is easily accounted for. Difficulties which arise with systems that exhibit flexible dynamics are highlighted, and suitable methods for dealing with these difficulties are developed and tested.

The second half of this thesis examines the issues that arise when a more accurate parameter-dependent model of the plant is used. In this case the system is not modelled by a set of linear time-invariant differential equations but rather by a set of linear differential equations which have parameter-dependent coefficients. For any chosen parameter trajectory this gives rise to a set of linear time-varying differential equations, each set merely being one element in the larger set generated by all feasible parameter trajectories. Much of our work concentrates on the problem of reducing the complexity of these models without incurring significant error. Techniques for synthesising controllers which are insensitive to uncertainty are also developed. This involves finding a parameter-dependent controller which internally stabilises the feedback interconnection and which bounds the induced L_2 gain of some closed-loop operator. As with the time-invariant case this has direct robustness interpretations in terms of the small gain theorem. Typically, the controllers exhibit the same complexity as the mathematical model used in their synthesis and the newly developed model reduction techniques can be used to generate reduced-order controllers which are more satisfactory for implementation.

1.3 Thesis overview

This thesis consists of nine chapters, and a brief overview of the contents of each chapter is as follows.

Chapter 2: Mathematical Preliminaries

In chapter 2 we gather relevant background information that will be useful throughout this thesis. We define the relevant signal and system spaces that find extensive application in control theory, and define the appropriate norms that are useful in the study of these spaces. We also gather background results relating to the factorisation of linear time-invariant systems. These are central to the techniques used in chapter 4. For linear parameter-dependent systems we introduce the notions of $\mathcal{Q}_e$ stability, $\mathcal{Q}_e$ stabilisability, $\mathcal{Q}_e$ detectability, and show how quadratic dissipation functions can be used to bound the induced norm of these systems.

Chapter 3: Mathematical Modelling: The Flexible Beam Example

In chapter 3 we introduce the mechanical system that is studied extensively in this thesis. Its study is motivated by the bowing problem, but it is representative of a much wider class of systems which exhibit similar dynamical characteristics. A detailed linear time-invariant model of the system is derived. This is indexed by a real parameter and captures the predominantly linear dynamics for each fixed value of the parameter. Pointwise application of standard modal truncation techniques are considered and physical arguments employed to show that this gives a continuous model approximant. One advantage of studying a specific system is that it highlights various issues that could otherwise be overlooked. In chapter 3 we take advantage of this to highlight difficulties that arise when we attempt to formulate more accurate parameter-dependent models (which account for the time-varying nature of the parameter) for this class of systems.

Chapter 4: A Topological Approach to Controller Synthesis

Chapter 4 deals with the problem of synthesising adequate controllers for parameter-dependent linear time-invariant plants. The synthesis problem is carefully formulated in a framework which is very natural for dealing with uncertainty, and chapter 4 serves to motivate this approach. We also introduce the various topologies and metrics that are useful in the analysis of feedback systems, and show that the chosen synthesis framework is the most natural one when robustness properties are measured with these metrics. Difficulties that arise when controlling systems that exhibit parameter-dependent flexible dynamics are highlighted, and techniques for dealing with these these difficulties developed. A number of example designs are performed.

Chapter 5: Switching controllers for LPV systems

Chapter 5 deals with the problem of switching between controllers in order to accommodate large parameter variations in the plant dynamics. Since elastic structures are very sensitive to sudden transients, careful attention is paid to the issue of switching between controllers without degrading overall performance. Techniques for introducing reference signals that are consistent with the switching objective are also considered, and these are applied to the example system examined in chapter 3.

Chapter 6: Experimental Evaluation of the LTI Approach

In chapter 6 we evaluate our chosen design methodology, at least for the class of systems being considered, by evaluating various controllers on an experimental test rig. Particular attention is paid to robustness/performance tradeoffs and how well our approach deals with this. By evaluating the performance of a number of different designs we show how important it is to account for errors in the mathematical model during the design phase. We also examine the effectiveness of the switching methodology developed in chapter 5 and show that this provides a useful technique for dealing with large parameter variations. An important aspect that is also worthy of study is the effectiveness of the controllers at controlling the plant when the parameter is truly time-varying. Experiments are performed to investigate this.

Chapter 7: Model Reduction of Parameter-Dependent Dynamical Systems

In chapter 7 we examine the issue of approximating a high-order model of a parameter-dependent dynamical system with a low-order model. Our approach is based on balanced realisations and Lyapunov inequalities, and makes use of factorisation theory to deal with unstable plants. We examine error bounds for this technique and show that error bounds that are known to hold for balanced truncation of time-invariant systems can, in some cases, be generalised to parameter-dependent systems. Special attention is paid to the continuity properties of the balancing transformation matrix and techniques developed for computing these transformations. A number of examples are presented.

Chapter 8: Synthesis of Parameter-Dependent Controllers for Parameter-Dependent Dynamical Systems

This chapter deals with the issue of synthesising gain-scheduled controllers for bounded-rate parameter-dependent systems. Necessary and sufficient conditions for the existence of a controller which bounds the L_2 gain of some closed-loop operator are stated, along with procedures for computing the controller. The four-block problem examined in chapter 4 is re-examined in this framework and shown to result in a particularly transparent solution. A direct approach to the problem of synthesising reduced-order controllers in the four-block setup is developed and it is shown that this can be performed in a very efficient manner. The technique is illustrated with a detailed example.

Chapter 9: Concluding Remarks

In chapter 9 we summarise the main contributions of this thesis and make some suggestions for future research.

2

Mathematical Preliminaries

In this chapter we gather important background material that will be used throughout this thesis. It is assumed that the reader is familiar with various fundamental concepts of linear systems theory such as controllability, observability and minimality ([15],[52]).

2.1 Signal spaces

The basic signal space used throughout this thesis is the Lebesgue space $L_2(-\infty,\infty)$ which consists of vector valued signals which are square integrable over the doubly-infinite time axis

$$L_2(-\infty,\infty) \stackrel{\triangle}{=} \{f(t) : \|f\|_2 < \infty\},$$

where $\|f\|_2$ is given by

$$\|f\|_2 = \left(\int_{-\infty}^{\infty} f^T(t)f(t)dt\right)^{\frac{1}{2}}.$$

This is a Hilbert space with inner product given by

$$(f,g) = \int_{-\infty}^{\infty} g^T(t)f(t)dt.$$

Two important closed subspaces of $L_2(-\infty,\infty)$ are the semi-infinite Lebesgue spaces $L_2[0,\infty)$ and $L_2(-\infty,0]$ consisting of functions that are square integrable over the semi-infinite time axis and zero everywhere else. We will use the notation L_2^+ and L_2^- to denote signals in $L_2[0,\infty)$ and $L_2(-\infty,0]$ respectively. We also introduce the extended 2-space $L_{2,e}^+$ defined by

$$L_{2,e}^+ \stackrel{\triangle}{=} \{f \in L_2[0,T) \ \text{ for all } T < \infty\}.$$

Associated with the time domain space $L_2(-\infty,\infty)$ is the frequency domain space L_2 consisting of functions of the complex variable s which are square integrable on the imaginary axis with the 2-norm defined by

$$\|f\|_2 \stackrel{\triangle}{=} \left(\frac{1}{2\pi}\int_{-\infty}^{\infty} f^*(j\omega)f(j\omega)d\omega\right)^{\frac{1}{2}}.$$

This is also a Hilbert space with inner product given by

$$(f,g) = \frac{1}{2\pi}\int_{-\infty}^{\infty} g^*(j\omega)f(j\omega)d\omega.$$

The Hardy spaces H_2 and $H_2^\perp$ are closed subspaces of L_2 consisting of vector valued functions square integrable on the imaginary axis and analytic in the open right-half and open left-half of the complex plane respectively. The bilateral Laplace transform, a Hilbert space isomorphism, and the Paley-Wiener theorem, are used to map between $L_2(-\infty,\infty) = L_2^+ \oplus L_2^-$ in the time domain and $L_2 = H_2 \oplus H_2^\perp$ in the frequency domain, L_2^+ being mapped onto H_2 and L_2^- being mapped onto $H_2^\perp$. Π^+ and Π^- denote the orthogonal projection operators which project $L_2(-\infty,\infty)$ onto L_2^+ and L_2^- in the time domain and L_2 onto H_2 and $H_2^\perp$ in the frequency domain. The duality between the time domain and frequency domain spaces results in little confusion if we use the notation L_2 for both.

2.2 System spaces

We will make extensive use of the space of linear finite-dimensional systems which have a state-space realisation given by

$$\begin{aligned} \dot{x}(t) &= A(t)x(t) + B(t)u(t) \\ y(t) &= C(t)x(t) + D(t)u(t). \end{aligned} \tag{2.1}$$

The vector $x(t) \in \mathbb{R}^{n\times 1}$ is the state, $u(t) \in \mathbb{R}^{m\times 1}$ is the input and $y(t) \in \mathbb{R}^{p\times 1}$ is the output. When $p = m = 1$ the system is single input-single output (SISO) otherwise it is multiple input-multiple output (MIMO). It is assumed that $A : \mathbb{R} \mapsto \mathbb{R}^{n\times n}$, $B : \mathbb{R} \mapsto \mathbb{R}^{n\times m}$, $C : \mathbb{R} \mapsto \mathbb{R}^{p\times n}$ and $D : \mathbb{R} \mapsto \mathbb{R}^{p\times m}$ are bounded piecewise continuous functions of time.

Remark 2.2.1 *By piecewise continuity of a matrix $A(t) : \mathbb{R} \mapsto \mathbb{R}^{n\times m}$ we imply that it is continuous everywhere except at a finite number of points. At these points it is assumed that the left hand limit and the right hand limit of the elements of the matrix are well defined and bounded.*

Definition 2.2.2 *[13]*
For all $t_0 \in \mathbb{R}$ define $\Phi(.,.) : \mathbb{R}\times\mathbb{R} \mapsto \mathbb{R}^{n\times n} : (t,t_0) \mapsto \Phi(t,t_0)$ as the unique continuous solution to the homogeneous differential equation

$$\frac{d}{dt}\Phi(t,t_0) = A(t)\Phi(t,t_0), \qquad \Phi(t_0,t_0) = I.$$

Proposition 2.2.3 *[45]*
Given $x(0) = 0$, the state-space equation (2.1) defines a causal linear operator $P : L_{2,e}^+ \mapsto L_{2,e}^+$, $u(t) \mapsto y(t)$ according to

$$y(t) = \int_0^t C(t)\Phi(t,\tau)B(\tau)u(\tau)d\tau + D(t)u(t).$$

By causal we mean that the output at any given instant is only dependent on past inputs, more succinctly $P_T P P_T = P_T P$, where P_T is the truncation operator

$$(P_T w)(t) \stackrel{\triangle}{=} \begin{cases} w(t) & t \leq T \\ 0 & t > T. \end{cases}$$

An equally important concept to that of causality is the concept of stability. We say that a system is stable if given any $u \in L_2^+$, Pu is also in L_2^+. That is, stable systems map bounded energy inputs into bounded energy outputs. This definition is independent of the chosen state-space realisation and is equivalent to the definition of internal stability (ie: asymptotic stability of the state) if the realisation is stabilisable and detectable. For presentation purposes we will make extensive use of the notation

$$P \stackrel{s}{=} \left[\begin{array}{c|c} A(t) & B(t) \\ \hline C(t) & D(t) \end{array}\right],$$

to represent a state-space realisation of the operator P.

In the case where A, B, C and D are all time invariant we recover the important class of finite-dimensional linear time-invariant (LTI) systems with p outputs and m inputs. We denote this important class of systems by $\mathcal{P}^{p\times m}$. We examine various properties of LTI systems in section 2.3 before examining the class of linear parameter-varying (LPV) systems, a class of time-varying systems where the time dependence enters the equations in a special way, in section 2.4.

2.3 LTI systems

When the matrices in equation (2.1) are time invariant we can take the bilateral Laplace transform to get

$$y(s) = P(s)u(s); \qquad P(s) = C(sI - A)^{-1}B + D.$$

This allows us to consider the system as being a frequency domain Laurent operator with symbol P

$$L_P : L_2 \mapsto L_2; \quad u \mapsto Pu,$$

provided it has no poles on the imaginary axis. While the Laurent operator is bounded, its domain $\mathcal{D}(L_P)$ being all of L_2, it is not necessarily causal. Causality is only preserved if P is stable (or as we will see $P \in H_\infty$). Alternatively, we can consider the system to be a possibly unbounded, but causal, multiplication operator with symbol P

$$M_P : H_2 \mapsto H_2; \quad u \mapsto Pu.$$

The domain of M_P, $\mathcal{D}(M_P)$, is defined as

$$\mathcal{D}(M_P) \stackrel{\triangle}{=} \{u \in H_2 : Pu \in H_2\}.$$

This leads us to the formal definitions of the spaces in which the transfer functions of linear time-invariant (possibly infinite-dimensional) systems are assumed to exist.

Definition 2.3.1 *The Banach space L_∞ is the space of matrix valued functions of the complex variable s, essentially bounded on the imaginary axis with L_∞ norm given by*

$$\|P\|_\infty = ess\sup_{\omega\in\mathbb{R}} \bar{\sigma}(P(j\omega)).$$

Definition 2.3.2 *The Hardy space H_∞ is a closed subspace of L_∞ whose elements are analytic and bounded on the open right-half plane. The H_∞ norm is defined as*

$$\|P\|_\infty \stackrel{\triangle}{=} ess\sup_{\Re(s)>0} \bar{\sigma}(P(s)) = ess\sup_{\omega\in\mathbb{R}} \bar{\sigma}(P(j\omega)).$$

The symbols RL_∞ and RH_∞ are used to denote the subspaces of L_∞ and H_∞ consisting of matrix valued functions whose elements are rational functions with real coefficients. The space H_∞ defines the space of all stable systems, that is, a system with transfer function P is stable if, and only if, $P \in H_\infty$. RH_∞ defines the space of all stable finite-dimensional systems. Given a minimal state-space realisation of a system with transfer function P, then $P \in RH_\infty$ if, and only if, $\Re(\lambda_i(A)) < 0$ for all i. Similarly, given a minimal state-space realisation of a system with transfer function P, $P \in RL_\infty$ if, and only if, $\Re(\lambda_i(A)) \neq 0$ for all i.

The importance of the L_∞ norm stems from the fact that it represents the induced norm of the Laurent operator.

Proposition 2.3.3 *Given any $P \in L_\infty$, then*

$$\|P\|_\infty = \sup_{u\in L_2, u\neq 0} \frac{\|Pu\|_2}{\|u\|_2} = \sup_{u\in H_2, u\neq 0} \frac{\|Pu\|_2}{\|u\|_2}.$$

The H_∞ norm is the restriction of the L_∞ norm to the class of stable systems and the duality of the time and frequency domain spaces shows that it is the maximum energy gain of the system.

Proposition 2.3.4 *Given any $P \in H_\infty$, then*

$$\|P\|_\infty = \sup_{u\in H_2, u\neq 0} \frac{\|Pu\|_2}{\|u\|_2}.$$

Another operator which is used extensively in system and control theory in the Hankel operator H with symbol P,

$$H_P : H_2^\perp \mapsto H_2, u \mapsto \Pi^+ Pu.$$

The Hankel norm is defined as

$$\|P\|_H \stackrel{\triangle}{=} \sup_{u\in H_2^\perp, u\neq 0} \frac{\|\Pi^+ Pu\|_2}{\|u\|_2}.$$

We will also require the conjugate transpose of a finite-dimensional system with transfer function P. When $P \in RL_\infty$ this represents the adjoint of the Laurent operator $L_P : L_2 \mapsto L_2$.

Definition 2.3.5 *The conjugate transpose of P is defined as follows*

$$P^*(s) \stackrel{s}{=} \left[\begin{array}{c|c} -A^T & C^T \\ \hline -B^T & D^T \end{array}\right].$$

When evaluated on the imaginary axis, $P^*(j\omega) = (P(j\omega))^*$.

For a scalar transfer function $g(s)$ we define the winding number about the origin wno $g(s)$ to be the total number of counterclockwise encirclements of the origin traced out by the image of $g(s)$ (assuming this to be continuous) when evaluated on the standard $\mathcal{D}$ contour[1].

We next state some important results concerning the factorisation of transfer functions of finite-dimensional LTI systems over the ring of matrices with elements in RH_∞. Such factorisations have played a central role in the development of multivariable control theory ([45],[60],[84],[103]) providing useful characterisations of closed-loop stability, a transparent parameterisation of stabilising feedback schemes and a powerful tool in approximation (model reduction) theory. The transfer function of a finite-dimensional system can always be written in terms of a quotient of transfer functions in RH_∞

$$P = NM^{-1}, \quad N, M \in RH_\infty.$$

An important concept in controller synthesis is the prevention of unstable pole-zero cancellations as would arise if N and M had common right-half plane zeros. This has led to the concept of coprime factorisations over RH_∞.

Definition 2.3.6 *[84]*
Given $N, M \in RH_\infty$, with the same number of columns, then N and M are right coprime if there exist $X, Y \in RH_\infty$ such that

$$XM + YN = I.$$

This definition requires any common right divisor of N and M to be a unit (invertible) in RH_∞. Specifically, if $N = N_1 D$ and $M = M_1 D$, then N and M are right coprime implies D and $D^{-1} \in RH_\infty$.

Definition 2.3.7 *The ordered pair $[N, M]$ is a right coprime factorisation (rcf) of the transfer function P if*

i. *M^{-1} exists.*

ii. *$P = NM^{-1}$.*

iii. *$N \in RH_\infty$ and $M \in RH_\infty$ are right coprime.*

Proposition 2.3.8 *Any finite-dimensional system with transfer function P has a rcf $[N, M]$.*

[1] Down the imaginary axis, indenting around any imaginary axis poles of $g(s)$, and around an sufficiently large circle in the right-half plane so that the winding number remains invariant for any larger circle.

Coprime factorisations are by no means unique and it can be shown [84] that if the ordered pair $[N, M]$ represents a rcf of P over RH_∞ then $[NQ, MQ]$ also represents a rcf of P when $Q, Q^{-1} \in RH_\infty$. In fact by varying Q over the open set of all units in RH_∞ we obtain every right coprime factorisation of P. A particular coprime factorisation which has useful norm preserving properties is the normalised coprime factorisation.

Definition 2.3.9 *The ordered pair $[N, M]$ is a normalised rcf over RH_∞ if $[N, M]$ is a rcf of P and*

$$N^*N + M^*M = I.$$

Proposition 2.3.10 *Any finite-dimensional system with transfer function P has a normalised rcf over RH_∞ which is unique up to right multiplication by a unitary matrix.*

Analogous results hold for left coprime factors.

Definition 2.3.11 *Given $\tilde{M}, \tilde{N} \in RH_\infty$ with the same number of rows, then $\tilde{M}$ and $\tilde{N}$ are left coprime if there exist $\tilde{X}, \tilde{Y} \in RH_\infty$ such that*

$$\tilde{M}\tilde{X} + \tilde{N}\tilde{Y} = I.$$

Definition 2.3.12 *The ordered pair $[\tilde{N}, \tilde{M}]$ is a left coprime factorisation (lcf) of the transfer function P if*

i. $\tilde{M}^{-1}$ *exists.*

ii. $P = \tilde{M}^{-1}\tilde{N}$.

iii. $\tilde{N} \in RH_\infty$ *and* $\tilde{M} \in RH_\infty$ *are left coprime.*

Proposition 2.3.13 *Any finite-dimensional system with transfer function P has a lcf $[\tilde{N}, \tilde{M}]$ which is unique up to left multiplication by a unit in RH_∞. Furthermore, all left coprime factorisations are of the form $[Q\tilde{N}, Q\tilde{M}]$ and can be obtained by varying Q over the open set of units in RH_∞.*

Definition 2.3.14 *The ordered pair $[\tilde{N}, \tilde{M}]$ is a normalised lcf of P if $[\tilde{N}, \tilde{M}]$ is a lcf of P and*

$$\tilde{N}\tilde{N}^* + \tilde{M}\tilde{M}^* = I.$$

Proposition 2.3.15 *Any finite-dimensional system with transfer function P has a normalised lcf $[\tilde{N}, \tilde{M}]$ which is unique up to left multiplication by a unitary matrix.*

In the spirit of Vinnicombe [87] we introduce the normalised left and normalised right graph symbols $\tilde{G}$ and G of a plant with transfer function P. Let $[\tilde{N}, \tilde{M}]$ and $[N, M]$ represent a normalised left and normalised right coprime factorisation of P, then

$$\tilde{G} \stackrel{\triangle}{=} [-\tilde{M}, \ \tilde{N}] \quad \text{and} \quad G \stackrel{\triangle}{=} \begin{bmatrix} N \\ M \end{bmatrix},$$

represent the normalised left and normalised right graph symbols of P respectively. Similarly, given a controller with transfer function C, let $[\tilde{N}_c, \tilde{M}_c]$ and $[N_c, M_c]$ denote a normalised left and a normalised right coprime factorisation of C respectively, then

$$\tilde{K} \stackrel{\triangle}{=} [-\tilde{N}_c, \tilde{M}_c] \quad \text{and} \quad K \stackrel{\triangle}{=} \begin{bmatrix} M_c \\ N_c \end{bmatrix},$$

represent the normalised left and normalised right graph symbols of C respectively. In terms of these definitions $\tilde{G}G = \tilde{K}K = 0$, while $[G, \ \tilde{G}^*]$ and $[K, \ \tilde{K}^*]$ are unitary on $L_2 \otimes L_2$.

2.4 LPV systems

Linear parameter-varying systems are a special class of time-varying systems where the time dependence enters the state equations through one, or possibly more, exogenous parameters. Consider a system which has a state-space realisation given by

$$\begin{aligned} \dot{x}(t) &= A(\rho(t))x(t) + B(\rho(t))u(t) \\ y(t) &= C(\rho(t))x(t) + D(\rho(t))u(t). \end{aligned} \tag{2.2}$$

The matrices $A : \mathbb{R}^s \mapsto \mathbb{R}^{n\times n}, B : \mathbb{R}^s \mapsto \mathbb{R}^{n\times m}, C : \mathbb{R}^s \mapsto \mathbb{R}^{p\times n}$ and $D : \mathbb{R}^s \mapsto \mathbb{R}^{p\times m}$ are here assumed to be continuous functions of the parameter vector $\rho \in \mathbb{R}^s$.

Definition 2.4.1 *We define the set of feasible parameter trajectories F_ρ to be a subset of*

$$F \stackrel{\triangle}{=} \{\rho(t) : \mathbb{R} \mapsto \mathbb{R}^s, \rho_i(t) \in C^1 \ \forall \ i\}.$$

In terms of F, the set of feasible trajectories is given by

$$F_\rho \stackrel{\triangle}{=} \{\rho(t) \in F : \rho_{i_{\min}} \leq \rho_i \leq \rho_{i_{\max}}, \dot{\rho}_{i_{\min}} \leq \dot{\rho}_i \leq \dot{\rho}_{i_{\max}} \ \forall \ i\}.$$

Remark 2.4.2 *At this stage we stress that in the definition of an LPV system it is not assumed that the parameter dependence of the state-space matrices is linear.*

Continuity of the state-space matrices implies that they are bounded on compact subsets of $\mathbb{R}^s$ which ensures that for each $\rho(t) \in F_\rho$ the state transition matrix in definition 2.2.2 is both unique and continuous.

Definition 2.4.3 *Given a state-space representation of an LPV system define the linear operator $P_\rho : L_{2,e}^+ \mapsto L_{2,e}^+, \ u(t) \mapsto y(t)$ as*

$$y(t) = \int_0^t C(\rho(t))\Phi_\rho(t,\tau)B(\rho(\tau))u(\tau)d\tau + D(\rho(t))u(t).$$

Remark 2.4.4 *We use the notation P_ρ to emphasise that the input-output operator is different for each specific path $\rho(t) \in F_\rho$.*

The state-space representation of an LPV system is not unique because the input-output operator P_ρ is invariant under parameter-dependent similarity transformations. However, when introducing parameter-dependent similarity transformations care must be taken to ensure that the solution of the state equation exists and remains unique.

Definition 2.4.5 *Given a state-space realisation of an LPV system, a continuous matrix $T(\rho)$ such that $T^{-1}(\rho)$ exists for all $\rho \in F_\rho$, and let $T(\rho)$ have continuous partial derivatives with respect to the parameters in the parameter vector. When $T(\rho)$ satisfies these conditions define the parameter-varying state transformation $x(t) = T(\rho(t))\tilde{x}(t)$. This gives*

$$\begin{aligned} \dot{\tilde{x}}(t) &= (T^{-1}(\rho(t))A(\rho(t))T(\rho(t)) - T^{-1}(\rho(t))\dot{T}(\rho(t)))\tilde{x}(t) + T^{-1}(\rho(t))B(\rho(t))u(t) \\ y(t) &= C(\rho(t))T(\rho(t))\tilde{x}(t) + D(\rho(t))u(t). \end{aligned}$$

For this class of systems we now define a notion of stability which we call extended quadratic stability ($\mathcal{Q}_e$ stability). This definition is a natural extension of the much studied notion of quadratic stability.

Definition 2.4.6 *Given the state-space equation*

$$\dot{x}(t) = A(\rho(t))x(t), \quad \rho(t) \in F_\rho \tag{2.3}$$

we say that the system is $\mathcal{Q}_e$ stable if there exists a real differentiable positive-definite matrix function $P(\rho) = P^T(\rho) > 0$ such that

$$\frac{d}{dt}P(\rho(t)) + A(\rho(t))^T P(\rho(t)) + P(\rho(t))A(\rho(t)) < 0 \qquad \forall \ \rho(t) \in F_\rho. \tag{2.4}$$

If we restrict the matrix P to be constant then we recover the familiar definition of quadratic stability ([7],[11],[12]), see also the review article in [17]. For presentation purposes we now drop ρ dependence in the equations although it will be implicitly assumed that the matrices are functions of ρ throughout.

Proposition 2.4.7 *The notion of $\mathcal{Q}_e$ stability is a system property, independent of any particular state-space realisation.*

Proof: Assume that

$$\frac{dP}{dt} + A^T P + PA < 0 \quad \forall\, \rho(t) \in F_\rho.$$

It is an easy matter to verify that $\hat{P} = T^T P T$ satisfies

$$\frac{d\hat{P}}{dt} + \hat{A}^T \hat{P} + \hat{P}\hat{A} < 0 \quad \forall\, \rho(t) \in F_\rho,$$

where $\hat{A}$ is the transformed A matrix given by $\hat{A} = T^{-1}AT - T^{-1}\dot{T}$. ■

Given a continuous state-space realisation of an LPV system we next define the notions of $\mathcal{Q}_e$ stabilisability and $\mathcal{Q}_e$ detectability.

Definition 2.4.8 *Any state-space realisation of an LPV system P_ρ having the basic structure given in equation (2.2) is said to be $\mathcal{Q}_e$ stabilisable if there exists a continuous matrix function $F(\rho) : \mathbb{R}^s \mapsto \mathbb{R}^{m\times n}$, such that the following system is $\mathcal{Q}_e$ stable for all $\rho(t) \in F_\rho$*

$$\dot{x}(t) = (A(\rho(t)) + B(\rho(t))F(\rho(t)))x(t).$$

Lemma 2.4.9 *An LPV system is $\mathcal{Q}_e$ stabilisable if, and only if, there exists a $Q(\rho) = Q^T(\rho) > 0$ and a continuous matrix function $R : \mathbb{R}^s \mapsto \mathbb{R}^{m\times n}$ such that*

$$-\dot{Q} + QA^T + AQ < -BR - R^TB^T \ \ \forall \rho(t) \in F_\rho. \tag{2.5}$$

Proof: Suppose the realisation is $\mathcal{Q}_e$ stabilisable, then $\exists\ P(\rho) = P^T(\rho) > 0$ and $F(\rho) : \mathbb{R}^s \mapsto \mathbb{R}^{m\times n}$ such that

$$\dot{P} + (A + BF)^T P + P(A + BF) < 0 \ \ \forall \rho(t) \in F_\rho. \tag{2.6}$$

Left and right multiplying equation (2.6) by P^{-1} gives

$$-\frac{d}{dt}P^{-1} + P^{-1}A^T + AP^{-1} < -P^{-1}F^TB^T - BFP^{-1},$$

and setting $Q = P^{-1}$ and $R = FP^{-1}$ gives equation (2.5). Conversely, suppose equation (2.5) holds, left and right multiplying by Q^{-1}, setting $P = Q^{-1}$ and $F = RQ^{-1}$ gives equation (2.6).

■

Remark 2.4.10 *Observe that the test condition given in equation (2.5) is affine in the unknown variables Q and R, and as we shall see, the problem of finding a Q and an R which satisfy equation (2.5) can be reformulated as a convex feasibility problem.*

Definition 2.4.11 *Any state-space realisation of an LPV system P_ρ having the basic structure given in equation (2.2) is said to be $\mathcal{Q}_e$ detectable if there exists a continuous matrix function $L(\rho) : \mathbb{R}^s \mapsto \mathbb{R}^{n\times p}$, such that the following system is $\mathcal{Q}_e$ stable for all $\rho(t) \in F_\rho$*

$$\dot{x}(t) = (A(\rho(t)) + L(\rho(t))C(\rho(t)))x(t).$$

Lemma 2.4.12 *An LPV system is $\mathcal{Q}_e$ detectable if, and only if, there exists a $Q(\rho) = Q^T(\rho) > 0$ and a continuous matrix function $Z(\rho) : \mathbb{R}^s \mapsto \mathbb{R}^{n\times p}$ such that*

$$\dot{Q} + A^TQ + QA < -C^TZ^T - ZC \ \ \forall \ \ \rho(t) \in F_\rho.$$

Although the notion of $\mathcal{Q}_e$ stability is weaker than the more commonly used notion of quadratic stability (which allows for unbounded rates of parameter variation), it is still a fairly strong form of stability. Given any initial state $x(0) = x_0$, when there is no external excitation (ie: $u(t) = 0$), a $\mathcal{Q}_e$ stable LPV system's state vector $x(t)$ approaches the origin at least as fast as a decaying exponential function for all feasible parameter trajectories.

Lemma 2.4.13 *Any $\mathcal{Q}_e$ stable system is exponentially stable, that is, there exist constants $c_0 > 0$ and $c_1 > 0$ such that*

$$\bar{\sigma}(\Phi_\rho(t, t_0)) \leq c_0 e^{-c_1(t-t_0)} \ \ \forall \ \ \rho(t) \in F_\rho. \tag{2.7}$$

Proof: Consider $V = x^T P(\rho) x$ where P satisfies equation (2.4) and note that

$$\lambda_{\min}\|x\|^2 \leq V \leq \lambda_{\max}\|x\|^2, \tag{2.8}$$

where $\lambda_{\min} = \min_{\rho \in F_\rho} \underline{\lambda}(P(\rho))$ and $\lambda_{\max} = \max_{\rho \in F_\rho} \bar{\lambda}(P(\rho))$. Differentiating V gives

$$\frac{dV}{dt} = x^T(A^T P + PA + \dot{P})x \leq -\gamma^2\|x\|^2 \tag{2.9}$$

for some $\gamma > 0$. The existence of such a γ is assured because the inequality in equation (2.4) holds on a compact subset of $\mathbb{R}^s$. So

$$\frac{dV}{dt} \leq \frac{-\gamma^2 V}{\lambda_{\max}}.$$

The Gronwall lemma [13] can now be used to get

$$\begin{aligned}
& V(x,t) \leq V(x_0,t_0)e^{-\frac{\gamma^2}{\lambda_{\max}}(t-t_0)} \\
\Rightarrow \quad & \|x\|^2 \leq \frac{V(x_0,t_0)}{\lambda_{\min}} e^{-\frac{\gamma^2}{\lambda_{\max}}(t-t_0)} \\
\Rightarrow \quad & \|x\|^2 \leq \frac{\lambda_{\max}}{\lambda_{\min}}\|x_0\|^2 e^{-\frac{\gamma^2}{\lambda_{\max}}(t-t_0)} \\
\Rightarrow \quad & \bar{\sigma}(\Phi(t,t_0)) \leq \sqrt{\frac{\lambda_{\max}}{\lambda_{\min}}} e^{-\frac{\gamma^2}{2\lambda_{\max}}(t-t_0)}.
\end{aligned}$$

■

Next we define the induced norm of a $\mathcal{Q}_e$ stable LPV system.

Definition 2.4.14 *Let P_ρ be a $\mathcal{Q}_e$ stable LPV system with $x(0) = 0$, then the induced norm is defined as follows*

$$\|P_\rho\| = \sup_{\rho \in F_\rho} \sup_{u \in L_2^+, u \neq 0} \frac{\|P_\rho u\|_2}{\|u\|_2}. \tag{2.10}$$

The following two results are standard results for exponentially stable linear time-varying systems [86] and consequently hold for LPV systems. The first shows that the induced norm of a $\mathcal{Q}_e$ stable system always exists while the second relates to the asymptotic behaviour of the state vector of a $\mathcal{Q}_e$ stable system.

Lemma 2.4.15 *The induced norm of any $\mathcal{Q}_e$ stable system is bounded.*

Lemma 2.4.16 *Given any $\mathcal{Q}_e$ stable system, any initial state vector $x(0) = x_0$, and any input $u \in L_2^+$, such that $\dot{x}(t) = A(\rho(t))x(t) + B(\rho(t))u(t)$, then*

$$\lim_{t\to\infty} \|x(t)\| \to 0.$$

We will make extensive use of quadratic dissipation functions to bound the induced norm of LPV systems. This leads us to define the notion of $\mathcal{Q}_\gamma$ performance. Once again, this is a natural extension of the notion of quadratic performance.

Definition 2.4.17 *Given an LPV system P_ρ with a continuous state-space realisation having the basic structure in equation (2.2), if $\exists\ X(\rho) = X^T(\rho) > 0$ such that the following two conditions hold,*

i. $\gamma^2 I - D^T D > 0$, *and*

ii. $\dot{X} + XA + A^T X + C^T C + (XB + C^T D)(\gamma^2 I - D^T D)^{-1}(B^T X + D^T C) < 0\ \forall \rho(t) \in F_\rho$,

then the following statements are true:

i. P_ρ *is $\mathcal{Q}_e$ stable.*

ii. $\|P_\rho\| \leq \gamma$.

Furthermore, if the two conditions are satisfied we say that the LPV system satisfies a $\mathcal{Q}_\gamma$ performance level[2].

Proof: We will give a full proof of the above statement in chapter 7. ■

Proposition 2.4.18 *The notion of $\mathcal{Q}_\gamma$ performance is independent of the chosen state-space realisation of an LPV system.*

Our work on LPV systems relies heavily on being able to cast the solution of various matrix differential inequalities into convex and quasi-convex optimisation problems involving linear matrix inequalities (LMI's). This makes them tractable, at least in a theoretical sense. The first application of LMI's dates back to Lyapunov's seminal work on stability theory. He showed that an LTI system with a state evolution equation given by

$$\dot{x}(t) = Ax(t),$$

is stable if, and only if, there exists a positive definite matrix $P \in \mathbb{R}^{n\times n}$ such that

$$A^T P + PA < 0. \tag{2.11}$$

[2]This is only a sufficient condition for the induced norm to be less than γ. That is, if we fail to find a quadratic dissipation function that satisfies the required conditions then we cannot make any conclusions.

Recent developments involving powerful and efficient interior point methods allow many problems arising in systems and control theory to be cast as LMI's and solved numerically. The book by Boyd et al [12] serves as an excellent review of these techniques and provides a comprehensive survey of the historical evolution of LMI's in control theory. We will be dealing with strict LMI's which take the form

$$F(x) \stackrel{\triangle}{=} F_0 + \sum_{i=1}^{m} x_i F_i < 0. \tag{2.12}$$

The vector $x \in \mathbb{R}^{m\times 1}$ is the unknown variable and the matrices $F_i = F_i^T$, $i = 0, 1 \ldots m$ are symmetric. The set $\{x \in \mathbb{R}^{m\times 1} : F(x) < 0\}$ is clearly convex. Multiple LMI's $F^1(x), F^2(x), \ldots F^p(x) < 0$ can be cast as a single LMI $\mathrm{diag}(F^1(x), F^2(x), \ldots F^p(x)) < 0$. Typically LMI's will not be explicitly in the form of equation (2.12) but will be left in a form where the unknown matrices are the variables. The example of the Lyapunov inequality in equation (2.11) represents an LMI in the unknown variable P and can be cast into the form of equation (2.12) by making use of a basis for the set of $n \times n$ symmetric matrices, $P_1, P_2 \ldots P_m$, where $m = n(n+1)/2$. This gives the constant matrices in the LMI problem as $F_0 = 0$ and $F_i = A^T P_i + P_i A$.

We conclude this very brief review of LMI's with a statement of the Shur-complement. This allows many seemingly non-convex problems to be convexified by posing them as an LMI involving a larger matrix.

Lemma 2.4.19 *Consider the following block partitioned matrix*

$$M = \begin{bmatrix} M_{11} & M_{12} \\ M_{12}^T & M_{22} \end{bmatrix}.$$

M is negative definite if, and only if,

$$M_{22} < 0 \qquad \textit{and} \qquad M_{11} - M_{12} M_{22}^{-1} M_{12}^T < 0.$$

As an example of its application, we use the Shur-complement to write the matrix differential inequality in definition 2.4.17 as an LMI which is affine in the unknown variable X. This allows us to state that an LPV system satisfies a $\mathcal{Q}_\gamma$ performance bound if, and only if:

i. $\gamma^2 I - D^T D > 0$.

ii. $\begin{bmatrix} \dot{X} + A^T X + X A & XB & C^T \\ B^T X & -\gamma^2 I & D^T \\ C & D & -I \end{bmatrix} < 0 \quad \forall \rho(t) \in F_\rho.$

2.5 The small gain theorem

The small gain theorem is the fundamental result upon which robust control theory has been developed. In order to state it in full generality we need to define the incremental gain of an operator.

Definition 2.5.1 *Let $P : L_{2,e}^{+} \mapsto L_{2,e}^{+}$ be a given operator, the incremental gain $\gamma(P)$ is defined as follows*

$$\gamma(P) \stackrel{\triangle}{=} \inf\{\gamma : \|Pw - P\tilde{w}\|_{2,[0,T]} \leq \gamma \|w - \tilde{w}\|_{2,[0,T]} \text{ for all } w, \tilde{w} \in L_{2,e}^{+} \text{ and for all } T > 0\}.$$

We note that any system having a finite incremental gain is causal, stable and has a finite induced norm. Furthermore, for linear systems the incremental gain and the induced norm are identical. The proof of the small gain theorem is based on the contraction mapping theorem due to Banach, the original proof can be found in [98].

Theorem 2.5.2 *Let the systems $\Delta_1 : L_{2,e}^{+} \mapsto L_{2,e}^{+}$ and $\Delta_2 : L_{2,e}^{+} \mapsto L_{2,e}^{+}$ in Figure 2.5 have finite incremental gains such that $\gamma(\Delta_1)\gamma(\Delta_2) < 1$. Then for all $w_1, w_2 \in L_2^{+}$, there exist unique solutions $e_1, e_2 \in L_2^{+}$.*

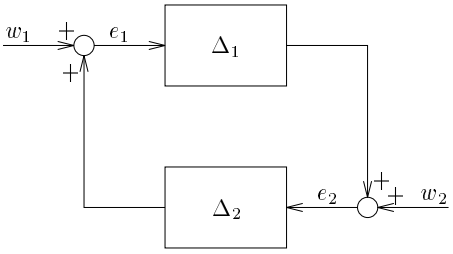

Figure 2.1 *Closed loop interconnection.*

This theorem indicates why so much theoretical effort has been expended on finding controllers which bound the induced norm of some closed-loop operator. Suppose Δ_1 denotes the closed-loop operator formed by interconnecting some nominal linear plant P with a linear stabilising controller C. By bounding the induced norm of Δ_1, $\|\Delta_1\| < \gamma$, we effectively guarantee closed-loop stability to any linear, possibly time-varying, infinite-dimensional perturbation Δ_2 having an induced norm less than or equal to γ^{-1}. The same is true for any nonlinear operator Δ_2 having an incremental gain less than or equal to γ^{-1}.

3

Mathematical Modelling: The Flexible Beam Example

3.1 Introduction

In this chapter we give a detailed definition of the mechanical system that is used as an example for much of this thesis, and develop mathematical models of it which are appropriate for the synthesis of model-based controllers. Since one of the objectives of this thesis is to investigate the control issues involved in violin bowing we consider a system which has many of the qualitative features of the bowing process, but which is simpler to model. We consider the problem of controlling the contact force between a flexible beam and a fixed object, allowing for variations in the position of the object on the beam. We require the contact force between the beam and the object to follow certain patterns of time variation as would be the case when trying to produce different bowing gestures with a violin bow. By allowing the contact position to vary we emulate the situation that arises during the bowing process where the contact point of the string on the bow is continually varying, so a controller must compensate for the considerable variation in dynamic properties which results.

It will be seen that this system has particularly severe parameter dependence, such that small variations in the contact position generate large variations in the open-loop dynamics. Although our motivation for studying this problem is strongly influenced by its application to the field of musical acoustics ([90],[91]), it is important to appreciate that many of the issues studied herein are inherent in any structural control problem [4]. The example system also provides a useful benchmark for studying the control issues that arise in a broad range of problems involving parameter-dependent structures. These can be anything from lightweight and highly flexible deployable manipulators and space structures used in space applications, to large rotating machinery used in an industrial environment. In fact, many vibration control problems involve systems whose dynamics vary in a predictable manner with some measurable exogenous parameter. Our interest here lies not so much in ad-hoc techniques which might work on our example system but rather in the fundamental control issues involved.

The system is shown in Figure 3.1; it consists of a highly flexible beam through which the force transmitted to a force transducer must be controlled. The force transducer is free to slide along the beam. An external torque can be applied to the base of the beam by a motor, with the

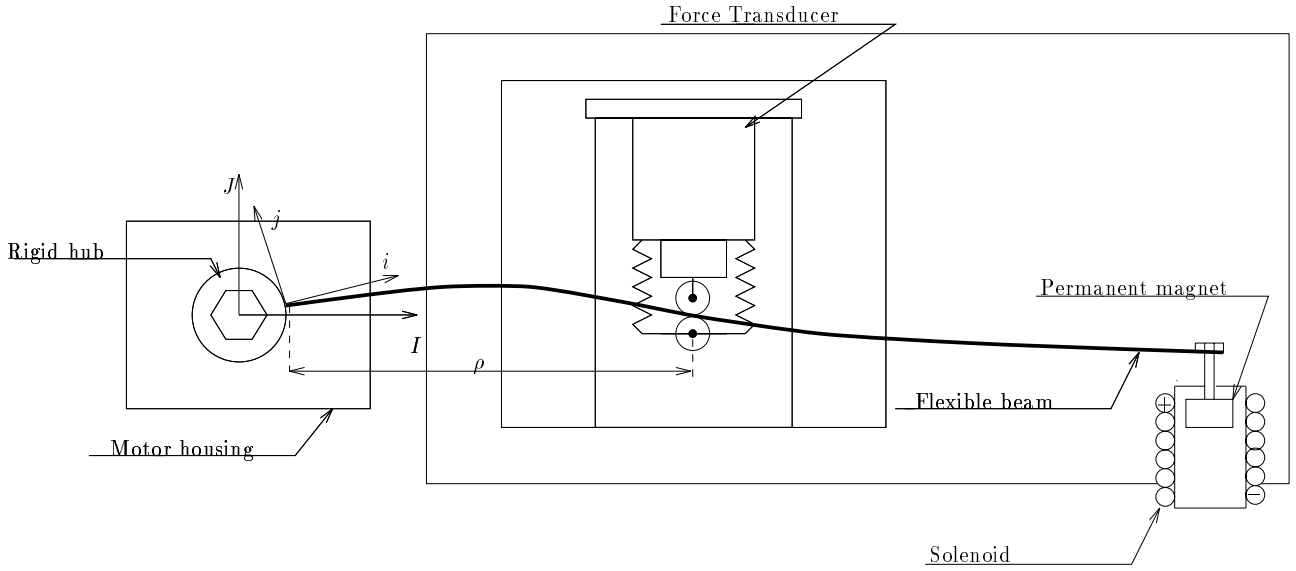

Figure 3.1 *The system under consideration.*

option of an additional input being provided by an electromagnetic actuator which can apply a force to the tip of the beam. Violinists manage to control bow pressure by applying a torque solely to the base of a bow so there is no physical justification for the additional force applied at the tip of the beam. However, our objective is to achieve tight control of the contact force between the flexible beam and the force transducer and if this performance can be improved by using additional actuators it is an issue that is worth investigating. Equally, it may be acceptable for a bowing machine to have additional actuators, and not to be restricted to a single actuator simply because players are restricted in this way.

Briefly, we list a number of features that are common to both the bowing problem and the problem studied herein which makes this an interesting and challenging control problem.

i. The system is subject to considerable dynamic uncertainty, even for the simple system considered here: boundary conditions, constraint dynamics and damping are only approximations of reality. Such modelling difficulties are likely to be even greater when modelling a real bow constrained by a violin string.

ii. The dynamics undergo parametric variations; while these are predictable they are also significant. The nature of the system is such that small variations in the contact position can cause a significant change in the open-loop dynamics. That these parameter variations make the system time varying further complicates the control issues.

iii. Flexible structures are infinite-dimensional and the vibration modes are lightly damped. This raises the issue of resonances appearing within the control bandwidth and the pos-

sibility of the controller interacting with unmodelled high frequency dynamics. Such interactions are generically referred to as modal spillover and can easily lead to closed-loop instabilities.

iv. Mathematical models of flexible structures typically involve a large number of modes. This raises a number of interesting implementation issues since many of the most recent control techniques produce controllers with a state dimension greater than or equal to that of the model from which they are designed ([2],[24],[32]).

We will develop two mathematical models of this system, the motivation for this becoming clearer as we commence. The first model gives a finite-dimensional LTI representation of the dynamics with the contact position as a free parameter. This model is used in the synthesis of LTI controllers that achieve a specified level of performance and robustness for all values of the free parameter in a chosen range. However, these controllers do not take into account the explicit time dependence of the system dynamics and we have to resort to the small gain theorem to ensure robustness in this case. One advantage of this approach is that for each fixed value of the free parameter we can make use of certain well known properties of mechanical systems to obtain an accurate finite-dimensional model. In particular, we can introduce co-ordinate transformations and view the system in a modal reference frame thus allowing us to incorporate physical measurements of damping into the model [29]. If we wish to account for the explicit time dependence of the system's dynamics we will need a finite-dimensional LPV model. In this case it becomes more difficult to incorporate physical measurements of damping[1] and we look instead for simple physical dissipation models to account for the observed damping.

3.2 An LTI model

In this section we develop a model for the idealised plant shown in Figure 3.2. It consists of a uniform beam of constant cross-section attached by a rigid hub to a motor. The right-handed triad $i-j-k$ is fixed to the edge of the hub whereas the triad $I-J-K$ is fixed in space and represents the inertial reference frame. The beam is constrained by a two-sided pinned constraint at a distance ρ from the edge of the hub and moves in the horizontal plane such that the effects of gravity can be neglected. For the purpose of analysis we consider the system to be acted upon by an externally applied torque T acting at the hub and a force F_1 applied by the constraint at the distance ρ from the hub. The forces F_{2x}, F_{2y} and the moment M are applied by a small detachable magnet which can be connected to the tip of the beam to give a second controllable input F. It is assumed that the elastic displacements are small such that the distance along the beam can be indexed by x, and that the constraint force remains normal to the beam. Shear deformation and rotary inertia are neglected. The equations of motion can be formulated using Hamilton's principle [43]. The kinetic energy can be written as

$$E_T = \int_0^l \frac{m}{2}(\dot{w}(x,t) + (x+r)\dot{\theta})^2 dx + \frac{I_h}{2}\dot{\theta}^2, \tag{3.1}$$

[1] This is primarily because modal damping models require the system to be transformed into a modal reference frame and these transformations are only applicable in the LTI case.

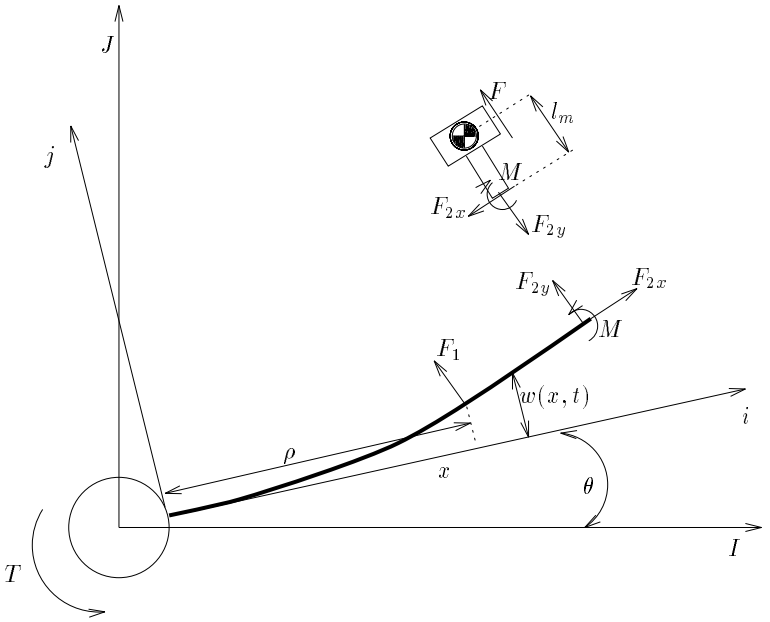

Figure 3.2 *Idealised system to be modelled.*

and the potential energy is given by[2]

$$E_V = \int_0^l \frac{EI}{2}(\frac{\partial^2 w(x,t)}{\partial x^2})^2 dx, \tag{3.2}$$

where E is Young's modulus, I is the second moment of area of the beam, m is the mass per unit length, I_h is the hub inertia, l is the length of the beam and r is the hub radius. Hamilton's principle states that

$$\delta I = \delta \int_0^{t_f} L = 0 \tag{3.3}$$

where $L = E_T - E_V$ and the variations at the terminal times are zero. Substituting equations (3.1) and (3.2) into equation (3.3), and using $'$ to denote differentiation with respect to x gives

$$\frac{\partial^2 w(x,t)}{\partial t^2} + \mathbf{L}w(x,t) + (x+r)\ddot{\theta} = \frac{F_1(t)}{m}\delta(x-\rho(t)) + \frac{F_{2y}(t)}{m}\delta(x-l) - \frac{M(t)}{m}\delta'(x-l) \tag{3.4}$$

$$I_h\ddot{\theta} - EI\frac{\partial^2 w}{\partial x^2}(0,t) + rEI\frac{\partial^3 w}{\partial x^3}(0,t) - T(t) = 0 \tag{3.5}$$

$$M_m(l\ddot{\theta} + \ddot{w}(l,t)) - F(t) + F_{2y}(t) = 0 \tag{3.6}$$

$$I_m(\ddot{\theta} + \frac{\partial^3 w}{\partial^2 t \partial x}(l,t)) + M(t) + l_m F_{2x}(t) = 0 \tag{3.7}$$

$$l_m M_m(\ddot{\theta} + \frac{\partial^3 w}{\partial^2 t \partial x}(l,t)) - F_{2x}(t) = 0. \tag{3.8}$$

[2]We neglect the small contribution resulting from axial compression of the beam due to the force F_{2x}.

Here M_m is the combined mass of the permanent magnet and its connecting rod which, when considered as a single component, has its centre of mass at a distance l_m from the centre-line of the beam. Similarly, I_m is the mass moment of inertia of the magnet and its connecting rod also taken about the combined mass centre. The differential operator $\mathbf{L}$ is given by

$$\mathbf{L} = \frac{EI}{m}\frac{\partial^4}{\partial x^4}$$

and the boundary conditions are as follows:

$$w(0,t) = 0 \qquad \frac{\partial w(0,t)}{\partial x} = 0$$
$$\frac{\partial^2 w(l,t)}{\partial x^2} = 0 \qquad \frac{\partial^3 w(l,t)}{\partial x^3} = 0.$$

These boundary conditions, obtained from the variational statement, correspond to ideal clamped conditions where the beam joins the hub and free conditions at the end of the beam. Since we are primarily interested in the low frequency dynamics of the beam we approximate the constraint as being perfectly rigid whence

$$(\rho(t) + r)\theta(t) + w(\rho(t), t) = 0. \tag{3.9}$$

The correct setting for the solution of these equations is the Hilbert space $L_2[0,l]$ ([94]) with inner product given by

$$(f(x), g(x)) = \int_0^l g(x)f(x)dx \qquad \forall\, f(x), g(x) \in L_2[0,l].$$

Consider the unforced homogeneous differential equation with $F_1 = F_{2x} = F_{2y} = M = 0$ and $\theta = 0$ (this is just the differential equation governing the response of a clamped/free flexible beam)

$$\frac{\partial^2 w(x,t)}{\partial t^2} + \mathbf{L}w(x,t) = 0. \tag{3.10}$$

This equation admits a solution of the form $w(x,t) = a(t)\phi(x)$, with $\phi(x) \in L_2[0,l]$, which on being substituted into equation (3.10) gives

$$\frac{\ddot{a}(t)}{a(t)} = -\frac{\mathbf{L}\phi(x)}{\phi(x)} = -\lambda^2.$$

The result is a standard Sturm-Liouville system with its associated boundary conditions.

$$\begin{aligned} \mathbf{L}\phi(x) &= \lambda^2\phi(x) \\ \phi(0) &= \phi'(0) = 0 \\ \phi''(l) &= \phi'''(l) = 0. \end{aligned}$$

The Sturm-Liouville system admits an infinite sequence of real eigenvalues $\{\lambda_j^2\}$ and an infinite sequence of eigenfunctions $\{\phi_j(x)\}$ which form a complete orthonormal system on $L_2[0,l]$, the first six of which are shown in Figure 3.3.

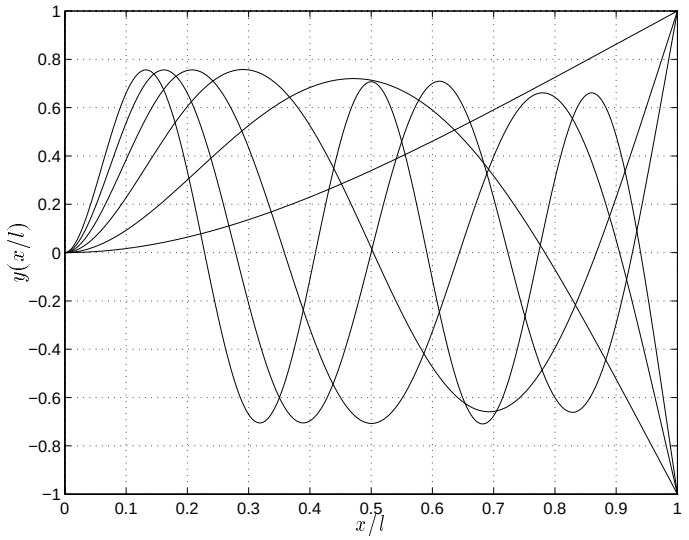

Figure 3.3 *The first six eigenfunctions.*

The operator $\mathbf{L}$ is Hermitian on its domain of definition[3] and the eigenfunctions satisfy the following orthogonality relations

$$\begin{aligned}(\phi_i(x), \phi_j(x)) &= \delta_{i,j} \\ (\phi_i(x), \mathbf{L}\phi_j(x)) &= \lambda_i^2 \delta_{i,j},\end{aligned}$$

where $\delta_{i,j}$ is the Kronecker delta. The completeness properties of the set of eigenfunctions $\{\phi_i(x)\}$ can be exploited to write a solution to the inhomogeneous equation (3.4) as

$$w(x,t) = \sum_i a_i(t)\phi_i(x). \tag{3.11}$$

Substituting equation (3.11) into equations (3.4) gives

$$\ddot{a_i}(t) + \lambda_i^2 a_i(t) + \gamma_i \ddot{\theta} = \frac{F_1(t)}{m}\phi_i(\rho(t)) + \frac{F_{2y}(t)}{m}\phi_i(l) + \frac{M(t)}{m}\phi_i'(l) \qquad i = 1,2,3... \tag{3.12}$$

$$\text{and} \qquad Ih\ddot{\theta}(t) = T(t) + EI\sum_i a_i(t)\phi_i''(0) - rEI\sum_i a_i(t)\phi_i'''(0) \tag{3.13}$$

$$\text{where} \quad (\rho(t)+r)\theta(t) + \sum_i a_i(t)\phi_i(\rho(t)) = 0 \quad \text{and} \qquad \gamma_i = \int_0^l (x+r)\phi_i(x)dx.$$

The constraint force is uniquely determined by the condition that the displacement at its position must be zero, and is easily eliminated when the constraint is assumed to be stationary in which

[3] The equivalence class of all functions in $L_2[0,l]$ which satisfy the boundary conditions and have continuous fourth derivatives.

case

$$\frac{d^2}{dt^2}(\sum_i a_i(t)\phi_i(\rho) + (\rho + r)\theta(t)) = \sum_i \ddot{a}_i(t)\phi_i(\rho) + (\rho + r)\ddot{\theta}(t).$$

In the parameter-varying case the assumption of a perfectly rigid constraint leads to a significant complication of the formulae and the undesirable result that the model depends on ρ, $\dot{\rho}$ and $\ddot{\rho}$. This is confirmed in Appendix A where the governing equations are derived without the above assumption.

Returning to the LTI approximation the constraint is given by

$$\sum_i \ddot{a}_i(t)\phi_i(\rho) + (\rho + r)\ddot{\theta}(t) = 0. \tag{3.14}$$

Multiplying equation (3.12) by $\phi_i(\rho)$ and summing over all i gives

$$\sum_i \phi_i(\rho)\ddot{a}_i(t) + \sum_i \lambda_i^2\phi_i(\rho)a_i(t) + \sum_i \gamma_i\phi_i(\rho)\ddot{\theta}(t) = \frac{F_1(t)}{m}\sum_i \phi_i^2(\rho) + \frac{F_{2y}(t)}{m}\sum_i \phi_i(\rho)\phi_i(l) + \frac{M(t)}{m}\sum_i \phi_i(\rho)\phi_i'(l). \tag{3.15}$$

We now exploit the completeness properties of the set $\{\phi_i(x)\}$ to get

$$\begin{aligned} x + r &= \sum_i (x + r, \phi_i(x))\phi_i(x) = \sum_i \gamma_i\phi_i(x) \qquad (3.16)\\ \delta(x - \rho) &= \sum_i \phi_i(\rho)\phi_i(x) = 0 \quad \forall x \neq \rho \\ \delta'(x - \rho) &= -\sum_i \phi_i'(\rho)\phi_i(x) = 0 \quad \forall x \neq \rho, \end{aligned}$$

which on substituting equation (3.14) into equation (3.15) gives

$$\frac{F_1(t)}{m}\sum_i \phi_i^2(\rho) = \sum_i \lambda_i^2\phi_i(\rho)a_i(t). \tag{3.17}$$

To keep the equations as simple and transparent as possible it is convenient to make the transformation

$$z_i(t) = \lambda_i^2 a_i(t).$$

A further observation which ensures that the equations remain symmetric is the following

$$\begin{aligned} \frac{EI}{m}\phi_i''''(x) &= \lambda_i^2\phi_i(x) \\ \Rightarrow \frac{EI}{m}\int_0^l (x + r)\phi_i''''(x)dx &= \lambda_i^2\gamma_i \\ \Rightarrow -\frac{EI}{m}\phi_i'''(0)r + \frac{EI}{m}\phi_i''(0) &= \lambda_i^2\gamma_i. \end{aligned}$$

This allows us to write equation (3.13) as

$$I_h\ddot{\theta}(t) = T(t) + m\sum_j \gamma_j z_j(t). \tag{3.18}$$

Using equations (3.12), (3.17) and equation (3.18), the frozen-parameter representation of the system dynamics is given by

$$\frac{\ddot{z}_i(t)}{\lambda_i^2} + z_i(t) + \frac{m}{I_h}\sum_j \gamma_i\gamma_j z_j(t) - \sum_j \frac{\phi_i(\rho)\phi_j(\rho)}{\sum_k \phi_k^2(\rho)} z_j(t) = \frac{F_{2y}(t)}{m}\phi_i(l) + \frac{M(t)}{m}\phi_i'(l) - \frac{\gamma_i}{I_h}T(t)$$

$$\begin{aligned} I_m(\ddot{\theta} + \sum_i \frac{\ddot{z}_i}{\lambda_i^2}\phi_i'(l)) + l_m^2 M_m(\ddot{\theta} + \sum_i \frac{\ddot{z}_i}{\lambda_i^2}\phi_i'(l)) + M(t) &= 0 \\ M_m(l\ddot{\theta} + \sum_i \frac{\ddot{z}_i}{\lambda_i^2}\phi_i(l)) + F_{2y}(t) - F &= 0. \end{aligned}$$

This is an infinite-dimensional model of the system but can be approximated by a finite-dimensional model by retaining only a finite number of eigenfunctions $\phi_i(x)$ in the series expansion of $w(x,t)$. This statement is particularly relevant when we consider that the constraint is not actually rigid and that we are tacitly assuming that the system is being excited at frequencies well below the first natural frequency of the force transducer. In so doing we obtain a finite-dimensional, albeit possibly high dimensional, LTI model of the system; the number of modes retained in the eigenfunction expansion of $w(x,t)$ effectively determining the frequency range over which we expect the model to be accurate. When our interest lies primarily in the first n modes of vibration of the constrained system it is typically necessary to retain $N > n$ terms in the series expansion of $w(x,t)$. Consequently, the number of differential equations retained in the model will be far larger than is necessary for the synthesis of adequate controllers since there will be numerous superfluous high frequency modes in the model. We can expect to have to perform further model reduction at a later stage.

3.3 An LPV model

In this section we make some modifications to the LTI model in order to make it more applicable when we wish to account for continuous variations in the constraint position. In section 3.2 particular care was taken to ensure that the mass and stiffness matrices were symmetric when the constraint was modelled as being rigid. The motivation for this will become clear in the next section where we will introduce parameter-dependent modal transformations. In the LPV case such modal transformations assume far less importance since it is not possible to find a single transformation that uncouples the equations for all feasible trajectories. Consequently, we need to look for more appropriate techniques of performing model reduction and this issue is addressed in greater detail in chapter 7. In section 3.2 we also pointed out that assuming a rigid constraint complicates the model in the time-varying case. Fortunately, this problem is

easily overcome by modelling the constraint as having a finite, but sufficiently high, stiffness. So by modelling the constraint by a stiff spring we obtain a model that depends solely on ρ. Not only does this simplify the model, but as we shall see, it also has important consequences for the synthesis of gain-scheduled controllers.

It is our view that the concept of modal damping is only applicable when the system is time invariant. This is because the combined effect of different physical dissipation mechanisms becomes particularly transparent when the system is represented in this special co-ordinate frame. Similar drawbacks hold for other popular structural damping models: for example hysteretic damping ([29],[61]) requires the system to have a frequency response, which is not the case when the system is time varying. For this reason modelling damping in parameter-varying structures is considerably more difficult, and hence likely to be even more approximate, than the methods typically used to model damping in LTI structures. In the LPV case we will model dissipation using simple physical models. For the given system the main physical mechanism of damping seems to be friction in the motor assembly, and we approximate this by a simple dashpot at the base of the beam. Experimental measurements can be used to obtain a suitable value for the damping rate of the dashpot (this is done in chapter 6). We can also model dissipation in the beam in an ad-hoc way by a proportional damping term, where the force per unit length depends on the linear velocity of the beam. Such a simple model of damping will result in a less accurate LTI model for each fixed value of ρ but we believe it to be a better representation in the LPV case. These difficulties in modelling different aspects of the system dynamics only serve to further motivate the use of a robust control approach when designing controllers for this class of systems. A schematic representation of the LPV model is given in Figure 3.4.

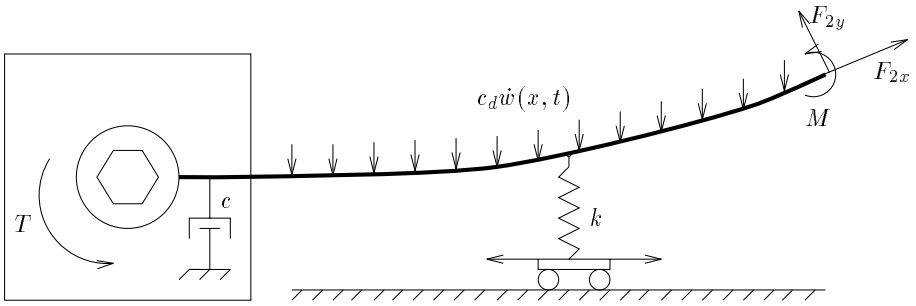

Figure 3.4 *Idealised system to be modelled.*

If we expand the elastic deformation of the beam in terms of the series $w(x,t) = \sum_{i=1}^{N} a_i(t)\phi_i(x)$,

the equations of motion are given by

$$\begin{aligned}
\ddot{a}_i(t) + c_d\dot{a}_i(t) + c_d\gamma_i\dot{\theta}(t) + \lambda_i^2 a_i(t) + \gamma_i\ddot{\theta}(t) &= \frac{F_1(t)}{m}\phi_i(\rho) + \frac{F_{2y}(t)}{m}\phi_i(l) + \frac{M(t)}{m}\phi_i'(l) \\
Ih\ddot{\theta}(t) + c\dot{\theta}(t) &= T(t) + EI\sum_{i=1}^{N} a_i(t)\phi_i''(0) \\
F_1(t) &= -k((\rho + r)\theta(t) + \sum_{i=1}^{N} a_i(t)\phi_i(\rho))
\end{aligned}$$

for sufficiently large k. When the magnet is attached to the tip of the beam, the moment $M(t)$ and the force $F_{2y}(t)$ are determined by the inertial properties of the magnet and the force applied by the magnetic field.

3.4 Basic properties of the frozen-parameter dynamics

In this section we undertake a thorough examination of the frozen-parameter dynamics of our constrained flexible beam. Our objective is to provide insight into the physical behaviour of this particular system, emphasising those properties that could be important form a control perspective. Throughout this section we will neglect the inertial properties of the tip magnet. This simplifies the formulas and makes the presentation clearer but does not alter any of the conclusions. It will be assumed that the infinite-dimensional model has been truncated so that only N vibration modes remain in the model and that the truncated system accurately reflects the properties of the infinite-dimensional model over some specified frequency range. Since it may be necessary to retain numerous vibration modes in order to accurately capture the constrained system's dynamics, we will consider an approach to reducing the resulting model complexity based on modal truncation. We will pay particular attention to the continuity properties of the model approximant as determined by the modal transformation matrices since these will be important when designing controllers for this system. We begin with an examination of the observability properties of the system.

3.4.1 Observability and pole-zero cancellations

Intuitively, we might expect difficulties controlling the contact force when the force transducer is located at or near a node point corresponding to a vibration mode of the unconstrained system.[4] This is because the system has the unusual property of having pole-zero cancellations at these discrete constraint positions. We show this formally in the following theorem.

Theorem 3.4.1 *Given the constraint force $F_1(t)$ as the only measured output, then the system is unobservable if, and only if, the force transducer is located at a node point of the unconstrained system.*

[4] By the unconstrained system we imply the given system when $F_1 = T = 0$ (and by assumption $F_{2x} = F_{2y} = M = 0$).

Proof: First consider the free response of the unconstrained system governed by

$$\frac{\ddot{z}_i(t)}{\lambda_i^2} + z_i(t) + \gamma_i \ddot{\theta}(t) = 0 \qquad \forall\ i = 1, 2, ...N \tag{3.19}$$

$$\ddot{\theta}(t) = \frac{m}{I_h} \sum_{j=1}^{N} \gamma_j z_j(t). \tag{3.20}$$

For the free vibration system there exist N natural frequencies denoted $\{w_n\}$, such that for each w_n there exists a real vector $z^n \in \mathbb{R}^{N\times 1}$ with components $\{z_i^n\}$ satisfying

$$-w_n^2 \frac{z_i^n}{\lambda_i^2} + z_i^n + \frac{m}{I_h}\gamma_i \sum_{j=1}^{N} \gamma_j z_j^n = 0 \qquad \forall\ i = 1, 2, ...N. \tag{3.21}$$

Now consider a node point, if one exists, for this mode of vibration (clearly the rigid body mode only has a node point at $x = 0$). These node points are just those points x_n which satisfy

$$\begin{aligned}
(x_n + r)\theta(t) + \sum_{j=1}^{N} \frac{z_j(t)}{\lambda_j^2}\phi_j(x_n) &= 0 \\
\Rightarrow (x_n + r)\ddot{\theta}(t) + \sum_{j=1}^{N} \frac{\ddot{z}_j(t)}{\lambda_j^2}\phi_j(x_n) &= 0 \\
\Rightarrow (x_n + r)\ddot{\theta}(t) - \sum_{j=1}^{N} \phi_j(x_n)(z_j(t) + \gamma_j\ddot{\theta}(t)) &= 0 \qquad \text{(using equation (3.19))} \\
\Rightarrow \sum_{j=1}^{N} \phi_j(x_n) z_j(t) &= 0 \qquad \text{(taking } \lim_{N\to\infty} \text{ and using equation (3.16)).}
\end{aligned}$$

In particular, when the system is vibrating at the natural frequency w_n this implies that

$$\sum_{j=1}^{N} \phi_j(x_n) z_j^n e^{iw_n t} = 0, \tag{3.22}$$

where to avoid confusion $i = \sqrt{-1}$. Next consider a free vibration mode for the constrained system. Its natural frequency Ω_k will satisfy

$$-\frac{\Omega_k^2}{\lambda_i^2} z_i^k + z_i^k + \frac{m}{I_h}\gamma_i \sum_{j=1}^{N} \gamma_j z_j^k - \frac{\phi_i(\rho)}{\sum_{j=1}^{N} \phi_j^2(\rho)} \sum_{j=1}^{N} \phi_j(\rho) z_j^k = 0 \quad \forall\ i = 1, 2, ...N$$

for some real vector $z^k \in \mathbb{R}^{N\times 1}$ with components $\{z_i^k\}$. This equation is automatically satisfied by $\Omega_k = w_n$, $\rho = x_n$ and $\{z_i^k\} = \{z_i^n\}$ by virtue of equation (3.21) and equation (3.22). So when

$\rho = x_n$, w_n is a natural frequency of both the free and constrained systems. Now we just show that $F_1 = 0$ and the result follows. But this follows from

$$F_1(t) = \frac{m \sum_{j=1}^{N} z_j^n \phi_j(\rho) e^{i w_n t}}{\sum_{j=1}^{N} \phi_j^2(\rho)}$$

when the system is vibrating at the natural frequency w_n. By virtue of equation (3.22) this implies that $F_1(t) = 0$.

Conversely, suppose that the plant is unobservable but the force transducer is not located at a node point of the unconstrained system. This implies that there exists an Ω_n of some vibration mode of the constrained system and a real vector $z^n \in \mathbb{R}^{N\times 1}$ with components $\{z_i^n\}$ such that

$$\begin{aligned} \sum_{j=1}^{N} z_j^n \phi_j(\rho) &= 0 \qquad \text{and} \\ -\frac{\Omega_n^2}{\lambda_i} z_i^n + z_i^n + \frac{m}{I_h}\gamma_i \sum_{j=1}^{N} \gamma_j z_j^n - \frac{\phi_i(\rho)}{\sum_{j=1}^{N} \phi_j^2(\rho)} \sum_{j=1}^{N} \phi_j(\rho) z_j^n &= 0 \quad \forall \ i = 1, 2, 3, \ldots N \end{aligned}$$

But this gives

$$-\frac{\Omega_n^2}{\lambda_i} z_i^n + z_i^n + \frac{m}{I_h}\gamma_i \sum_{j=1}^{N} \gamma_j z_j^n = 0.$$

So if the plant is unobservable then ρ is a node point of the unconstrained system and we have a contradiction. ■

This result has a number of implications which could be of importance. Since the system is unobservable when the contact position coincides with a node point of the unconstrained system we cannot control the corresponding vibration mode of the constrained system (since the constrained and unconstrained modes coincide). This is not necessarily a disadvantage since even if the system is excited at the frequency of the unobservable mode the subsequent vibration will not affect the contact force. Near a node point of the unconstrained system the constrained system is close to having an imaginary axis pole-zero cancellation. Were it not for damping the system would be undetectable (in the LTI sense) at these points. In the next section we will show that these points are actually stationary points of the corresponding natural frequencies so in their vicinity the natural frequencies will vary slowly but the modal amplitudes (residues) will vary rapidly. Since the exact position of the node points predicted by the model will never match those of the physical system precisely we also expect the modelling errors to be relatively large in their vicinity.

3.4.2 Modal truncation

Having obtained a mathematical model of the constrained system which consists of a finite number of second order differential equations it is easily written in standard form

$$M\ddot{z}(t) + K(\rho)z(t) = \Phi u(t), \tag{3.23}$$

where $z^T(t) = [z_1(t)\, z_2(t)\, z_3(t)...z_n(t)]$ and $u^T(t) = [T(t)\ \ F(t)]$. Since the mass and stiffness matrices are symmetric it is well known ([49],[64]) that for each $\rho \in (0, l)$ there exists an orthonormal matrix function $\Psi(\rho)$ which simultaneously diagonalises M and $K(\rho)$. Even though the mass and stiffness matrices are real and infinitely differentiable matrix functions (in fact they are analytic) it is not immediately obvious what continuity properties the state transformation matrix $\Psi(\rho)$ will process. In order to answer this question we begin by showing that the natural frequencies of the constrained system can never cross each other. To show this we need the following statement of the interlacing theorem.

Theorem 3.4.2 *[49]*
Let $A \in \mathbb{R}^{N\times N}$ be a given symmetric matrix, let $y \in \mathbb{R}^{N\times 1}$ be a given vector, and let $a \in \mathbb{R}$ be a given real number. Let $\hat{A} \in \mathbb{R}^{(N+1)\times(N+1)}$ be the real symmetric matrix obtained by bordering A as follows:

$$\hat{A} \triangleq \left[\begin{array}{c|c} A & y \\ \hline y^T & a \end{array}\right].$$

Let the eigenvalues of A and $\hat{A}$ be denoted by $\{\kappa_i\}$ and $\{\hat{\kappa}_i\}$, respectively, and assume that they have been arranged in increasing order $\kappa_1 \le \kappa_2 \le \ldots \kappa_n$ and $\hat{\kappa}_1 \le \hat{\kappa}_2 \le \ldots \hat{\kappa}_{n+1}$. Then

$$\hat{\kappa}_1 \le \kappa_1 \le \hat{\kappa}_2 \le \kappa_2 \ldots \kappa_{n-1} \le \hat{\kappa}_n \le \kappa_n \le \hat{\kappa}_{n+1}.$$

It is a straightforward matter to verify that a direct application of Lagranges equations yields the following representation of the unconstrained system's dynamics

$$\begin{bmatrix} 1 & 0 & 0 & \ldots & \gamma_1 \\ 0 & 1 & 0 & \ldots & \gamma_2 \\ \vdots & & \ddots & & \\ \gamma_1 & \gamma_2 & \ldots & \gamma_n & I_e \end{bmatrix} \begin{bmatrix} \ddot{a}_1 \\ \vdots \\ \ddot{a}_n \\ \ddot{\theta} \end{bmatrix} + \begin{bmatrix} \lambda_1^2 & 0 & 0 & \ldots & 0 \\ 0 & \lambda_2^2 & 0 & \ldots & 0 \\ \vdots & & \ddots & & \\ 0 & 0 & 0 & \ldots & 0 \end{bmatrix} \begin{bmatrix} a_1 \\ \vdots \\ a_n \\ \theta \end{bmatrix} = \frac{1}{m} \begin{bmatrix} \phi_1(\rho) \\ \phi_2(\rho) \\ \vdots \\ \phi_n(\rho) \\ \rho + r \end{bmatrix} F_1 \tag{3.24}$$

where $I_e = \frac{1}{m}(I_h + m(l+r)^3/3)$. Define the similarity transformation

$$\begin{bmatrix} q_1 \\ q_2 \\ \vdots \\ q_n \\ q_{n+1} \end{bmatrix} = \Psi^T(\rho) \begin{bmatrix} a_1 \\ a_2 \\ \vdots \\ a_n \\ \theta \end{bmatrix},$$

where the transformation matrix is given by

$$\begin{aligned}\Psi^T(\rho) &\triangleq \begin{bmatrix} & & \Psi^\perp & & \\ s\phi_1(\rho) & s\phi_2(\rho) & \dots & s\phi_n(\rho) & s(\rho+r) \end{bmatrix} \\ s^{-2} &= \phi_1^2(\rho)+\phi_2^2(\rho)+\dots\phi_n^2(\rho)+(\rho+r)^2,\end{aligned}$$

and $\Psi^\perp(\rho)$ is the orthonormal completion of the last row (which is recognised as being the constraint equation). The transformed system now satisfies

$$\Psi^T(\rho)\hat{M}\Psi(\rho)\ddot{q}+\Psi^T(\rho)\hat{K}\Psi(\rho)q=\begin{bmatrix}0\\0\\\vdots\\\frac{1}{ms}\end{bmatrix}F_1,$$

where $\hat{M}$ and $\hat{K}$ are the mass and stiffness matrices of the unconstrained system in equation (3.24). When the constraint is satisfied $q_{n+1}(t)$ is identically zero. So the unconstrained natural frequencies $\{\hat{w}_n\}$ are the eigenvalues of $\Psi^T(\rho)(\hat{M}^{-1}\hat{K})\Psi(\rho)$, whereas the constrained natural frequencies $\{w_n(\rho)\}$ are the eigenvalues of the sub-matrix obtained by eliminating the last row and column. Theorem 3.4.2 is now applicable and shows that

$$\hat{w}_{n+1}\geq w_n(\rho)\geq\hat{w}_n\geq w_{n-1}\dots\hat{w}_3\geq w_2(\rho)\geq\hat{w}_2\geq w_1(\rho)\geq\hat{w}_1. \tag{3.25}$$

In fact on purely physical grounds it can be seen that the equalities in equation (3.25) can never be achieved from both sides simultaneously. To see why this should be so consider the case where at some $\rho\in(0,l)$ two constrained natural frequencies coalesce. Theorem 3.4.2 shows that if this occurs then the constrained natural frequencies must both be equal to an unconstrained natural frequency. Theorem 3.4.1 shows that this can only occur at a point where the unconstrained system has a degeneracy. Since this is not a feature of the one dimensional system under study this can never occur.

Proposition 3.4.3 *[53]*
Since M is symmetric positive definite and $K(\rho)$ is symmetric and analytic for all $\rho\in(0,l)$, there exists a real, analytic orthonormal matrix function $\Psi(\rho)$ such that

$$\Psi(\rho)^T M\Psi(\rho)=I \qquad \textit{and} \qquad \Psi(\rho)^T K(\rho)\Psi(\rho)=diag(w_i^2(\rho)),$$

where $w_1(\rho)<w_2(\rho)<\dots w_n(\rho)$.

Remark 3.4.4 *Analyticity of the matrix $\Psi(\rho)$ depends on the fact that the continuous curves representing the constrained natural frequencies $w_i(\rho)$ do not cross one another.*

An important consequence is that we can make a co-ordinate transformation [64] $z(t)=\Psi(\rho)q(t)$ and write equation (3.23) in terms of the modal co-ordinates $q(t)$

$$\ddot{q}(t)+\begin{bmatrix} w_1^2(\rho) & 0 & \dots & 0 \\ 0 & \ddots & & \\ 0 & & & w_n^2(\rho)\end{bmatrix}q(t)=\Psi^T(\rho)\Phi u(t).$$

With the equations in this form it is a simple matter to add a modal damping matrix

$$\ddot{q}(t) + \begin{bmatrix} 2\zeta_1(\rho)w_1(\rho) & \dots & 0 \\ 0 & \ddots & \\ 0 & & 2\zeta_n(\rho)w_n(\rho) \end{bmatrix} \dot{q}(t) + \begin{bmatrix} w_1^2(\rho) & \dots & 0 \\ 0 & \ddots & \\ 0 & & w_n^2(\rho) \end{bmatrix} q(t) = \Psi^T(\rho)\Phi u(t)$$

where the modal damping factors $\zeta_i(\rho)$ can be obtained from experimental measurements [29]. Having the equations in this form we can truncate the model by retaining only those modes in the frequency range of interest and in so doing obtain a reduced-order model which is more appropriate for controller synthesis. Since the modal overlap of this system is small, it is relatively straight-forward to select an appropriate number of modes to retain in the reduced-order model. The continuity properties of the modal transformation matrix $\Psi(\rho)$ are sufficient to ensure that the reduced-order model will have continuous mass and stiffness matrices. This also ensures that the reduced-order model is continuous in the graph topology, the importance of which will be discussed in the next chapter[5].

In the subsequent chapters we will make frequent use of the standard state-space representation of the system dynamics

$$\begin{aligned} \dot{x}(t) &= A(\rho)x(t) + B(\rho)u(t) \\ y(t) &= C(\rho)x(t) + D(\rho)u(t), \end{aligned} \tag{3.26}$$

where all matrices are continuous and the matrix $A(\rho)$ is constructed from the mass, stiffness and damping matrices while $B(\rho)$ and $C(\rho)$ depend on the chosen combination of sensors and actuators. The direct throughput term $D(\rho)$ represents the DC behaviour of the high frequency modes. The vector $y(t)$ is the vector of measured outputs and the vector $u(t)$ is the vector of controlled inputs.

We have already gained some important physical insights into the behaviour of our example system. We conclude by examining the characteristics of the transfer functions from the two actuators to the contact force. In order to do so we need values for the different physical parameters that appear in the model. The values we use are taken from the experimental system outlined, in detail, in chapter 6. Some of these parameters are trivial to obtain, for example, the relevant properties of the elastic beam (we will neglect the inertial properties of the tip magnet here). Others, such as the hub inertia and the modal damping factors (for the LTI model) are obtained from experimental measurements. The physical dimensions of the experimental equipment restrict variations in the position of the force transducer to thirty percent of the total length of the beam ($0.45 \leq \rho/l \leq 0.75$), however, the dynamics vary dramatically over this interval and have a number of properties which make the synthesis of controllers suitably challenging.

[5] These continuity properties do not necessarily hold for a model approximant obtained by pointwise application of the balanced truncation procedure, or the optimal Hankel norm truncation procedure.

Insight into the nature of the parameter variations can be obtained by plotting the frequency response as a function of the contact position. In Figure 3.5 we show a contour plot of the calculated frequency response with the motor torque as input and the constraint force as output. This is the response function of primary interest. The contour plot has been shaded so that the peaks in the response function appear as white lines and the troughs appear as black lines. There are several distinct unobservable points (these are easily discernible from the contour plots where white lines and black lines cross each other). Theorem 3.4.1 shows that each of these unobservable points is a node point of some vibration mode of the unconstrained system. Furthermore, at each one of these points the constrained mode shape of interest coincides with an unconstrained mode shape.

Physical insight into the behaviour of the system around these points is aided by considering the displacement of the beam when it is excited by a torque applied at the base with the constraint force absent. If the response generated by the applied torque is obtained in terms of a modal expansion using the unconstrained mode shapes then, considering one mode at a time, the displacement changes from being in phase to being out of phase with the torque, or visa versa, at positions just to the left and just to the right of a node of the given mode. Since the constraint force always opposes the displacement of the beam we can see that it too changes from being in or out of phase with the torque as the node point is crossed. Since these node points are also node points of the constrained system we can see that one of the residues in the modal expansion from the applied torque to the constraint force will change sign as the constraint moves past this position on the beam (being precisely zero at the node). Consequently, the position of an antiresonant frequency (or zero) will change from lying between one pair of resonant peaks to lying between an adjacent pair of resonant peaks as the constraint crosses the node. This is precisely what is observed in Figure 3.5[6]. Since the torque and force actuators are located at opposite ends of the beam we expect that for any ρ, one will behave more like a transfer response and the other more like a driving point response. This is confirmed by examining the antiresonant frequencies in Figure 3.6 and comparing them with those in Figure 3.5.

[6] We also note that the node points are stationary points for the constrained natural frequencies, as predicted by the interlacing theorem.

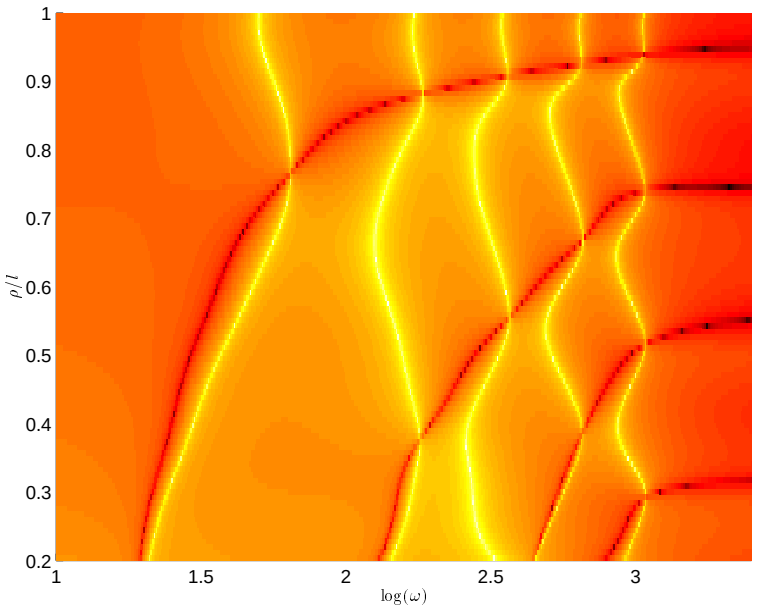

Figure 3.5 *Graded contour plot of the frequency response from the motor torque to the contact force.*

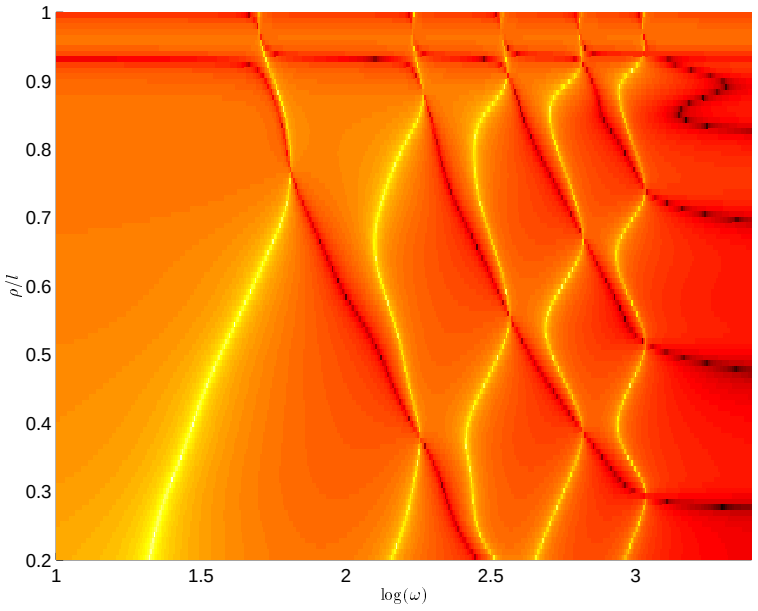

Figure 3.6 *Graded contour plot of the frequency response from the tip actuator to the contact force.*

3.5 Summary

In this chapter we have considered various aspects involved in the modelling of LPV structures by developing an analytical model for our example system. For these systems obtaining pointwise LTI models is relatively straightforward, and more complicated systems could easily be modelled using various approximate methods (such as the finite element method [6]) to obtain finite-dimensional models. For the frozen-parameter models it is also relatively straightforward to introduce modal transformations to allow physical damping measurements to be incorporate into the model. We also pointed out that this is not the case when we explicitly account for the time-varying nature of the parameter(s) since modal transformations become far less important. Since the detailed physical mechanisms involved in structural damping are poorly understood, the best we can do in the LPV case is to make use of fairly crude physical models to account for the observed dissipation. Model reduction of LPV structures must also be approached with some care and in chapter 7 we will consider these issues in greater detail. For the example system we were able to use purely physical arguments to show that we can obtain a continuous modal transformation matrix which allows us to perform pointwise modal truncation to obtain a continuous model approximant. The importance of obtaining a continuous approximant will become apparent in chapter 4, and again in chapter 8, where we will consider the problem of synthesising gain-scheduled controllers for this class of systems.

4

A Topological Approach to Controller Synthesis

4.1 Introduction

In this chapter we consider the problem of controlling the contact force developed between a highly flexible elastic beam and a movable constraint. We will examine various issues that arise when attempting to synthesise a controller for the strongly parameter-dependent elastic structure detailed in chapter 3. There are essentially two approaches that can be taken when controlling parameter-dependent systems of this type. One approach is to neglect the inherent time-varying nature of the parameter(s) and model the plant as being LTI, treating the time variations as perturbations. Alternatively, we can explicitly take into account the time-varying nature of the parameter(s) which complicates both the analysis and synthesis problems considerably. This and the next two chapters will be concerned with the LTI approach, in chapter 7 and chapter 8 we will consider the issues that arise when we approach the problem in its full generality. In this chapter our objective is to design a controller that robustly stabilises a family of LTI plants, indexed by some real parameter, and which also achieves a desired level of performance for all parameter values. We believe that by examining this problem from an optimal control perspective such questions as controller existence, achievable performance and the tradeoff between performance and robustness can be methodically addressed. We will also examine other issues, for example, can performance be enhanced by the use of additional actuators? If additional actuators are used, is there a way of placing them so as to make the system easier to control? Indeed, in what sense is a system "easier to control"? It is felt that the H_∞ formulation is ideally suited to addressing many of these issues, primarily because it allows us to incorporate intuition gained from classical control techniques and deals in a systematic manner with uncertainty and multivariable plants.

For the rest of this chapter we will model the plant as being finite-dimensional and LTI. Of course the plant is really infinite-dimensional and LTV, so we will need to justify our approach. By modelling the plant as time invariant we can use a number of powerful results that hold for this class of systems. For each fixed value of the variable parameter ρ we can obtain a controller that is robust to unmodelled high frequency dynamics, uncertain physical parameters such as the hub inertia and the modal damping factors, and various other modelling errors. In fact we will show that this is not only possible for a single value of ρ but is possible for all values of ρ lying within some specified interval with a single controller. If necessary we can invoke the small gain

theorem [98] to deduce robustness to a class of time-varying uncertainty, although it is difficult to characterise this class precisely. In chapter 8 we consider the latter problem more carefully and develop a theory for synthesising scheduled controllers that overcomes this difficulty. A final motivating factor for the approach taken here concerns practical implementation. LTI controllers synthesised from LTI models consist of a finite number of differential equations that must be solved in real time. Provided the state dimension is not unduly high, these controllers can be implemented relatively easily with modern computational facilities, making them ideal for use in applications.

The analysis of LTI systems, the dynamics of which depend on one or more exogenous parameters has been greatly facilitated by the development of the structured singular value, or μ-analysis ([21],[66]). This involves writing a parameter-dependent system as a linear fractional transformation involving a fixed LTI plant with a structured perturbation operator. The parameter dependence in our system gives rise to a repeated real perturbation block when considered in this framework with the contact position ρ acting as the real parameter. Incorporating other closed-loop performance/robustness objectives into this analysis framework results in an analysis problem involving a linear fractional transformation of a fixed LTI plant with a block-diagonal perturbation operator made up of one repeated real block and at least one unstructured norm-bounded block.

For plants that are subjected to structured uncertainty it is possible to make use of μ-synthesis [22] to design controllers which meet certain performance objectives for all permissible perturbations. Unfortunately, this is an iterative procedure which is not guaranteed to find a controller when one exists, and is not ideally suited to problems involving repeated real perturbation blocks. This stems from a weakness in the original μ-analysis framework, namely, the conservativeness that results when dealing with repeated real blocks of the type which arise in the analysis of parameter-dependent structures. Typically, these systems have state matrices that exhibit complex parameter dependence and this leads to high order perturbation blocks. Recent extensions that reduce this conservatism on so called mixed-μ problems can be found in Young [95] and the references therein. Young [96] has also extended the synthesis machinery to account for the phase information inherent in repeated real blocks. However, this involves state space approximations to certain scaling matrices[1] which are only known at discrete frequencies during each step of the iteration. This makes its application to problems involving large repeated real blocks (as arise with systems that have complicated parameter dependence) essentially intractable. In this thesis we take a different approach to the problem of controlling parameter-dependent systems, one which is based on certain topological notions of robustness and the use of appropriate metrics to measure how parameter variations change the important feedback properties of the system.

We begin with an examination of the fundamental properties of linear feedback systems. Our aim is to expose those properties that are important in the feedback setting. It is only once

[1] Repeated real uncertainty requires rational function approximation of both the "D" and "G" scales which are both full matrices.

we have established what these are that it is possible to see how specific parameter variations influence them. In section 4.2 we introduce the graph topology, motivating this as providing the correct setting for the analysis of feedback systems. We then examine various metrics which induce the graph topology and review the H_∞ loop-shaping design procedure, indicating how this fits into the topological framework. Having established the relevant background theory we consider a novel application of these techniques to flexible structures. By way of example, we show how parameter dependence can lead to difficulties when synthesising controllers for this class of systems. The remainder of the chapter then concentrates on procedures for overcoming these difficulties when synthesising controllers in the chosen topology.

4.2 The graph topology

One approach to the problem considered in this thesis is to consider it as being a special case of the general setup in Figure 4.1. This consists of the interconnection of a linear finite-dimensional plant P with a linear finite-dimensional controller C and we denote this interconnection structure by (P, C).

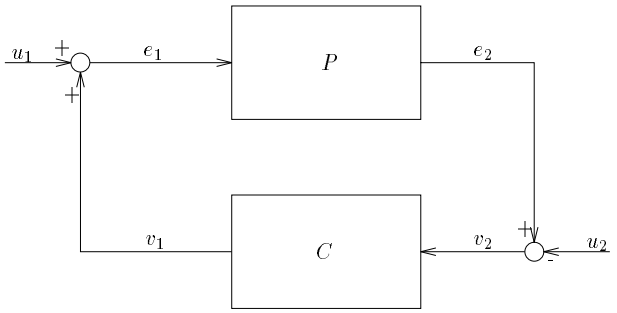

Figure 4.1 *The standard feedback setup.*

A fundamental requirement for this feedback interconnection is internal stability [32] . That is, given bounded energy inputs u_1 and u_2, we require the mapping

$$H(P,C) : H_2 \otimes H_2 \mapsto H_2 \otimes H_2, \qquad \begin{bmatrix} u_2 \\ u_1 \end{bmatrix} \mapsto \begin{bmatrix} e_2 \\ e_1 \end{bmatrix},$$

to be unique and bounded on all of $H_2 \otimes H_2$, where

$$H(P,C) \stackrel{\triangle}{=} \begin{bmatrix} P \\ I \end{bmatrix} (I - CP)^{-1} [-C \quad I].$$

Since stability is not the only requirement we also require the closed-loop mapping $H(P,C)$ to satisfy certain performance objectives. For example, u_1 and u_2 might model disturbances injected at the plants input and output respectively. So we can bound the signals e_1, e_2, v_1 and v_2 by bounding $\|H(P,C)\|$ with an appropriate norm. The correct choice of operator norm depends on the underlying class of signals used to model the disturbances. If the disturbances

are modelled as being stochastic then it is appropriate to pose the problem in an LQG setting thereby minimising the variance of the output signals ([2],[45],[103]). Alternatively, if the signal power spectra are not fixed but are modelled as having bounded energy then it is appropriate to minimise $\|H(P,C)\|_\infty$ thereby minimising the energy in the output signals for the worst case input ([31],[99],[100]). The stability and performance properties just stated are generically referred to as nominal performance and nominal stability and while they are necessary, in general, they are not sufficient. This is because we have not considered the behaviour of the closed loop when the operators are subjected to the inevitable perturbations which arise from abstracting a physical plant to a mathematical model.

Our model, as is our controller through discretization or approximation, is subject to uncertainty. Thus we would also like the interconnection to have the property of being robust. Specifically, when both the plant and the controller are LTI, let $\Lambda : \lambda \mapsto P_\lambda$ be a mapping from a countable topological space (eg: $\mathbb{R}^n$) onto the space of finite-dimensional LTI systems and let $\lambda_0 \mapsto P_{\lambda_0}$ represent the nominal plant as captured by our model. Suppose that we have a controller C such that (P_{λ_0}, C) is stable and $H(P_{\lambda_0}, C)$ meets the nominal performance objectives. For the interconnection to be robust we require (P_λ, C) to be stable and the mapping $\lambda \to H(P_\lambda, C)$ to be continuous (in the chosen performance metric) for some neighbourhood $\mathbf{N}$ of λ_0. Clearly this requires a suitable topology to be defined on the set of LTI plants which, by definition, captures all perturbations to the nominal plant that can be stabilised by feedback and for which the mapping $\lambda \to H(P_\lambda, C)$ is continuous. For stable systems such a topology is the norm topology, that is, the natural topology induced by $\|.\|_\infty$ consisting of open balls given by

$$\mathcal{B}(P_0, \epsilon) \stackrel{\triangle}{=} \{P : \|P - P_0\|_\infty < \epsilon\} .$$

In other words, if P_λ and P_{λ_0} are both stable and (P_{λ_0}, C) is stable, then given any $\delta > 0$ there will exist a $\epsilon > 0$ such that (P_λ, C) is stable and $\|H(P_\lambda, C) - H(P_{\lambda_0}, C)\|_\infty < \delta$ provided $\|P_\lambda - P_{\lambda_0}\|_\infty < \epsilon$. Indeed, this property of the H_∞ norm does not carry over to the LQG setting and has been the primary motivation behind the development of H_∞ control theory starting with the seminal paper by Zames [99]. Doyle [19] has pointed out that LQG controllers do not give any stability guarantees and in so doing has highlighted one of the major shortcomings of LQG control theory.

The inability to include unstable plants in the norm topology is a major drawback and has led to the development of the graph topology ([82],[83],[104]). The fundamental importance of this topology is captured in the following proposition.

Proposition 4.2.1 *[84]*
Suppose that $\lambda \mapsto P_\lambda$, $\lambda \mapsto C_\lambda$ are functions mapping a first countable topological space Λ into the set of finite-dimensional LTI systems, and suppose that the pair $(P_{\lambda_0}, C_{\lambda_0})$ is stable.

i. Suppose the functions $\lambda \mapsto P_\lambda$, $\lambda \mapsto C_\lambda$ are continuous at λ_0 in the graph topology. Then there exists a neighbourhood $\mathbf{N}$ of λ_0 such that (P_λ, C_λ) is stable for all $\lambda \in \mathbf{N}$, and in addition $H(P_\lambda, C_\lambda)$ is continuous at λ_0 in the norm topology.

ii. Conversely, suppose there is a neighbourhood $\mathbf{N}$ *of* λ_0 *such that* (P_λ, C_λ) *is stable for all* $\lambda \in \mathbf{N}$*, and such that* $H(P_\lambda, C_\lambda)$ *is continuous at* λ_0 *in the norm topology. Then the functions* $\lambda \to P_\lambda$*,* $\lambda \mapsto C_\lambda$ *are continuous at* λ_0 *in the graph topology.*

A better understanding of the graph topology can be obtained by defining a suitable base for it as follows. Given an LTI system P, let $[N, M]$ be a rcf of P over RH_∞. It is well known [84] that there exists a positive constant $\mu(N, M)$ such that given $[N_1, M_1]$ of compatible dimension, $[N_1, M_1]$ are also right coprime whenever $\|((N_1 - N)^T, (M_1 - M)^T)^T\|_\infty < \mu(N, M)$. Thus, given an LTI plant P, it is possible to define a basic neighbourhood of $P = NM^{-1}$ consisting of the set

$$\mathbf{N}(N, M, \epsilon) \stackrel{\triangle}{=} \left\{ P_1 = N_1 M_1^{-1} : \left\| \begin{pmatrix} N - N_1 \\ M - M_1 \end{pmatrix} \right\|_\infty < \epsilon < \mu(N, M) \right\}.$$

By varying ϵ over all positive numbers less than $\mu(N, M)$, similarly by varying $[N, M]$ over all possible right coprime factorisations of P and by varying P over all finite-dimensional LTI systems we obtain a collection of neighbourhoods that form a base for the graph topology [84].

The graph topology represents the correct setting for the study of robust control in the presence of plant and/or controller uncertainty since it captures all perturbations that can be stabilised by feedback while causing gradual degradation in performance. To be of any use in practical problems we require a metric on the set of finite-dimensional LTI systems such that if (P, C) is perturbed to (P_1, C_1) then the perturbation is permissible (in the above sense) if, and only if, P_1 is close to P and C_1 is close to C in the metric. In other words, we require a metric that induces the graph topology. A number of metrics having this property have been introduced, these include the graph metric [83], the gap metric ([26],[37],[97]), the pointwise gap metric [72] and more recently, the ν-gap metric [88]. Only two, the gap metric and the ν-gap metric are amenable to computation ([36],[88]) and consequently have practical application. In the next two sections we give a more thorough discussion of the gap and ν-gap metrics stating various important robust stability results as we commence.

4.2.1 The gap metric

The gap metric is defined in terms of the distance between closed manifolds of a Hilbert space $\mathcal{H}$ [53] and was first introduced into control theory in ([26],[97]). It has application in a number of areas of applied mathematics. Of particular interest to us, it provides a natural measure of the distance between two systems when they are to be used in a feedback context. As will be seen, two systems are considered to be close in the gap metric if given any stable input-output pair of the first system, there is a corresponding stable input-output pair of the second system that is close to it. This makes sense intuitively where, subject to a perturbation in the plant, it is unlikely that a fixed controller will maintain a desired output if the inputs required to maintain it differ dramatically for the perturbed and unperturbed plants.

Finite dimensional LTI systems can be considered as unbounded multiplication operators $M_P : H_2 \mapsto H_2,\ u \mapsto Pu$, that is, their domain $\mathcal{D}(M_P)$ is not the whole of H_2 [32]. The graph of such a system is defined as follows.

Definition 4.2.2 *The graph of a finite-dimensional LTI system is defined as the totality of all stable input-output pairs*

$$\mathcal{G}(P) \stackrel{\triangle}{=} \left\{ \begin{pmatrix} Pu \\ u \end{pmatrix} : u \in \mathcal{D}(P) \right\}$$

considered as a subspace of $H_2 \otimes H_2$.

For stable systems the domain of the multiplication operator is the whole of H_2 whereas for unstable systems it is a proper subset of H_2. In either case, the graph of a given system can be generated through the use of coprime factors.

Proposition 4.2.3 *Let* $P = NM^{-1}$ *be a right coprime factorisation of the LTI plant with transfer function* P*, then its graph* $\mathcal{G}(P)$ *is given by*

$$\mathcal{G}(P) = \begin{bmatrix} N \\ M \end{bmatrix} q,\ \ q \in H_2.$$

Proof: Given $q \in H_2$, $y = Nq$ and $u = Mq$ are both in H_2. Since M is invertible $q = M^{-1}u$ which implies that $y = NM^{-1}u$. Conversely, given any element in the graph we can find a $q \in H_2$ which acts as a generator because $\begin{bmatrix} N \\ M \end{bmatrix}$ is left invertible. That is, there exists $[X,\ Y] \in H_\infty$ such that $[X,\ Y] \begin{bmatrix} y \\ u \end{bmatrix} = [X,\ Y] \begin{bmatrix} N \\ M \end{bmatrix} q = q$. ■

An important property of the graph of any finite-dimensional LTI system is that it is a closed subspace of $H_2 \otimes H_2$ which means that for any $x \in H_2 \otimes H_2$ we can define a unique distance from x to $\mathcal{G}(P)$ [57]. This motivates the definition of the directed gap between two systems P_1 and P_2 as follows.

$$\vec{\delta}_g(P_1, P_2) = \sup_{\begin{bmatrix} y_1 \\ u_1 \end{bmatrix} \in \mathcal{G}(P_1)} \inf_{\begin{bmatrix} y_2 \\ u_2 \end{bmatrix} \in \mathcal{G}(P_2)} \frac{\left\| \begin{bmatrix} y_1 \\ u_1 \end{bmatrix} - \begin{bmatrix} y_2 \\ u_2 \end{bmatrix} \right\|_2}{\left\| \begin{bmatrix} y_1 \\ u_1 \end{bmatrix} \right\|_2}. \tag{4.1}$$

From equation (4.1) it is clear that the directed gap is bounded above by unity (put $\begin{bmatrix} y_2^T, & u_2^T \end{bmatrix}^T = 0$) but that it does not satisfy the properties of a metric (consider the case when $\mathcal{G}(P_1) \subset \mathcal{G}(P_2)$). The gap metric is defined as being the maximum of two directed gaps.

Definition 4.2.4 *The gap metric* $\delta_g(.,.) : \mathcal{P}^{p\times m} \otimes \mathcal{P}^{p\times m} \mapsto \mathbb{R}$ *is defined as being the maximum of the two directed gaps*

$$\delta_g \stackrel{\triangle}{=} \max\left\{ \stackrel{\rightarrow}{\delta}_g (P_1, P_2), \stackrel{\rightarrow}{\delta}_g (P_2, P_1) \right\}.$$

Let $\Pi_{\mathcal{G}(P_1)} : H_2 \otimes H_2 \mapsto \mathcal{G}(P_1)$ and $\Pi_{\mathcal{G}(P_2)} : H_2 \otimes H_2 \mapsto \mathcal{G}(P_2)$ denote the orthogonal projection operators onto the respective graph space of P_1 and P_2. We can reformulate the formula for the directed gap as follows.

$$\begin{aligned}
\stackrel{\rightarrow}{\delta}_g (P_1, P_2) &= \sup_{\left[\begin{smallmatrix} y_1 \\ u_1 \end{smallmatrix}\right] \in \mathcal{G}(P_1)} \frac{\left\| \left[\begin{smallmatrix} y_1 \\ u_1 \end{smallmatrix}\right] - \Pi_{\mathcal{G}(P_2)} \left[\begin{smallmatrix} y_1 \\ u_1 \end{smallmatrix}\right] \right\|_2}{\left\| \left[\begin{smallmatrix} y_1 \\ u_1 \end{smallmatrix}\right] \right\|_2} \\
&= \frac{\|(I - \Pi_{\mathcal{G}(P_2)})\Pi_{\mathcal{G}(P_1)} q\|_2}{\|q\|_2}, \quad q \in \mathcal{G}(P_1) \\
&= \|\Pi^{\perp}_{\mathcal{G}(P_2)} \Pi_{\mathcal{G}(P_1)}\|.
\end{aligned}$$

This gives the more familiar formula for the gap metric [53]

$$\delta_g(P_1, P_2) = \|\Pi_{\mathcal{G}(P_1)} - \Pi_{\mathcal{G}(P_2)}\| = \max\{\|\Pi^{\perp}_{\mathcal{G}(P_2)} \Pi_{\mathcal{G}(P_1)}\|, \|\Pi^{\perp}_{\mathcal{G}(P_1)} \Pi_{\mathcal{G}(P_2)}\|\}.$$

Georgiou [36] obtained an explicit formula for the gap between two systems and showed that it can be computed in terms of two standard two-block H_∞ optimisation problems.

Proposition 4.2.5 *[36]*

$$\begin{aligned}
\delta_g(P_1, P_2) = \|\Pi_{\mathcal{G}(P_1)} - \Pi_{\mathcal{G}(P_2)}\| &= \max\{\|\Pi^{\perp}_{\mathcal{G}(P_2)} \Pi_{\mathcal{G}(P_1)}\|, \|\Pi^{\perp}_{\mathcal{G}(P_1)} \Pi_{\mathcal{G}(P_2)}\|\} \\
&= \max\{\inf_{Q\in H_\infty} \|G_1 - G_2 Q\|_\infty, \inf_{Q\in H_\infty} \|G_2 - G_1 Q\|_\infty\}.
\end{aligned}$$

G_1 and G_2 are the normalised right graph symbols of P_1 and P_2 respectively (these symbols were defined in chapter 2).

Georgiou and Smith [37] have demonstrated that when $\delta_g(P_1, P_2) < 1$ the two directed gaps $\stackrel{\rightarrow}{\delta}_g (P_1, P_2)$ and $\stackrel{\rightarrow}{\delta}_g (P_2, P_1)$ are equal. So to compute the gap between two systems only one of the directed gaps needs to be computed, it then being sufficient to verify that the other directed gap is less than unity. Georgiou [36] has also shown that the gap metric induces the graph topology by showing the equivalence between the gap metric and the graph metric, the latter being known to have this property [83].

4.2.2 The ν-gap metric

Since the gap metric induces the graph topology it becomes a useful tool for robustness optimisation when dealing with unstructured neighbourhoods about the nominal plant captured by

our mathematical model. More specifically, given any mapping $\Lambda : \lambda \to P_\lambda$ from a countable topological space onto the space of LTI systems with $\lambda_0 \mapsto P_{\lambda_0}$ representing our model, we would like to find a controller C that stabilises P_λ for the "largest" possible neighbourhood about λ_0. Since the gap metric captures all perturbations that can be stabilised by feedback and, by the definition of dynamic uncertainty, we don't actually know what the mapping Λ is, the best we can do is to find a controller C which stabilises the largest possible gap ball about the nominal plant.

The situation is very different in the case of parametric uncertainty. In the latter case we have precise knowledge about how various changes in operating conditions map into changes in the dynamics of the nominal plant. Clearly the graph topology remains the correct setting for robust stabilisation since there will always be dynamic uncertainty associated with the plant in addition to the parametric uncertainty. So we would like to incorporate our knowledge about the expected parametric variations in the plant dynamics into the controller, yet still maximise robustness to unstructured neighbourhoods. This is a difficult problem and one that is not well addressed by the gap metric which, having an operator-theoretic definition, makes it difficult to relate physical changes in the plant to changes in the gap. The ν-gap metric introduced by Vinnicombe ([87],[88]) is much better suited in this regard.

Given two plants P_1 and P_2, the ν-gap between these systems is defined to be the gap between their L_2 graph spaces provided a winding number constraint is satisfied. If we consider a finite-dimensional LTI system to be a Laurent operator $L_P : L_2 \mapsto L_2,\ u \to Pu$, then the domain of this operator $\mathcal{D}(L_P)$ is all of L_2 when the system has no poles on the imaginary axis (the operator being causal only when the system is stable).

Definition 4.2.6 *The L_2 graph of a finite-dimensional LTI system is defined to be the totality of all input-output pairs*

$$\mathcal{G}_{L_2}(P) \stackrel{\triangle}{=} \left\{ \begin{pmatrix} Pu \\ u \end{pmatrix} : u \in L_2 \right\}$$

considered as a subspace of $L_2 \otimes L_2$.

Proposition 4.2.7 *Let $P = NM^{-1}$ be a right coprime factorisation of the LTI plant with transfer function P, then the L_2 graph $\mathcal{G}_{L_2}(P)$ of P is given by*

$$\mathcal{G}_{L_2}(P) = \begin{bmatrix} N \\ M \end{bmatrix} q,\ \ q \in L_2.$$

Proof: The proof follows identical reasoning to the proof of proposition 4.2.3. ■

The winding number constraint ensures that the ν-gap metric, which we define next, induces the graph topology.

Definition 4.2.8 *[88]*
The ν-gap metric $\delta_v(.,.) : \mathcal{P}^{p\times m} \otimes \mathcal{P}^{p\times m} \to \mathbb{R}$ is given by

$$\delta_v(P_1,P_2) = \begin{cases} \|\tilde{G}_2 G_1\|_\infty & \text{if } \det(G_2^* G_1)(jw) \neq 0 \ \forall \omega \in (-\infty,\infty) \\ & \text{and } wno\det(G_2^* G_1) = 0 \\ 1 & \text{otherwise.} \end{cases}$$

Here G_1 denotes the normalised right graph symbol of P_1 and $\tilde{G}_2$ denotes normalised the left graph symbol of P_2.

While the winding number constraint appears cumbersome it turns out not to present significant difficulties in practice provided the plant behaves sufficiently smoothly. There are two fundamental advantages that the ν-gap metric has over the gap metric. Firstly, it is tighter [87], being the weakest metric that can be defined on the set of finite dimensional LTI systems for which feedback is a robust property in the sense of our earlier definitions. Secondly, the distance between two plants depends entirely on their frequency responses which makes the ν-gap metric much better suited as a tool for dealing with parametric uncertainty.

4.2.3 Performance measures and robust stability theorems

Returning to the feedback interconnection in Figure 4.1, the closed-loop transfer function matrix $H(P,C)$ represents a useful and practical measure of performance. MacFarlane and Glover [59] have shown that by bounding the size of $\|H(P,C)\|_\infty$ we bound the size of the sensitivity function, the complementary sensitivity function and the actuator effort when noise is injected at various points around the closed loop. In fact this observation has led to the development of the H_∞ loop-shaping design procedure ([41],[59]) and the equivalent weighted gap metric design procedure [27]. We will discuss the H_∞ loop-shaping design procedure at greater length in section 4.3. It turns out that the size of the closed-loop transfer function $H(P,C)$ provides more than just a useful performance measure, it is also closely related to robustness to perturbations as measured by the gap metric, the ν-gap metric and to perturbations of a normalised coprime factor representation of the nominal plant. Since this concept plays a central role in this thesis we give it further motivation.

Definition 4.2.9 *For the feedback pair (P,C) define the generalised stability margin $b_{P,C}$ [37] as*

$$b_{P,C} \triangleq \begin{cases} \left\| \begin{bmatrix} P \\ I \end{bmatrix} (I - CP)^{-1} [-C \ \ I] \right\|_\infty^{-1}, & \text{if } (P,C) \text{ is stable} \\ 0 & \text{otherwise.} \end{cases}$$

The first two theorems concern robust stability to gap metric perturbations.

Theorem 4.2.10 *[37]*
Given a plant P_1, a compensator C_1 and a number β, then:
(P_2,C_1) is stable for all plants P_2 satisfying $\delta_g(P_1,P_2) \leq \beta$ if, and only if, $b_{P_1,C_1} > \beta$.

This theorem show that maximisation of b_{P_1,C_1} is equivalent to maximising stability to unstructured neighbourhoods about P_1 as measured by the gap metric. Maximising b_{P_1,C_1} is also equivalent to minimising $\|H(P_1,C_1)\|_\infty$, so optimising robustness is equivalent to optimising performance for the nominal plant. In fact Qui and Davison [72] have shown that maximising b_{P_1,C_1} is equivalent to maximising performance when both the plant and the controller are subject to perturbations in the gap metric.

Theorem 4.2.11 *[72]*
Let (P_1,C_1) be stable. Then (P_2,C_2) is stable for all P_2 satisfying $\delta_g(P_2,P_1) < r_1$ and C_2 satisfying $\delta_g(C_2,C_1) < r_2$ if, and only if

$$\arcsin r_1 + \arcsin r_2 + \arccos b_{P_1,C_1} \leq \frac{\pi}{2}$$

in which case

$$\inf\{b_{P_2,C_2} : P_2 \in \mathcal{B}_g(P_1,r_1) \text{ and } C_2 \in \mathcal{B}_g(C_1,r_2)\} = \cos(\arcsin r_1 + \arcsin r_2 + \arccos b_{P_1,C_1}).$$

Using the ν-gap metric, Vinnicombe [88] has weakened these results even further.

Theorem 4.2.12 *[88]*

i. Given a nominal plant P_1, a compensator C_1 and a number $\beta < b_{\max}(P_1)$, then: (P_2,C_1) is stable for all plants P_2 satisfying $\delta_v(P_1,P_2) \leq \beta$ if, and only if, $b_{P_1,C_1} > \beta$.

ii. Given a nominal plant P_1, a perturbed plant P_2, and a number $\beta < b_{\max}(P_1)$, then: (P_2,C_1) is stable for all compensators C_1 satisfying $b_{P_1,C_1} > \beta$ if, and only if, $\delta_v(P_1,P_2) \leq \beta$.
Here $b_{\max}(P) = \sup_C b_{P,C}$.

Again, maximising b_{P_1,C_1} is equivalent to optimising robustness to unstructured neighbourhoods in the ν-gap metric. While equivalent to the gap metric in this sense, the second part of this theorem indicates that if two plants are far apart, when this distance is measured in the ν-gap metric, then it is possible to find a controller that performs adequately with the first plant but which actually destabilises the second plant. This indicates that the ν-gap metric is more fundamental than the gap metric since it allows us to make some important conclusions when the distance between two plants is large. Vinnicombe [88] also shows that maximising b_{P_1,C_1} is equivalent to maximising $b_{P,C}$ for all perturbed plants and compensators lying in a ν-gap ball.

Theorem 4.2.13 *[88]*
Given a nominal plant P_1, and a nominal compensator C_1 such that (P_1,C_1) is stable, then:

$$\arcsin b_{P_2,C_2} \geq \arcsin b_{P_1,C_1} - \arcsin \delta_v(P_2,P_1) - \arcsin \delta_v(C_2,C_1).$$

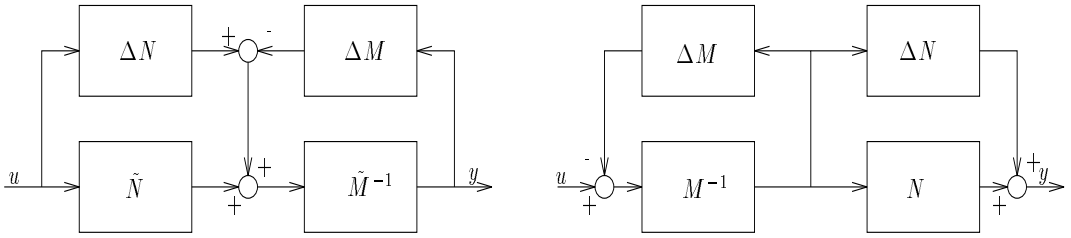

Figure 4.2 *Left coprime factor and right coprime factor perturbation models.*

There is an alternative interpretation of the performance measure $b_{P,C}$ which relates to robust stability of a coprime factor representation of the nominal plant [85]. This interpretation is more in line with early results on robust stabilisation of unstructured neighbourhoods generated by multiplicative and additive uncertainty models ([20],[32]) which preserve the number of closed right-half plane poles of the nominal model. Coprime factor perturbations are less restrictive than the additive and multiplicative models of uncertainty since they allow the number of closed right-half plane poles of the nominal plant and the perturbed model set to differ. This is highly desirable for unstable plants and for plants having poles on, or near, the imaginary axis, particularly if the plant might be time-varying[2].

Definition 4.2.14 *Let $P = \tilde{M}^{-1}\tilde{N}$ be a lcf of the nominal plant and define the family of plants*

$$\mathbf{N}\{\tilde{N},\tilde{M},\epsilon\} \triangleq \{P_1 = (\tilde{M}+\Delta M)^{-1}(\tilde{N}+\Delta N) : \|(\Delta N, \Delta M)\|_\infty < \epsilon, \quad \textit{and} \quad \Delta N, \Delta M \in RH_\infty\}$$

to be a norm-bounded left coprime factor perturbation set.

Identically, we can define a norm-bounded rcf perturbation set using a rcf of the nominal plant. Block diagram representations of the coprime factor model sets are shown in Figure 4.2.

Theorem 4.2.15 *[85]*
Suppose that (P,C) is stable and $P = \tilde{M}^{-1}\tilde{N}$ is a left coprime factorisation of the nominal plant P. Then (P_1,C) is stable for all $P_1 = (\tilde{M}+\Delta M)^{-1}(\tilde{N}+\Delta N)$ where ΔM, $\Delta N \in RH_\infty$ and $\|(\Delta N, \Delta M)\|_\infty < \beta$ if, and only if

$$\left\| \begin{bmatrix} C \\ I \end{bmatrix} (I-PC)^{-1}\tilde{M}^{-1} \right\|_\infty \leq \frac{1}{\beta}.$$

Proof: This follows directly from the small gain theorem which gives necessary and sufficient conditions for robust stability for stable norm-bounded perturbations [103]. ■

A similar result is easily obtained for rcf perturbations, although in terms of a norm bound on a different closed-loop transfer function. When the coprime factorisation of the nominal plant is normalised, ie: $N^*N + M^*M = I$ for the rcf and $\tilde{N}\tilde{N}^* + \tilde{M}\tilde{M}^* = I$ for the lcf, then the stability conditions for the normalised left and normalised right coprime factor perturbations

[2] When the plant is time-varying extracting a stable LTI model is somewhat arbitrary.

become identical. That is, for a norm-bounded perturbation to a normalised lcf representation of the nominal plant, $\|(\Delta N, \Delta M)\|_\infty \leq \beta$, or a norm-bounded perturbation to a normalised rcf representation of the nominal plant, $\|(\Delta N^T, \Delta M^T)^T\|_\infty \leq \beta$, the closed loop remains stable if, and only if, $b_{P,C} > \beta$. Finally, it is evident that optimising robustness to normalised coprime factor perturbations is identical to optimising robustness to gap metric and ν-gap metric perturbations.

4.3 H_∞ loop-shaping

MacFarlane and Glover [59] have observed that the problem of optimising $b_{P,C}$ over the class of all stabilising controllers has an explicit solution (unlike most H_∞ optimisation problems). Their solution makes use of the isometry properties of the normalised coprime factors to reduce the optimisation to a standard Nehari extension for which there exists an efficient state space solution [39]. Optimising stability robustness is most certainly not the only objective of control design and we would like to achieve a specified level of performance as well. In this regard, MacFarlane and Glover [41] have suggested introducing frequency weights to shape the open-loop frequency response of the nominal plant in much the same way as is done in the classical control of SISO plants. In any loop-shaping design technique a controller is selected so as to achieve sufficiently high loop gain at low frequency, low loop gain at high frequency, and the correct phase around crossover to give closed-loop stability ([25],[60]). This allows certain guarantees to be made concerning closed-loop performance [20].

For example, given a plant P and a stabilising controller C, then for good performance we require the sensitivity function $S = (I - PC)^{-1}$ to be small, ie: $\bar{\sigma}((I - PC)^{-1}(j\omega))$ must be bounded from above. Returning to Figure 4.1, it can be seen that by making the sensitivity function small we make the transfer function from u_2 to e_2 close to unity. If u_2 represents a reference signal this implies that the plant output, represented by e_2, will follow the reference signal closely. Similarly, for good robust stability we require the complementary sensitivity function $T = (I - PC)^{-1}PC$ to be small, ie: $\bar{\sigma}((I - PC)^{-1}PC(j\omega))$ must be bounded from above. If we use u_2 in Figure 4.1 to model additive sensor noise at the plant output then by making the complementary sensitivity function small we make the effect of this noise on the plant output, again modelled by e_2, small. This requirement is typically important at high frequency where sensor outputs become erroneous due to the presence of unmodelled high frequency dynamics. For example, the output from the force transducer will only be a useful measure of the contact force at frequencies well below the first natural frequency of the transducer. These conflicting design objectives[3] are typically satisfied over different frequency ranges reflecting such things as model accuracy, disturbance spectra and available actuator effort.

A number of typical design objectives can be specified in terms of the singular values of various closed-loop transfer functions. These provide a measure of the gain from disturbances injected

[3]We cannot make both S and T small at any specific frequency because the relation $S - T = I$ must always hold.

at various points in the loop to important physical outputs. Table 4.1 gives a summary of the important transfer functions along with an interpretation of the signals they bound. Where

Transfer function	Loop gain interpretation	Mapping	Physical interpretation
$\bar{\sigma}((I-CP)^{-1}(j\omega))$	$\underline{\sigma}(CP(j\omega)) \gg 1$	$u_1 \mapsto e_1$	u_1 : Additive input noise e_1 : Actuator demand
$\bar{\sigma}(C(I-PC)^{-1}(j\omega))$	•	$u_2 \mapsto e_1$	u_2 : Additive output noise e_1 : Actuator demand
$\bar{\sigma}((I-PC)^{-1}(j\omega))$	$\underline{\sigma}(PC(j\omega)) \gg 1$	$u_2 \mapsto v_2$	u_2 : Reference signal v_2 : Tracking error
$\bar{\sigma}((I-PC)^{-1}P(j\omega))$	•	$u_1 \mapsto e_2$	u_1 : Additive input noise e_2 : Plant output
$\bar{\sigma}((I-PC)^{-1}PC(j\omega))$	$\bar{\sigma}(PC(j\omega)) \ll 1$	$u_2 \mapsto e_2$	u_2 : Additive output noise e_2 : Plant output
$\bar{\sigma}(P(I-CP)^{-1}(j\omega))$	•	$u_1 \mapsto v_2$	u_1 : Additive input noise v_2 : Tracking error

Table 4.1 *Design objectives in terms of closed-loop transfer functions.*

there is no ambiguity we give an interpretation of the design objectives, which are specified in terms of the singular values of closed-loop transfer functions, in terms of the singular values of the loop gain operator given by $L_g = PC$ when the loop is broken at the input to the controller and $L_g = CP$ when the loop is broken at the input to the plant. Some of the design objectives in Table 4.1 can be conflicting. Consider a SISO plant which is free of the complications arising from directionality issues. An example of the type of contradiction that might arise is given by the second and third entries in Table 4.1. If the plant has low gain in a particular frequency range then for good tracking performance we require the controller to have high gain over the same frequency range. Now if the sensor measuring the plant output is particularly noisy over this frequency range then it is possible for the noise to be amplified to give large actuator demand signals at the plant input. This is highly undesirable and typifies the type of tradeoff that exists in control problems: the contradiction merely indicates that for good tracking over a certain frequency range we require good measurement signals over that range. An important observation is that all of the transfer functions appearing in Table 4.1 can be bounded by bounding $\|H(P,C)\|_\infty$ which follows from the fact [37] that $\|H(P,C)\|_\infty = \|H(C,P)\|_\infty$.

The closed-loop transfer functions appearing in Table 4.1 also have useful robust stability interpretations. These stability interpretations provide the motivation for using singular value loop-shaping to give performance/robustness tradeoffs in the classical sense. Table 4.2 lists three transfer functions along with the class of uncertainty for which they provide a measure of stability. The stability test is based on the small gain theorem and provides a frequency by frequency measure of the size of tolerable perturbations from each of the uncertainty classes. These tests only apply to stable perturbations (unlike those in section 4.2.3) and can be highly

conservative, especially when uncertainty enters into the loop at different locations [21]. In the latter case the structured singular value ([66],[95]) provides a less conservative analysis tool. The fact that requirements on many of the closed-loop singular values can be converted into

Transfer function	Uncertainty model	Stability test
$(I-CP)^{-1}C$	$P_1 = P + \Delta,\ \Delta \in RH_\infty$	$\bar{\sigma}((I-CP)^{-1}C(j\omega))\bar{\sigma}(\Delta(j\omega)) < 1$
$(I-CP)^{-1}CP$	$P_1 = P(I + \Delta),\ \Delta \in RH_\infty$	$\bar{\sigma}((I-CP)^{-1}CP(j\omega))\bar{\sigma}(\Delta(j\omega)) < 1$
$(I-PC)^{-1}PC$	$P_1 = (I + \Delta)P,\ \Delta \in RH_\infty$	$\bar{\sigma}((I-PC)^{-1}PC(j\omega))\bar{\sigma}(\Delta(j\omega)) < 1$

Table 4.2 *Stability interpretations of closed-loop transfer functions.*

requirements on the singular values of the loop gain operator forms the basis of the H_∞ loop-shaping design procedure. Figure 4.3 shows typical bounds on the singular values of the loop gain operator for a plant having one crossover region. The bound $L(j\omega)$ represents a hard lower

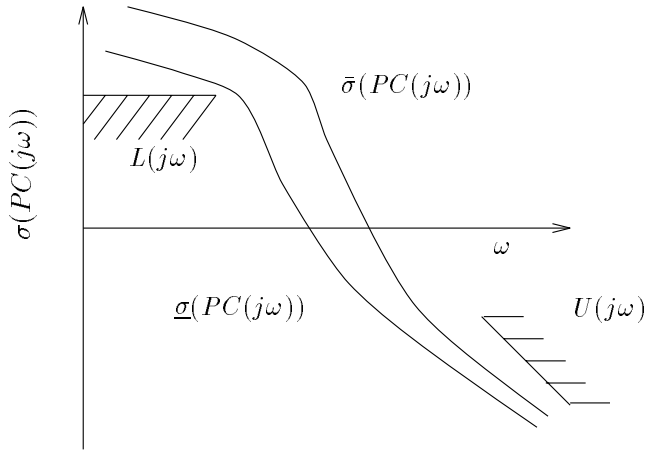

Figure 4.3 *Typical bounds required of the open-loop singular values.*

bound on the minimum singular value of the loop gain operator, typically required to ensure a bound on tracking error. $U(j\omega)$ represents a hard upper bound on the maximum singular value of the loop gain operator and can be used to limit control action at high frequency, ensure stability to unmodelled high frequency dynamics and reduce the effect of sensor noise. Returning to the H_∞ loop-shaping design procedure, shaping of the open-loop singular values is achieved by pre- and post-multiplying the plant with weights W_1 and W_2 without strict regard for phase. A controller is then sought which optimally stabilises this weighted plant to normalised coprime factor, gap metric and ν-gap metric perturbations by solving the following H_∞ problem

$$b_{\max} = \inf_{C} \left\| \begin{bmatrix} P_s \\ I \end{bmatrix} (I - CP_s)^{-1} [-C \quad I] \right\|_\infty^{-1},$$

where P_s is the shaped plant given by $P_s = W_2 P W_1$. If $b_{\max} << 1$, the achieved stability margin, which is bounded above by unity, is too small. This indicates a mismatch between the properties

of the nominal plant and the selected weights and may be the result of choosing weights which reflect unreasonable performance objectives. This makes it necessary to adjust the weights and repeat the procedure. Once a sufficiently large stability margin $b_{\max}$ has been obtained (this will of course depend on the accuracy of the model), the weights are absorbed into the controller to give the final controller as W_1CW_2. In [41] a solution for the maximal stability margin $b_{\max}$ is given as

$$b_{\max} = (1 - \|[\tilde{N}_s, \tilde{M}_s,]\|_H^2)^{\frac{1}{2}}$$

where $\|[\tilde{N}_s, \tilde{M}_s]\|_H$ denotes the norm of the Hankel operator with symbol $[\tilde{N}_s, \tilde{M}_s]$ and $[\tilde{N}_s, \tilde{M}_s]$ is a normalised lcf of P_s. Extensive experience gained from the selection of weights for the Harrier model has led Hyde [50] to the following conclusion regarding the selection of suitable weights which give a satisfactory stability margin.

i. The loop gain $\bar{\sigma}(P_s(j\omega))$ should be small around frequencies corresponding to the modulus of any right-half plane zeros of the nominal plant.

ii. The loop gain $\underline{\sigma}(P_s(j\omega))$ should be large around frequencies corresponding to the modulus of any right-half plane poles of the nominal plant.

iii. The roll-off rate around crossover should not be much greater than about 20 dB/dec.

Similar restrictions on the loop shape of SISO plants have been known to hold for some time [25]. These rules are given further justification by Vinnicombe [87] but are not always easy to apply, particularly when the plant has multiple unity-gain crossover frequencies. For example, in the problem considered here there is a conflict between keeping the roll-off rate at cross over sufficiently low and maintaining stability in the presence of unmodelled high frequency vibration modes.

In reality the designer only has the freedom to shape the singular values of the weighted plant P_s, whereas the bounds on the desired loop shape depend on the singular values of PW_1CW_2. Bounds on the degradation of the desired loop shape, as reflected by the singular values of P_s, due to the introduction of the controller C have been obtained by MacFarlane and Glover [59]. Given a compensator C with $b_{P_s,C} \geq \beta$, then:

i. In any frequency range where $\underline{\sigma}(P_s(j\omega)) \gg \frac{\sqrt{1-\beta^2}}{\beta}$, it can be shown that $\underline{\sigma}(C(j\omega)) \gtrsim \frac{\beta}{\sqrt{1-\beta^2}} > \beta$; where $\gtrsim$ denotes asymptotically greater than or equal to as $\underline{\sigma}(P_s) \to \infty$. This can be used to give an upper bound on the sensitivity function

$$\bar{\sigma}((I - P_sC)^{-1}(j\omega)) \lesssim \left(\underline{\sigma}(P_s(j\omega))\frac{\beta}{\sqrt{1-\beta^2}} - 1\right)^{-1}.$$

ii. In any frequency range where $\bar{\sigma}(P_s(j\omega)) \ll \frac{\beta}{\sqrt{1-\beta^2}}$ it can be shown that $\bar{\sigma}(C(j\omega)) \lesssim \frac{\sqrt{1-\beta^2}}{\beta}$ and this can be used to give an upper bound on the complementary sensitivity function.

$$\bar{\sigma}(P_sC(I-P_sC)^{-1}(j\omega)) \lesssim \left(\frac{1}{\bar{\sigma}(P_s(j\omega))}\frac{\beta}{\sqrt{1-\beta^2}} - 1\right)^{-1}.$$

These bounds indicate that where $\underline{\sigma}(P_s(j\omega)) \gg 1$, the sensitivity function will be small provided $b_{P_s,C}$ is bounded from below. Similarly, where $\bar{\sigma}(P_s(j\omega)) \ll 1$, the complementary sensitivity function will be small provided $b_{P_s,C}$ is bounded from below. The performance bounds together with the robust stability theorems of section 4.2.3 indicate that the H_∞ loop-shaping design procedure is ideally suited to the problem of robustness optimisation when dealing with unstructured neighbourhoods about the nominal plant. This design technique has been the basis of a very challenging multivariable control application which has resulted in a successful implementation on a Harrier VSTOL aircraft [51]. Briefly, we summarise the advantages of this design procedure which make it particularly attractive for the class of problems we are considering.

i. We can incorporate intuition gained from classical control techniques in the selection of weights to give performance/robustness tradeoffs.

ii. The weights can be selected to reflect available actuator effort. If there is more than one actuator present the relative capabilities of the actuators can be accounted for. Another advantage of the H_∞ loop-shaping design procedure stems from the fact that each loop can be shaped on its own leaving decoupling between loops to the H_∞ optimisation.

iii. There exist useful bounds on the achieved sensitivity and complementary sensitivity functions in terms of the singular values of the shaped plant P_s and the achieved stability margin $b_{P_s,C}$.

iv. The explicit formula for the optimal stability margin makes it a simple matter to investigate the effect of changing loop shapes or actuator/sensor placement on robust stability.

v. The H_∞ loop-shaping design procedure does not introduce stable pole-zero cancellations between the plant and the controller [79]. Cancellation of stable poles with stable zeros can, and most certainly does, arise in other H_∞ synthesis techniques, for example the mixed sensitivity formulation. This is highly undesirable for plants having stable poles and zeros near the imaginary axis, particularly if these are subject to uncertainty due to parameter variations.

vi. The central controller [24] for the suboptimal problem has a particularly simple structure and can be written as a plant observer with state feedback. This structure has been exploited by Hyde ([50],[51]) to gain-schedule controllers for the Harrier aircraft.

Up to this point we have focused on the problem of stabilisation in the presence of dynamic uncertainty. By shaping the frequency response of the nominal plant we ensure that the class of

tolerable perturbations is sensible from an engineering perspective, but what of parametric uncertainty? It must be true that if we design a controller that stabilises our parameter-dependent plant (in the graph topology) for a fixed value of the contact parameter ρ_0, then the closed loop will be stable for some open ball $\mathcal{B}(P_{\rho_0}, \epsilon) = \{P_\rho : |\rho - \rho_0| < \epsilon\}$. If this is not the case then there does not exist a finite-dimensional LTI controller that can stabilise the plant and which gives gradual degradation in performance when the contact position varies slightly. One fundamental question that immediately arises concerns just how large the neighbourhood about ρ_0 will be. Alternatively, if we bury the parametric uncertainty in a ball of dynamic uncertainty, will we end up with a conservative controller, or will a sensible design result?

It turns out that for the class of systems considered in this thesis the result can be very disappointing. We will see that the properties of flexible mechanical systems can take seemingly innocuous variations in the physical parameter into a plant well beyond the maximally stabilisable gap and ν-gap balls. One interpretation of this is that if we synthesise a controller without taking into account prior knowledge of how changes in the physical parameter map into changes in the coprime factors then it is possible to end up with a poor controller. This is a disappointing observation because robust stabilisation in the graph topology clearly represents the correct setting for approaching the problem. In fact Safanov [47] using simple examples of mechanical systems has argued that this implies that gap type controllers, and indeed the gap metric, are not useful tools when used on this class of systems. In this thesis we will argue that the converse is true.

4.3.1 H_∞ loop-shaping applied to LPV structures

Returning to the system defined in chapter 3, consider the application of the H_∞ loop-shaping technique to the problem of controlling the contact force with a fixed value of the contact parameter. In this section we restrict attention to the SISO case. To be more specific, consider controlling the contact force with the contact point located at the centre of the beam, actuation coming from the motor and the measured output being the contact force. Before doing any theoretical design we point out that the model used here corresponds to the physical plant discussed in chapter 6, which has a beam of length $670mm$. This model incorporates modal damping factors which were measured experimentally at $\rho_0 = 350mm$. During the design stage variation in the physical damping associated with changes in the contact position is covered by tolerance to dynamic uncertainty making it unnecessary to measure the modal damping factors for all possible contact positions. Figure 4.4 shows a theoretical 8-state Bode magnitude plot with the motor torque as input and the contact force as output when the constraint is located at $\rho_0 = 350mm$.

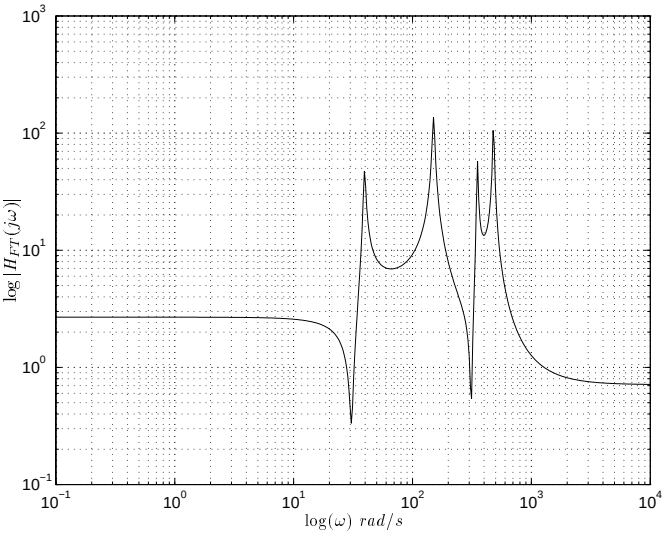

Figure 4.4 *Predicted frequency response* $\rho_0 = 350mm$.

For performance we would like to achieve robust force tracking with a bandwidth of approximately 10 rad/s over the largest possible physical interval about the nominal contact position[4]. We also require an increase in the level of damping associated with the first two vibration modes in order to reduce the effect of low frequency disturbances which are generated from movement of the force transducer. We approach the problem using classical loop-shaping ideas, increasing the loop gain at low frequency by using an integrator of the form

$$W_a = \frac{11.2}{s},$$

and increasing the level of damping in the second vibration mode as well as reducing the control effort at high frequency with a weight of the form

$$W_b = \frac{160^2(s^2 + 240s + 600^2)}{600^2(s^2 + 32s + 160^2)}.$$

The rationale behind the selection of these weights is as follows. The integral action at low frequency is introduced to give small sensitivity and good tracking performance; the effective closed-loop bandwidth being determined by the crossover frequency of this integrator. The idea behind the selection of the weight W_b is to increase the loop gain around frequencies corresponding to the second natural frequency of vibration and, thereafter, to roll it off quickly. By increasing the loop gain around the second resonant peak we are effectively specifying an increase in the level of closed-loop damping for this vibration mode. By reducing the loop gain at high frequency we limit control action and attempt to "gain stabilise" the unmodelled vibration

[4]This bandwidth being representative of the transients that we would like to track with a real violin bow.

modes. Unfortunately, there is a limit on the rate at which the loop gain can be rolled off and it is well known, at least in the case of stable minimum phase SISO plants, that roll-off rate is closely related to phase margin [25]. It was found that the first order lag

$$W_c = \frac{200}{s + 200},$$

with a cut off frequency just above crossover helped to further improve robustness to the unmodelled dynamics. With these weights the shaped plant is given by $P_s = P_{\rho_0} W_1$ where $W_1 = W_a W_b W_c$.

The optimal stability margin for the weighted model was computed as being $b_{P_s,C} = 1/3$. Figure 4.5 shows the open-loop gain of the weighted model P_s as well as the degradation in the desired loop shape due to including a slightly suboptimal controller achieving $b_{P_s,C} = 1/3.1$. One of the first issues we consider concerns robust stability to unmodelled high frequency dynamics. To this end we compute the gap $\delta_g(P_s, P_{\rho_0} W_1)$ between the nominal weighted plant P_s and the weighted plant $P_{\rho_0} W_1$ obtained by retaining more vibration modes in the model. These values are presented in Table 4.3. The difference between these systems is effectively zero[5] indicating good robustness to the unmodelled dynamics. Next we evaluate the gap and the ν-gap between the weighted nominal plant P_s and a weighted 12-state model under perturbations in the contact position. These results are tabulated in Table 4.4.

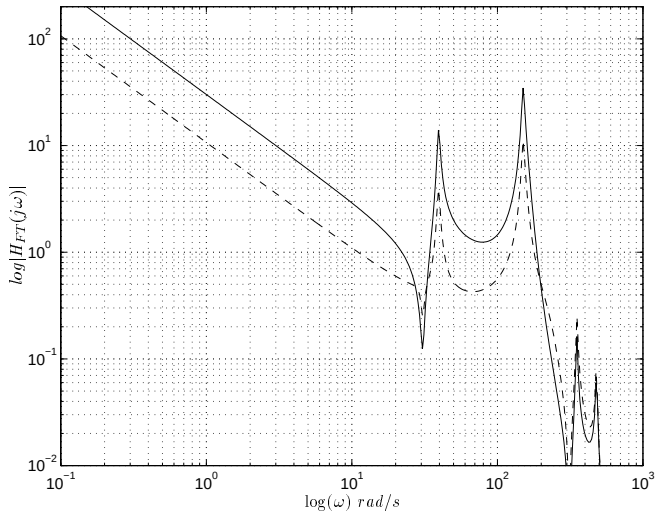

Figure 4.5 *Loop gain of P_s (solid), loop gain of $P_s C$ (dashed).*

[5] The ν-gap $\delta_v(P_s, P_{\rho_0} W_1)$ shows these systems to be indistinguishable.

States retained in the model	$\delta_g(P_s, P_{\rho_0}, W_1)$
8 states	0
10 states	$9.76E^{-4}$
12 states	$2.00E^{-3}$
14 states	$2.00E^{-3}$

Table 4.3 *Robustness to unmodelled dynamics.*

Contact position ρ	$\delta_g(P_s, P_\rho W_1)$	$\delta_v(P_s, P_\rho W_1)$
$\rho = 320mm$	$\delta_g = 0.7327$	$\delta_v = 0.7325$
$\rho = 330mm$	$\delta_g = 0.5424$	$\delta_v = 0.5417$
$\rho = 340mm$	$\delta_g = 0.2897$	$\delta_v = 0.2888$
$\rho = 350mm$	$\delta_g = 0$	$\delta_v = 0$
$\rho = 360mm$	$\delta_g = 0.2839$	$\delta_v = 0.2831$
$\rho = 370mm$	$\delta_g = 0.5239$	$\delta_v = 0.5234$
$\rho = 380mm$	$\delta_g = 0.7053$	$\delta_v = 0.7038$

Table 4.4 *Robustness to perturbations in the contact position.*

It turns out that only small perturbations in the contact position take the plant well beyond the maximally stabilisable gap and ν-gap balls given by $b_{\max} = 1/3$. Once the plant moves beyond this gap ball then we cannot guarantee closed-loop stability, even for the mathematical model. This fact is made clear by computing $b_{P_\rho W_1, C}$ with the contact position perturbed to the left and to the right of the nominal position and plotting the result in Figure 4.6.

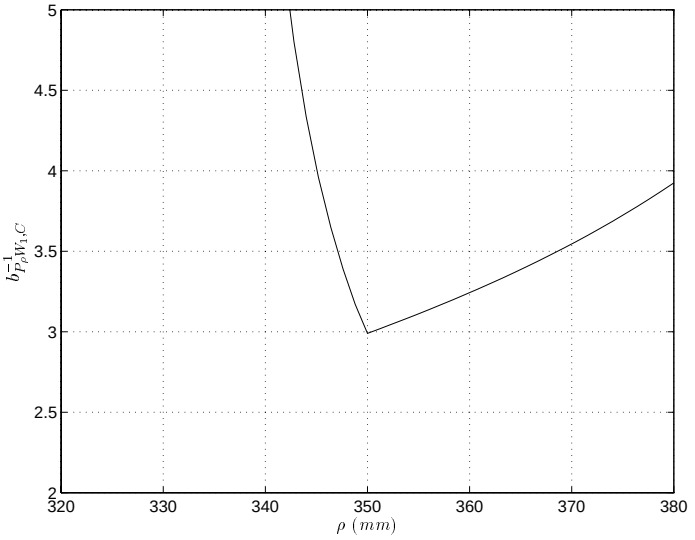

Figure 4.6 *Achieved stability margin vs ρ.*

Figure 4.6 indicates that the central H_∞ controller gives very poor robust stability to perturbations in the contact position. In fact, this controller actually destabilises the model when $\rho < 340mm$ although it gives a more gradual degradation in performance when $\rho > 350mm$. Safanov and Heise [47] have pointed out that the gap metric is very sensitive to zeros lying within the control bandwidth and poles lying beyond the control bandwidth. Using a simple model of two masses connected by a spring of variable stiffness they were able to construct a lead controller that gave satisfactory performance to the allowable variations in the spring stiffness. When they computed the gap between these plants for different values of the stiffness parameter they found it to be large and concluded that the gap metric was a highly conservative stability measure for flexible structures. The ν-gap metric, like the gap metric, has the same sensitivity to the pole-zero configuration of the plant.

However, if we recall part (ii.) of Theorem 4.2.12 we come to a very different conclusion. What this tells us is that when the ν-gap between two plants is large (as occurs under perturbations in the contact position), then it is possible to construct a controller that performs satisfactorily with the nominal plant but which actually destabilises the perturbed plant. For example, the ν-gap between the nominal weighted plant at $\rho_0 = 350mm$ and the perturbed weighted plant at $\rho = 370mm$ is given by $\delta_\nu(P_\rho W_1, P_{\rho_0} W_1) = 0.5234$. So it is possible to find a controller that stabilises P_s with a stability margin of $b_{P_s,C} = 0.5234$ but which destabilises the perturbed plant. This does not mean that all controllers performing satisfactorily with the nominal plant will perform poorly with the perturbed plant, but it does mean that we should account for the expected changes in the dynamics when synthesising the controller. For the plant we are examining it turns out that the central controller is a poor choice, but the set of all suboptimal controllers is huge (in fact homeomorphic to the unit ball in RH_∞ [24]), and we just need to find a way of choosing a more satisfactory controller. As an aside, it was observed that any attempt to increase the loop gain around frequencies corresponding to the zeros within the control bandwidth gave worse robust stability to variations in the contact position. From this we conclude that any controller that results in pole-zero cancellations is likely to have very poor stability properties.

4.3.2 The ν-gap metric as a design tool for LPV systems

Limitations associated with robustness to parametric uncertainty of controllers designed using H_∞ loop-shaping have been alluded to in section 4.3.1. One way of ensuring that any satisfactory controller for the nominal plant will perform satisfactorily under perturbations in the contact position is to modify the plant in such a way as to reduce the sensitivity of the ν-gap metric to this parameter. Unfortunately, it is not immediately obvious how one should modify a physical plant in order to achieve this. In chapter 3 we plotted the frequency response of two transfer functions. The first transfer function was from the motor torque to the measured contact force (Figure 3.5), the second transfer function was from the force applied by an actuator at the tip of the beam to the same contact force (Figure 3.6). It was pointed out that these transfer functions have a different pole-zero configuration. For example, the appearance of an antiresonance before the first natural frequency in the motor loop is not mimicked by the force loop. A little physical

intuition shows that the ν-gap metric can be exploited to make the system less sensitive to the parameter variations.

In definition 4.2.8 it was stated that, when the winding number constraint is satisfied, the ν-gap metric can be computed from the frequency response of the plants. In section 4.4 it will be shown that provided the ν-gap metric remains less than unity under continuous perturbations to the plant, these being assessed in the graph topology, then the winding number constraint will not be violated. This is a weak assumption and most certainly holds for the system under study where the mapping from the physical parameter ρ onto the state-space realisation is continuous in any matrix norm. The ν-gap metric can be regarded as the supremum over frequency of the following pointwise metric

$$\kappa_{P_1,P_2}(\omega) = \bar{\sigma}(\tilde{G}_2 G_1(j\omega)).$$

For the contact interval $320mm \leq \rho \leq 380mm$, we compute $\kappa(\omega)$ for the weighted plant used in section 4.3.1 and plot the result in Figure 4.7. The distance between the plants on this parameter interval is dominated by two frequency regions, the first being around the low frequency antiresonance, the second corresponding to the natural frequency of the third mode of vibration. Since the ν-gap metric allows us to identify those frequency regions contributing most to the distance between these plants, and since we can link these frequency regions with various physical properties of the plant, we can use this information to modify the plant in such a way as to make it easier to control.

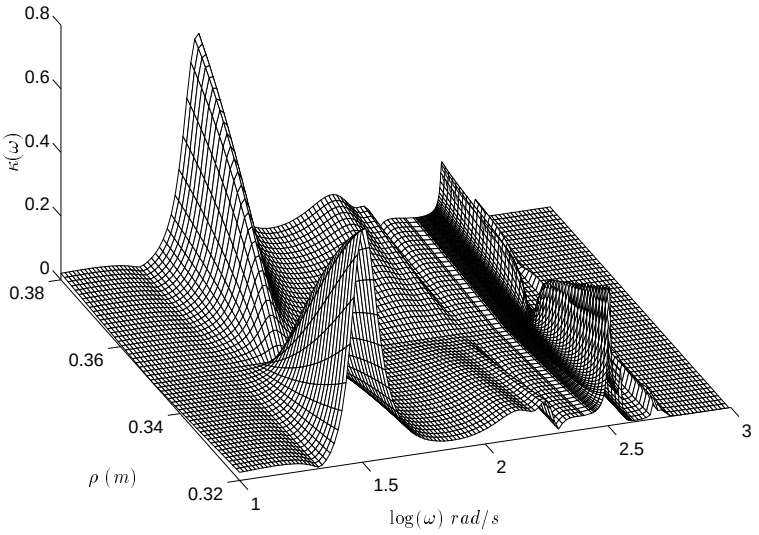

Figure 4.7 $\kappa(\omega)$ *computed over the parametric model set.*

The setup is as before, the nominal contact position being at $\rho_0 = 350mm$, but with inputs from the motor at the base of the beam and a force actuator at the tip of the beam. Since the plant has two inputs and one output we can shape the loop from each of the actuators to the measured output independently of each other by using weights at the plant input. For the motor loop we use the weight selected in section 4.3.1 except we reduce the crossover frequency of the integrator slightly giving

$$W_a = \frac{8.0}{s}.$$

We use the force actuator to increase the control bandwidth and to improve damping in the first vibration mode. More importantly, we can use this actuator to eliminate the effect of the antiresonance lying within the control bandwidth of the motor loop. To this end a weight of the form

$$W_d = \left(\frac{800s}{s^2 + 20s + 20^2}\right)\left(\frac{40}{s + 40}\right),$$

gives the force loop high gain over the desired frequency range. This weight also ensures that the force loop has suitably low gain at both low and high frequencies respectively. This effectively assigns the low frequency tracking performance to the motor loop and, using similar reasoning to section 4.3.1, prevents the force loop from interacting with unmodelled high frequency vibration modes. Figure 4.8 shows the open-loop frequency response of both loops of the shaped plant along with the maximum singular value. It may seem strange to use a weight that makes

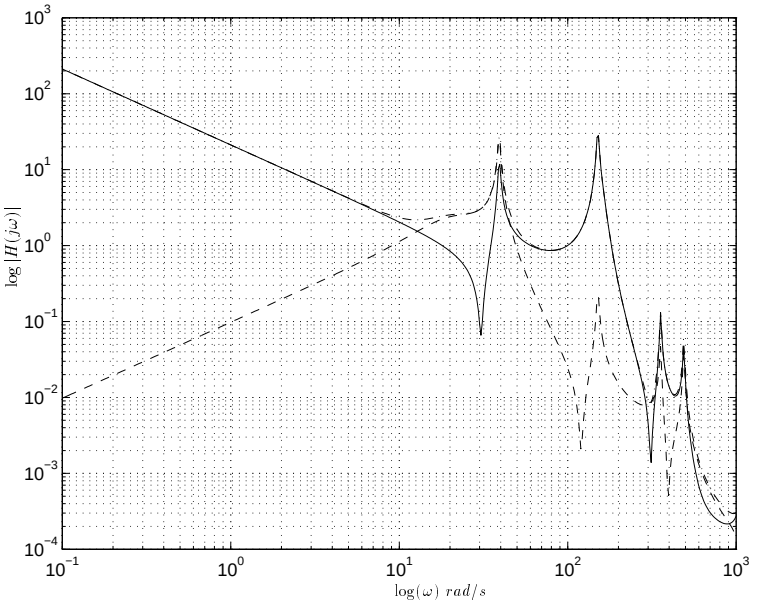

Figure 4.8 *Loop shapes, motor loop (solid), force loop (dashed), maximum singular value (dot-dashed).*

the plant look ill-conditioned from the input based on the fact that ill-conditioned plants are

notoriously difficult to control [81]. However, such difficulties do not arise with this plant since it only has one output. Since the high gain and low gain directions are effectively decoupled [81] we do not expect the usual difficulties that arise from directionality. This is confirmed by using standard checks such as robustness to multiplicative uncertainty at the plant input (ie: between the input weight and the plant). As in section 4.3.1 we compute the gap between the nominal shaped plant P_s and the weighted plant obtained by retaining more vibration modes in the model; these results are tabulated in Table 4.5. Once again, this shows that the selected weights give good robust stability to unmodelled high frequency dynamics. Similarly, we compute the gap and the ν-gap between the nominal shaped plant P_s and a 12-state weighted model $P_\rho W_1$ due to perturbations in the contact position. These results are tabulated in Table 4.6. It

States retained in the model	$\delta_g(P_s, P_{\rho_0} W_1)$
8 states	0
10 states	$9.97E^{-4}$
12 states	$2.00E^{-3}$
14 states	$2.00E^{-3}$

Table 4.5 *Robustness to unmodelled dynamics.*

Contact position ρ	$\delta_g(P_s, P_\rho W_1)$	$\delta_v(P_s, P_\rho W_1$
$\rho = 320mm$	$\delta_g = 0.3502$	$\delta_v = 0.3491$
$\rho = 330mm$	$\delta_g = 0.2673$	$\delta_v = 0.2665$
$\rho = 340mm$	$\delta_g = 0.1902$	$\delta_v = 0.1901$
$\rho = 350mm$	$\delta_g = 0$	$\delta_v = 0$
$\rho = 360mm$	$\delta_g = 0.1200$	$\delta_v = 0.1194$
$\rho = 370mm$	$\delta_g = 0.2156$	$\delta_v = 0.2155$
$\rho = 380mm$	$\delta_g = 0.3268$	$\delta_v = 0.3265$

Table 4.6 *Robustness to perturbation in the contact position.*

is clear from Table 4.6 that we have successfully exploited the extra freedom afforded by the second actuator to make the ν-gap metric (and the gap metric) less sensitive to variations in the physical parameter. This demonstrates the power of this metric as a design tool. Rather than simply designing, building and thereafter attempting to control a physical system, we can use the ν-gap metric (which is more easily related to the physical properties of the plant) to ascertain exactly what properties of the plant are important from a feedback viewpoint and then account for these when designing the plant itself. The use of only one additional actuator judiciously placed to account for the pole-zero distribution of the plant guarantees that any controller that performs satisfactorily with the nominal plant will also perform adequately under predictable perturbations. This is confirmed by computing $\kappa(\omega)$ over the specified parameter interval for the two-input plant and plotting the result in Figure 4.9.

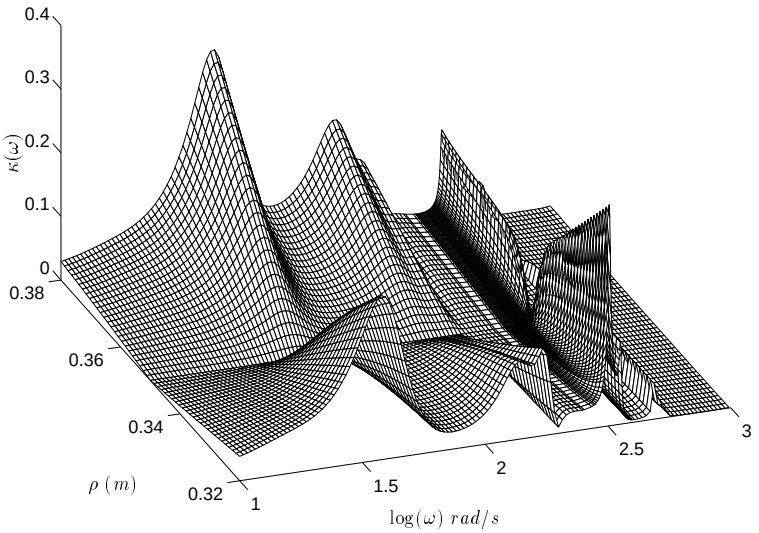

Figure 4.9 $\kappa(\omega)$ *computed over the parametric model set.*

With the additional input the optimal controller for the weighted plant P_s gives $b_{P_s,C} = 1/2.92$. From this we can guarantee stability, at least for the mathematical model, over the range $320mm < \rho < 380mm$. For a slightly suboptimal controller $b_{P_s,C} = 1/2.94$ we compute the achieved stability margin $b_{P_\rho W_1,C}$ over this interval, and obtain the result shown in Figure 4.10. This shows that the controller not only stabilises the model over the specified parameter interval but actually achieves a satisfactory level of robustness to dynamic uncertainty as well.

In this section we have shown how, at least for control problems involving parameter-dependent flexible structures, the ν-gap metric can be used in selecting actuator (and possibly sensor) placements in order to improve robustness. This is an important and difficult problem for this class of systems because there is so much freedom allowed in the placement of sensors and actuators, particularly for vibration attenuation problems [4]. It has been argued that the ν-gap metric is a fundamental measure of the pertinent properties of any LTI system when used in a feedback configuration. We have used this metric to identify the particular properties of the flexible manipulator under study which make this system difficult to control. This was demonstrated in section 4.3.1 where it was shown that even sensible robust controllers can give poor stability properties when the plant dynamics undergo parametric variations. We then exploited this knowledge by modifying the plant so that any controller that works adequately at the chosen nominal contact position also works adequately over a restricted interval about that point. In section 4.4 we return to the problem of incorporating the known parametric variations when synthesising a controller.

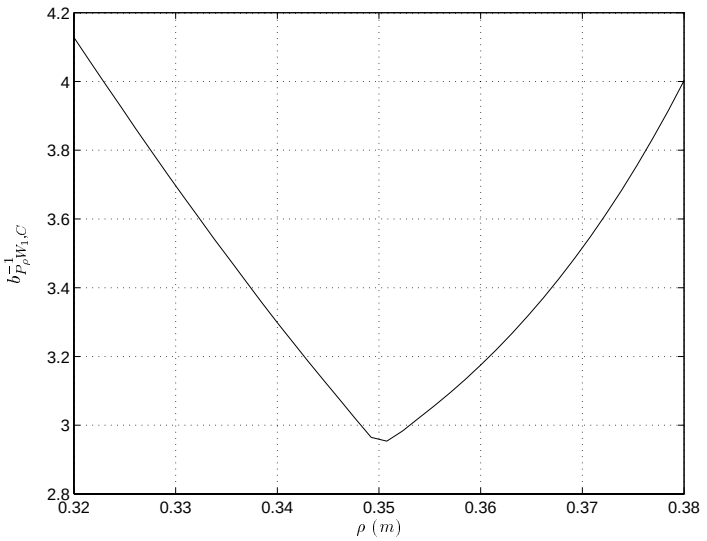

Figure 4.10 *Achieved stability margin vs ρ.*

4.4 Incorporating structure into the controller synthesis

We have observed that the H_∞ loop-shaping design approach can result in poor controllers for flexible mechanical systems, particularly when used to cover parametric uncertainty. We have also seen that one solution to this problem was to make use of the ν-gap metric in order to modify the physical properties of the plant in such a way as to make any controller more robust to the predictable parametric variations. This approach may not always be viable and may, in some situations, be undesirable. In particular, for the violin bowing problem a human player manages to control the bow pressure with a *single* actuator and it would be desirable to mimic this in a bowing machine. We address now, using an extension of the H_∞ loop-shaping design technique, the problem of incorporating structure into the controller synthesis. It will be shown that incorporating structure has an appealing physical interpretation. In effect we find a weight $w, w^{-1} \in RH_\infty$ which weights the ball of uncertainty in the normalised coprime factor interpretation of the stabilisation problem thereby accounting for the manner in which physical parameter variations map into changes in the coprime factors. Suppose we have a nominal plant P and let $[N, M]$ denote a normalised rcf of this plant, incorporation of the weight w into the stabilisation problem is depicted in Figure 4.11.

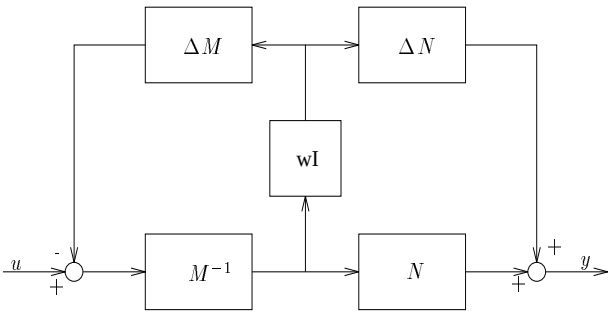

Figure 4.11 *Weighting the ball of uncertainty.*

4.4.1 A closer look at the ν-gap metric

Since the ν-gap metric is fundamental to this approach to incorporating parametric uncertainty, we examine it more closely in this section. We begin with a result concerning the internal stability of the feedback pair (P, C).

Lemma 4.4.1 *[32]*
Given the feedback pair (P, C), let $[N, M]$ denote a rcf of P and $[\tilde{U}, \tilde{V}]$ a lcf of C, then the following are equivalent:

i. The feedback pair (P, C) is internally stable.

ii. $(\tilde{V}M - \tilde{U}N)$ is a unit in RH_∞.

For conciseness of exposition it is convenient to use the normalised left and the normalised right graph symbols of the controller given by $\tilde{K}$ and K respectively. Similarly, we will use the normalised left and normalised right graph symbols of the plant given by $\tilde{G}$ and G respectively. These symbols were defined in chapter 2. The key to including parametric uncertainty is the answer to the following question. Given a nominal plant P_0 and a stabilising controller C which achieves a certain level of stability $b_{P_0,C} > \beta$, what is the largest set of plants that can be stabilised by this controller? Since (P_0, C) is stable we are assured, by Lemma 4.4.1, that $\tilde{K}G_0$ is a unit in RH_∞. So given a perturbed plant P_1 with graph symbol G_1 it is stabilised by C if, and only if, $\tilde{K}G_1$ is a unit in RH_∞. The following lemma proves useful in determining whether $\tilde{K}G_1$ is a unit.

Lemma 4.4.2 *[84]*
Given $A, A^{-1}, B \in RL_\infty$, $wno\det(A+B) = wno\det(A)$ *if* $\underline{\sigma}(A(j\omega)) > \bar{\sigma}(B(j\omega))$. *Also, given* $A, B \in RL_\infty$, $wno\det(AB) = wno\det A + wno\det B$.

Another useful result comes from [37] and shows that $b_{P,C}$ can be related to $\underline{\sigma}(\tilde{K}G)$.

Proposition 4.4.3 *[37]*
Given a plant P *and a stabilising controller* C, *then*

$$b_{P,C} = \inf_w \underline{\sigma}(\tilde{K}G(j\omega))$$

where $\tilde{K}$ *is the normalised left graph symbol of* C *and* G *is the normalised right graph symbol of* P.

$\tilde{K}G_1$ is a unit in RH_∞ if, and only if, $\det(\tilde{K}G_1(j\omega)) \neq 0$ and $\mathrm{wno}\det(\tilde{K}G_1) = 0$. Making use of the fact that $[G_0, \tilde{G_0}^*]$ is unitary we get

$$\begin{aligned} \tilde{K}G_1 &= \tilde{K}(G_0G_0^* + \tilde{G_0}^*\tilde{G}_0)G_1 \\ \Rightarrow \underline{\sigma}(\tilde{K}G_1) &\geq \underline{\sigma}(\tilde{K}G_0G_0^*G_1) - \bar{\sigma}(\tilde{K}\tilde{G}_0^*\tilde{G}_0G_1). \end{aligned}$$

So if

$$\underline{\sigma}(\tilde{K}G_0G_0^*G_1(jw)) > \bar{\sigma}(\tilde{K}\tilde{G}_0^*\tilde{G}_0G_1(j\omega)) \ \forall \ \omega \in \mathbb{R},$$

then

$$\begin{aligned} \det(\tilde{K}G_1(j\omega)) &\neq 0 \qquad \text{and} \\ \mathrm{wno}\det(\tilde{K}G_1) &= \mathrm{wno}\det(\tilde{K}G_0) + \mathrm{wno}\det(G_0^*G_1) \\ \Rightarrow \mathrm{wno}\det(\tilde{K}G_1) &= 0 \ \text{ if, and only if } \ \mathrm{wno}\det(G_0^*G_1) = 0. \end{aligned}$$

Vinnicombe [88] has shown that for a controller achieving $b_{P,C} > \beta$, if $\delta_v(P_1, P_0) \leq \beta$ then $\underline{\sigma}(\tilde{K}G_0G_0^*G_1) > \bar{\sigma}(\tilde{K}\tilde{G}_0^*\tilde{G}_0G_1)$. As part of the necessity proof of Theorem 4.2.12 it is shown that if $\delta_v(P_1, P_0) > \beta$ then it is possible to construct a plant P_1, lying in this set, such that $\det(\tilde{K}G_1) = 0$ at some frequency. This shows that the winding number constraint in Definition 4.2.8 arises in a very natural way as part of the robust stability result in Theorem 4.2.12.

Since $[K, \tilde{K}^*]$ is also a unitary function it can be used in a similar manner to obtain the following relation

$$\underline{\sigma}(\tilde{K}G_1) \geq \underline{\sigma}(\tilde{K}G_0)\sqrt{1-\bar{\sigma}^2(\tilde{G}_0G_1)} - \bar{\sigma}(\tilde{G}_0G_1)\sqrt{1-\underline{\sigma}^2(\tilde{K}G_0)}.$$

This suggests that the minimum value of $\underline{\sigma}(\tilde{K}G_1)$ depends on the size of $\bar{\sigma}(\tilde{G}_0G_1)$ provided $\text{wno}\det(G_0^*G_1) = 0$ and this motivates the metric given in Definition 4.2.8. That the ν-gap metric is symmetric and satisfies the triangle inequality is shown in [88]. The metric depends entirely on the frequency response of the plants and can be regarded as the supremum over frequency of the pointwise metric

$$\kappa_{P_1,P_2}(\omega) = \bar{\sigma}(\tilde{G}_2G_1(j\omega)),$$

with G_1 and G_2 being the normalised right graph symbols of P_1 and P_2 respectively. We defined the generalised stability margin $b_{P,C}$ in Definition 4.2.9 using its interpretation as both a performance and robustness indicator as motivation. Proposition 4.4.3 shows that the achieved stability margin is given by the infimum over frequency of the following pointwise version thereof

$$\tau_{P,C}(\omega) = \underline{\sigma}(\tilde{K}G(j\omega)).$$

These frequency response measures $\tau(\omega)$ and $\kappa(\omega)$ are the key to including parametric uncertainty into the controller synthesis.

Although quantitatively sharper than the gap metric, the ν-gap metric has only been used for its robust stability interpretations in covering an unstructured neighbourhood about the nominal plant in the graph topology. In order to include parametric uncertainty into the controller synthesis we need a way of dealing with the winding number constraint in Definition 4.2.8.

Theorem 4.4.4 *Given a metric space Λ, a mapping $\Lambda : \lambda \mapsto P_\lambda$, continuous in the graph topology, and a piecewise connected subset $\bar{U} \in \Lambda$, with $\lambda_0 \in \bar{U} \mapsto P_{\lambda_0}$ then*

$$\sup_{\lambda\in\bar{U}} \delta_v(P_{\lambda_0}, P_\lambda) = \sup_{\omega} \sup_{\lambda\in\bar{U}} \kappa_{P_{\lambda_0},P_\lambda}(\omega). \tag{4.2}$$

Proof: Continuity of the mapping $\lambda \mapsto P_\lambda$ implies that the mapping onto the normalised graph symbol of P_λ, $\lambda \mapsto G_\lambda$ is continuous (proposition 4.2.1) on the closed right-half plane. This implies that equation (4.2) holds provided the winding number constraint is not violated. Furthermore, continuity of the mapping $\lambda \mapsto G_\lambda$ implies that $\lambda \mapsto \det(G_\lambda^*G_{\lambda_0}(j\omega))$ is continuous for all $\omega \in \mathbb{R}$. So if $\text{wno}\det(G_\lambda^*G_{\lambda_0}) \neq 0$ for some $\lambda \in \bar{U}$ then $\det(G_\lambda^*G_{\lambda_0}(jw)) = 0$ for some $\lambda \in \bar{U}$ and $\omega \in \mathbb{R}$. Now noting that $[G_\lambda, \tilde{G}_\lambda^*]$ is unitary we get

$$\begin{aligned} G_\lambda G_\lambda^* + \tilde{G}_\lambda^*\tilde{G}_\lambda &= I \qquad \text{and} \qquad G_{\lambda_0}^*G_{\lambda_0} = I \\ \Rightarrow \underline{\sigma}^2(G_{\lambda_0}^*G_\lambda) &= 1 - \bar{\sigma}^2(\tilde{G}_\lambda G_{\lambda_0}). \end{aligned}$$

Thus we see that when $\det(G_\lambda^*G_{\lambda_0}(j\omega)) = 0$, $\bar{\sigma}^2(\tilde{G}_{\lambda_0}G_\lambda(j\omega)) = 1$ at the same frequency and for the same $\lambda \in \bar{U}$. ■

This is an important result because it ensures that the winding number constraint is not violated provided $\kappa(\omega)$ does not become unity at any given frequency and the parametrised model set is obtained by continuous variations in the physical parameters. Actually the assumption that the mapping $\lambda \mapsto P_\lambda$ is continuous in the graph topology is not a strong assumption and will hold provided the mapping of λ onto a state-space realisation of P_λ is continuous in the Euclidean norm [84]. This is most certainly the case for the system studied here since ρ is mapped continuously onto the mass and stiffness matrices.

In the sequel we need the following family of plants. Given P_0 and $f(\omega)$ satisfying $0 \leq f(\omega) < 1 \quad \forall \omega \in \mathbb{R}$, define the set of plants

$$\bar{B}(P_0; f(\omega)) \stackrel{\triangle}{=} \{P : \delta_v(P_0, P) < 1, \kappa_{P_0,P}(\omega) \leq f(\omega) \quad \forall \omega \in \mathbb{R}\}.$$

We now state a generalisation of Theorem 4.2.12 which allows us to incorporate structured uncertainty into the synthesis problem.

Theorem 4.4.5 *[87]*
Provided $\exists$ *g(s) satisfying* $|g(j\omega)| = f(\omega)$ *and* $g, g^{-1} \in RH_\infty$ *then:*

1. *Given* P_0*, and a compensator* C*, then:*
   $b_{P_1,C} > \alpha$ *for all* $P_1 \in \bar{B}(P_0, f(\omega))$ *if, and only if,* (P_0, C) *is stable and*

$$\arcsin \tau_{P_0,C}(\omega) > \arcsin f(\omega) + \arcsin \alpha \quad \forall \omega \in \mathbb{R}.$$

2. *Given* P_0 *and* P_1 *then, provided there exists a* C *such that* (P_0, C) *is stable and which satisfies* $\arcsin \tau_{P_0,C}(\omega) > \arcsin f(\omega) + \arcsin \alpha$*, then* $b_{P_1,C} > \alpha$ *for all* C *for which* (P_0, C) *is stable and which satisfy* $\tau_{P_0,C}(\omega) > \arcsin f(\omega) + \arcsin \alpha$ *if, and only if,* $P_1 \in \bar{B}(P_0, f(\omega))$.

4.4.2 Extended H_∞ loop-shaping

Suppose we have a nominal plant P_0 which lies within a parametrised family of plants $\mathcal{B}$. Furthermore, suppose the parametrised family of plants has associated with it some dynamic uncertainty - we may not know the exact value of certain physical parameters, or for any given value of the physical parameters there may be a mismatch between the model and the true plant. Having motivated the maximisation of $b_{P,C}$ as both a robust stability margin and as a performance criterion we consider the following problem

$$\sup_C \inf_{P \in \mathcal{B}} b_{P,C},$$

where $\mathcal{B}$ is the parametrised family of plants. This is a difficult problem and is similar to the mixed-μ setup of Young [96]. If, instead, we consider a slightly larger family of plants then the supremisation can be carried out as a one-block H_∞ synthesis problem. Firstly we obtain $f(\omega)$

as the maximum distance from the nominal plant P_0 to the boundary of the parametrised set as follows

$$f(\omega) = \sup_{P \in \mathcal{B}} \kappa_{P_0,P}(\omega).$$

We now bury the parametrised model set $\mathcal{B}$ in the larger set

$$\bar{B}(P_0; f(\omega)) := \{P : \delta_v(P_0, P) < 1, \kappa_{P_0,P}(\omega) \leq f(\omega) \quad \forall \omega \in \mathbb{R}\}.$$

To find $\sup_C \inf_{P \in \bar{B}} b_{P,C}$ we require the largest α such that $\arcsin \tau_{P_0,C}(\omega) > \arcsin f(\omega) + \arcsin \alpha$. This is equivalent to finding the largest α such that

$$\inf_C \sup_\omega \frac{w(\omega)}{\tau_{P_0,C}(\omega)} < 1 \tag{4.3}$$

where $w(\omega) = \sin(\arcsin f(\omega) + \arcsin \alpha)$. For fixed α, the infimum on the left hand side of equation (4.3) can be found using the following H_∞ optimisation. Recall that

$$\frac{1}{\tau_{P_0,C}(\omega)} = \bar{\sigma}\left(\begin{bmatrix} P_0 \\ I \end{bmatrix} (I - C P_0)^{-1} [-C \quad I](j\omega) \right).$$

Let $P_0 = N_0 M_0^{-1}$ be a normalised rcf of the nominal plant P_0. Using the fact that G_0, the normalised right graph symbol of P_0, is an isometry, this is equivalent to

$$\frac{1}{\tau_{P_0,C}(\omega)} = \bar{\sigma}(M_0^{-1}(I - C P_0)^{-1}[-C \quad I](j\omega)). \tag{4.4}$$

So we require the largest α such that

$$\inf_C \| w_1 I M_0^{-1} (I - C P_0)^{-1} [-C \quad I] \|_\infty < 1, \tag{4.5}$$

where $w_1, w_1^{-1} \in RH_\infty$ satisfies $w_1^* w_1(j\omega) = w^2(\omega)$. This is easily shown to be equivalent to the closed-loop transfer function from $\begin{bmatrix} u_1 \\ u_2 \end{bmatrix}$ to y in Figure 4.12. This can be solved by using the Riccati equation solution for all suboptimal H_∞ controllers [24], or by using the Youla parametrisation of all stabilising controllers ([32],[60],[103]) to reduce the optimisation to a Nehari extension. In the SISO case the latter approach is advantageous because it can be solved using interpolation theory [25] without the need to fit the weight $w(\omega)$ with a rational approximation. Furthermore, if interpolation theory is used in the SISO case then for a fixed value of α it is not necessary to iterate to find the optimal infinity norm. If the solution procedure of Doyle and Glover is used, then for each trial value of α it is necessary to iterate to get the controller that comes arbitrarily close to minimising the infinity norm. This makes the overall procedure significantly slower and because it is also necessary to fit $w(\omega)$ with a stable minimum phase rational function it can be less accurate as well.

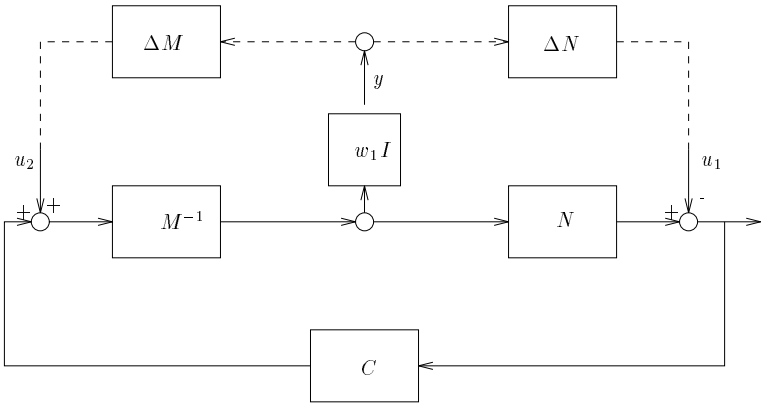

Figure 4.12 *Physical setup for the H_∞ optimisation problem.*

Let $\tilde{X}_0$ be a left inverse of G_0 which can be obtained from the doubly coprime factorisation ([32],[60]), ie: $\tilde{X}_0 G_0 = I$. Equation (4.4) can be simplified to

$$\frac{1}{\tau_{P_0,C}(\omega)} = \bar{\sigma}(((\tilde{K}G_0)^{-1}\tilde{K})(j\omega)), \tag{4.6}$$

where $\tilde{K}$ is the normalised left graph symbol of C. Substituting the Youla parametrisation [84] of all stabilising controllers gives

$$\tilde{K} = Z(\tilde{X}_0 + Q\tilde{G}_0),$$

where $Q \in RH_\infty$ is an arbitrary stable parameter and $Z, Z^{-1} \in RH_\infty$ is such that $\tilde{K}\tilde{K}^* = I$. Equation (4.6) now becomes

$$\begin{aligned}\frac{1}{\tau_{P_0,C}(\omega)} &= \bar{\sigma}(((Z(\tilde{X}_0 + Q\tilde{G}_0)G_0)^{-1}Z(\tilde{X}_0 + Q\tilde{G}_0))(j\omega)) \\ &= \bar{\sigma}((\tilde{X}_0 + Q\tilde{G}_0)(j\omega)).\end{aligned}$$

Thus, equation (4.5) can be written as

$$\inf_C \|w_1 I M^{-1}(I - CP_0)^{-1}[-C \quad I]\|_\infty = \inf_{Q \in RH_\infty} \|w_1 I(\tilde{X}_0 + Q\tilde{G}_0)\|_\infty,$$

and multiplying on the right by $[G_0, \quad \tilde{G}_0^*]$, which is unitary, we get

$$\inf_C \|w_1 I M^{-1}(I - CP_0)^{-1}[-C \quad I]\|_\infty = \inf_{Q \in RH_\infty} \|w_1 I[I, \quad \tilde{X}_0\tilde{G}_0^* + Q]\|_\infty.$$

So equation (4.4) is equivalent to finding a $Q \in RH_\infty$ such that

$$\begin{aligned} w^2(\omega)(1 + \bar{\sigma}^2((\tilde{X}_0\tilde{G}_0^* + Q)(j\omega))) &< 1 \; \forall \, \omega \in \mathbb{R} \\ \Rightarrow \|w_2 I(\tilde{X}_0\tilde{G}_0^* + Q)\|_\infty &< 1 \end{aligned}$$

$$\text{where} \qquad w_2^*(j\omega)w_2(j\omega) = \frac{w^2(\omega)}{1 - w^2(\omega)}.$$

In the SISO case this problem can be solved using Nevanlinna-Pick interpolation [25], the Hilbert Transform to generate phase information for w_2 and the Poisson integral to evaluate w_2 at the right-half plane poles of $\tilde{X}_0\tilde{G}_0^*$. This makes it unnecessary to extract a rational approximation of the controller during the iteration since it suffices to work with the controller's frequency response. An iteration over α (for which a bisection algorithm works adequately) gives the largest α for which the inequality in equation (4.3) holds. The result of the first stage of the design is a controller C which achieves

$$\inf_{\omega\in\mathbb{R}} \inf_{P\in\bar{B}(P_0;f(\omega))} \tau_{P,C} = \alpha$$

and since $\mathcal{B} \subset \bar{B}(P_0, f(w))$

$$\inf_{\omega\in\mathbb{R}} \inf_{P\in\mathcal{B}} \tau_{P,C} = g(\omega) \geq \alpha.$$

At frequencies where $g(\omega) > \alpha$, indicating unnecessary excess stability (the consequence of optimising over a larger model set), the weight $f(\omega)$ is relaxed according to a simple rule

$$f(\omega) = \sin(\arcsin f(\omega) - \epsilon(\arcsin g(\omega) - \alpha)) \tag{4.7}$$

where ϵ is a small positive constant. The whole procedure is then repeated until $g(\omega)$ is approximately flat against frequency. This indicates that the compensator does no more than is necessary to achieve the desired stability margin for the parametrised model set.

4.4.3 Improving parameter robustness using extended H_∞ loop-shaping

We consider, once again, the problem of robust force control through our flexible beam. The nominal contact point is fixed at a distance of $\rho_0 = 350mm$ and we investigate the possibility of controlling the force over a specified interval about the nominal contact position using only the motor loop. Here the physical parameter used to parametrise the family of plants is the distance ρ. We will keep the same design objectives as outlined previously, namely to achieve good force tracking with no steady state error and also to increase the level of damping in the first two flexible modes.

In much the same way as before we weight the plant to achieve our nominal design objectives. The same weight as used in section 4.3.1 is used again, except that we make use of a single parameter K_p to trade off robustness against performance

$$W_1 = \left(\frac{K_p}{s}\right)\left(\frac{200}{s+200}\right)\left(\frac{s^2+240s+600^2}{s^2+32s+160^2}\right).$$

In terms of performance, increasing K_p results in a decrease in sensitivity, an increase in the level of damping in the controlled vibration modes and an increase in the controller bandwidth. Three different values of K_p are investigated, as specified in table 4.7. Since we do not attempt to invert the lightly damped zeros within the control bandwidth the loop gain is always small

around their frequency. Some initial designs indicated that a reasonable interval over which to expect good performance was approximately $60mm$, therefore we concentrate on the region $320mm < \rho < 380mm$.

K_p	$b_{P_\rho W_1, C}$	$b_{P_\rho W_1, \hat{C}}$	Order of C	Order of $\hat{C}$	$\delta_v(C, \hat{C})$
0.80	0.30	0.29	44 states	14 states	0.007
1.10	0.25	0.23	47 states	20 states	0.016
1.33	0.20	0.19	44 states	15 states	0.011

Table 4.7 *Design example controller properties.*

The first step in the design procedure is to measure the boundary of the set

$$f(\omega) = \max_{\rho} \kappa_{P_{\rho_0} W_1, P_\rho W_1}(\omega),$$

where $\rho_0 = 350mm$.

This is achieved by discretizing the $60mm$ interval by covering it with a mesh consisting of 21 equally spaced grid points, denoted ρ_j. At each of the grid points $\kappa_{P_{\rho_0} W_1, P_{\rho_j} W_1}(\omega_i)$ is computed over a suitably dense frequency list, denoted ω_i. The weight $f(\omega_i)$ is evaluated at each frequency in the frequency list as the maximum over the set of points ρ_j. The maximum value of α for which equation (4.3) holds is then computed using a simple bisection algorithm. Following this, the excess stability margin $g(\omega_i)$ is computed, the weight $f(\omega_i)$ relaxed in accordance with equation (4.7) and the whole procedure repeated. Figure 4.13 shows the initial and the final shape of the weight $f(\omega)$, before, and after completion of the iteration (both of these weights correspond to $K_p = 1.10$). The final weight is largest at frequencies corresponding to the zeros lying within the control bandwidth and at frequencies corresponding to the third vibration mode. Interpreted in the coprime factor framework the original norm-bounded ball has been weighted to emphasise perturbations in the frequency range where $f(\omega)$ is large. It can be seen from Figure 4.13 that the weight $f(\omega)$ is a complicated function of frequency and consequently it can only be well approximated by a high order rational function. In the three examples computed with the three different values of the parameter K_p a high order weight was necessary when extracting a rational approximation of the optimal controller, as can be deduced by examining table 4.7. Attempts to extract a controller based on a lower order approximation of the weight were unsuccessful mainly because small mismatches between the weight $f(\omega)$ and the approximation resulted in unacceptable degradation of the ideal stability margin. If we add to this the state dimension of the weighted plant it can be seen that the cost of incorporating knowledge about the parametric changes in the plant dynamics has been a considerable increase in the state dimension of the controller.

From an implementation perspective it is important to reduce the state dimension of the controller as much as possible. It was found that an optimal Hankel norm approximation of the controller's normalised graph symbol [62] produced satisfactory reduced order controllers without considerable degradation in the achieved stability margin. Table 4.7 lists the design factor

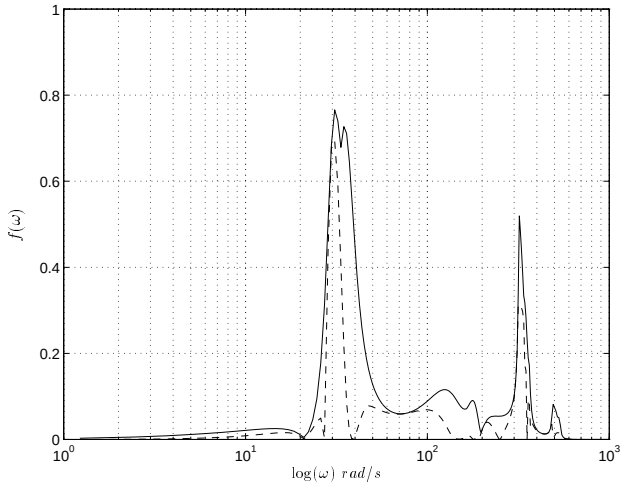

Figure 4.13 *Weight $f(\omega)$, original estimate (solid), final solution (dashed).*

K_p, the stability margin $b_{P_\rho W_1,C}$ achieved by the full order controller and $b_{P_\rho W_1,\hat{C}}$ achieved by the reduced order controller. A plot of the stability margin achieved by the reduced-order controller $\hat{C}$ over the parametric model set with $K_p = 1.10$ can be found in Figure 4.14. Although this should be flat against frequency there is a rapid rise in the achieved stability margin above 200 rad/s. This is the result of taking a slightly suboptimal controller when extracting a rational approximation of the controller which makes the stability margin approximately flat against frequency. For $K_p = 1.10$, Figure 4.15 shows the frequency response of the controller which makes the stability margin approximately flat against frequency together with the frequency response of $\hat{C}$.

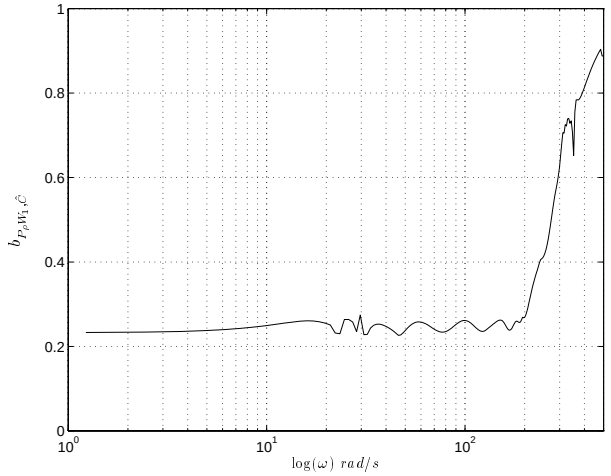

Figure 4.14 *Stability margin achieved by the reduced order controller $\hat{C}$.*

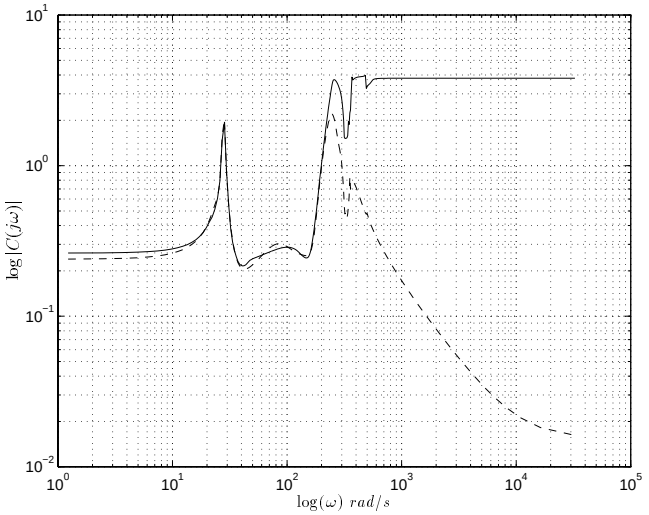

Figure 4.15 *Frequency response of the optimal controller (solid), frequency response of $\hat{C}$ (dashed).*

We have already argued that the ν-gap metric provides a fundamental measure of the properties of a system which are important from a feedback perspective. We have also demonstrated that the ν-gap metric is a powerful tool that allows us to account for parametric uncertainty in the plant when designing the controller. To evaluate the resulting controllers (a thorough experimental evaluation is undertaken in chapter 6) we simulate the closed-loop performance achieved by the reduced order controller with $K_p = 1.10$. In terms of improving damping we examine the effectiveness of the controller at attenuating a $50ms$ pulse disturbance applied at the plant input. We compute the response at three positions $\rho = 325mm$, $\rho = 350mm$ and $\rho = 375mm$, these being representative of the entire parametric model set. Figure 4.16 shows the open-loop response to the pulse disturbance which can be compared with Figure 4.17 which shows the closed-loop pulse response. The controller maintains performance over the entire interval, significantly increasing the damping in the first two modes.

Increasing damping is not the only objective of the controller design: we are also interested in assessing the effectiveness of the controller at tracking reference signals. To this end we compute the contact force in response to a step change in the reference signal. A suitable technique for introducing reference signals will be given in chapter 5. Figure 4.18 shows the step response at the three specified positions. The slightly oscillatory response is not the result of poor damping but relates to the manner in which the reference signal is introduced into the closed loop. Improved response comes at the cost of using a high order prefilter but these issues will be discussed in more detail in chapter 5.

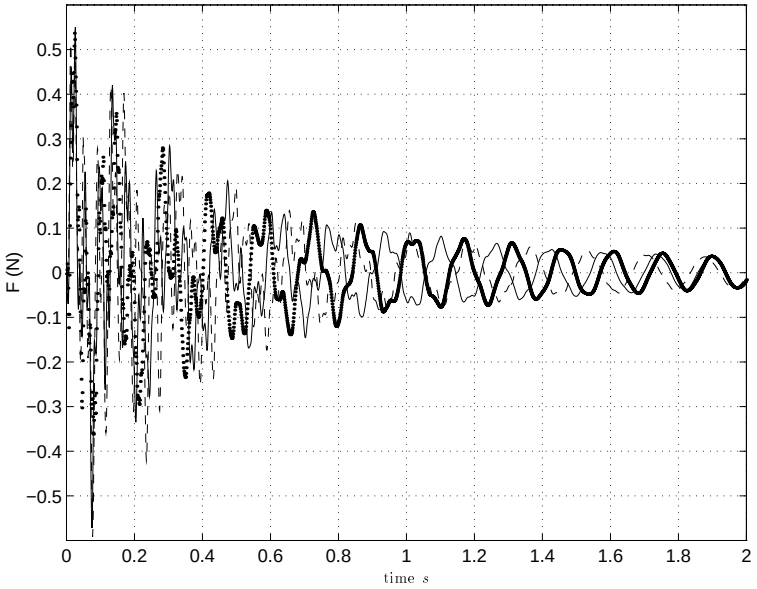

Figure 4.16 *Open-loop pulse response, $\rho = 325mm$ (dashed), $\rho = 350mm$ (solid), $\rho = 375mm$ (dotted).*

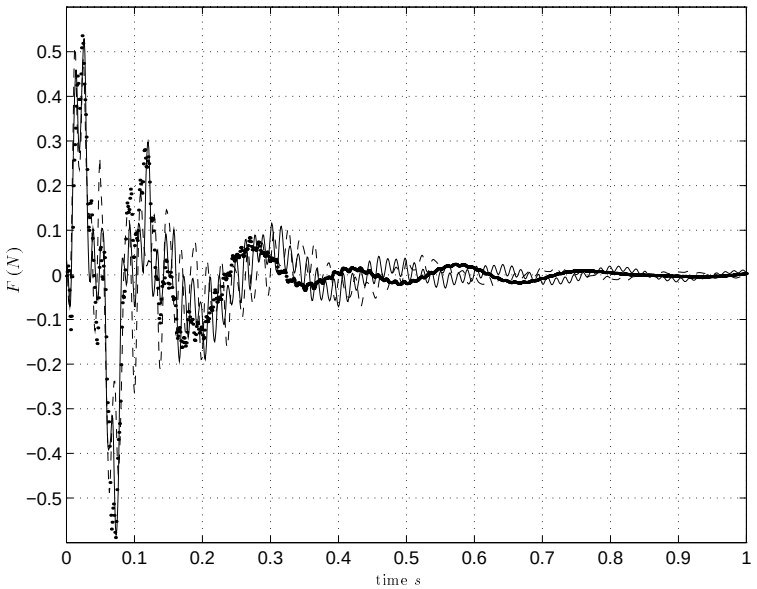

Figure 4.17 *Closed-loop pulse response ($K_p = 1.10$), $\rho = 325mm$ (dashed), $\rho = 350mm$ (solid), $\rho = 375mm$ (dotted).*

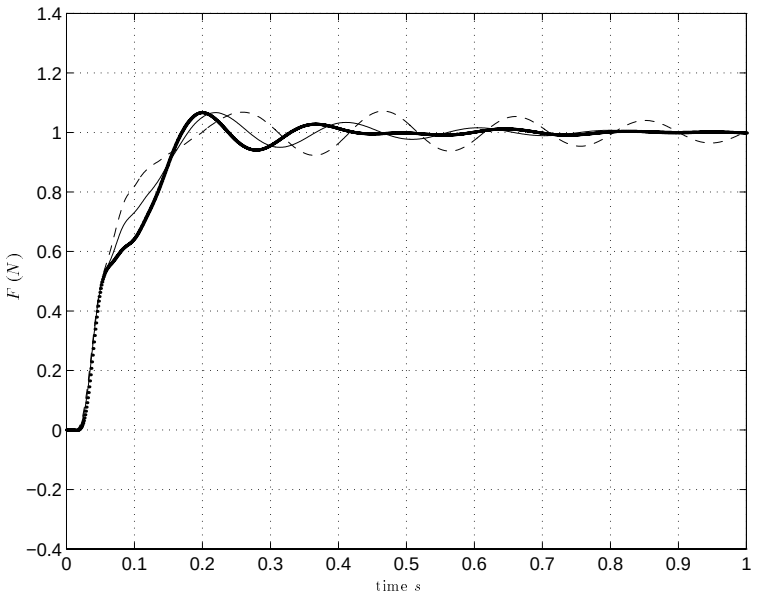

Figure 4.18 *Closed-loop step response ($K_p = 1.10$), $\rho = 325mm$ (dashed), $\rho = 350mm$ (solid), $\rho = 375mm$ (dotted).*

4.5 Summary

In this chapter we have examined the problem of controlling a parameter-dependent flexible structure. It is evident that the strong parameter dependence exhibited by this class of systems must be treated with some care. Attempts to cover the parameter variations by tolerance to norm-bounded dynamic uncertainty can easily result in controllers that are very sensitive to the expected parametric variations. This is even true when the controller is designed using a highly sensible formulation such as the H_∞ loop-shaping procedure. Our approach has relied heavily on the ν-gap metric and its frequency response interpretation which we have exploited in order to incorporate knowledge of the predictable parameter variations into the controller synthesis. The ν-gap metric can be used to expose the important feedback properties of any system which is something that is lacking in the μ-analysis framework. This allowed us to answer some very open ended questions in a fairly precise manner, for example, in what sense is one system easier to control than another? We then demonstrated how the ν-gap metric can be used both as a heuristic design tool and as a powerful analysis tool to aid in control design. Of course there are still a number of limitations with this approach. Firstly, a single controller can only cover a limited range of parameter variation, which is why we consider the problem of extending this range in the next chapter. Secondly, we have no guarantees that the controller will perform adequately when the parameter is time varying. This motivates a thorough experimental examination in order to determine the effectiveness of the LTI approach under realistic conditions.

5

Switching controllers for LPV systems

5.1 Introduction

In chapter 4 it was shown that it is possible to get a single controller that is robust to a limited range of real parametric uncertainty while still being robust to a sensible class of dynamic uncertainty. Intuitively, there is a limit to what can be achieved by a single controller and if we attempt to cover too large a range of parameter variation with only one controller then it becomes plausible that the controller will have to be detuned to such an extent that it becomes useless from a performance perspective. In fact the parameter $b_{P,C}$, when used in conjunction with the ν-gap metric as a synthesis tool, makes this tradeoff particularly transparent. Any attempt to stabilise an unrealistic range of parameter variation results in a small generalised stability margin and this brings with it an associated reduction in performance and tolerance to plant/model mismatch. In this chapter we consider how the limited range of parameter variation that can be tolerated by a single controller can be extended by designing a controller for each set in a finite cover of the parameter space and then switching between the controllers according to real time measurements of the parameter.

Driving a feedback loop with the output of one of a number of possible controllers means that only the selected controller will actually have its output consistent with the plant input. If this is the case then substituting one of the off-line controllers into the loop could easily generate a step in the actuator demand signal and this can seriously degrade the performance of the overall controller. One approach which overcomes this difficulty is to design a discrete set of controllers which cover the parameter space, interpolating between the controllers as the parameter space is traversed. This approach, usually referred to as gain-scheduling, requires the controllers designed at each of the chosen points to have a definite structure. In classical control this is not a significant problem and often amounts to little more than having to interpolate the proportional, integral and derivative gains of a PID controller. For controllers designed using H_∞ techniques this structure is often lacking and this will almost certainly be the case for the design technique outlined in chapter 4. There it was observed that the weight used to give robustness to parametric uncertainty is often a complicated function of frequency requiring high order rational function approximation when extracting the controller. So controllers designed at selected points using this technique are unlikely to even have the same state dimension, let

alone an easily identifiable structure. This merely highlights one of the difficulties that can arise when scheduling controllers designed using H_∞ control techniques. Others include the problem of choosing appropriate design points, the number of design points required to get satisfactory performance at intermediate points and the requirement for extensive simulation to verify performance when the scheduling parameter is truly time varying.

A significant advance which addresses a number of these issues can be found in the work of Hyde [50]. In his work, difficulties associated with the structural properties of H_∞ controllers were overcome by scheduling the central controller solving the normalised coprime factor robustness problem. Unlike most H_∞ controllers, which have a worst case disturbance signal entering into the controller equations [24], the coprime factor setup gives a controller that can be written as an observer with state feedback [79]. So by scheduling the state feedback and observer gains separately it is possible to obtain a controller having a definite structure and the same state complexity as the weighted plant. Unfortunately, there are still no guarantees on stability or performance when the parameter space is traversed at a finite rate, which is why we will delay examining this particular scheduling setup until chapter 8 where these issues will be addressed in greater detail.

For the present we examine the idea that the ability to cover sizeable parameter variations with a single controller makes a switching methodology a viable alternative to scheduling. This still leaves the problem of dealing with undesirable bumps when a controller switch is effected. A related problem arises when the plant has a saturation nonlinearity at any of its inputs. For example, the motor at the base of the flexible beam and the actuator at the tip of the beam are both driven by output-limited current amplifiers. If saturation occurs during closed-loop operation then the output of the controller and the input to the plant will differ, resulting in an inconsistency between the controller states and the physical plant input. This inconsistency is generically referred to as controller windup and is particularly pronounced if the controller has either slow or unstable dynamics [23]. For multivariable plants the effects of windup can be even more pronounced. Saturation in any one of the input channels results in a rotation of the input vector (relative to the unsaturated input) and this can have serious consequences, particularly for ill-conditioned plants [81]. A number of different strategies have been developed for dealing with controller windup. These range from conventional high gain antiwindup and the observer-based techniques of Astrom [3] to the self-conditioned form of Hanus [46]. Recently Campo [14] and Kothare et al [56] have shown that many of the conventional antiwindup techniques are equivalent to a coprime factor implementation of the controller, each technique merely being associated with a different coprime factorisation[1]. In section 5.2 we will outline Campo's approach in greater detail. Section 5.3 deals with the problem of introducing a reference signal into the loop to give good tracking properties. In section 5.4 we apply the technique to our example system and design both single input and multiple input controllers that cover the entire range of contact variation.

[1] Recall that coprime factors are only unique up to multiplication by a unit in RH_∞.

5.2 The antiwindup/ bumpless transfer formulation

Consider Figure 5.1 which shows an LFT interconnection of an LTI controller with a generalised plant P.

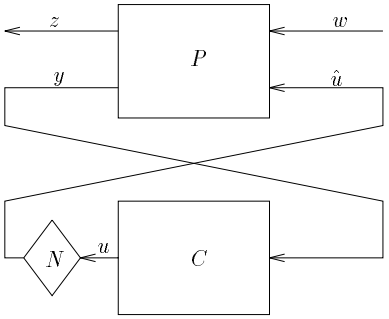

Figure 5.1 *LFT interconnection of a generalised plant and controller.*

New to the setup is the nonlinear operator N which could be a saturation nonlinearity or a discrete switch selecting one of a number of possible outputs from the controller. The controller and the generalised plant are both assumed to be LTI and it is further assumed that in the absence of the nonlinearity the controller (or selected output thereof) internally stabilises the feedback interconnection. To limit the effect of windup, the controller is now modified by the inclusion of an antiwindup operator Δ as shown in Figure 5.2.

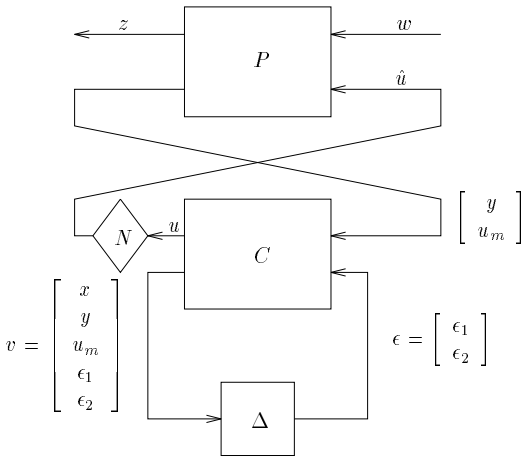

Figure 5.2 *Antiwindup implementation.*

It is assumed that the controller is provided with the measured output y together with a measurement or approximation of the actual plant input $\hat{u}$. In many cases it is not possible to measure the physical plant input so u_m and $\hat{u}$ may differ. For complete generality the antiwindup operator Δ may be any causal nonlinear operator and it is allowed to operate directly on the state of the controller through ϵ_1 and directly on the output of the controller through ϵ_2.

The antiwindup operator is also supplied with full information through v. That is, v contains the state of the controller x and the measurements y, u_m, ϵ_1 and ϵ_2. Observing that many of the antiwindup techniques found in the literature still result in an LTI controller, Campo [14] suggests the following assumptions on the operator Δ.

i. The operator Δ must be casual, linear and time invariant.

ii. When $u_m = u$, the constraint $\epsilon = 0$ must hold.

These conditions imply that the antiwindup operator must have no memory and consequently must be a constant matrix. Partitioning Δ conformally with ϵ gives

$$\begin{bmatrix} \epsilon_1 \\ \epsilon_2 \end{bmatrix} = \begin{bmatrix} \Delta_1 \\ \Delta_2 \end{bmatrix} v,$$

and incorporating the antiwindup block into C, Campo has shown that the setup gives

$$C = [\tilde{U}, \quad I - \tilde{V}], \tag{5.1}$$

where $C = \tilde{V}^{-1}\tilde{U}$ is a left coprime factorisation of the controller. LTI antiwindup schemes found in the literature differ to the extent that for different antiwindup operators Δ a different coprime factorisation of the controller results. The factorisation in equation (5.1) is equivalent to a controller realisation with internal feedback and in the case of perfect measurement $\hat{u} = u_m$ corresponds to the block diagram in Figure 5.3. The equivalence between the two blocks during normal operation (ie: $N = I$) is easily established.

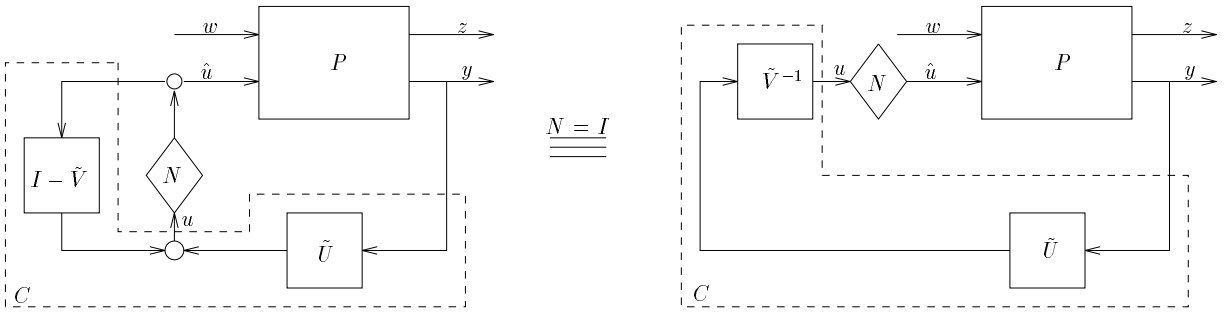

Figure 5.3 *Coprime factor realisation of the antiwindup scheme with perfect measurement.*

We now give a heuristic interpretation of how this scheme limits the effects of windup either during an input saturation or when the controller is running off-line. The scheme in Figure 5.3 has $\tilde{U}$ updated by the measured plant output and $\tilde{V}$ updated by the measured plant input. Since both operators are stable their states will be consistent with the physical signals used to update their respective state-spaces. So if an actuator saturates, the states of $\tilde{V}$ will tend to the equilibrium value consistent with the saturated level while the states of $\tilde{U}$ will continue to follow the measured output as required. The faster the dynamics of $\tilde{V}$ the quicker we can expect

the controller to resume normal operation when the input comes out of saturation. The same comments apply when the controller is off-line in which case we would like the states of $\tilde{V}$ to be consistent with the output of the online controller. Since many of the known LTI antiwindup schemes can be expressed in this form we shall use it as our starting point and consider other closed-loop objectives when selecting a particular factorisation of the controller.

5.3 Bumpless transfer and the extended H_∞ loop-shaping design procedure

Consider, without loss of generality, the problem of switching between two controllers designed using the extended H_∞ loop-shaping design procedure. The setup is depicted in Figure 5.4.

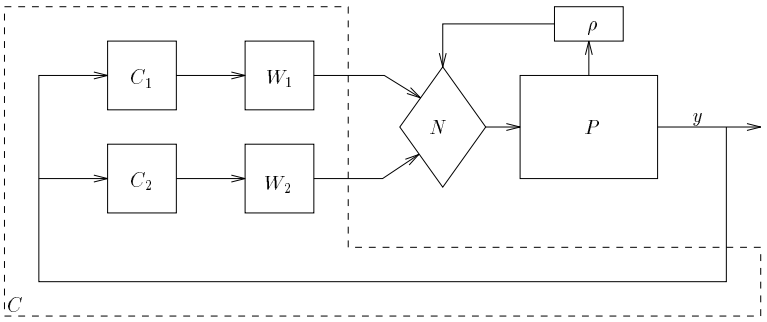

Figure 5.4 *The switching setup.*

The switching problem is complicated somewhat by the need to deal with the loop-shaping weights and the task of finding a suitable technique whereby reference signals can be introduced into the loop in a manner which is consistent with the original loop-shaping design objectives. In this section we argue that there is a particular coprime factorisation of the controller that is consistent with the antiwindup setup developed by Campo and which is also natural when introducing reference signals into the feedback loop. We will also show that the same approach can be used to design a filter to achieve the desired tracking objectives while leaving the factorisation of the controller essentially arbitrary.

We begin by taking each controller and absorb the corresponding loop-shaping weights into the respective controllers. We then obtain a left coprime factorisation of the weighted controller to express it in the form

$$WC = \tilde{V}^{-1}\tilde{U}.$$

Now consider any rcf [2] of the plant P

$$P = NM^{-1}.$$

Lemma 5.3.1 *Let the ordered pair $[N, M]$ denote a rcf of the plant P, then $[N, W^{-1}M]$ denotes a rcf of the weighted plant PW if $W, W^{-1} \in RH_\infty$.*

[2] Here we are using the unweighted plant because the weight has been absorbed into the controller.

Proof: This is a trivial consequence of the right coprimeness of the pair $[N, M]$ which implies the existence of $X, Y \in RH_\infty$ such that

$$\begin{aligned} [X, \quad Y] \begin{bmatrix} N \\ M \end{bmatrix} &= I \\ \Rightarrow [X, \quad YW] \begin{bmatrix} N \\ W^{-1}M \end{bmatrix} &= I. \end{aligned}$$

■

Our objective is to obtain a normalised rcf of the weighted plant in terms of the selected rcf of the unweighted plant and the selected lcf of the weighted controller. To this end the following lemma proves useful.

Lemma 5.3.2 *[103]*
Given the state-space realisation

$$\begin{bmatrix} N \\ W^{-1}M \end{bmatrix} \stackrel{s}{=} \left[\begin{array}{c|c} A & B \\ \hline C & D \end{array}\right], \quad D^TD > 0,$$

define $\Phi(s) = N^*N + M^*(W^*)^{-1}W^{-1}M$. *Then there exists* $Z, Z^{-1} \in RH_\infty$ *such that*

$$\Phi = Z^*D^TDZ, \tag{5.2}$$

and a state-space realisation of Z *is given by*

$$Z \stackrel{s}{=} \left[\begin{array}{c|c} A & B \\ \hline -F & I \end{array}\right], \quad \textit{where}$$

$F = -R^{-1}(D^TC + B^TX)$, $R = D^TD$ *and* X *is the unique real symmetric stabilising solution of the Riccati equation*

$$(A - BR^{-1}D^TC)^TX + X(A - BR^{-1}D^TC) - XBR^{-1}B^TX + C^TC - C^TDR^{-1}D^TC = 0.$$

Proof: This follows directly from coprimeness of the pair $[N, W^{-1}M]$ and the assumptions made in [103]. ■

Lemma 5.3.3 *Given* $P = NM^{-1}$, *the weight* $W, W^{-1} \in RH_\infty$ *together with* Z *and* R *obtained from lemma 5.3.2, then*

$$PW = (NZ^{-1}R^{-\frac{1}{2}})(W^{-1}MZ^{-1}R^{-\frac{1}{2}})^{-1}$$

is a normalised rcf of the weighted plant PW.

Proof: To show that this factorisation is normalised it suffices to use equation (5.2) to show that

$$R^{-\frac{1}{2}}(Z^*)^{-1}N^*NZ^{-1}R^{-\frac{1}{2}} + R^{-\frac{1}{2}}(Z^*)^{-1}M^*(W^*)^{-1}W^{-1}MZ^{-1}R^{-\frac{1}{2}} = I.$$

Coprimeness follows from $Z, Z^{-1} \in RH_\infty$ and $W, W^{-1} \in RH_\infty$. ■

Recall that our aim is to find a way of introducing the reference signal that is consistent with the original loop-shaping design objectives. Given the lcf $WC = \tilde{V}^{-1}\tilde{U}$, define

$$F \stackrel{\triangle}{=} R^{\frac{1}{2}} Z(\tilde{V}M - \tilde{U}N)^{-1},$$

with Z and R defined according to lemma 5.3.2 and $P = NM^{-1}$ the chosen rcf of the unweighted plant. Two different approaches to introducing the reference signal are shown in Figure 5.5, where

$$[\tilde{U}_1, \tilde{V}_1] = F[\tilde{U},\ \tilde{V}].$$

Recall that any lcf is only unique up to left multiplication by a unit in RH_∞, so $[\tilde{U}_1, \tilde{V}_1]$ still represents a lcf of the weighted controller because F is a unit in RH_∞[3]. Both methods of reference signal injection give the transfer function from r to y as the following

$$y = NZ^{-1}R^{-\frac{1}{2}}r. \tag{5.3}$$

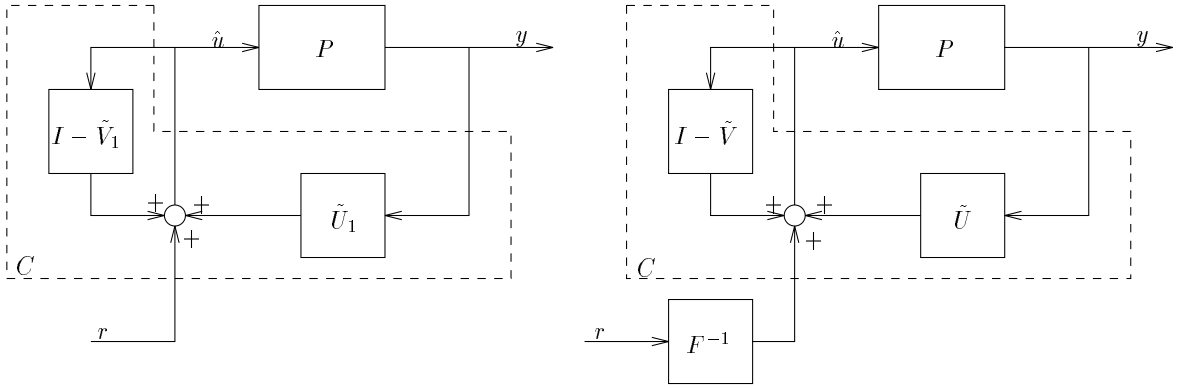

Figure 5.5 *Two alternative techniques for injecting the reference signal.*

In both cases we are assured that the transfer function from the reference signal to the plant output is given by the numerator of a normalised rcf of the weighted plant

$$PW = N_s M_s^{-1} \qquad N_s^* N_s + M_s^* M_s = I,$$

and it is easily shown that the following relation holds

$$\sigma_i(N_s(j\omega)) = \frac{\sigma_i(PW(j\omega))}{\sqrt{1 + \sigma_i^2(PW(j\omega))}}.$$

So where $\underline{\sigma}(PW(j\omega)) \gg 1$ we have $N_s \approx I$. Hence either of these techniques is entirely consistent with the original loop-shaping design objectives as determined by the choice of loop-shaping weights. Although equivalent from this perspective it is felt that the second technique is somewhat advantageous for the following reasons.

[3] In fact $F, F^{-1} \in RH_\infty$ is both necessary and sufficient for the feedback loop to be internally stable.

i. The first technique inflates the McMillan degree of the controller considerably.

ii. Using a prefilter it is possible to approximate the frequency response of the filter without affecting closed-loop stability properties. In fact it is only necessary to approximate the filter response over the frequency range corresponding to the bandwidth of the closed loop, it then being sufficient to roll the filter gain off at higher frequencies where tracking performance is poor anyway.

iii. Prefiltering the reference signal allows complete freedom when factorising the weighted controller. Thus it is possible to choose $[\tilde{U}, \tilde{V}]$ to meet other objectives. For example, we could minimise the Hankel norm of the controller as suggested by Campo [14]. This has the intuitively appealing interpretation of minimising the controller's memory. Alternatively, the techniques being developed by Romanchuk and Smith [76] can be used to select a factorisation which attempts to minimise the incremental gain of some closed-loop operator when the input has a saturation nonlinearity.

5.4 Application to the example system

We now consider an application of the switching technique given in section 5.3 to the mechanical system under consideration. In the first example the only actuation comes from the motor at the base of the beam while in the second example we make use of both actuators.

5.4.1 SISO control

Using the extended H_∞ loop-shaping design technique it was possible to partition the contact range $300mm \leq \rho \leq 500mm$ into four separate intervals and to design an acceptable controller for each interval. Each controller was designed with the following performance objectives in mind.

i. To achieve good reference signal tracking with a bandwidth of approximately 10 rad/s and no steady state error.

ii. To increase the level of damping in the first two vibration modes and to ensure stability in the presence of unmodelled high frequency dynamics.

iii. To achieve an acceptable level of robust stability in order to accommodate model/plant mismatch and to ensure stability to time-varying perturbations.

The first objective is in line with what would be expected of a high performance violin bowing machine. The second objective arises out of a need to damp out vibrations in the low frequency vibration modes which are easily excited by movement of the force transducer. The third objective relates to an interesting but open question. By bounding $b_{P,C}$ from below, the small gain theorem guarantees stability of the closed loop even when the contact position is time varying; provided these variations are sufficiently slow. However, analytical techniques for determining the stability of non-autonomous linear systems tend to be highly conservative, making it difficult to characterise the trajectories for which the system remains stable. For systems which have time-invariant real parameter dependence available robust stability tests include Kharitonovs theorem and recent extensions [5] and the real-μ upper bound with frequency dependent D and G scales. For systems having real time-varying parameter dependence there are essentially two tests for robust stability, quadratic stability and the real-μ upper bound with constant D and G scales. Since both allow for arbitrary rates of parameter variation they are seen as being conservative. Of course this was our motivation for introducing the notion of $\mathcal{Q}_e$ stability for LPV systems in chapter 2.

Recent advances in LMI techniques indicate that finding a Lyapunov function to guarantee stability for a specified class of real parameter trajectories can be posed as a convex feasibility problem [12] and is thus amenable to computation. These techniques also allow an explicit constraint to be placed on the rate of parameter variation thereby reducing conservativeness. For systems having linear parameter dependence Gahinet et al [35] have considered the problem of establishing stability using a parameter-dependent quadratic dissipation function and LMI techniques to search for the dissipation function. Similarly, LMI's allow the induced-norm properties

of the closed loop to be investigated when the system is subjected to bounded-rate parameter variations. By making use of the bounded real lemma[4] this can also be posed as a convex feasibility problem [12]. From a theoretical viewpoint convexity is very important because it means that a solution to the specified problem can always be found when one exists. From a practical viewpoint the computations are numerically intensive and it was found that the state dimension of the controllers designed in this section made the analysis unrealistic, even after performing model reduction on the controllers. So we will have to be satisfied with an experimental investigation of the stability properties which we undertake in chapter 6, returning to make a more thorough examination of the LMI techniques in chapter 7.

The relevant properties of each of the controllers and their respective loop-shaping weights are given in Table 5.1 and Table 5.2.

Controller	Weight	Filter	$\min_{\rho\in F_\rho} b_{P,C}$	$\min_{\rho\in F_\rho} b_{P,\hat{C}}$	dim $\hat{C}$	Range
C_1	W_1	F_1	0.2583	0.2416	15 states	$300mm \leq \rho \leq 365mm$
C_2	W_2	F_2	0.2726	0.2451	15 states	$360mm \leq \rho \leq 425mm$
C_3	W_3	F_3	0.2587	0.2401	18 states	$420mm \leq \rho \leq 460mm$
C_4	W_4	F_4	0.2627	0.2429	10 states	$460mm \leq \rho \leq 500mm$

Table 5.1 *Relevant properties of the loop-shaping controllers.*

Controller	Weight	Filter
C_1	$W_1 = \left(\frac{16}{s}\right)\left(\frac{200}{s+200}\right)\left(\frac{180^2}{600^2}\frac{s^2+240s+600^2}{s^2+64s+180^2}\right)$	$F_1 = \left(\frac{18}{s+18}\right)$
C_2	$W_2 = \left(\frac{14}{s}\right)\left(\frac{200}{s+200}\right)\left(\frac{200^2}{600^2}\frac{s^2+240s+600^2}{s^2+160s+200^2}\right)$	$F_2 = \left(\frac{20}{s+20}\right)$
C_3	$W_3 = \left(\frac{15}{s}\right)\left(\frac{200}{s+200}\right)\left(\frac{160^2}{600^2}\frac{s^2+240s+600^2}{s^2+128s+160^2}\right)$	$F_3 = \left(\frac{20}{s+20}\right)$
C_4	$W_4 = \left(\frac{15}{s}\right)\left(\frac{200}{s+200}\right)\left(\frac{160^2}{600^2}\frac{s^2+240s+600^2}{s^2+128s+160^2}\right)$	$F_4 = \left(\frac{15}{s+15}\right)$

Table 5.2 *Loop-shaping weights and filters.*

The integral action in the weights ensures no steady state tracking error and allows the bandwidth to be adjusted easily. The weights also ensure a sufficiently high roll-off rate above the second natural frequency, to gain-stabilise unmodelled high frequency dynamics. For robust stability it was decided that $b_{P,C}$ should be bounded from below with $b_{P,C} \geq 0.25$ for all permissible values of ρ. In light of the results of chapter 4 where it was observed that high order rational function approximations are necessary when extracting the controller obtained from the extended loop-shaping design procedure, it is unrealistic to expect to be able to implement the controllers without performing model reduction first. For this reason each of the weights was adjusted to

[4]The bounded real lemma only gives sufficient conditions for bounding the induced norm of an LPV system.

ensure that the controllers performed slightly better than necessary for each of their respective intervals. This gave a small margin of tolerable degradation in $b_{P,C}$ which was exploited when performing model reduction (recall theorem 4.2.13).

Model reduction of the respective controllers was performed by approximating the normalised graph symbol of each controller [62] using optimal Hankel norm approximation [39]. To determine the degradation in performance resulting from approximation, the achieved stability margin was computed for the full-order controllers and for the reduced-order approximants over a grid of 40 equally spaced points covering each of the physical intervals. The controllers listed in Table 5.1 represent an acceptable tradeoff between the state dimension of the reduced-order controllers and degradation in $b_{P,C}$ for the chosen model reduction technique. Figures 5.6 and 5.7 show the loop shapes of the weighted plant at the centre of each design interval together with the achieved loop shape after introduction of the reduced-order controllers. The controller bandwidth is approximately the same in all four cases although the loop gain around the first natural frequency is lower for the final design $460mm \leq \rho \leq 500mm$ than for the other designs. This is not surprising when we consider that the first mode becomes unobservable as ρ tends to $500mm$, resulting is rapid variation in the frequency response around this frequency over the last design interval. We can also see that the effect of the controller is not limited to the first two vibration modes and for positions where the modal amplitude of the third vibration mode is large we can also expect some attenuation. To check for interaction with high frequency modes ν-gap measurements were performed and once again indicated a high level of robustness to unmodelled dynamics.

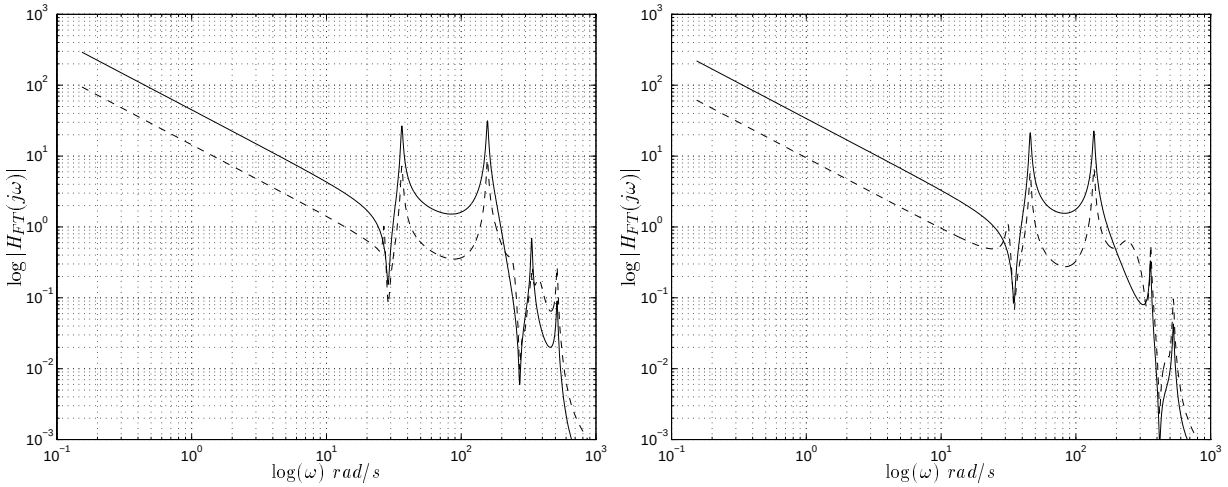

Figure 5.6 *Nominal loop shape (solid), achieved loop shape (dashed),* $\rho = 330mm$ *and* $\rho = 390mm$.

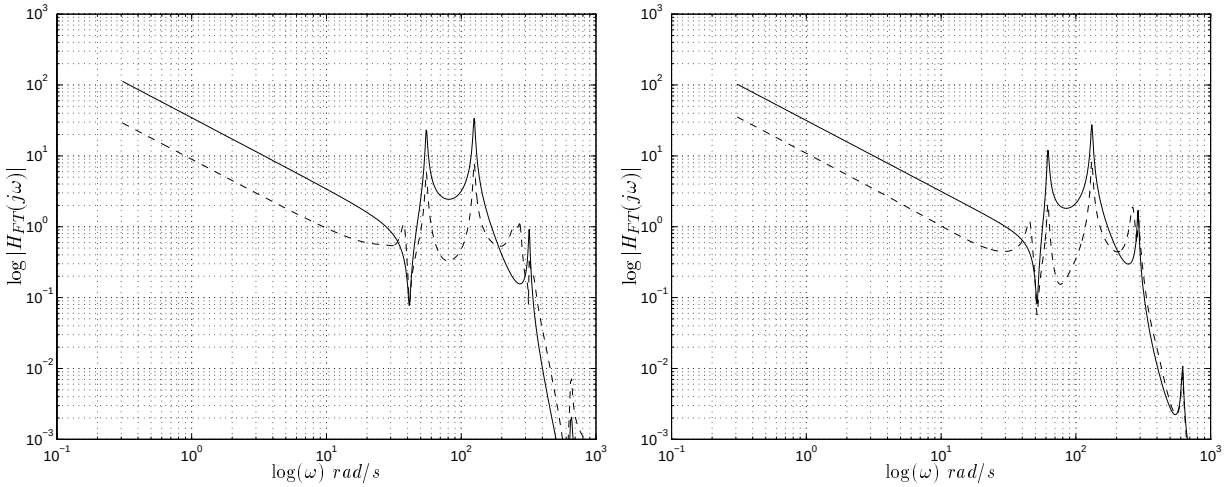

Figure 5.7 *Nominal loop shape (solid), achieved loop shape (dashed),* $\rho = 440mm$ *and* $\rho = 480mm$.

Having performed model reduction to obtain satisfactory reduced-order controllers it is now possible to absorb the loop-shaping weights into the respective reduced-order controllers and to compute prefilters using the technique outline in section 5.3. Although the loop-shaping weights are not invertible they can be approximated arbitrarily closely by stable minimum phase rational functions to facilitate computation of the prefilters. On doing this it was found that the frequency response of each of the prefilters was approximately flat over the controller bandwidth. This made it possible to approximate the prefilters with first order lags while still achieving good tracking performance. From an implementation perspective this is ideal since it reduces the number of states that must be updated in real time. Since we are essentially free to choose any factorisation of the weighted controller when implementing the switching scheme it was decided that a normalised coprime factorisation would be preferable. This ensures that there is no direct feedthrough from the measured plant input to the controller output which could give rise to problems with noisy measurements. A block diagram representation of the final switching scheme is given in Figure 5.8.

To gain some insight into the tracking performance of this controller we simulate the closed-loop step response at $20mm$ intervals covering each of the four design intervals. The results can be found in Figures 5.9 and 5.10. To investigate the effectiveness of this scheme at achieving bumpless transfer we simulate the step response of the closed loop at the three switching positions $\rho = 360mm$, $\rho = 420mm$ and $\rho = 460mm$. The results can be found in Figures 5.11 and 5.12. In each plot the output of the online controller (solid) can be compared to the output of the next scheduled controller (dashed). The two distinct curves correspond to the two switching possibilities that arise at each switching point (ie: at $\rho = 360mm$ C_1 online and C_2 off-line, or alternatively, C_2 online and C_1 off-line). In each of these simulations the off-line controller follows the actual plant input very closely indicating that satisfactory performance should be

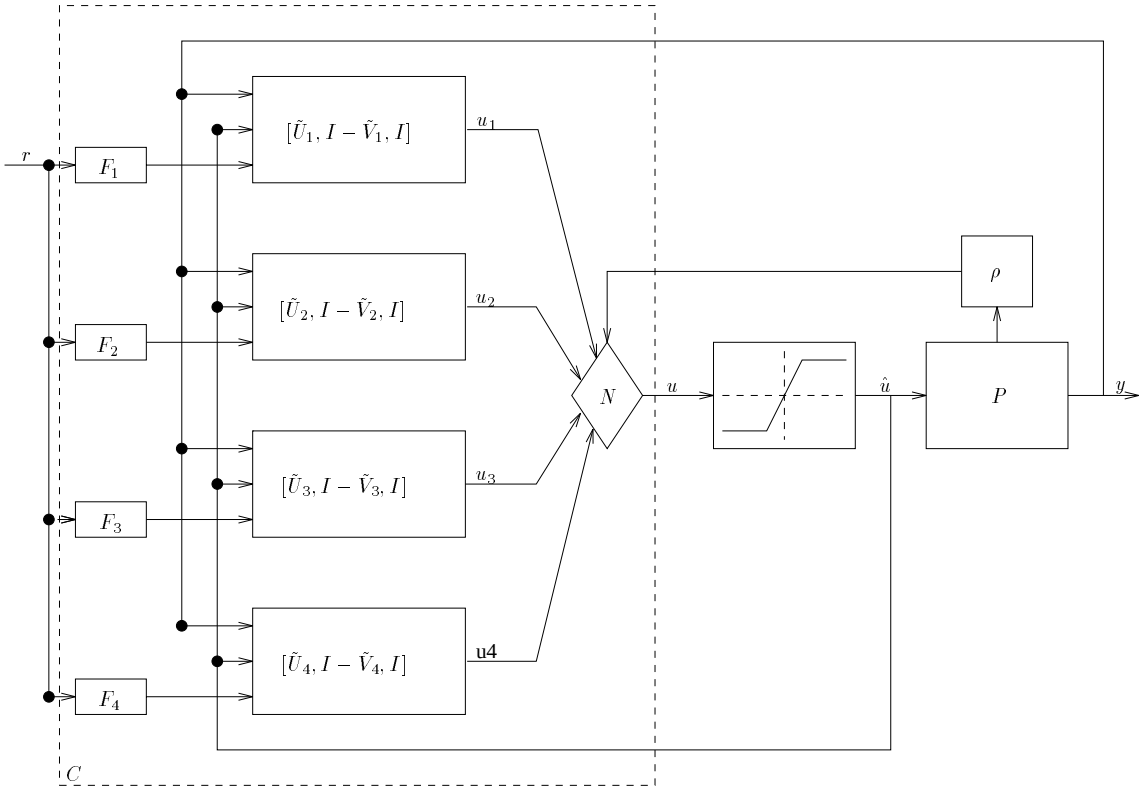

Figure 5.8 *Switching implementation.*

achieved by the switching scheme (although these are only frozen-parameter results). The true effectiveness of this scheme is best characterised experimentally on a real rig when switching under more general conditions. This is examined in chapter 6.

We conclude this section by observing that the cost of controlling this particular system is high. This can be attributed to the properties of the underlying class of systems being considered and to the severe parameter dependence exhibited by this particular system. Models of flexible structures invariably contain a relatively large number of states in order to accurately reflect the behaviour of the physical system and to ensure that the controller does not destabilise modes lying beyond the control bandwidth. When combined with strong parameter dependence this leaves us with the task of switching between a number of high-order controllers all of which must be simultaneously updated to ensure satisfactory switching characteristics. We will require relatively extensive computational power to implement this controller.

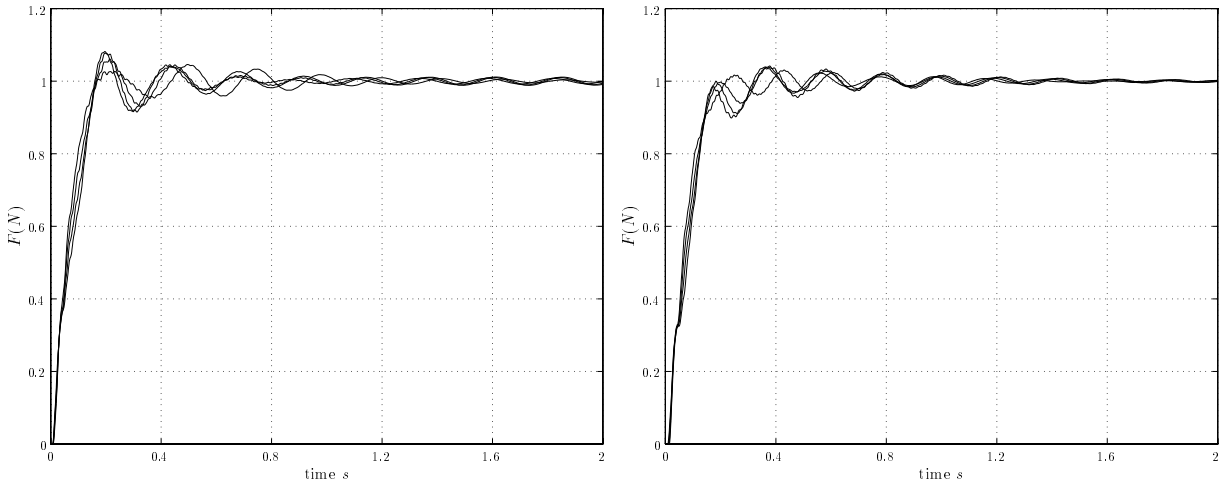

Figure 5.9 *Frozen-parameter closed-loop step responses,* $300mm \leq \rho \leq 360mm$ *and* $360mm \leq \rho \leq 420mm$ *respectively.*

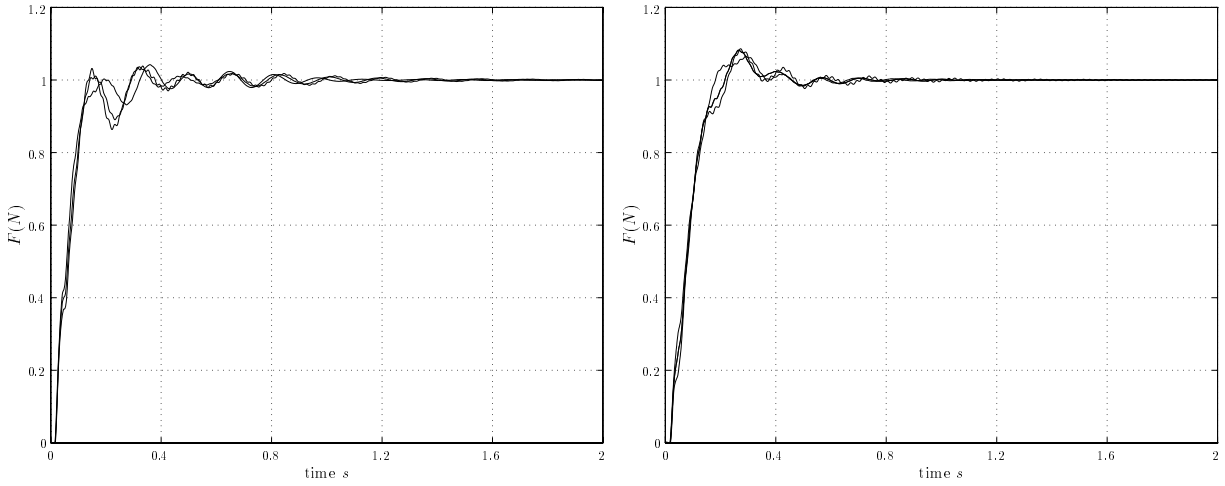

Figure 5.10 *Frozen-parameter closed-loop step responses,* $420mm \leq \rho \leq 460mm$ *and* $460mm \leq \rho \leq 500mm$ *respectively.*

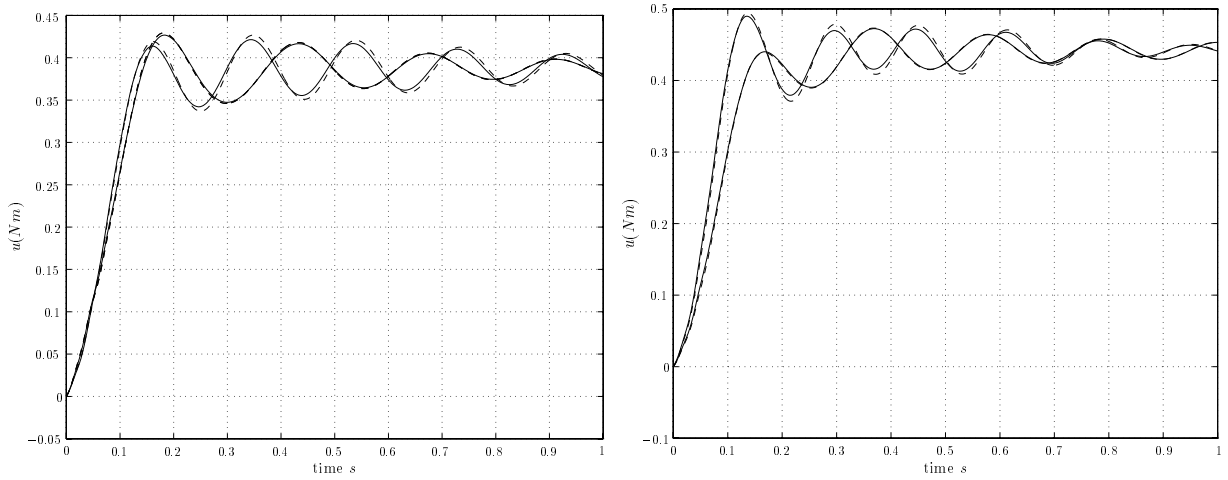

Figure 5.11 *Controller output signals, solid lines - online controller, dashed lines - next scheduled controller,* $\rho = 360mm$ *and* $\rho = 420mm$ *respectively.*

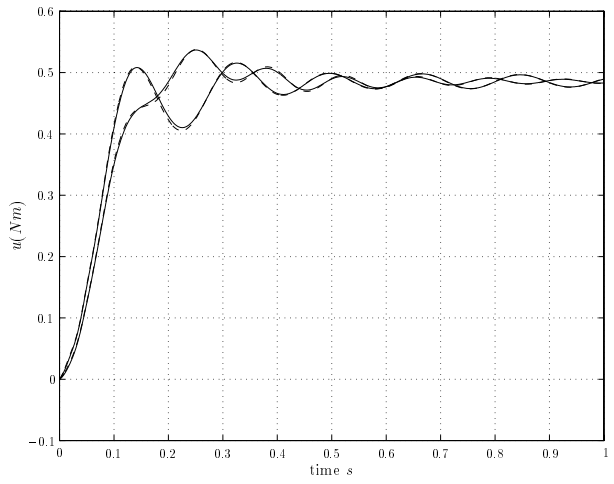

Figure 5.12 *Controller output signals, solid lines - online controller, dashed lines - next scheduled controller,* $\rho = 460mm$.

5.4.2 MISO control

In chapter 4 we demonstrated how the ν-gap metric can be used as a design tool to help in the selection of actuator placements to make the system easier to control (in the sense that any acceptable controller at some nominal contact position will be less sensitive to the given parameter variations). Even when this is done, the range of parameter variation that can be tolerated by a single controller is limited. This makes it necessary to use more than one controller to cover large parameter variations. The switching problem considered here is essentially the same as that considered in the previous section except we now have more choice when selecting the controller at the chosen design points. In particular, if the central controller solving the normalised coprime factor robustness problem is selected then it is possible to use the observer structure of this controller (shown in Figure 5.13) to inject reference signals without inflating the McMillan degree of the controller (or the need for prefilters) [87]. The observer-based controller shown is for the weighted plant PW which is assumed to have a strictly proper state-space realisation $(A, B, C, 0)$. The state feedback gain F and the observer gain L are obtained by solving two algebraic Riccati equations. This observer structure ensures that the transfer function from the reference signal to the controlled output is given by the numerator of a normalised coprime factorisation of the weighted plant. Its structure is ideal for switching because, with the exception of the weight in the forward loop, the controller is implicitly in a factorised form and has a state dimension equal to that of the weighted plant.

Since we now have two actuators and only one controlled output there is a lot of freedom when selecting the relative contribution made by each actuator. When using this extra freedom it is necessary to take care to match the transfer function from the reference signal to the output of each of the individual controllers. If this is not done it is possible to obtain a controller that has very poor switching characteristics. This is essentially because the plant has a nontrivial kernel, so the mapping from its inputs to its output is not unique. Failure to account for this fact makes it plausible that two different controllers could produce different actuator demand signals when regulating the output to the same level. If at some instant of time a switch is made between two such controllers then a step in the actuator signal would result.

Following the procedure developed in chapter 4 it is possible to use the tip actuator to eliminate the effect of the antiresonance lying within the control bandwidth, thereby reducing sensitivity to variations in the contact position[5]. Additionally, if a single weight can be used to shape the open-loop frequency response over the entire parameter interval then the overall complexity of the controller can be significantly reduced. This important practical consideration makes it worthwhile trying to find a weight that achieves a satisfactory loopshape for all parameter values. Since the motor loop and force loop both have gains that are inversely proportional to ρ we will need to use a parameter-dependent weight if the same performance objectives are to be met for all feasible parameter values. Using the performance objectives given previously, a

[5]The model has been updated to account for the inertial properties of the tip magnet.

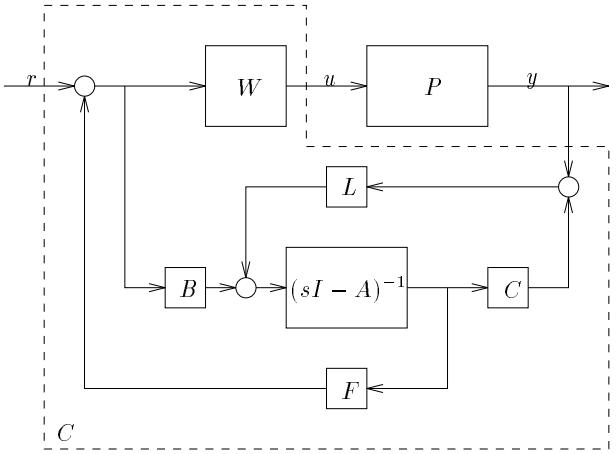

Figure 5.13 *The observer structure of the central H_∞ loop-shaping controller.*

weight of the form

$$W_1(\rho) = \rho\tilde{W}_1 = \frac{\rho}{10.5}\left(\frac{s+200}{s}\right)\left(\frac{120^2}{600^2}\frac{s^2+240s+600^2}{s^2+120s+120^2}\right),$$

was used to shape the frequency response of the motor loop. This weight rolls off at a lower frequency than the corresponding weights used in previous designs in order to reduce the loop gain around the third natural frequency (we have to settle for a compromise because the roll-off characteristics of the weight have to be acceptable for all parameter values). Following the same reasoning used in chapter 4, the weight used to shape the frequency response of the force loop was selected to increase the loop gain around frequencies near the antiresonance in the control bandwidth and around the first vibration mode, thereafter rolling it off to gain-stabilise the high frequency modes. The weight

$$W_2(\rho) = \rho\tilde{W}_2 = 2.2\rho\left(\frac{s}{2s+30}\right)\left(\frac{80^2}{s^2+80s+80^2}\right),$$

achieved a satisfactory loop shape. Using the diagonal input weight

$$W(\rho) = \begin{bmatrix} W_1(\rho) & 0 \\ 0 & W_2(\rho) \end{bmatrix},$$

it was possible to partition the parameter interval into three closed intervals $300mm \leq \rho \leq 390mm$, $390mm \leq \rho \leq 450mm$ and $450mm \leq \rho \leq 500mm$ with the central controller designed at the middle of each interval achieving a satisfactory stability margin $b_{P,C}$. The details of each controller are listed in Table 5.3. In order to implement the switching scheme the observer structure of each controller was implemented in the feedback path with the output of the appropriate controller being selected at the input to the loop-shaping weight. This form of controller allows

Controller	$\min_\rho b_{P,C}$	dim C	Range
C_1	0.2554	14 states	$300mm \leq \rho \leq 390mm$
C_2	0.2638	14 states	$390mm \leq \rho \leq 450mm$
C_3	0.2674	14 states	$450mm \leq \rho \leq 500mm$

Table 5.3 *Relevant properties of the loop-shaping controllers.*

the reference signal to have two components whereas there is only one controlled output. Where the loop gain of the shaped plant is high it is possible to inject the reference signal with arbitrary directionality provided its magnitude corresponds to the magnitude of the desired output. This allows the inherent lack of uniqueness at the plant input to be exploited by the designer to select the relative actuator effort. To keep this consistent with the capabilities of the actuators on the physical system, and with the objective of achieving bumpless transfer, the reference signal was injected into the individual controllers with a directionality that made the input to the weight driving the force loop zero at DC. To prevent windup the loop-shaping weight was factorised to get

$$W(\rho) = \rho \tilde{V}_w^{-1} \tilde{U}_w = \rho \begin{bmatrix} \tilde{W}_1 & 0 \\ 0 & \tilde{W}_2 \end{bmatrix},$$

and implemented with internal feedback using a measurement of the physical plant input. Once again, a normalised coprime factorisation was chosen to prevent measurement noise from being coupled directly its output. The overall structure of the controller is shown in Figure 5.14. Simulations of the closed-loop step response performed at equally spaced contact positions covering the three controller ranges $300mm \leq \rho \leq 390mm$, $390mm \leq \rho \leq 450mm$ and $450mm \leq \rho \leq 500mm$ are shown in Figures 5.15 and 5.16. These are comparable to the SISO step responses except the MISO controllers exhibit less oscillation and settle to a constant level more quickly. In order to gain insight into the effectiveness of the observer-based technique at achieving good switching characteristics we simulate the closed-loop response to obtain the signals generated at the input to the loop-shaping weight following a step change in the reference signal. Two simulations were performed corresponding to the two switching positions $\rho = 390mm$ and $\rho = 450mm$. For bumpless transfer the output of the online controller, which is connected to the loop-shaping weight, and the controller that is about to be switched into the loop should be identical. In Figure 5.17 the solids lines correspond to the output of the online controller and the dashed line correspond to the output of the off-line controller at the switching point $\rho = 390mm$. The separate plots correspond to the two different switching configurations that can occur. Similarly, Figure 5.18 shows the same information at the switching point $\rho = 450mm$. Although the correspondence between the outputs of the online and off-line controllers is worse than that achieved in the previous section, the discrepancy between the signals is still fairly small. We expect that the controller will have satisfactory switching characteristics since the results presented here correspond to a rapid transient (although the parameter is fixed). We will examine this is detail in chapter 6.

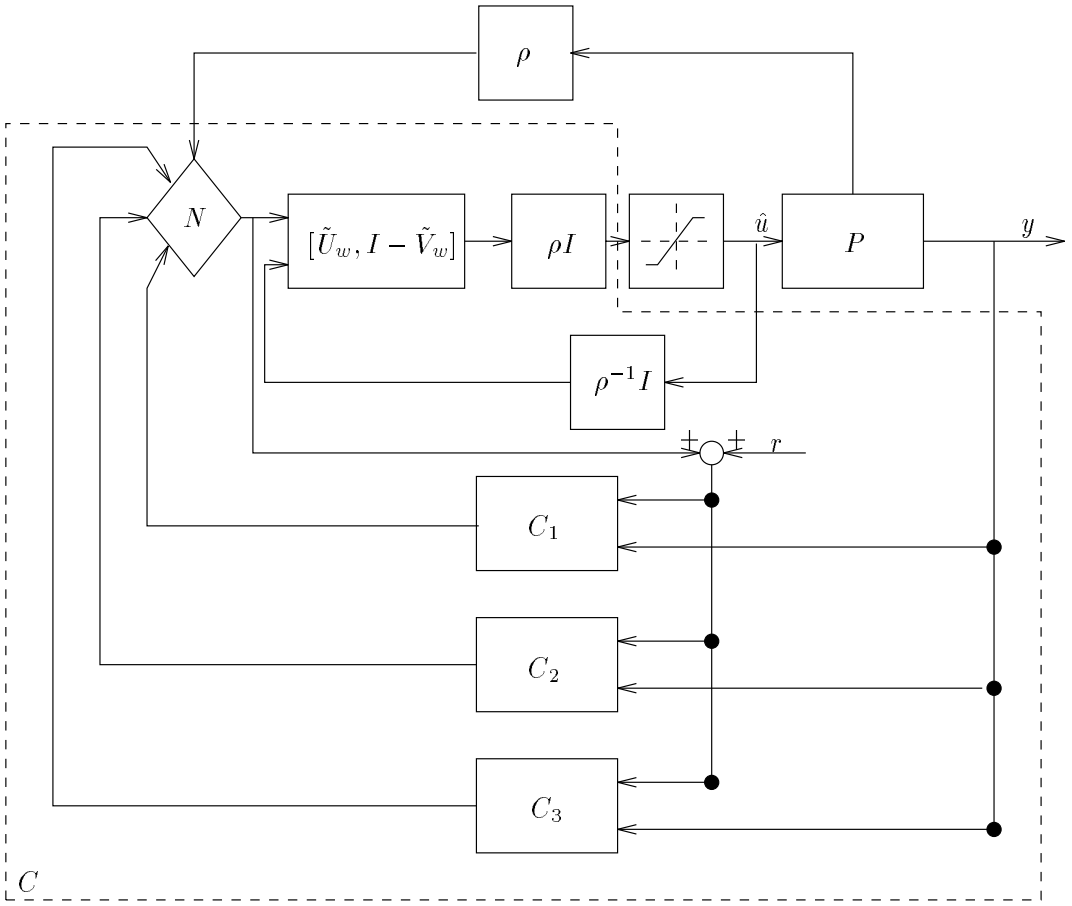

Figure 5.14 *Implementation structure of the MISO controller.*

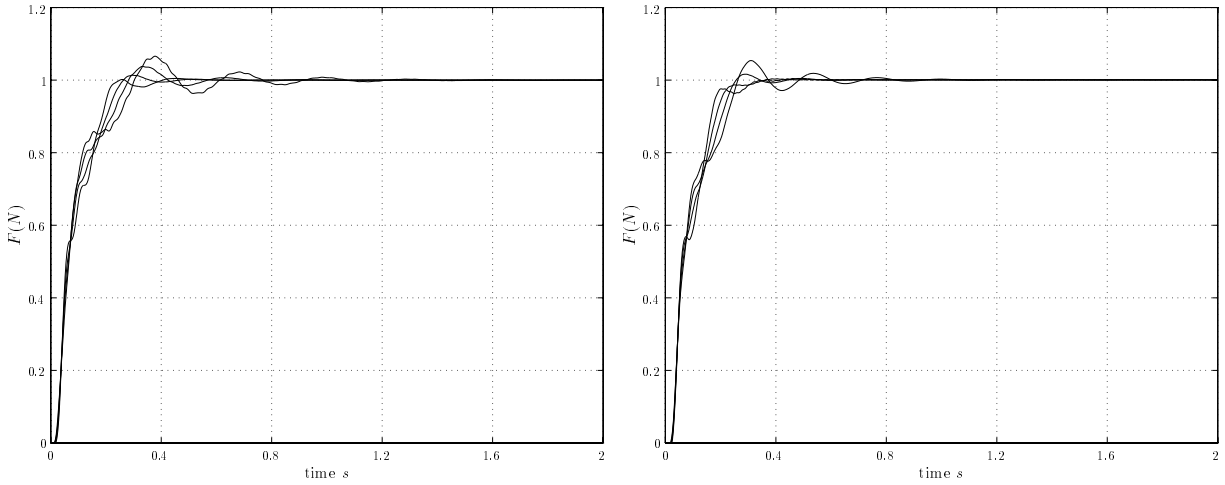

Figure 5.15 *MISO step response* $300mm \leq \rho \leq 390mm$ *and* $390mm \leq \rho \leq 450mm$.

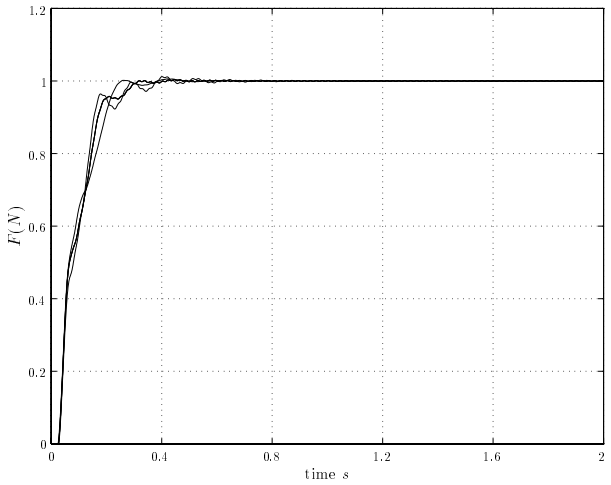

Figure 5.16 *MISO step response* $450mm \leq \rho \leq 500mm$.

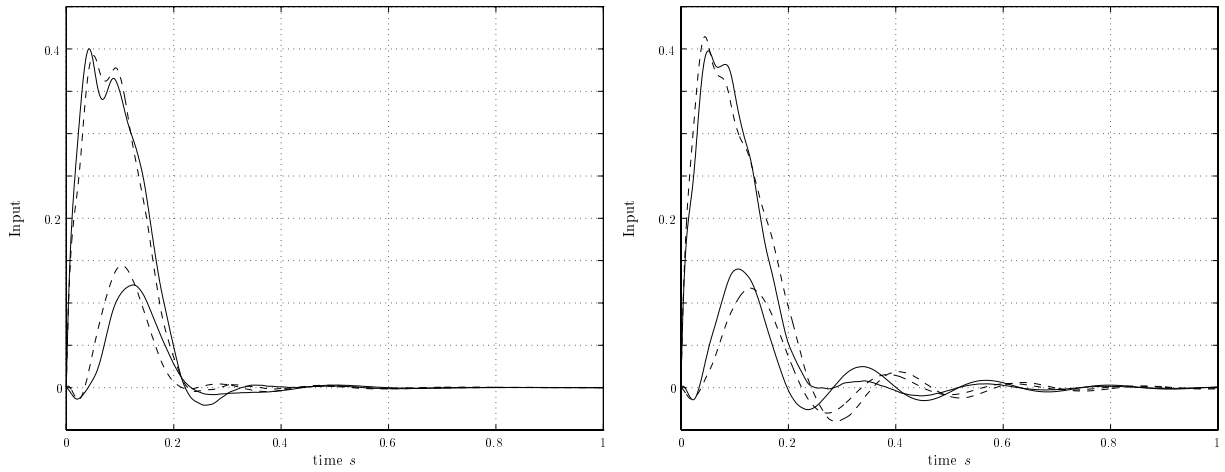

Figure 5.17 *Inputs to the loop-shaping weight following a step change in the demand signal ($\rho = 390mm$).*

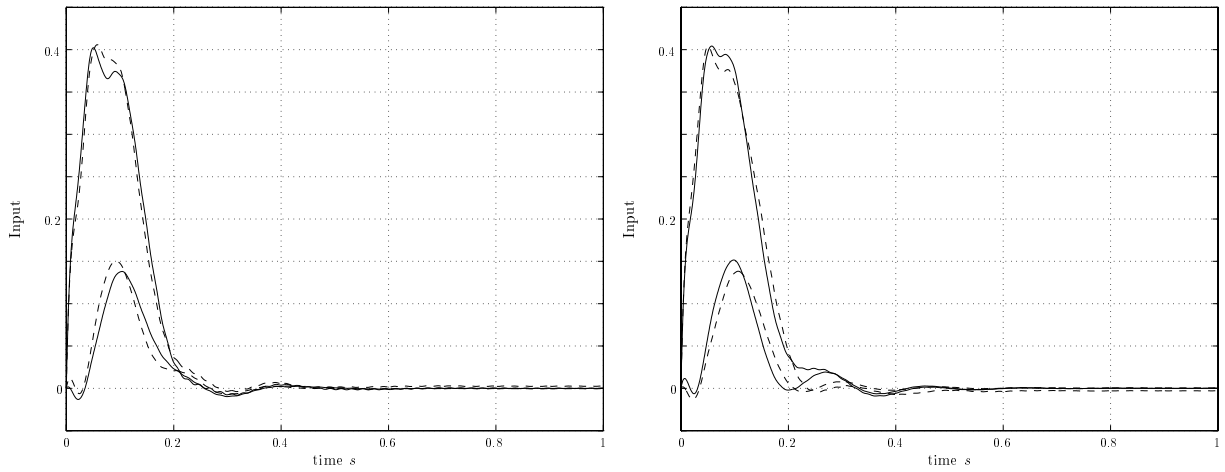

Figure 5.18 *Inputs to the loop-shaping weight following a step change in the demand signal ($\rho = 450mm$).*

5.5 Summary

In this chapter we have considered the problem of extending the range of parameter variation that can be tolerated by a single LTI controller using switching techniques. This allowed us to use a family of robust LTI controllers to cover large parameter variations while still achieving certain closed-loop performance objectives. The unified anti-windup and bumpless transfer framework developed by Campo has been central to our approach, allowing us to switch between controllers without exciting flexible modes. We have also considered the problem of introducing reference signals into the closed loop within the bumpless transfer framework in a manner which is consistent with the H_∞ and the extended H_∞ loop-shaping design procedures. Two alternative techniques for reference signal injection have been outlined, one of which allows the controller to be factorised so as to meet other closed-loop objectives. Although we have not exploited this freedom, choosing to implement a normalised coprime factorisation of the controller, this freedom could be exploited to improve anti-windup characteristics. We have also examined various difficulties that can arise when applying these switching techniques to non-square plants indicating why these difficulties arise and how they can be overcome. Closed-loop simulations suggest that the switching technique should achieve satisfactory closed-loop performance. In chapter 6 we will undertake a thorough experimental evaluation of the switching performance, allowing us to evaluate the effectiveness of the LTI design approach for this class of systems.

6

Experimental Evaluation of the LTI Approach

6.1 Purpose of the experiments

In this chapter we examine the problem of force control through a constrained flexible manipulator experimentally. In the previous chapters we have shown that it is possible to design LTI controllers that are robust to both plant/model mismatch and to predictable variations in the plant dynamics. The purpose of this chapter is to evaluate the performance of these controllers under realistic conditions. We will investigate the tradeoff between performance and robustness as encapsulated by the parameter $b_{P,C}$ by implementing the three controllers designed in chapter 4. We also investigate the effectiveness of the switching methodology developed in chapter 5 and determine how easy it is to extend the range of tolerable parameter variation using this technique. Of particular interest is the effectiveness of the switching technique at achieving bumpless transfer and we will examine this under some fairly general parameter trajectories. As an aside, this also allows us to evaluate the antiwindup properties of the controller. The final objective of these experiments is a thorough evaluation of closed-loop performance under general time-varying perturbations. The difficulties associated with characterising closed-loop performance in a non-conservative manner using theoretical techniques makes an experimental evaluation particularly worthwhile. By examining the performance of the controllers when subjected to a series of trajectories of increasing complexity it is possible to gain some insight into the effectiveness of the LTI design methodology.

6.2 Experimental equipment

6.2.1 The test rig

A photograph of the experimental equipment is shown in Figure 6.1. The system is built around a rigid steel air table having dimensions $600mm \times 150mm \times 80mm$. At one end of the air table is a brushless DC motor which is housed in an adjustable aluminium housing so that the vertical position of the motor can be varied relative to the air table. A $670mm \times 25.4mm \times 1.6mm$ steel beam is mounted directly to the shaft of the motor via an aluminium hub which approximates an ideal clamp. The air table carries a $250mm \times 190mm \times 35mm$ steel block which, when levitated by an air supply, is free to slide along the length of the table without the effects of friction and without generating excessive background vibration. Mounted on this block is a force transducer

Figure 6.1 *Mechanical components of the experimental equipment.*

(strain gauge variety) which is used to measure the contact force developed between itself and the elastic beam. Contact between the beam and the force transducer is made through a small roller bearing in order to accommodate changes in the contact position. The exact position of the steel block relative to the table is measured by an LVDT having a stroke of $250mm$. A small high intensity permanent magnet can be attached to the tip of the beam using a locknut arrangement. This allows a force to be exerted on the tip of the beam by placing the magnet in the core of a copper coil. The length of the coil is such that nonlinearities arising from movement of the magnet within the magnetic field generated by the coil are small. The coil is suspended independently of the beam and can be adjusted vertically to align the magnet along its axis.

The force transducer is connected to a bridge amplifier. This energises the strain gauge circuitry with a $3kHz$ carrier signal and demodulates the transducer output to produce a voltage which is proportional to the contact force. The output of the bridge amplifier can be filtered by a Kemo filter to prevent aliasing when the controllers are implemented digitally. The motor at the base of the beam is driven by a $180W$ current amplifier which has a gain of $1A/V$ and a

$\pm 10V$ limit on the output voltage. This ensures that the motor produces a torque which is proportional to the voltage applied to the amplifier, making it unnecessary to account for the dynamics of the motor. The output from the current amplifier is linear over the range $0-200Hz$ and gradually rolls off above $200Hz$ (well beyond the bandwidth of any of the controllers). An identical amplifier capable of delivering $100W$ is used to drive the coil at the tip of the beam.

6.2.2 The controller implementation environment

Controller synthesis using LQG, H_∞ and μ-synthesis techniques often results in controllers which have a high state dimension, possibly multiple inputs and outputs, and no simple structure. Implementation of these controllers using analogue circuitry is infeasible, if not impossible. This means that the controllers must be discretized and implemented digitally and if they are to perform comparably with their ideal continuous time counterparts, high sampling rates and accurate conversion of analogue signals is called for. These challenging requirements are being met through the development of high performance digital signal processing (DSP) chips which have already reached a stage of development where the implementation of complicated controllers is less time consuming. One of the commercially available DSP based products is produced by dSPACE GmbH as the "DSP CIT pro Control Implementation Tool". This is supplied as a series of add-on cards for an IBM compatible PC.

The main processor board (dSPACE no DS1003) runs the Texas Instruments TMS320 C40 DSP chip which supports floating point arithmetic. This runs at clock speed of $33MHz$ and has a $40ns$ single cycle execution time with 40×32 bit single cycle floating point multipliers and 12×40 bit accumulators. The board has its own high speed memory for storing the controller instructions as well as 8192×32 bit words of dual port memory for monitoring key variables. The DS1003 board is connected to its peripheral boards via a high speed bus which allows for stand-alone operation independent of the PC. Analogue to digital conversion is performed by the DS2002 board. This has two independent 16-bit sequential analogue to digital converters with separate sample and holds. Each converter has a $5\mu s$ conversion time on top of a $0.9\mu s$ sample/hold acquisition time. The converters can be multiplexed to give up to 32-channels of input (16 for each converter) with a multiplexing time of $1.2\mu s$. The board has programmable gain which allows the input voltage range to be selected as either $\pm 10V$ or $\pm 5V$ to best match the range of the analogue signals, thereby reducing quantisation effects. Digital to analogue conversion is performed by the DS2101 board which has five fully parallel 12-bit D/A converters. Each converter has a $3\mu s$ settling time and has programmable gain which allows the output range to be toggled between $\pm 10V$ and $\pm 5V$.

Development time is greatly reduced by the implementation package Impex. This allows LTI controllers developed in a Matlab environment to be converted directly into C-code in a form that is suitable for real time implementation. The controller is read into Impex as the state-space quadruple (A, B, C, D), and if it is not already in discrete form, it can be discretized using either step invariant, ramp invariant or bilinear discretization. Impex also facilitates state transformation of the LTI controller matrices in order to reduce the number of multiplications and

additions required during real time implementation. To this end the controller A matrix can be converted into a real modal form, or if this causes numerical difficulties, into an upper triangular Schur form using unitary state transformation matrices. The various inputs and outputs of the controller can then be assigned to different channels of the A/D and D/A converters and following this, C-code can be generated. The C-code can be downloaded to the DSP directly and implemented as a real time controller or it can be adjusted by incorporating switching logic or gain-scheduling to allow implementation of switched or LPV controllers.

6.3 SISO tests

6.3.1 Calibration

Theoretical models of the mechanical system were developed in chapter 3. The LTI model was developed to approximate the frozen-parameter behaviour of the system while the LPV model is believed to be a more accurate representation when the system is time varying. Both of these models require experimental identification of various physical parameters. For example, both models require an estimate of the combined inertia of the motor and hub assembly, while the LTI model also requires measurements of the modal damping factors. We are also interested in determining to what extent simple physical dissipation models, which provide a more appropriate method of modelling damping in the LPV case, can account for the observed physical damping. Again, this requires us to estimate the coefficients that appear in the damping models, and this is another objective of this section.

The different physical parameters were obtained from calibration tests performed with the force transducer fixed at a set of equally spaced points along the accessible length of the beam. Contact between the beam and the force transducer was maintained by preloading the beam with a constant force generated by an elastic spring pressing against the beam from the opposite side to the force transducer. For the SISO experiments the magnet was not attached to the tip of the beam making it unnecessary to account for the inertial properties of the magnet initially. Logarithmic sine sweeps were applied to the amplifier driving the motor loop to ensure a flat excitation spectrum over the frequency range $0 - 80Hz$. The excitation signal was generated digitally at a sampling rate of $250Hz$ covering the frequency interval over a $40s$ period. Once the excitation had stopped the system response was sampled for a further $10s$ to ensure that it had decayed to zero by the end of each test. This made the response truly periodic hence preventing spectral leakage ([10],[64]) and making accurate computation of the systems transfer function less difficult (no windowing was needed when computing the spectra). Aliasing of any high frequency components in the measured signal due to sampling was prevented by low pass filtering the measured response using the Kemo filter with a cut off frequency of $125Hz$. During identification it was found that fairly large amplitude excitation signals were required to get a linear response from the beam. It was observed that small excitation signals resulted in a nonlinear response around the second natural frequency (identifiable by a warping of the resonant peak). This was attributed to unavoidable friction between the motor shaft and its housing, which was clearly not negligible.

When estimating modal damping factors for the LTI model the small modal overlap made it possible to use simple circle fitting techniques [29] to obtain the damping estimates. In fact it was found that each of the respective modal damping constants could be approximated reasonably accurately as being constant along the accessible length of beam. The hub inertia was estimated by adjusting its value in the model until the predicted and measured frequency responses coincided at a chosen measurement position ($\rho = 350mm$). To be certain that this was correct it was then verified that the measured and predicted frequency responses matched accurately at the other measurement positions. Suitable damping constants for the LPV model were obtained in a similar manner. As expected, it was found that the simple dashpot damping factor c and the viscous dissipation factor c_d (which were used to model damping in our flexible beam in chapter 3) were capable of producing reasonably accurate damping estimates for the first two vibration modes but imposed a somewhat artificial variation in the higher frequency modes. This indicates that the use of simple models to account for damping in LPV structures will generate models of limited accuracy, a fact that should always be considered during controller synthesis. Values of the physical parameters estimated from these calibration sweeps are listed in Table 6.1.

Model	Damping parameters	Inertia
LTI	$\zeta_1 = 1.5\%$ $\zeta_2 = 1.5\%$ $\zeta_3 = 1.0\%$ $\zeta_4 = 1.0\%$	$I_h = 5.3 \times 10^{-4} kg.m^2$
LPV	$c = 4.5 \times 10^{-3} Nm.s$ $c_d = 7 \times 10^{-1} Ns/m^2$	$I_h = 5.3 \times 10^{-4} kg.m^2$

Table 6.1 *Estimated physical parameter values.*

The frequency responses measured at $\rho = 300mm, 350mm, 400mm, 450mm$ and $500mm$ can be compared to the frequency responses generated by the theoretical models in Figures 6.2 through 6.4. These indicate that the LTI model is slightly more accurate than the LPV model, both in terms the natural frequency estimates and the frozen-parameter damping estimates, although for both models agreement is good over the measured frequency range. This gives us some confidence when using them to design controllers. In fact the LTI model formed the basis of an interesting model validation study in [18]. We give a brief discussion of this and its implications in section 6.3.2.

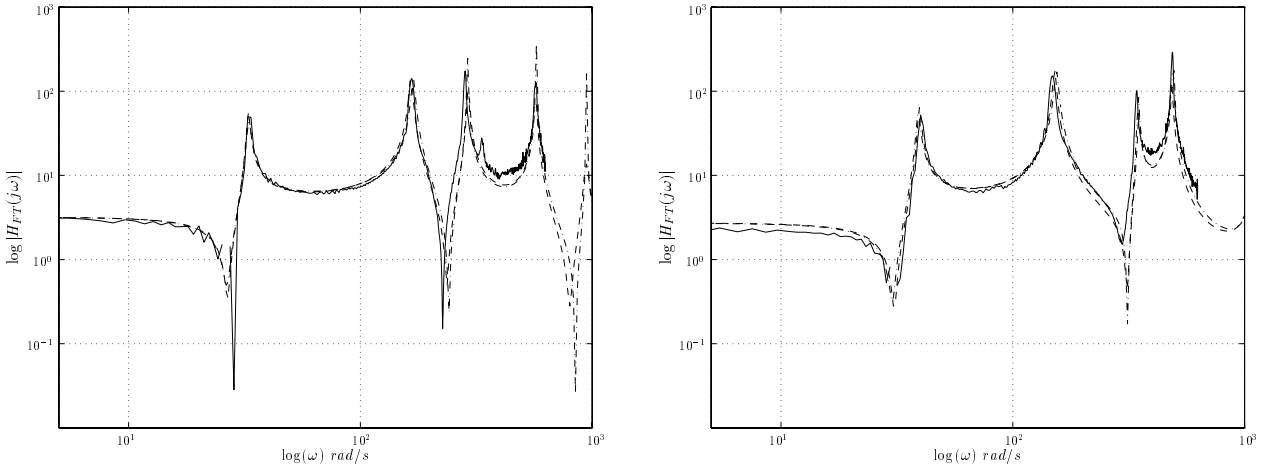

Figure 6.2 *Measurement at $\rho = 300mm$ and $\rho = 350mm$, Experimental data (solid), LTI model (dashed), LPV model (dot-dashed).*

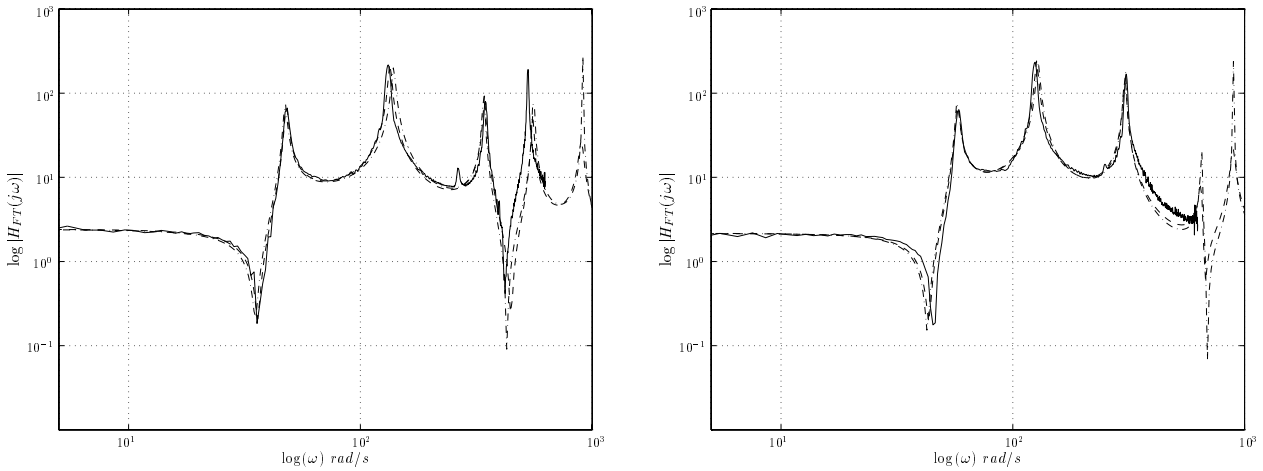

Figure 6.3 *Measurement at $\rho = 400mm$ and $\rho = 450mm$, Experimental data (solid), LTI model (dashed), LPV model (dot-dashed).*

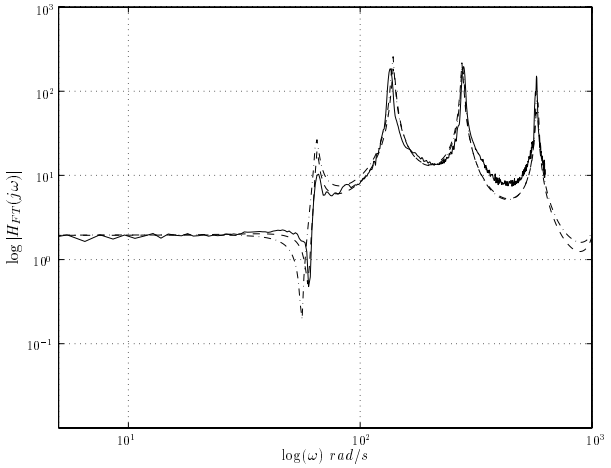

Figure 6.4 *Measurement at* $\rho = 500mm$*, Experimental data (solid), LTI model (dashed), LPV model (dot-dashed).*

6.3.2 Frozen-parameter tests

The aim of this section is to evaluate the controllers designed in chapter 4. These controllers were designed to be robust to both parametric and dynamic uncertainty by ensuring the same generalised stability margin $b_{P,C}$ for each of the plants in the parametric model set. The parametric uncertainty arises from measurable changes in the contact position which produce predictable changes in the plant dynamics. Dynamic uncertainty arises due to the difference between the true physical plant at each contact position and the mathematical model used to describe its behaviour. The generalised stability margin $b_{P,C}$ provides a measure of how large the dynamic uncertainty can be before instability results.

Acceptable behaviour of the controllers would indicate that the class of perturbations allowed for at the design stage actually captures the perturbations arising in practice. Our evaluation of the controllers will pay particular attention to the tradeoff between performance and robustness, as determined by the scaling factor K_p at the design stage. In chapter 4 three designs were undertaken, each producing a different value of $b_{P,C}$ over the contact range $320mm \leq \rho \leq 380mm$. Experimental measurements were limited to three measurement positions, $\rho = 325mm$, $\rho = 350mm$ and $\rho = 375mm$, these being representative of the entire parametric model set. In the first set of tests we characterised the performance of the controller obtained with $K_p = 1.10$ and which achieved a generalised stability margin of $b_{P,C} = 0.25$ over the specified physical interval. For implementation the reduced-order controllers obtained in chapter 4 were discretized using a step invariant discretization at a sampling rate of 1 kHz (approximately 30 times the open-loop bandwidth). Aliasing problems were avoided by low pass filtering the transducer output using the Kemo filter with a cut off frequency of $500Hz$.

To determine the increase in the level of damping achieved for the first two vibration modes we applied a $50ms$ pulse disturbance through the motor and measured both closed-loop and open-loop responses to this disturbance. Figure 6.5 shows the open-loop response to the disturbance. This can be compared to Figure 6.6 which shows the closed-loop response to the same disturbance (see also Figure 4.16 and 4.17 which give the simulated response to this disturbance). Figure 6.7 shows the actuator demand signal and indicates that the control activity was limited to the frequency range of the first two flexible modes. This is consistent with the design objective of avoiding interaction with the high frequency modes. The controller is seen to have a stable response at all three test positions and has clearly achieved the objective of increasing the level of damping associated with the first two vibration modes, showing little sensitivity to parameter variation. A better characterisation of the closed-loop damping can be obtained from transfer function measurements with a disturbance injected at the plant input. Figures 6.8, 6.9 and 6.10 show measurements of the closed-loop and open-loop frequency responses at the chosen measurement positions. In all three cases the peak response of the first mode has been drastically reduced while that of the second mode also shows a noticeable reduction relative to the open-loop response (except at $\rho = 325mm$ where the modal amplitude of the second mode is small anyway).

Investigation of the tracking performance of this controller (using the method outlined in chapter 5 to inject reference signals) was undertaken using step demand signals. Figure 6.11 shows the open-loop step response at the three measurement positions using a naive open-loop approach (simply applying a step to the input when it is well known that this will excite the flexible modes). Figure 6.12 shows the closed-loop step response for the same three measurement positions. All three cases track the step reasonably well, and the response is much less sensitive to variations in the physical parameter, although the response has a larger overshoot than predicted.

The tradeoff between robustness and performance is of particular interest. By increasing the parameter K_p at the design stage we should obtain an increase in the level of damping in the controlled modes (at least for the mathematical model) and an increase in bandwidth which should manifest itself in a quicker response. Decreasing K_p should have the opposite effect. As before, we examine the closed-loop step response at the three measurement positions $\rho = 325mm$, $\rho = 350mm$ and $\rho = 375mm$. Figure 6.13 shows the step response of the controller generated when K_p was reduced to 0.80 and for which the achieved stability margin was $b_{P,C} = 0.30$. There is little to choose between this and the step response obtained with $K_p = 1.10$, although the rise time and the settling time are slightly better with $K_p = 1.10$ (particularly at $\rho = 325mm$). Figure 6.14 shows the step response for the controller obtained by setting $K_p = 1.33$ and for which the achieved stability margin was $b_{P,C} = 0.20$. Closed-loop instabilities in the form of nonlinear limit cycles (probably the result of friction at the motor shaft) are present at two of the contact positions. The frequency of these oscillations corresponds to the crossover frequency between the second and third vibration modes. Clearly the level of robustness was too low to cover the discrepancy between the real plant and the model used to design the controller in this case.

These tests indicate that the differences between the real plant and the mathematical model used to design the controller are not important provided the achieved stability margin is sufficiently large. They also demonstrate that it is possible to build robustness to both parametric and dynamic uncertainty into the controller. For SISO systems Vinnicombe [87] has provided a particularly sharp interpretation of the class of dynamic uncertainty that can be tolerated by a controller known only to satisfy a bound on $b_{P,C}$. He has shown that the frequency by frequency interpretation of the ν-gap metric is equivalent to measuring the chordal distance between the Nyquist plots of two systems when they are projected onto the Riemann sphere. For flexible structures this graphical interpretation shows that the controller will be robust to large perturbations where the weighted plant has either high or low loop-gain. This implies that the feedback loop will be insensitive to errors such as imperfect damping estimates for modes within the control bandwidth (which is highly desirable since damping estimates are often poor) and unmodelled dynamics beyond the bandwidth (provided sensible weighting is used). In terms of the tradeoff between performance and robustness, it is felt that this is encapsulated very nicely by the parameter $b_{P,C}$. The cost of increasing the controller bandwidth and the level of damping in the controlled modes is reflected by a reduction in $b_{P,C}$ and hence by a reduction in robust stability. Unrealistic attempts to increase the level of performance forces the controller to make

greater use of the specific properties of the model and eventually such a scheme will have to break down when the controller is applied to the real plant because the properties of the model no longer reflect those of the plant. This has been clearly demonstrated here.

It is worth pointing out that while the parameter $b_{P,C}$ encapsulates the robustness/performance tradeoff very nicely, it is still very much an engineering judgement that determines what value we finally settle for. In other words, we are still in the undesirable position where the designer has to make quantitative judgements about the required stability margin based on various qualitative properties of the model. Systematic attempts to address these difficulties can be found in the model validation literature ([18],[69]). For example, the time domain approach to model validation attempts to answer the following question: given a nominal mathematical model, a set of allowable models, physical input-output measurements and realistic bounds on noise, does there exist a model in the allowable model set that interpolates the data? Actually, the term model validation is somewhat of a misnomer since we can never validate a model, only not invalidate it (principally because we can only perform a limited number of input-output tests). These questions prompted a thorough model validation study on this experimental equipment which can be found in [18]. Based on the success of the controllers, attempts were made to determine whether experimental input-output data could be accounted for using a coprime factor perturbation model set with weighted norm bounded uncertainty[1]. In Davis [18] it was shown that norm bounded LTI uncertainty could not account for the observed data, whereas, when the uncertainty was allowed to be time varying, the model could not be invalidated. In other words, allowing the uncertainty to be time varying it was possible to interpolate the measured input-output data, so this specific measurement data could not invalidate the model set. Of course the small gain theorem allows us to consider the uncertainty as being time invariant, time varying, or even nonlinear, provided it is bounded and has a norm less than the achieved stability margin. This raises a number of interesting philosophical questions, if we believe the uncertainty to be time invariant but can only account for the measured data by allowing it to be nonlinear, how much faith do we have in the model of the plant and the uncertainty set given that we can only test the model with a limited number of data sets? On the other hand, if we believe the uncertainty to be time invariant and interpolate the data with a norm bounded time-invariant perturbation then it is much easier to accept the bound on the uncertainty as being meaningful. For our model it was felt that time-varying uncertainty was reasonable because the system has nonlinearities that are not accurately modelled by time-invariant perturbations. It is beyond the scope of this thesis to go into the details of model validation theory, our point is merely that practical techniques that allow the designer to quantify the size of the required stability margin, and so make a realistic tradeoff between robustness and performance, are being developed.

[1] The weight was used so that the model validation was consistent with the extended H_∞ loop-shaping design procedure which was used to synthesise the controllers.

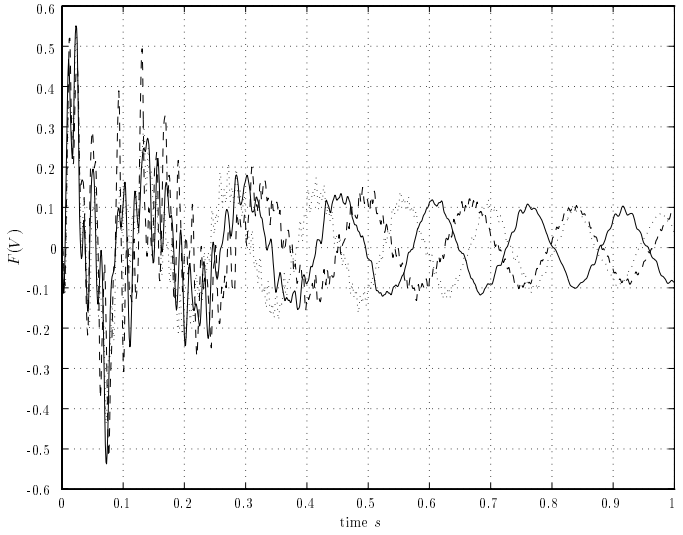

Figure 6.5 *Open-loop response to a* 50*ms pulse disturbance applied at the plant input.*

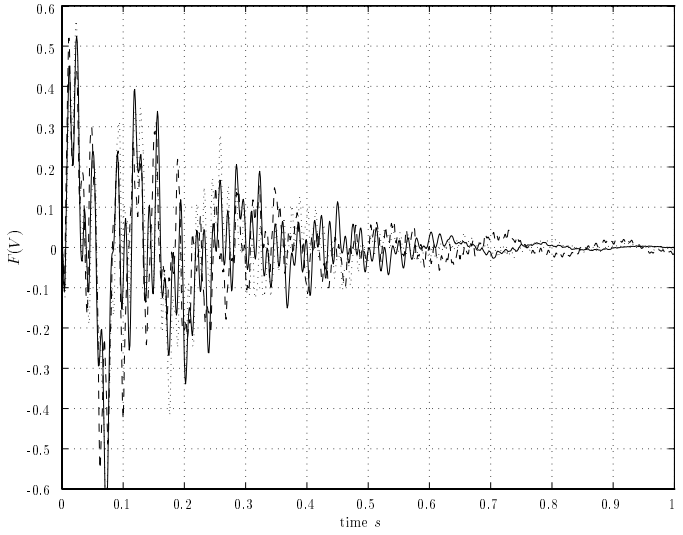

Figure 6.6 *Closed-loop response to a* 50*ms pulse disturbance applied at the plant input.*

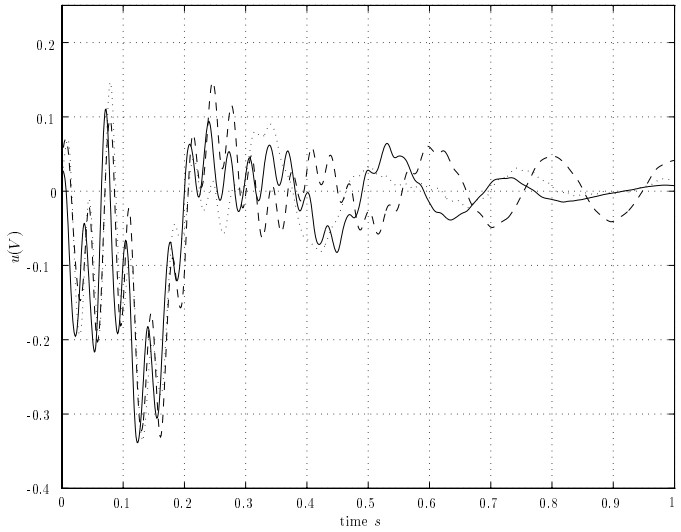

Figure 6.7 *Actuator demand to a* 50*ms pulse disturbance applied at the plant input.*

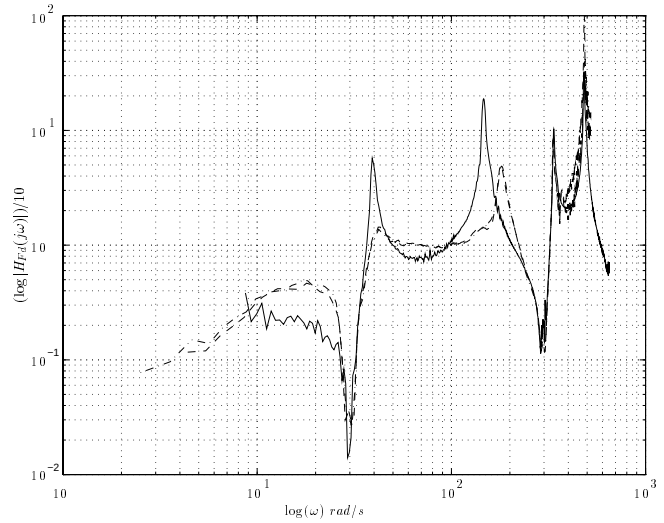

Figure 6.8 $|H_{Fd}(j\omega)|$, *Open loop (solid), Closed loop (dashed),* $\rho = 350mm$.

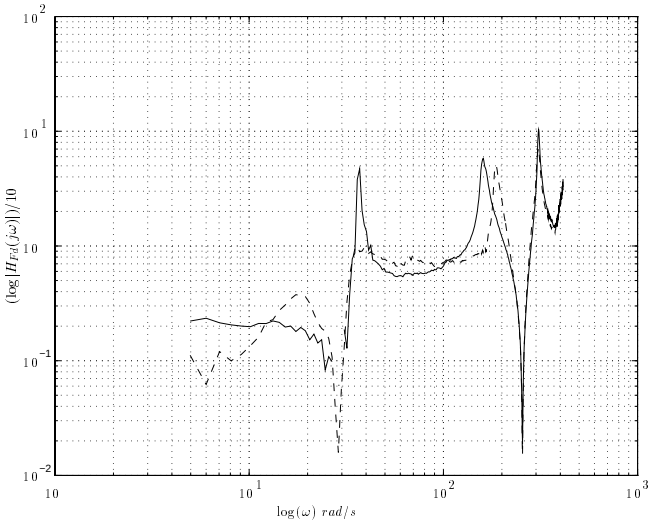

Figure 6.9 $|H_{Fd}(j\omega)|$ *Open loop (solid), Closed loop (dashed),* $\rho = 325mm$.

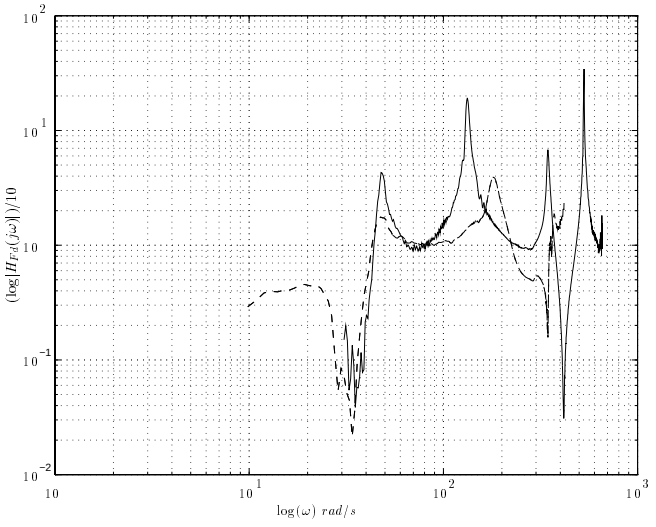

Figure 6.10 $|H_{Fd}(j\omega)|$ *Open loop (solid), Closed loop (dashed),* $\rho = 375mm$.

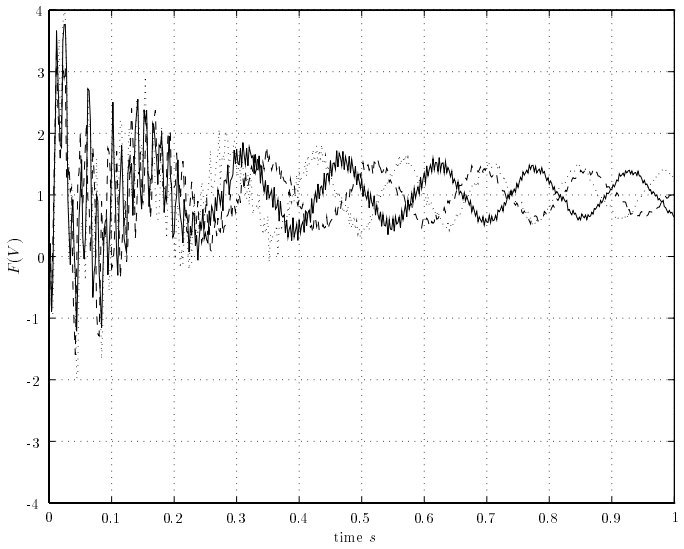

Figure 6.11 *Open-loop step response.*

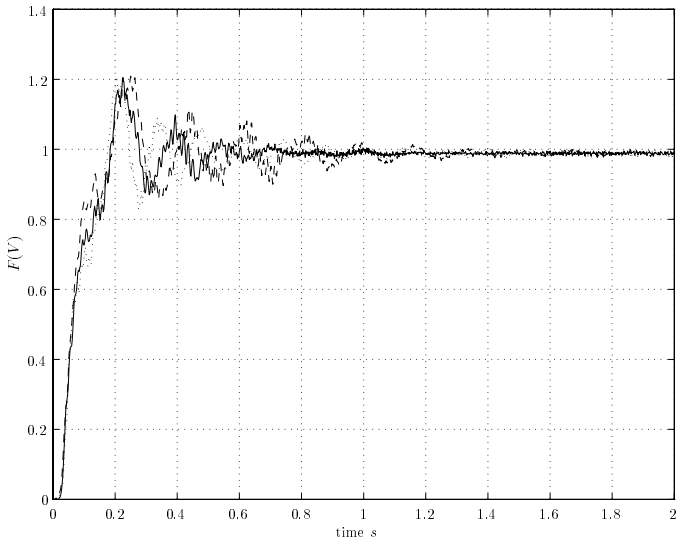

Figure 6.12 *Closed-loop step response.*

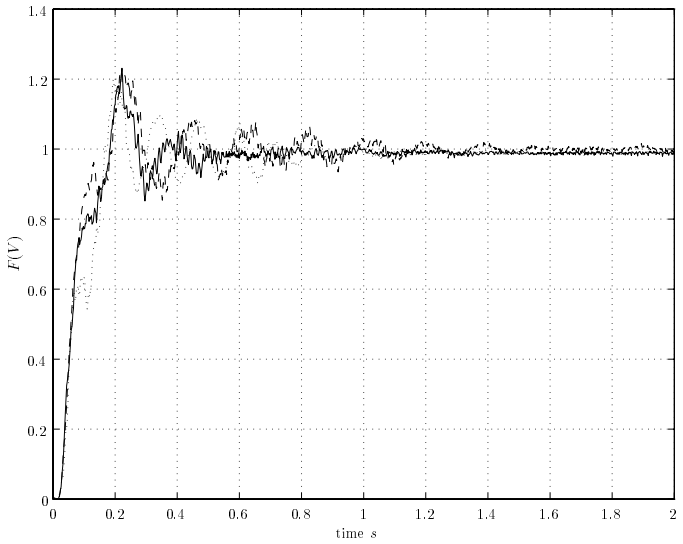

Figure 6.13 *Closed-loop step response* $K_p = 0.80$.

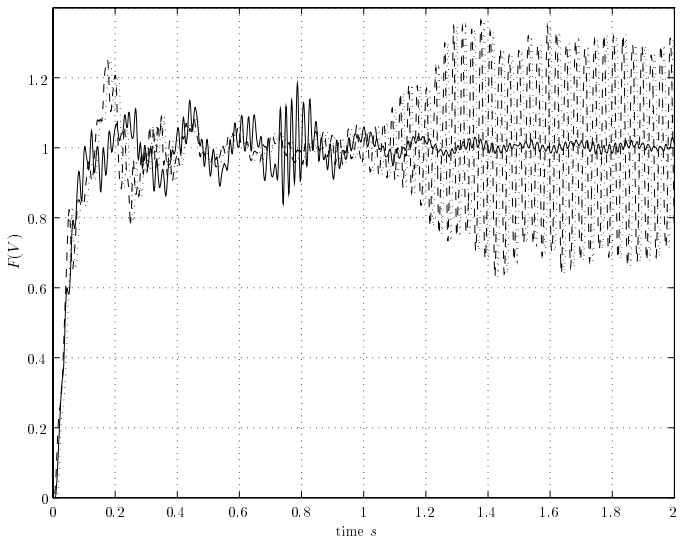

Figure 6.14 *Closed-loop step response* $K_p = 1.33$.

6.3.3 Time-varying tests and switching performance

In this section we investigate the switching methodology developed in chapter 5 by implementing the controller designed in section 5.4.1. There are a number of issues that require experimental verification, including:

i. The effectiveness of the switching scheme at achieving bumpless transfer between controllers, and in particular, whether this technique is appropriate for the class of system considered in this thesis.

ii. Stability properties under time-varying parametric uncertainty. Recall that this is difficult to characterise analytically in a non-conservative manner.

iii. The level of performance degradation resulting from movement of the force transducer.

Another interesting issue relates to the effectiveness of the coprime factor implementation methodology at achieving good anti-windup characteristics. A number of these issues can be partially addressed experimentally, although by no means completely resolved. For example, we cannot use the experimental equipment to characterise the class of trajectories for which the system remains stable. All we can do is examine the performance properties of the given system with a chosen set of parameter trajectories[2]. However, using the fact that the chosen system has particularly severe parameter variations and by choosing a representative class of parameter trajectories, we can still draw some useful conclusions about the applicability of these control techniques.

To this end, the controller designed to cover the entire parameter interval in section 5.4.1 was discretized at a sampling rate of $2kHz$ using a step invariant transformation (a slightly faster sampling rate was needed to ensure that it remained approximately 30 times as fast as the open-loop bandwidth). The discrete time realisation was then transformed into a real modal form in order to reduce processor load during implementation. The C-code for the basic LTI controller was generated with the Impex package and subsequently modified by incorporating the switching logic. To prevent aliasing the output from the force transducer was low pass filtered using the Kemo filter with a cutoff frequency of $500Hz$ and the output of the LVDT was filtered with a cutoff of $20Hz$. Even with a combined state dimension of 75 states the processing power of the DSP chip was more than adequate to implement the controller at this sampling rate.

We begin by examining the effectiveness of the switching scheme. To this end we examined the effectiveness of the controller at tracking constant reference signals under simple parameter trajectories where the force transducer traverses from the tip of the beam to the base and back again. Two such measurements are shown in Figure 6.15, the second with a more rapid traverse. Recall that the controller is made up of four individual controllers C_1, C_2, C_3 and C_4, covering the ranges $300mm \leq \rho \leq 365mm$, $360mm \leq \rho \leq 425mm$, $420mm \leq \rho \leq 465mm$ and $460mm \leq \rho \leq 500mm$ respectively, so each traverse of the beam involves six controller switches.

[2]The issue of stability is more difficult to deal with. Intrinsically, stability is an infinite horizon concept whereas our experimental evaluation can only be performed on a finite horizon.

As predicted from simulations, the switching performance is good with little evidence of the switches between the individual controllers. The controller also maintains the output close to the reference value despite the time-varying nature of the parameter.

Next we consider the effectiveness of the switching scheme when the controller is required to follow more ambitious reference signals. To this end we characterised the step response achieved by the controller with the force transducer traversing the full length of the beam. By considering closed-loop performance under a series of increasingly rapid traverses we can evaluate performance degradation as well as obtain a much better characterisation of the switching performance. For example, how effective is the switching scheme when a switch is effected during a rapid transient following a step change in the reference signal? The results of these tests can be found in Figures 6.16 through 6.18. It is evident from these results (and from numerous other experimental evaluations which cannot all be reported here) that the controller maintains a high level of robustness even when faced with rapid parameter variations. The controller has the desirable property of showing gradual degradation in performance as the severity of the parameter trajectories becomes increasingly worse. There is no evidence of any instabilities resulting from interaction with high frequency vibration modes (although movement of the force transducer certainly excites some high frequency modes), and little evidence of sudden step changes in the controlled output resulting from controller switching. It appears that the perturbation class allowed for when designing the controllers covers a sensible class of time-varying perturbations as well.

We conclude with a simple characterisation of the antiwindup properties of the controller. With the contact position fixed at $\rho = 300mm$, a reference signal which periodically switched between two discrete levels was injected into the loop. The maximum value of the reference signal required the motor to produce a torque which was well beyond its physical saturation level while the minimum value of the reference signal required a torque that was within the actuators linear region. This made the feedback loop switch between open-loop operation and closed-loop operation each time the level of the reference signal changed. Of interest is the speed with which the controller resumes normal linear operation when coming out of saturation. The results of this test can be found in Figure 6.19. It can be seen that the controller comes out of saturation very quickly giving a response close to the desired linear response. When the controller was implemented without the coprime factor antiwindup strategy the closed-loop behaviour was very different, tending to remain in saturation for much longer, even resulting in closed-loop instability if it remained in saturation for too long.

Although the switching methodology has been successfully implemented and shown to be a useful procedure when designing against large parametric variations it does have some drawbacks. From a practical perspective the requirement of having to run all controllers simultaneously even when they are off-line so that good switching characteristics are achieved is far from ideal. Depending on the number of controllers required to cover the physical parameter range it is plausible that similar performance might be achieved by a scheduled controller having a much lower state dimension than a switching controller formed from a set of individual controllers.

This said, the reduction in state dimension must be offset against the requirement of having to update the state matrices of the scheduled controller continuously, making it difficult to determine which approach will be computationally less demanding.

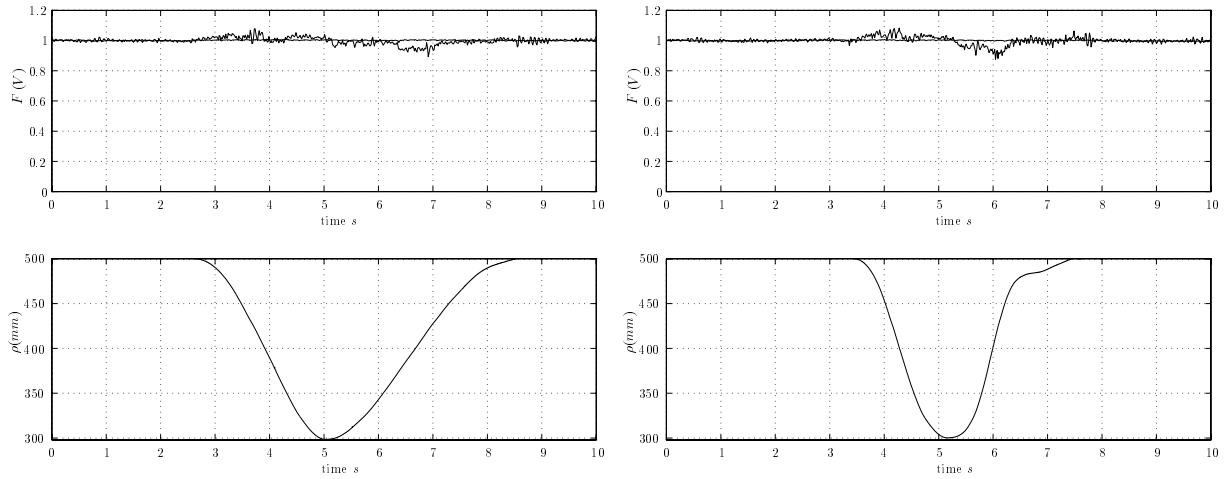

Figure 6.15 *Response to a constant reference signal.*

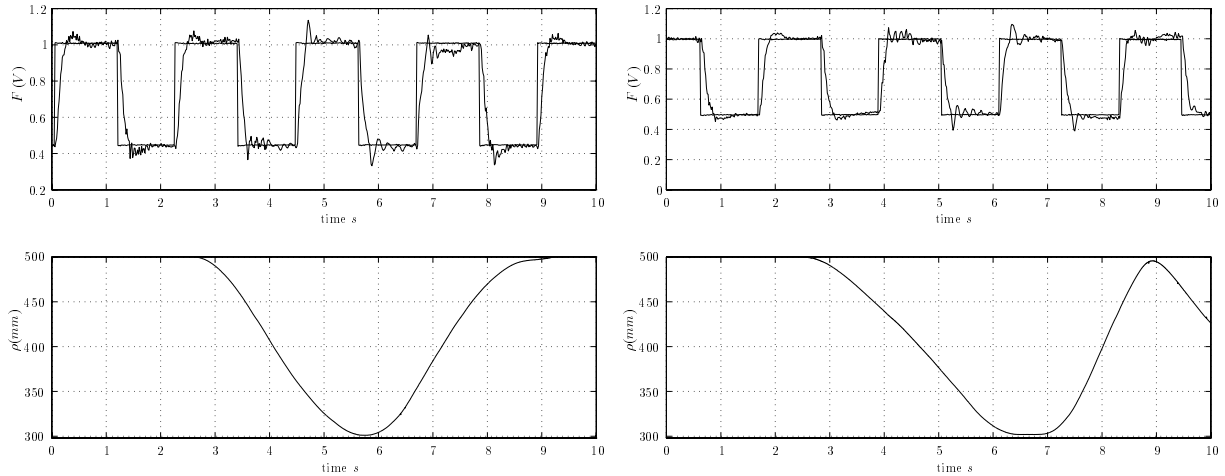

Figure 6.16 *Step response.*

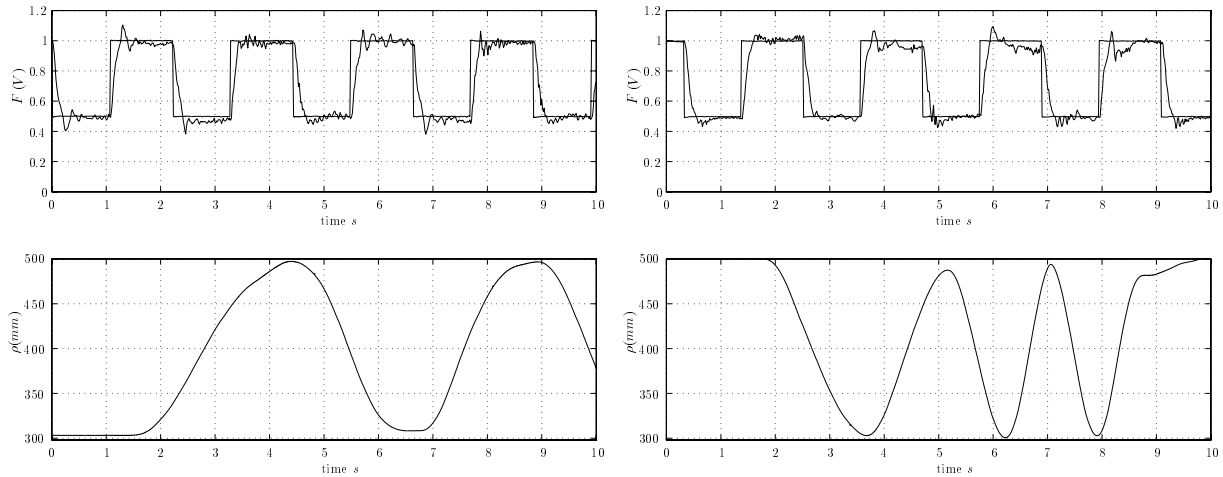

Figure 6.17 *Step response.*

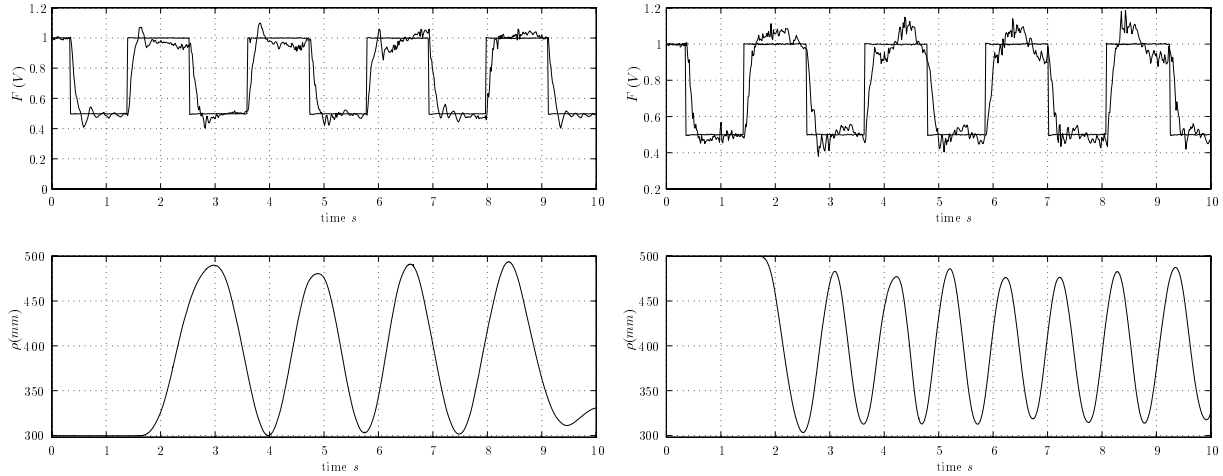

Figure 6.18 *Step response.*

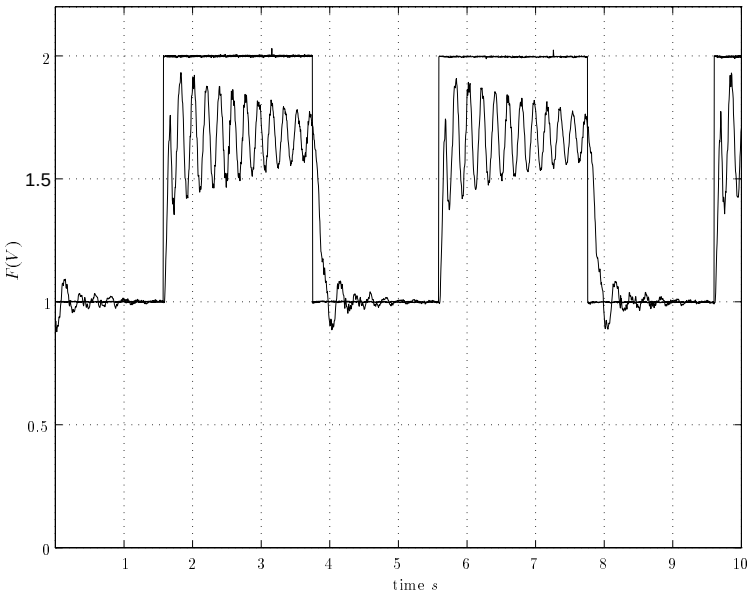

Figure 6.19 *Experimental characterisation of the antiwindup properties of the controller.*

6.4 MISO tests

The objective of these tests is to verify the claim that modifications to the physical plant suggested by examining its feedback properties using the ν-gap metric can make it easier to control (in the sense already discussed). To this end we will implement the central H_∞ loop-shaping controller and determine whether the additional input does in fact reduce sensitivity to the class of parametric uncertainty arising in this problem. The experimental evaluation will also allow us to determine performance degradation when the plant is time varying and allows the switching characteristics of the controller to be fully explored.

6.4.1 Calibration

For the MISO experiments the magnet was attached to the tip of the beam using the locknut arrangement. Although the mass of the magnet was only $67g$ it had a significant effect on the frequency response, making it necessary to recalibrate the experimental equipment and to update the theoretical model. The model update required the inertial force generated by the tip magnet to be accounted for and it was also found that suitable accuracy required the rotary inertia of the tip magnet to be included. This is because certain of the constrained mode shapes involve only small tip deflections but relatively large slopes at the tip of the beam. For these vibration modes the rotary inertia of the magnet has a strong constraining effect. The calibration procedure was essentially identical to that outlined previously involving a sequence of logarithmic sine sweeps with the constraint fixed at equally spaced intervals across the accessible length of the beam.

Two complicating factors arose in these tests: the possibility of the tip magnet changing the observed modal damping and the nonlinear effect of friction acting at the motor shaft. Electrical damping can easily arise from the reactance of the coil. This reactance is proportional to the velocity of the magnet in the coil and is only present when the coil is connected to its amplifier and the amplifier is switched on. When measuring the transfer functions from the two excitation sources it was therefore essential that all equipment was connected and powered up to guarantee that the characteristics of the system did not change from one test to another. The effect of friction was particularly prevalent in the response generated when an excitation signal was applied to the coil driving the tip magnet. In order to ensure that a linear driving force was generated by this actuator it was necessary to keep the excitation level and consequently, the tip deflection, relatively small. Unfortunately, small excitation levels were not enough to make the effect of static friction at the motor shaft negligible and led to strong nonlinearities being observed, especially near the second natural frequency, the mode shape of which involves large rotations at the base of the beam.

This problem was overcome by exciting both actuators simultaneously making the friction force negligible when compared to the torque applied by the motor. Reference signals were injected simultaneously into the amplifiers of the respective actuators, first in phase, and then in anti-phase. By either summing or subtracting the measured responses obtained from the two excitation configurations it was possible to obtain the individual frequency responses with

nonlinear effects largely eliminated. Logarithmic sine sweeps having a flat spectrum over the frequency range $0 - 80Hz$ were generated digitally at a sampling rate of $250Hz$ and applied over a $40s$ period. The measured response was low pass filtered at $125Hz$ using the Kemo filter and sampled for $50s$ to prevent spectral leakage. Circle fitting techniques were applied to obtain modal damping estimates which are tabulated in Table 6.2. The reactance of the coil is reflected in the increased level of damping observed in the first three vibration modes. Measured and predicted frequency responses at the measurement positions $\rho = 300mm, \rho = 350mm, \rho = 400mm, \rho = 450mm$ and $\rho = 500mm$ are compared in Figures 6.20 through 6.24. Errors are certainly discernible in these plots, particularly in the transfer function corresponding to the tip actuator. Possible sources other than friction at the motor shaft include: finite displacements of the magnet in the copper coil and rotation of the tip magnet resulting in misalignment of the magnetic fields. These errors manifest themselves particularly strongly in the low frequency modes when the constraint is located near the tip of the beam.

Model	Damping parameters	Magnet
LTI	$\zeta_1 = 2.0\%$ $\zeta_2 = 2.0\%$ $\zeta_3 = 2.0\%$ $\zeta_4 = 1.0\%$	$67g$

Table 6.2 *Estimated modal damping factors.*

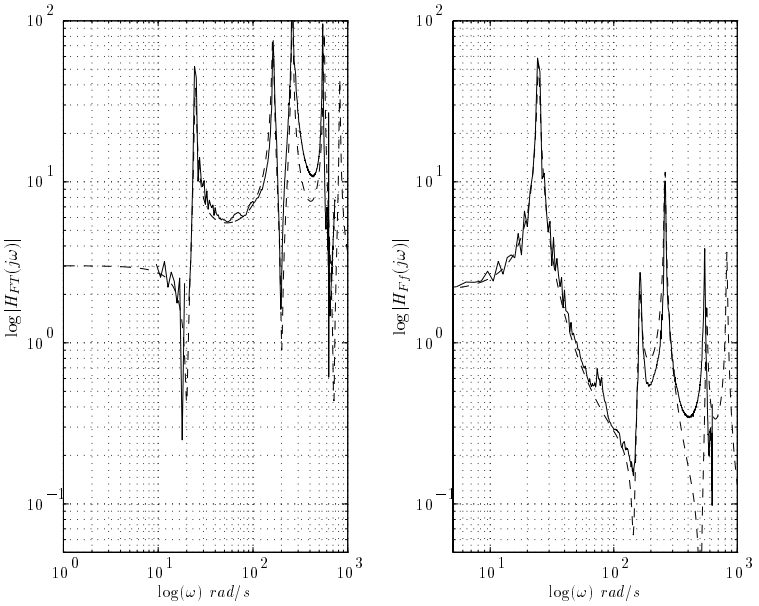

Figure 6.20 *Measured (solid) and predicted (dashed) transfer functions* $\rho = 300mm$.

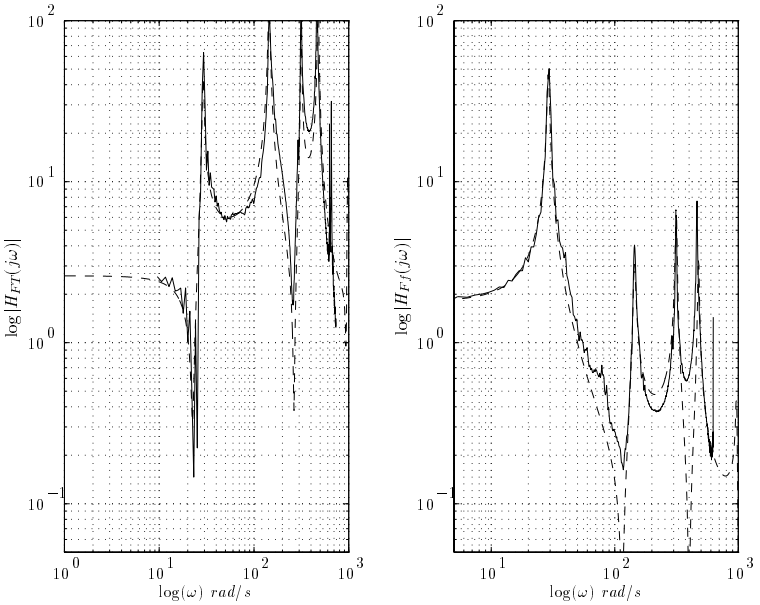

Figure 6.21 *Measured (solid) and predicted (dashed) transfer functions* $\rho = 350mm$.

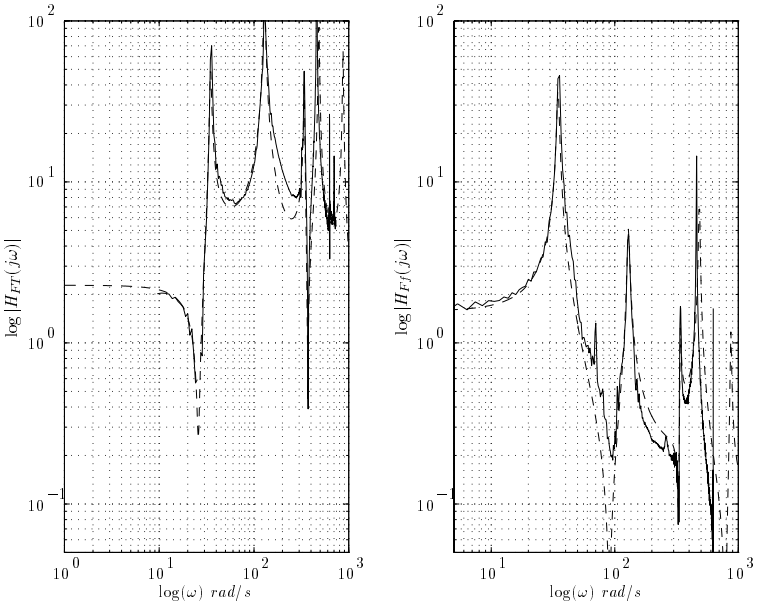

Figure 6.22 *Measured (solid) and predicted (dashed) transfer functions* $\rho = 400mm$.

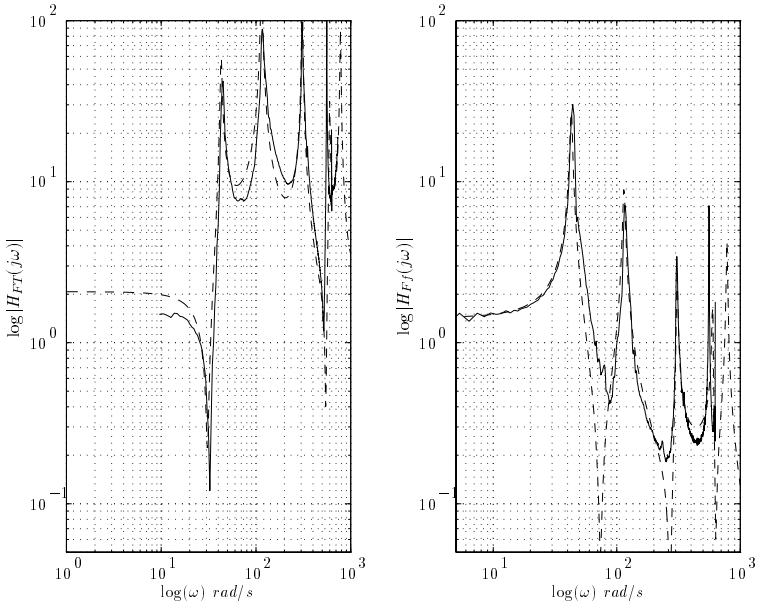

Figure 6.23 *Measured (solid) and predicted (dashed) transfer functions* $\rho = 450mm$.

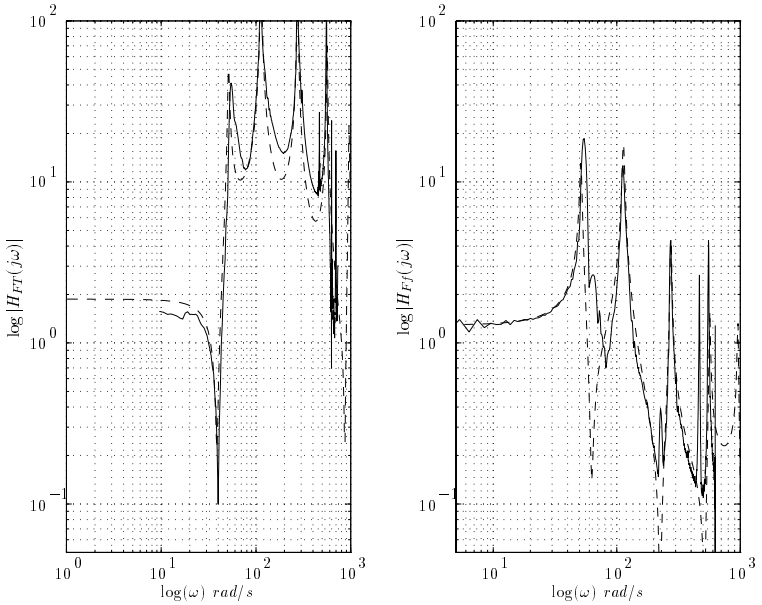

Figure 6.24 *Measured (solid) and predicted (dashed) transfer functions* $\rho = 500mm$.

6.4.2 Time-varying tests and switching performance

The actuator at the tip of the beam was introduced based on the feedback properties of the system when actuation was applied solely by the motor. Using the ν-gap metric, frequency by frequency measurements of the distance between the LTI plants representing the system at different contact positions indicated that a tip actuator could be used to make the system easier to control. That is, any controller designed at some chosen nominal contact position should be insensitive to variations in the contact position. In chapter 5 we selected the central controller solving the normalised coprime factor stabilisation problem as being appropriate, based on the fact that this has the same order as the weighted plant and its observer structure gives a factorisation of the controller over RH_∞ (making it a natural choice for switching). The second actuator made it relatively straightforward to select frequency weighting to meet the closed-loop performance objectives over the entire length of the beam using a single loop-shaping weight, and only three controllers were required to cover the entire range of parameter variation.

We begin our evaluation of this claim by examining the frozen-parameter performance of this controller. To keep this examination consistent with the previous section we investigate the effectiveness of the controller at rejecting a disturbance applied at the input to the motor by measuring the closed-loop transfer function from this disturbance to the contact force. Our interest is primarily in the level of closed-loop damping to determine whether the performance objectives have been met. Figures 6.25 through 6.27 compare the open-loop and closed-loop damping at the positions $\rho = 300mm$, $\rho = 350mm$, $\rho = 400mm$, $\rho = 450mm$ and $\rho = 500mm$. As desired, these indicate a large attenuation in the peak response for the controlled modes (except the second mode at $\rho = 300\ mm$ where little improvement was achieved) and little or no control activity in the higher frequency modes. This is a pleasing observation given that selecting an appropriate loop-shaping weight to meet the performance objectives was relatively straightforward due to the reduced level of sensitivity resulting from the new actuator configuration.

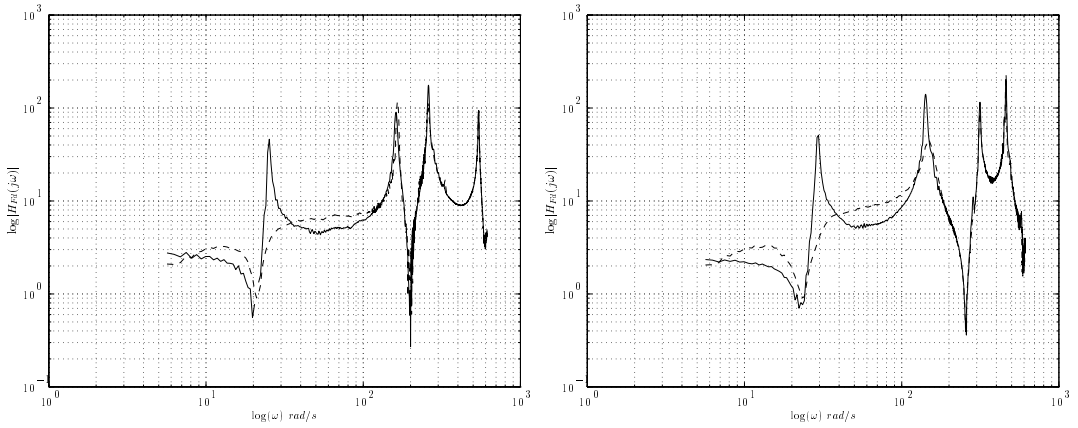

Figure 6.25 $H_{Fd}(j\omega)$ *open loop (solid), closed loop (dashed),* $\rho = 300mm$ *and* $\rho = 350mm$ *respectively.*

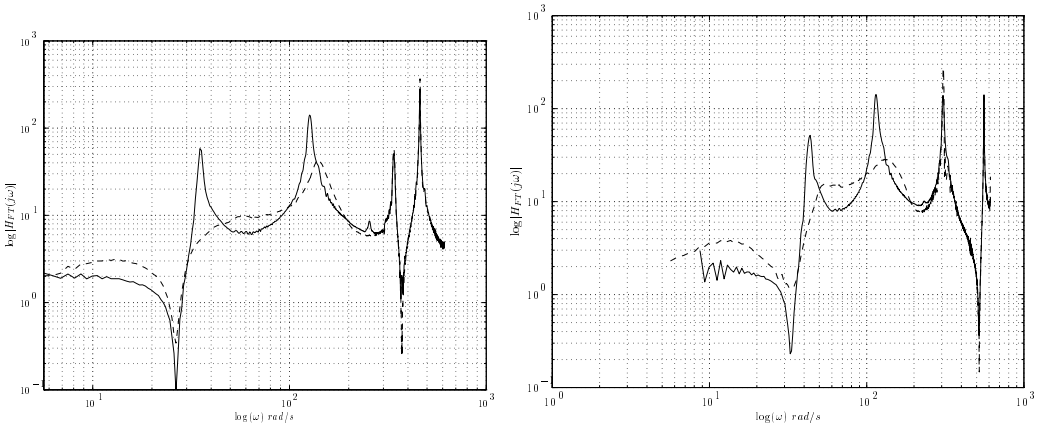

Figure 6.26 $H_{Fd}(j\omega)$ *open loop (solid), closed loop (dashed),* $\rho = 400mm$ *and* $\rho = 450mm$ *respectively.*

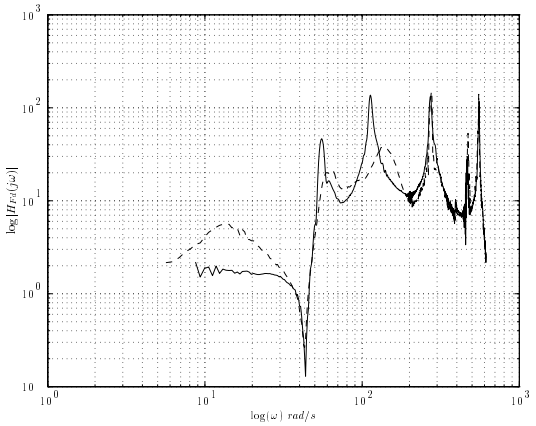

Figure 6.27 $H_{Fd}(j\omega)$ *open loop (solid), closed loop (dashed),* $\rho = 500mm$.

Our next objective is a thorough evaluation of the switching characteristics of the two-input controller under a general class of parameter variations. Recall that the two-input controller was generated from three individual controllers with switching occurring at $\rho = 390\ mm$ and $\rho = 450\ mm$. We again begin by evaluating the ability of the controller to maintain a constant contact force subject to the force transducer moving across the entire length of the beam. Any sudden transients resulting from controller switching should be easy to detect with this simple reference signal. The results for three separate traverses are to be found in Figures 6.28 through 6.30. These correspond to three successively more rapid traverses giving an indication of performance degradation resulting from time-varying uncertainty. The exact switching positions can be determined by the intersection of the horizontal dashed lines with the displacement plot in each of the figures. If bumps resulting from controller switching are present they are certainly not discernible in these plots.

An interesting observation from these tests is that the greatest deviation of the output from the desired level occurs at positions where the acceleration, not the velocity, is at a maximum. Once again, it is clear that the switching scheme gives an acceptable method for dealing with large parameter variations and the robust control methodology accounts for the time-varying nature of the parameter very satisfactorily.

We complete this experimental study by evaluating closed-loop performance with a step reference signal. This we do with a series of increasingly complicated parameter trajectories, the last of which involves very rapid traverses of the beam. The results are to be found in Figure 6.31 through 6.34. These are in keeping with the general observation so far: switching, when done correctly, provides a useful approach when controlling systems which are strongly parameter dependent. Similarly, the chosen robust control approach generates controllers that are robust to plant/model mismatch and to useful class of time-varying perturbations.

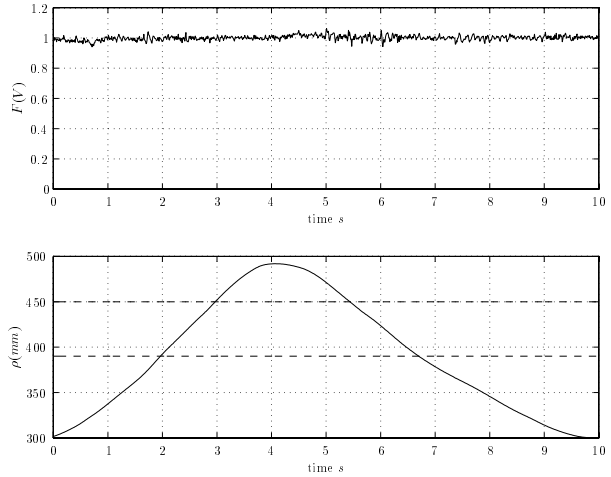

Figure 6.28 *Response to a constant reference signal.*

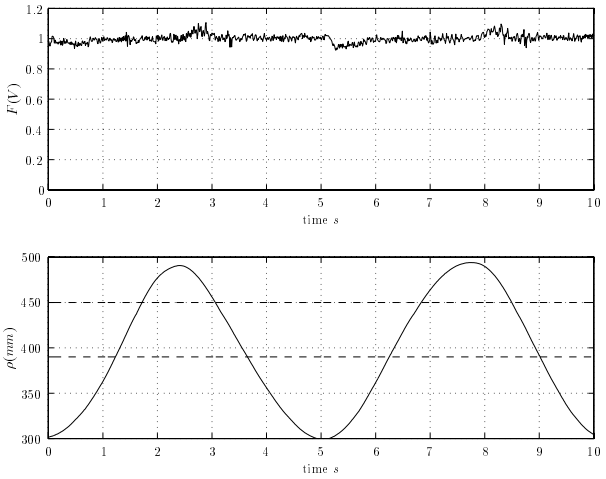

Figure 6.29 *Response to a constant reference signal.*

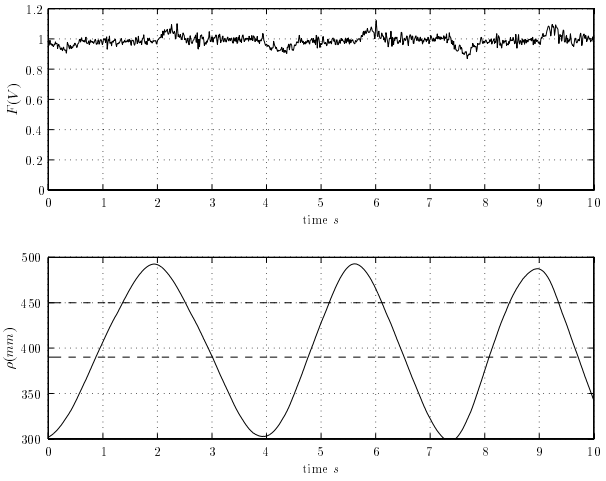

Figure 6.30 *Response to a constant reference signal.*

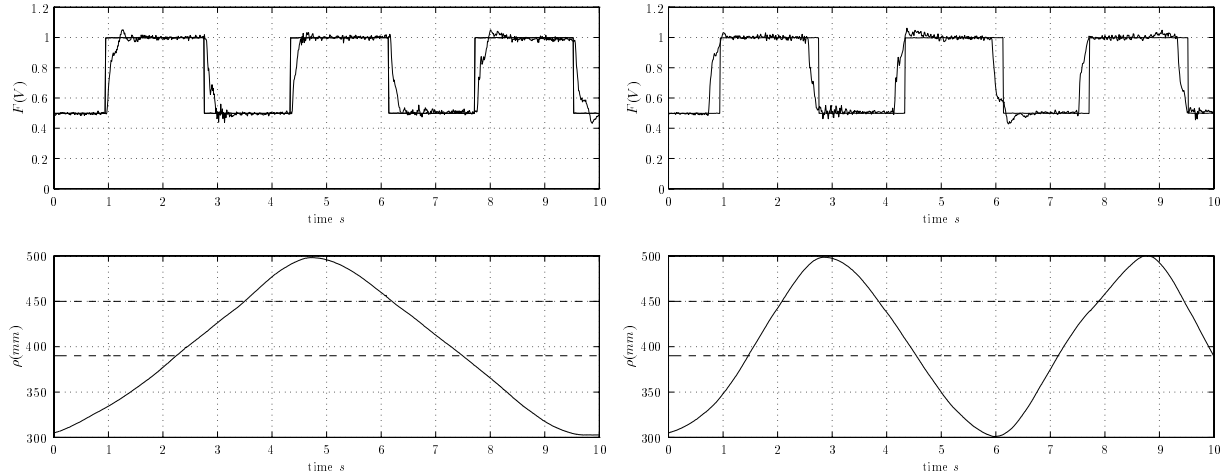

Figure 6.31 *Closed-loop step response.*

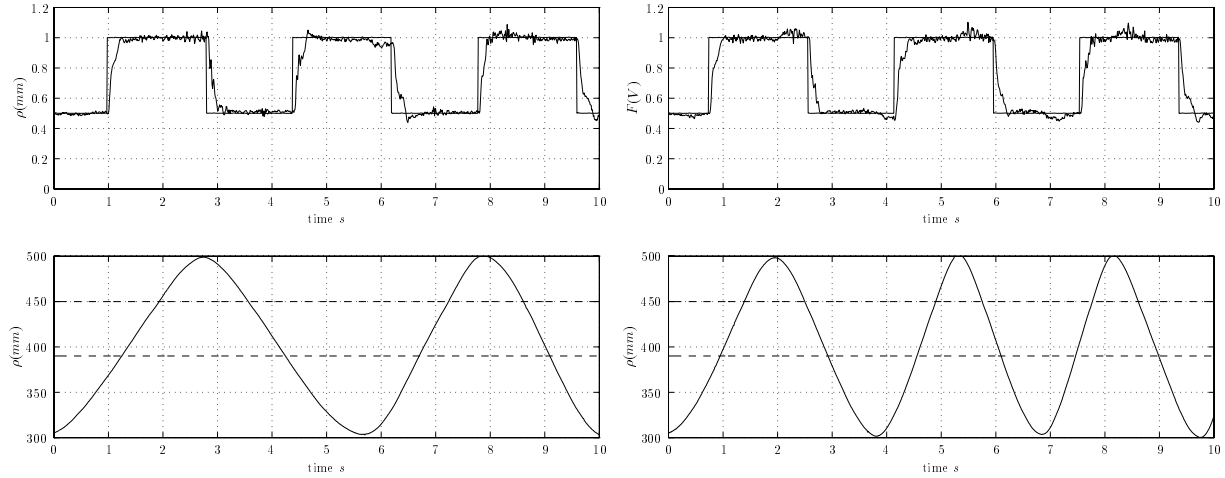

Figure 6.32 *Closed-loop step response.*

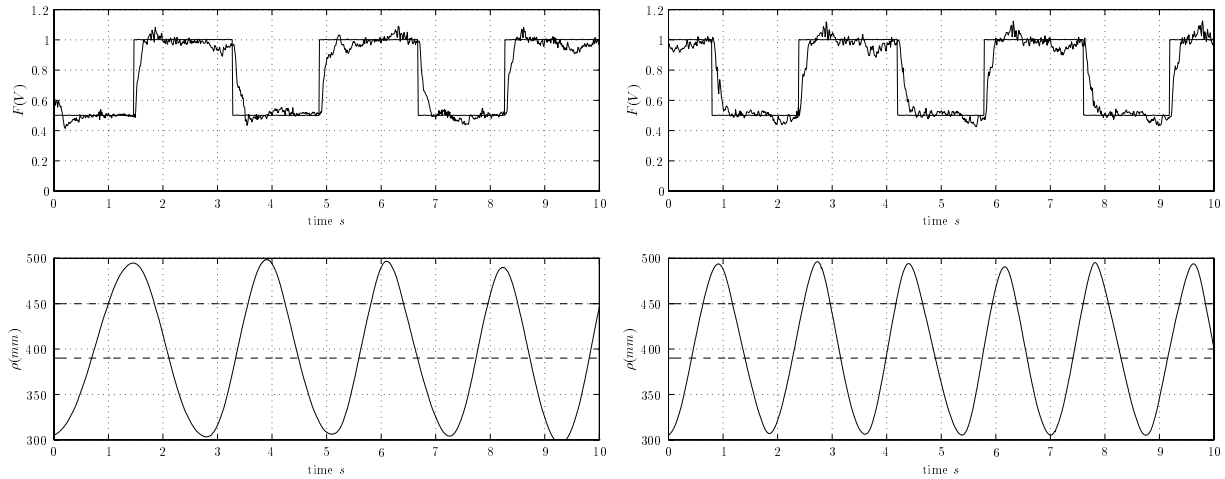

Figure 6.33 *Closed-loop step response.*

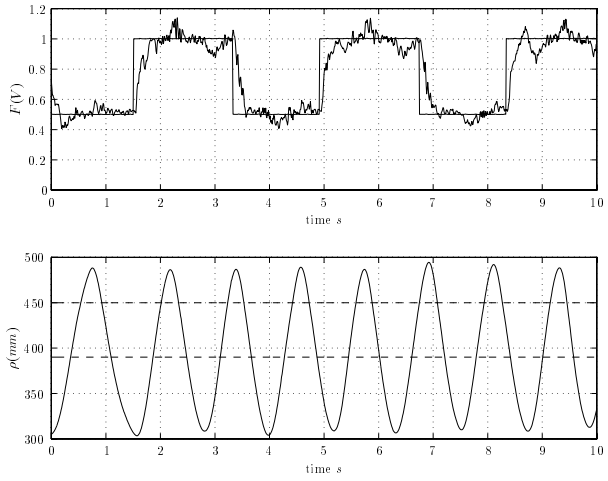

Figure 6.34 *Closed-loop step response.*

6.5 Summary

In this chapter we have examined the LTI design methodology on our example system which we believe to be representative of a large class of structural systems that exhibit strongly parameter-dependent dynamics. We have demonstrated the importance of the tradeoff between robustness and performance, vindicating the emphasis placed on these issues in chapter 4. Even though flexible structures are sensitive to sudden transients, we have demonstrated that the switching methodology developed in chapter 5 can be used in conjunction with suitable robust control techniques to generate a useful design methodology for this class of systems. Both single-input and multiple-input controllers have been shown to have good switching characteristics and satisfactory robustness properties when subjected to some fairly demanding parameter trajectories. The input-output setting and the ν-gap metric have been central to our approach and the lack of parameter sensitivity demonstrated by the controllers indicates the power of this metric, both as an analysis tool, and as a design tool. The fact that the two-input controllers performed very satisfactorily on the experimental system also indicates how useful this metric can be when selecting actuator placements. Intuitively, it might have been expected that a second actuator could be used to improve performance, but we have shown that a careful examination of the feedback properties of our example system leads to the somewhat surprising result that robustness can also be improved. In chapter 7 we will return to modelling issues that arise in the study of LPV systems. Our objective is to extend the LTI techniques by explicitly accounting for the time-varying nature of the parameter. In so doing we will develop a methodology for synthesising gain-scheduled controllers, examining the cost associated with such guarantees as we commence.

7

Model Reduction of Parameter-Dependent Dynamical Systems

7.1 Introduction

We now turn to various theoretical issues that arise in the study of LPV systems. These issues are important when one considers the problem of synthesising controllers that give performance and stability guarantees for this important class of systems. The theoretical work presented here concentrates on the single-parameter case, although there is no conceptual reason why these techniques cannot be applied to systems having multiple-parameter dependence.

The trade-off between model accuracy and model simplicity is a central theme of model-based control theory related to the design, analysis and implementation of controllers. For a given set of inputs, a complicated model might predict the outputs of some physical system very accurately, but for the purpose of control, this degree of accuracy may be unnecessary. For linear finite-dimensional systems which admit state-space realisations a natural measure of complexity is the state-dimension of a minimal realisation representing the given system. Since optimal control techniques such as LQG and H_∞ synthesis usually produce controllers that have the same state complexity as the models from which they are designed it is evident that the use of these design techniques on models having a high state-dimension will produce controllers having a high state-dimension. From an implementation perspective this is far from ideal because simple controllers are easier to implement, require less processing power and have higher integrity [50]. For these reasons the problem of reducing the state-dimension of a mathematical model in such a way as to ensure that its input-output behaviour is not unduly compromised has received much attention in the control literature ([42] and [92] contain a thorough review of these techniques). In our view two recent developments make re-examination of one of these techniques worthwhile. The first is the development of systematic methods that allow robust controllers to be designed for the class of LPV systems. The second is the development of highly efficient numerical techniques [12] which make the analysis of these systems feasible with present day computational facilities.

Model reduction schemes can be broadly separated into two different classes, open-loop techniques which attempt to match the input-output behaviour of a system as closely as possible ([1],[28],[39],[63]); and closed-loop techniques which attempt to retain the most salient aspects of the full-order model from a control perspective ([42],[92],[102]). For LTI systems the open-loop

techniques have reached a high level of maturity. For example, there exist efficient algorithms for obtaining optimal Hankel norm model approximants [39]. There are also useful L_∞ error bounds as well as stability guarantees for the balanced ([28],[39]), Hankel [39] and balanced stochastic [44] reduction techniques. This said, open-loop techniques do have drawbacks. Most noticeably, they do not address the problem of model reduction with the properties of the resulting closed loop in mind. Attempts to alleviate these drawbacks have led to the development of frequency weighted model reduction ([28],[58]) where the plant is weighted prior to reduction so as to emphasise frequency ranges that are particularly important to the behaviour of the resulting closed loop (usually the frequency range at or near unity gain crossover). When used in an open-loop context the frequency weights are either selected heuristically, or by considering various closed-loop stability measures, in order to give a better approximation over a specified frequency range. By contrast, closed-loop model reduction ([42],[92]) involves the explicit computation of weights which are based on the properties of the loop formed by the full-order controller and which give guarantees on stability and performance when the reduced-order controller is used.

When using model reduction as a design tool there is also some freedom regarding the order in which the reduction is performed. One may proceed either by taking a high order model of the plant, model-reduce this to obtain a low-order model and then design a controller based on the low-order model, or alternatively, by designing a high order controller based on the full-order model and then reduce the controller. These alternatives are depicted in Figure 7.1.

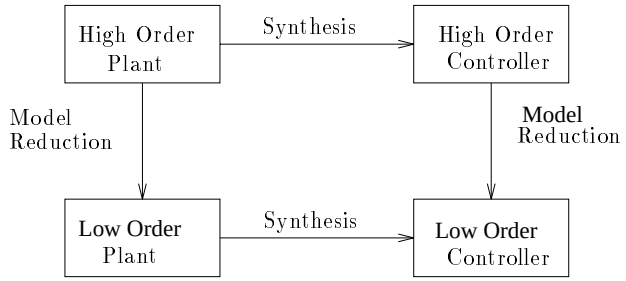

Figure 7.1 *Alternative reduced-order controller design techniques.*

In the case of closed-loop model reduction Goddard [42] argues that the latter approach is somewhat preferable. This is because a high order controller designed from a high order model contains all the essential information necessary to achieve closed-loop stability and performance, so it is possible to find weights which preserve this information. Similarly, Anderson and Liu [1] observe that if the plant is reduced prior to controller design then errors made during the approximation step will be propagated throughout the design procedure. Although closed-loop reduction techniques are certainly preferable to the open-loop techniques they are also considerably more complicated. The technique developed by Goddard [42] makes use of the parametrisation of all controllers that achieve a specified H_∞ norm bound on some closed-loop transfer function [24]. Since the set of all controllers bounding the induced norm of some closed-loop operator has yet to be obtained for the class of LPV systems it is not immediately

obvious how these techniques could be extended. For these reasons we will restrict attention to the problem of approximating the open-loop behaviour of an LPV system and pay particular attention to the issues of stability, approximation error and continuity.

Our approach will be based upon the notion of an internally balanced state-space realisation [63]. In order to justify this approach we give a brief review of certain popular reduction techniques in section 7.2, particularly those used routinely on flexible mechanical systems. We examine the disadvantages associated with these techniques when they are extended to the class of LPV systems, hence providing motivation for our chosen approach. In section 7.3 we define precisely what we mean by a balanced realisation and a balanced approximant of an LPV system, define what is meant by a set of $\mathcal{Q}_e$ singular values and show how these are related to the mapping from past inputs to future outputs. In section 7.4 we outline a "frequency weighted" generalisation of the balanced truncation procedure. For each frozen parameter value this has the interpretation of emphasising certain frequency ranges when extracting the model approximant. The problem of approximating unstable systems by approximating the symbol of the system's graph is examined in section 7.5. Section 7.6 examines the conditions under which known error bounds for LTI balanced truncation can be extended to LPV truncation. Numerical procedures for computing controllability and observability Gramians based on convex optimisation techniques are developed in section 7.7. In section 7.8 we show how the balancing state transformation can be computed once the controllability and observability Gramians have been found. Important issues concerning the continuity properties of the model approximant are also highlighted and computational techniques for obtaining a continuous model approximant are presented. Finally, in section 7.9 we apply the technique to various simple example problems.

7.2 Modal truncation of LPV systems

In this section we review open-loop model reduction techniques that are based on the principle of projection of dynamics [92], concentrating on those commonly used on flexible mechanical systems. For small amplitude vibrations about an equilibrium position it is well known ([61],[64]) that under the assumption of Rayleigh damping the equations of motion for this class of systems can be expressed in terms of a coupled system of second order differential equations

$$M(\rho)\ddot{x} + (\alpha M(\rho) + \beta K(\rho))\dot{x} + K(\rho)x = D(\rho)u, \tag{7.1}$$

where all matrices are assumed to be continuous functions of the parameter ρ. The vector x is a vector of generalised co-ordinates, the mass matrix $M(\rho) \in \mathbb{R}^{n\times n}$ is symmetric and assumed to be positive definite (it is unusual although not impossible to have co-ordinates with no associated mass), the stiffness matrix $K(\rho) \in \mathbb{R}^{n\times n}$ is symmetric and semi-definite and $D(\rho) \in \mathbb{R}^{n\times n_u}$ is a matrix of influence coefficients. The assumed damping model ensures that standard orthogonality conditions hold [64] and is based more on mathematical convenience than sound physical reasoning. More elaborate damping models might violate these orthogonality conditions but this does not pose serious problems from an analysis perspective. The continuity assumptions ensure that the dynamics vary smoothly with the parameter, and as pointed out

in chapter 3, these assumptions ensure the existence of a state transformation matrix $\Phi(\rho)$ such that

$$\Phi^T(\rho)M(\rho)\Phi(\rho) = I \tag{7.2}$$
$$\Phi^T(\rho)K(\rho)\Phi(\rho) = \mathrm{diag}(w_1^2(\rho), w_2^2(\rho), w_3^2(\rho), \ldots w_n^2(\rho)), \tag{7.3}$$

where $w_1(\rho) \leq w_2(\rho) \ldots \leq w_n(\rho)$ are the undamped natural frequencies for a fixed value of the parameter ρ. The continuity properties of the state transformation matrix depend to a large extent upon the behaviour of the undamped natural frequencies when considered as a function of the parameter. If these cross then it is possible that there might not exist a continuous state transformation matrix that decouples the equations of motion[1]. In other cases, for example the constrained flexible beam considered in chapter 3, continuity can be ascertained on purely physical grounds. We emphasise this point because it is necessary to differentiate the state transformation matrix when performing a similarity transformation if we explicitly account for the time-varying nature of the parameter. Since the eigenvectors of the transformation matrix can vary rapidly as a function of the parameter, failure to account for the derivative might lead to large modelling errors being introduced.

Supposing the parameter to be fixed and applying an input in the direction of the k'th generalised co-ordinate we can obtain the response of the i'th generalised co-ordinate. This is given by

$$x_i(j\omega) = \sum_{s=1}^{n}\sum_{m=1}^{n} \frac{\Phi_{is}\Phi_{ms}D_{mk}u_k(j\omega)}{(\omega_s^2 - \omega^2 + j2\zeta_s\omega_s\omega)}. \tag{7.4}$$

The frequency decomposition in equation (7.4) suggests that we retain only those modes in the frequency range of interest (typically low frequencies for control applications) and truncate the other modes. For example, if we retain the first r modes we get

$$x_i(jw) = \sum_{s=1}^{r}\sum_{m=1}^{r} \frac{\Phi_{is}\Phi_{ms}D_{mk}u_k(jw)}{(w_s^2 - w^2 + j2\zeta_s w_s w)} + \sum_{s=r+1}^{n}\sum_{m=1}^{n}(\Phi_{is}\Phi_{ms}D_{mk}/w_s^2)u_k(jw), \tag{7.5}$$

where the contribution of the high frequency modes has been converted into a throughput term.

Modal truncation has been used, and continues to be used, with great success on LTI models of flexible structures, allowing physical insight into the behaviour of the system to be fully exploited. In many problems a form of modal truncation is applied implicitly by either replacing the infinite-dimensional spatial operators of a continuum system with finite-dimensional matrix representations, as is done in the finite element method [6], or by measuring the modal parameters directly using experimental modal analysis techniques [29]. This implicit modal truncation and its implications are not primarily what we are interested in here; we assume that the given finite-dimensional model is sufficiently accurate and attempt to reduce this further while keeping errors to a minimum.

[1] This results from the chosen ordering of the natural frequencies. For systems which exhibit this behaviour it is possible to overcome the difficulties associated with the continuity properties of the transformation matrix by reordering the natural frequencies.

If we now allow the parameter to be time varying and attempt to apply the modal truncation procedure we immediately encounter a number of problems:

i. The frequency-domain decomposition in equation (7.4) no longer holds because the system does not have a frequency response. Consequently, we lose the physical insight afforded by this technique when applied in the LPV case.

ii. The transformation matrix no longer decouples the governing differential equations because derivatives of the transformation matrix enter into the problem. This can introduce large off-diagonal elements into the transformed mass and stiffness matrices.

iii. We require the transformation matrix to be twice differentiable with respect to the parameter[2] and by introducing the transformation we increase the parameter complexity of the model. For example, given a model that depends on ρ, introducing a parameter-dependent transformation generates a model with $\rho, \dot{\rho}$ and $\ddot{\rho}$ dependence.

iv. We cannot say anything concrete about the stability of the model approximant even if it is known that the full-order model is stable. Hence we cannot bound the error resulting from approximation.

Regarding the last statement, mechanical systems of this type are usually dissipative and stable for a fixed value of the parameter (assuming no rigid body modes), their domain being the whole of L_2^+. In the parameter-varying case this is not necessarily true (consider the Matteau equation [64]) unless a sufficiently strong limit is placed on the rate of parameter variation. Unfortunately, even when the rate of parameter variation is sufficiently restricted so as to ensure that the full-order model remains stable, modal truncation may still fail to produce a stable approximant.

More ambitious models of damping might destroy the orthogonality relations so crucial to the application of modal truncation. In this case the general state-space realisation given in equation (7.6) and which is applicable to a much larger class of systems is suitable:

$$P_\rho \stackrel{s}{=} \left[\begin{array}{c|c} A(\rho) & B(\rho) \\ \hline C(\rho) & D(\rho) \end{array}\right]. \tag{7.6}$$

The relevant assumptions concerning the dimensions and continuity properties of the state-space matrices made in chapter 2 are assumed to hold. These assumptions are sufficient to ensure that there exists a state transformation matrix $T(\rho)$ such that for fixed ρ

$$P_\rho \stackrel{s}{=} \left[\begin{array}{c|c} A_J(\rho) & B_J(\rho) \\ \hline C_J(\rho) & D(\rho) \end{array}\right] \tag{7.7}$$

$$P_\rho \stackrel{s}{=} \left[\begin{array}{c|c} T^{-1}(\rho)A(\rho)T(\rho) & T^{-1}(\rho)B(\rho) \\ \hline C(\rho)T(\rho) & D(\rho) \end{array}\right], \tag{7.8}$$

[2] Actually, this is not a serious problem because if $M(\rho)$ and $K(\rho)$ are both analytic matrix functions then the transformation matrix can always be chosen in such a way as to make it analytic.

where the matrix A_J is in Jordan canonical form

$$A_J = \begin{bmatrix} J_1(\lambda_1) & & & \\ & J_2(\lambda_2) & & \\ & & \ddots & \\ & & & J_k(\lambda_k) \end{bmatrix} \tag{7.9}$$

$$J_i = \begin{bmatrix} \lambda_i(\rho) & 1 & & \\ & \lambda_i(\rho) & 1 & \\ & & \ddots & \\ & & & \lambda_i(\rho) \end{bmatrix} \in \mathbb{C}^{n_i \times n_i} \tag{7.10}$$

and the matrices B_J and C_J are partitioned conformally

$$B_J = \begin{bmatrix} B_{J_1}(\rho) \\ B_{J_2}(\rho) \\ \vdots \\ B_{J_k}(\rho) \end{bmatrix} \qquad C_J = \begin{bmatrix} C_{J_1}(\rho) & C_{J_2}(\rho) & \dots & C_{J_k}(\rho) \end{bmatrix}. \tag{7.11}$$

The Jordan canonical form gives a frequency domain decomposition of the input-output operator

$$G = \sum_i C_{J_i}(\rho)(sI - A_{J_i}(\rho))^{-1} B_{J_i}(\rho) + D(\rho). \tag{7.12}$$

Reducing the state dimension by retaining only those states in the frequency range of interest constitutes a useful[3] and valid reduction technique in the time-invariant case. Extending this technique to the parameter-varying case we encounter similar problems to those outlined previously.

It is clear that if we are to retain stability and bound the approximation error we will need to guarantee stability of both the full-order model and the reduced-order approximant. We will also need knowledge of the continuity properties of the state transformation matrix since this must be differentiable with respect to the parameter. For LPV systems this can be achieved through the use of Lyapunov functions, which play a central role in the theory of balanced reduction of LTI systems. This is our motivation for extending the theory of balanced model reduction to LPV systems. The main result of this chapter will be to show that balanced truncation of LPV systems can be considered as a perturbation of the same technique when applied to LTI systems, at least for sufficiently slow rates of parameter variation.

[3] A major drawback associated with the Jordan form is numerical sensitivity.

7.3 Balancing of LPV systems

We defined LPV systems in chapter 2 and associated with the LPV system P_ρ the unique (for each parameter trajectory) state transition matrix $\Phi_\rho(t, t_0)$.

Proposition 7.3.1 *[13]*
The state transition matrix is nonsingular for all $(t, t_0) \in \mathbb{R} \times \mathbb{R}$.

We list, without proof, some useful properties of the state transition matrix. (Proofs can be found in [13].)

$$\begin{aligned} \frac{\partial}{\partial t_0}\Phi_\rho(t, t_0) &= -\Phi_\rho(t, t_0)A(\rho(t_0)) \\ \Phi_\rho(t, t_0) &= \Phi_\rho(t, t_1)\Phi_\rho(t_1, t_0) \\ \Phi^{-1}(t, t_0) &= \Phi(t_0, t). \end{aligned} \tag{7.13}$$

We now prove two results which provide a geometric interpretation of LPV systems and an intuitive basis for balanced truncation. For presentation purposes we drop the explicit time dependence in the parameter.

Theorem 7.3.2 *Given a continuous state-space realisation of an LPV system* P_ρ*, any initial state* $x(t_0) = x_0$ *and a differentiable* $Q(\rho) = Q^T(\rho) > 0$ *satisfying*

$$\frac{d}{dt}Q(\rho) + A^T(\rho)Q(\rho) + Q(\rho)A(\rho) + C^T(\rho)C(\rho) < 0 \quad \forall \quad \rho(t) \in F_\rho, \tag{7.14}$$

i. the LPV system P_ρ *is exponentially stable;*

ii. the energy in the output signal is bounded, from above, according to

$$\|y\|_2^2 < \max_{\rho \in F_\rho} x_0^T Q(\rho) x_0.$$

Proof:

i. This follows from the Lyapunov function $V = x^T Q(\rho)x$ which is positive definite, radially unbounded and decrescent. Since the derivative of this Lyapunov function is uniformly negative definite [4]

$$\frac{dV}{dt} \leq -\epsilon I,$$

the result is immediate.

[4] This follows from compactness of the feasible set of parameter trajectories.

ii. Given the initial state $x_0 = x(t_0)$, the output is given by

$$y = C(\rho)\Phi_\rho(t,t_0)x_0,$$

so the energy in the output signal is given by

$$\|y\|_2^2 = \int_{t_0}^{\infty} x_0^T \Phi_\rho^T(t,t_0)C^T(\rho)C(\rho)\Phi_\rho(t,t_0)x_0 dt,$$

where $\Phi_\rho(t,t_0)$ is the unique state transition matrix for the specified path $\rho(t) \in F_\rho$. Now consider equation (7.14): multiplying on the left by $\Phi_\rho^T(t,t_0)$ and on the right by $\Phi_\rho(t,t_0)$ gives

$$\Phi_\rho^T(t,t_0)\dot{Q}(\rho)\Phi_\rho(t,t_0) + \Phi_\rho^T(t,t_0)A^T(\rho)Q(\rho)\Phi_\rho(t,t_0) + \Phi_\rho^T(t,t_0)Q(\rho)A(\rho)\Phi_\rho(t,t_0) + \Phi_\rho^T(t,t_0)C^T(\rho)C(\rho)\Phi_\rho(t,t_0) < 0. \quad (7.15)$$

This, together with the definition of the state transition matrix, gives

$$\frac{d}{dt}\left(\Phi_\rho^T(t,t_0)Q(\rho)\Phi_\rho(t,t_0)\right) + \Phi_\rho^T(t,t_0)C^T(\rho)C(\rho)\Phi_\rho(t,t_0) < 0.$$

Integrating the last expression from t_0 to ∞ and using lemma 2.4.13 gives

$$Q(\rho(t_0)) > \int_{t_0}^{\infty} \Phi_\rho^T(t,t_0)C^T(\rho)C(\rho)\Phi_\rho(t,t_0)dt,$$

from which the result follows readily. ■

Thus $Q(\rho)$ can be used to define a set of observability ellipsoids, the length of the principal axes of which provide an upper bound on the energy in the output signal given the initial state $x(t_0) = x_0$ and the initial parameter $\rho(t_0) = \rho_0$.

Next we consider the largest set of state vectors $x(0) = x_0$ reachable with a unit energy input $u(t) \in L_2^-$.

Theorem 7.3.3 *Given a continuous state-space realisation on an LPV system P_ρ, a differentiable $P(\rho) = P^T(\rho) > 0$ satisfying*

$$-\frac{d}{dt}P(\rho) + A(\rho)P(\rho) + P(\rho)A^T(\rho) + B(\rho)B^T(\rho) < 0 \ \ \forall \ \ \rho(t) \in F_\rho, \quad (7.16)$$

and any initial state $x(0) = x_0$, then:

i. the LPV system P_ρ is exponentially stable;

ii. the energy required to drive the system from $x(-\infty) = 0$ to $x(0) = x_0$ with the input $u(t) \in L_2^-$ is bounded, from below, according to

$$\|u\|_2^2 > \min_{\rho \in F_\rho} x_0^T P^{-1}(\rho) x_0.$$

Proof:

i. This follows by left and right multiplying equation (7.16) by $P^{-1}(\rho)$ and using the Lyapunov function $V = x^T P^{-1}(\rho)x$. Again, the time derivative of this Lyapunov function is uniformly negative definite and this implies exponential stability.

ii. Using the fact that

$$x_0 = \int_{-\infty}^{0} \Phi_\rho(0,\tau)B(\rho(\tau))u(\tau)d\tau,$$

the energy in the input signal can be computed from

$$\|u\|_2^2 = \int_{-\infty}^{0} u^T(\tau)u(\tau)d\tau.$$

The minimum energy input $u(t)$ that achieves the desired state $x(0) = x_0$ is given by

$$\begin{aligned} u(t) &= B^T(\rho)\Phi_\rho^T(0,t)W_c^{-1}x_0 \quad \forall\, t \le 0, \\ \text{where} \qquad W_c &= \int_{-\infty}^{0} \Phi_\rho(0,\tau)B(\rho)B^T(\rho)\Phi_\rho^T(0,\tau)d\tau, \end{aligned}$$

from which it follows that

$$\|u\|_2^2 = x_0^T W_c^{-1} x_0.$$

To see that this is the minimum energy input, consider perturbing the input such that

$$\tilde{u}(t) = B^T(\rho)\Phi_\rho^T(0,t)W_c^{-1}x_0 + u_1(t) \qquad \text{and} \qquad \int_{-\infty}^{0} \Phi_\rho(0,t)B(\rho(t))u_1(t)dt = 0,$$

where the integral constraint is required to ensure that the condition $x(0) = x_0$ is met. It is easily shown that the energy in the perturbed input is given by

$$\|\tilde{u}\|_2^2 = \|u\|_2^2 + \|u_1\|_2^2.$$

Multiplying equation (7.16) on the left by $\Phi_\rho(0,t)$ and on the right by $\Phi_\rho^T(0,t)$ gives

$$\begin{aligned} -\Phi_\rho(0,t)\dot{P}(\rho)\Phi_\rho^T(0,t) + \Phi_\rho(0,t)A(\rho)P(\rho)\Phi_\rho^T(0,t) + \Phi_\rho(0,t)P(\rho)A^T(\rho)\Phi_\rho^T(0,t) + \\ \Phi_\rho(0,t)B(\rho)B^T(\rho)\Phi_\rho^T(0,t) < 0. \quad (7.17) \end{aligned}$$

Using the properties of the state transition matrix listed in equation (7.13), equation (7.17) can be written as

$$-\frac{d}{dt}(\Phi_\rho(0,t)P(\rho)\Phi_\rho^T(0,t)) + \Phi_\rho(0,t)B(\rho)B^T(\rho)\Phi_\rho^T(0,t) < 0,$$

which on integrating over the semi-infinite time axis $(-\infty, 0]$, and noting that $\lim_{t\to-\infty}\Phi_\rho(0,t) = 0$ gives

$$P(\rho(0)) > W_c. \quad (7.18)$$

The result follows directly from equation (7.18). ■

Remark 7.3.4 *If the state-space realisation is not minimal then it is possible that the controllability Gramian W_c might not be invertible. In this case it suffices to restrict attention to the controllable subspace in which case the above result goes through without modification.*

Thus $P^{-1}(\rho)$ can be used to define a family of parameter-varying controllability ellipsoids, the length of the principal axes of which bound, from below, the energy required to reach an initial state $x(0) = x_0$. Henceforth we shall refer to a $Q(\rho)$ satisfying equation (7.14) as a parameter-varying observability Gramian and a $P(\rho)$ satisfying equation (7.16) as a parameter-varying controllability Gramian[5]. Next we examine how the Gramians vary under a similarity transformation of the state vector.

Lemma 7.3.5 *Given a continuous state-space realisation of an LPV system P_ρ, an observability Gramian $Q(\rho)$ satisfying equation (7.14), a controllability Gramian $P(\rho)$ satisfying equation (7.16) and a parameter-varying state transformation matrix $T(\rho)$ then*

$$\begin{aligned} \tilde{Q}(\rho) &= T^T(\rho)Q(\rho)T(\rho) \\ \tilde{P}(\rho) &= T^{-1}(\rho)P(\rho)T^{-T}(\rho) \end{aligned}$$

are parameter-varying observability and controllability Gramians for the transformed system respectively.

Proof: We only prove the result for the observability Gramian, the proof for the controllability Gramian is essentially the same. Given

$$\frac{d}{dt}Q(\rho) + A^T(\rho)Q(\rho) + Q(\rho)A(\rho) + C^T(\rho)C(\rho) < 0 \quad \forall \quad \rho(t) \in F_\rho, \tag{7.19}$$

multiplying this on the left by $T^T(\rho)$ and on the right by $T(\rho)$ gives

$$\frac{d}{dt}(T^T(\rho)Q(\rho)T(\rho)) + T^T(\rho)A^T(\rho)Q(\rho)T(\rho) + T^T(\rho)Q(\rho)A(\rho)T(\rho) + T^T(\rho)C^T(\rho)C(\rho)T(\rho) - \dot{T}^T(\rho)Q(\rho)T(\rho) - T^T(\rho)Q(\rho)\dot{T}(\rho) < 0.$$

This can be written as

$$\frac{d}{dt}\tilde{Q}(\rho) + (T^T(\rho)A^T(\rho)T^{-T}(\rho) - \dot{T}^T(\rho)T^{-T}(\rho))\tilde{Q}(\rho) + \tilde{Q}(\rho)(T^{-1}(\rho)A(\rho)T(\rho) - T^{-1}(\rho)\dot{T}(\rho)) + T^T(\rho)C^T(\rho)C(\rho)T(\rho) < 0$$

which is the desired result. ■

Definition 7.3.6 *Given an n-state LPV system P_ρ, an observability Gramian $Q(\rho)$ satisfying equation (7.14) and a controllability Gramian $P(\rho)$ satisfying equation (7.16), define the $\mathcal{Q}_e$ singular values as:*

$$\sigma_i(\rho) = \sqrt{\lambda_i(Q(\rho)P(\rho))} \quad i = 1, 2, 3 \ldots n.$$

[5]Observe that we have taken care to emphasise the inherent lack of uniqueness in the solutions of equations (7.14) and (7.16). If $Q(\rho)$ satisfies equation (7.14) then so does $\alpha Q(\rho)$ for any constant $\alpha \geq 1$. A similar conclusion holds for $P(\rho)$.

For LTI systems, when the inequalities are replaced by equalities, the $\mathcal{Q}_e$ singular values are unique input-output invariants referred to as Hankel singular values. Although not unique, the $\mathcal{Q}_e$ singular values do provide useful insight into the input-output mapping of a given LPV system; in particular, they bound the mapping from past inputs to future outputs.

Proposition 7.3.7 *The $\mathcal{Q}_e$ singular values bound, from above, the norm of the Hankel operator with symbol P_ρ*

$$\|P_\rho\|_H = \sup_{\rho \in F_\rho} \sup_{u \in L_2^-} \frac{\|\Pi^+ P_\rho u\|_2}{\|u\|_2},$$

according to

$$\|P_\rho\|_H \leq \max_{\rho \in F_\rho} \sigma_1(\rho).$$

Proof: We have already shown that for any $x(0) = x_0$, any feasible path $\rho(t) \in F_\rho$ with $\rho(0) = \rho_0$ and an input $u(t) \in L_2^-$ which takes the system from $x(-\infty) = 0$ to $x(0) = x_0$,

$$\begin{aligned} \|\Pi^+ y\|_2^2 &< x_0^T Q(\rho_0) x_0 \quad \text{and} \\ \|u\|_2^2 &> x_0^T P^{-1}(\rho_0) x_0. \end{aligned}$$

This implies that

$$\begin{aligned} \sup_{\{\rho(t) \in F_\rho | \rho(0) = \rho_0\}} \sup_{\{u \in L_2^- | x(0) = x_0\}} \frac{\|\Pi^+ y\|_2^2}{\|u\|_2^2} &\leq \frac{x_0^T Q(\rho_0) x_0}{x_0^T P^{-1}(\rho_0) x_0} \\ \Rightarrow \|P_\rho\|_H &\leq \max_{\rho \in F_\rho} \sigma_1(\rho). \end{aligned}$$

■

Remark 7.3.8 *For LTI systems the inequalities can be replaced by equalities and this bound becomes tight in the sense that it is achieved by an input $u(t) \in L_2^-$.*

We are now in a position to define precisely what we mean by a balanced parameter-varying realisation. In order to do so we require the existence of a balancing state transformation matrix. The balancing transformation matrix will be used to diagonalise the Gramians, allowing us to extend the above Hankel norm bound to each component of the state vector.

Proposition 7.3.9 *Given a continuous state-space realisation on an LPV system P_ρ, an observability Gramian $Q(\rho)$ satisfying equation (7.14) and a controllability Gramian $P(\rho)$ satisfying equation (7.16), then it is possible to find a parameter-dependent state transformation matrix $T(\rho)$ such that the transformed Gramians $\tilde{P}(\rho) = \tilde{Q}(\rho) = \Sigma(\rho)$. $\Sigma(\rho)$ is a diagonal matrix which, for each $\rho \in F_\rho$, has the $\mathcal{Q}_e$ singular values arranged along its diagonal in descending order $\sigma_1(\rho) \geq \sigma_2(\rho) \geq \sigma_3(\rho) \geq \ldots \sigma_n(\rho) > 0$.*

Proof: This follows from the well-known result for LTI systems [63] where for each $\rho \in F_\rho$ it is possible to find a $T(\rho)$ such that $\tilde{P}(\rho) = \tilde{Q}(\rho) = \Sigma(\rho)$. ■

At this point it is worth clarifying a number of points about the continuity properties of the balancing state transformation matrix and the existence of its derivative. The non-increasing ordering of the $\mathcal{Q}_e$ singular values can give rise to difficulties at certain exceptional points in the parameter space where two or more of the continuous curves[6] representing the $\mathcal{Q}_e$ singular values cross each other. For systems having single parameter dependence we will show that the balancing state transformation matrix is everywhere differentiable except at these exceptional points where it may even fail to be continuous. Indeed, this would indicate that it does not satisfy our requirements of continuity and so does not constitute a valid transformation.

Since the transformation matrix and its derivative has well-defined and bounded left hand and right hand limits at the exceptional points we might be tempted to define the value of the derivative at these points using an appropriate limit. For example, let ρ_i denote an exceptional point and define

$$\frac{dT}{d\rho}_{|_{\rho_i}} = \lim_{\rho \to \rho_i^+} \frac{dT}{d\rho}.$$

Then provided

$$\frac{d\Sigma}{d\rho}_{|_{\rho_i}} \triangleq \lim_{\rho \to \rho_i^+} \left(\frac{dT^T}{d\rho} Q T + T^T \frac{dQ}{d\rho} T + T^T Q \frac{dT}{d\rho}\right) = \lim_{\rho \to \rho_i^+} \left(\frac{dT^{-1}}{d\rho} P T^{-T} + T^{-1} \frac{dP}{d\rho} T^{-T} + T^{-1} P \frac{dT^{-T}}{d\rho}\right),$$

is defined consistently, we are assured that the controllability and the observability inequalities of the transformed system will be satisfied. However, while the solution of the state evolution equation of the transformed system will still be unique and continuous, it may not be consistent with the solution of the original system. We demonstrate this with a simple example. Consider the first-order system

$$\dot{x}(t) + t x(t) = 0, \qquad x(0) = 1. \tag{7.20}$$

Introduce the similarity transformation $\tilde{x}(t) = T(t)x(t)$, where

$$T(t) \triangleq \begin{cases} (2-t) & t \in [0,1] \\ (1+t) & t \in (1,2]. \end{cases}$$

The transformation is everywhere differentiable except at $t = 1$ where it fails to be continuous. Now define

$$\frac{dT}{dt}_{|_1} = \lim_{t \to 1^-} \frac{dT}{dt} = -1,$$

in which case the transformed system becomes

$$\begin{aligned} \dot{\tilde{x}}(t) + t\tilde{x}(t) + \frac{\tilde{x}(t)}{(2-t)} &= 0 \qquad t \in [0,1], \tilde{x}(0) = 2, \\ \dot{\tilde{x}}(t) + t\tilde{x}(t) - \frac{\tilde{x}(t)}{(1+t)} &= 0 \qquad t \in (1,\infty). \end{aligned}$$

[6] That the $\mathcal{Q}_e$ singular values are continuous functions of ρ follows from the differentiability of $P(\rho)$ and $Q(\rho)$ and standard results from matrix analysis concerning the continuity of eigenvalues [49].

The transformed system has a unique continuous solution given by

$$\tilde{x}(t) = \begin{cases} (2-t)e^{-\frac{t^2}{2}} & t \in [0,1] \\ \frac{(1+t)}{2}e^{-\frac{t^2}{2}} & t \in (1,\infty]. \end{cases}$$

Transforming back to the original state we get

$$x(t) = \begin{cases} e^{-\frac{t^2}{2}} & t \in [0,1] \\ \frac{1}{2}e^{-\frac{t^2}{2}} & t \in (1,\infty), \end{cases}$$

which is clearly not equal to the unique continuous solution of equation (7.20) which is given by $x(t) = e^{-\frac{t^2}{2}}$.

Fortunately, for systems which do have such singular value crossings we can rectify the situation by defining a reordering of the columns of $T(\rho)$ and we will show how this can be done in section 7.8. For systems which exhibit this behaviour we define a variant of the balancing state transformation which we call the natural-balancing state transformation.

Proposition 7.3.10 *Given a continuous realisation of an LPV system P_ρ, an analytic[7] observability Gramian $Q(\rho)$ satisfying equation (7.14) and an analytic controllability Gramian $P(\rho)$ satisfying equation (7.16), then it is possible to find a parameter-dependent state transformation matrix $\tilde{T}(\rho)$ such that $\tilde{P}(\rho) = \tilde{Q}(\rho) = \tilde{\Sigma}(\rho)$. $\tilde{\Sigma}(\rho)$ is a diagonal matrix which, for each $\rho \in F_\rho$, has the $\mathcal{Q}_e$ singular values arranged along its diagonal. The $\mathcal{Q}_e$ singular values are not necessarily in descending order.*

Remark 7.3.11 *The relationship between the balancing state transformation matrix $T(\rho)$ and the natural-balancing state transformation matrix $\tilde{T}(\rho)$ is that the latter results from a reordering of the columns of the former. That is, when the Gramians are analytic, there always exists an ordering of the columns of the balancing transformation matrix that makes them differentiable.*

Definition 7.3.12 *Given a continuous realisation of an LPV system and a balancing (alternatively, naturally-balancing) state transformation matrix $T(\rho)$ such that $\tilde{P}(\rho) = \tilde{Q}(\rho) = \Sigma(\rho)$, define the balanced (naturally-balanced) parameter-varying realisation as follows*

$$P_\rho \stackrel{s}{=} \left[\begin{array}{c|c} T^{-1}(\rho)A(\rho)T(\rho) - T^{-1}(\rho)\dot{T}(\rho) & T^{-1}(\rho)B(\rho) \\ \hline C(\rho)T(\rho) & D(\rho) \end{array}\right].$$

Remark 7.3.13 *The balanced realisation of P_ρ is a function of both ρ and of $\dot{\rho}$, the implication being that state complexity can be reduced at the expense of parameter complexity. Actually, we will see that this is not necessarily true since it is always possible, at least in theory, to remove the rate dependence from the model approximant.*

[7] Analytic in some domain $\mathcal{D}$ such that $F_\rho \subset \mathcal{D}$.

The balanced realisation leads immediately to a balanced truncation procedure for bounded-rate parameter-varying systems which is essentially identical to the procedure used on LTI systems [63].

Definition 7.3.14 *Given a balanced (naturally-balanced) realisation of an exponentially stable n-state LPV system partitioned as follows*

$$P_\rho \stackrel{s}{=} \left[\begin{array}{cc|c} A_{11}(\rho,\dot{\rho}) & A_{12}(\rho,\dot{\rho}) & B_1(\rho) \\ A_{21}(\rho,\dot{\rho}) & A_{22}(\rho,\dot{\rho}) & B_2(\rho) \\ \hline C_1(\rho) & C_2(\rho) & D(\rho) \end{array}\right],$$

where $A_{11} \in \mathbb{R}^{r\times r}, A_{12} \in \mathbb{R}^{r\times(n-r)}, A_{21} \in \mathbb{R}^{(n-r)\times r}, A_{22} \in \mathbb{R}^{(n-r)\times(n-r)}, B_1 \in \mathbb{R}^{r\times m}, B_2 \in \mathbb{R}^{(n-r)\times m}, C_1 \in \mathbb{R}^{p\times r}$ *and* $C_2 \in \mathbb{R}^{p\times(n-r)}$*, define the r-state balanced model approximant as follows*

$$\hat{P}_\rho \stackrel{s}{=} \left[\begin{array}{c|c} A_{11}(\rho,\dot{\rho}) & B_1(\rho) \\ \hline C_1(\rho) & D(\rho) \end{array}\right].$$

A physical interpretation of balanced truncation can now be given. When the system is balanced, the contribution of a given state to the input-output mapping is exposed. States corresponding to large $\mathcal{Q}_e$ singular values are easy to excite from the input and are strongly reflected in the output. States corresponding to small $\mathcal{Q}_e$ singular values are hard to excite from the input and are weakly reflected in the output. So truncating those states that are associated with small $\mathcal{Q}_e$ singular values is equivalent to removing the states that do not contribute strongly to the input-output mapping. For systems where we use the natural-balancing state transformation more care is required in this interpretation because for certain parameter values we might not be eliminating the most important states.

A useful property of the balanced truncation procedure is that for any exponentially stable LPV system the resulting model approximant is exponentially stable. So balanced truncation of stable LPV systems preserves stability and guarantees that the error resulting from approximation will be bounded.

Lemma 7.3.15 *The balanced (naturally-balanced) model approximant $\hat{P}_\rho$ of an exponentially stable LPV system P_ρ is itself balanced (naturally-balanced) and exponentially stable.*

Proof: Stability follows from the $(1,1)$ block of either of the Lyapunov inequalities. Partition $\tilde{Q}(\rho)$ conformally with the balanced realisation of P_ρ to get

$$\tilde{Q}(\rho) = \left[\begin{array}{cc} \Sigma_1(\rho) & 0 \\ 0 & \Sigma_2(\rho) \end{array}\right].$$

The $(1,1)$ block of the transformed observability inequality gives

$$\dot{\Sigma}_1(\rho) + A_{11}^T(\rho,\dot{\rho})\Sigma_1(\rho) + \Sigma_1(\rho)A_{11}(\rho,\dot{\rho}) + C_1^T(\rho)C_1(\rho) < 0 \;\; \forall\, \rho(t) \in F_\rho.$$

$V = x^T\Sigma_1(\rho)x$ is clearly a Lyapunov function for the reduced-order approximant. Since $\Sigma(\rho)$ is diagonal and satisfies equation (7.14) and equation (7.16), it is evident that the controllability and observability Gramians of the truncated system are balanced. ■

We conclude this section by showing how the rate dependence can be removed from the model approximant. It should be clear that the balanced approximant has affine rate dependence which implies that it has a state-space realisation of the form

$$\hat{P}_\rho \stackrel{s}{=} \left[\begin{array}{c|c} A_{11}^0(\rho) + \dot{\rho}A_{11}^1(\rho) & B_1(\rho) \\ \hline C_1(\rho) & D(\rho) \end{array}\right].$$

Introducing a similarity transformation $L(\rho)$, this becomes

$$\hat{P}_\rho \stackrel{s}{=} \left[\begin{array}{c|c} L^{-1}(\rho)A_{11}^0(\rho)L(\rho) + \dot{\rho}(L^{-1}(\rho)A_{11}^1(\rho)L(\rho) - L^{-1}(\rho)\frac{dL}{d\rho}) & L^{-1}(\rho)B_1(\rho) \\ \hline C_1(\rho)L(\rho) & D(\rho) \end{array}\right].$$

If the transformation matrix is chosen to satisfy

$$L^{-1}(\rho)A_{11}^1(\rho)L(\rho) - L^{-1}(\rho)\frac{dL}{d\rho} = 0,$$

or equivalently,

$$\frac{dL}{d\rho} = A_{11}^1(\rho)L(\rho), \tag{7.21}$$

then the new realisation will be independent of $\dot{\rho}$. Since $A_{11}^1(\rho)$ is continuous and F_ρ is compact, we can solve equation (7.21) numerically with an arbitrary initial condition (presumably a normalisation condition). This shows that the rate dependence is actually a realisation phenomenon, not an intrinsic property of the approximation procedure[8].

7.4 Frequency-weighted generalisation

Balanced truncation of LTI systems produces zero error at infinite frequency because it does not influence the system's D matrix, but from a control perspective we would like the approximation error to be small at low and intermediate frequencies. In the case of LTI systems it is well known that there is an upper bound on the truncation error which is tight and actually achieved at DC when only one state is truncated [28]. It is also known that in the general case where more than one state is truncated the maximum approximation error resulting from balanced truncation occurs at low frequency. This has led to the development of several alternative approximation schemes which emphasise low frequency approximation rather than giving good approximation at high frequencies. Of course parameter-varying systems do not have a frequency response but we can still draw on intuition gained from LTI systems in order to improve the approximation for the purpose of control design. In this regard the frequency-weighted technique introduced by Enns [28] proves particularly useful since it can be regarded as weighting (or filtering) the signal space to emphasise particular frequency regions. In this section we will examine this frequency-weighted approximation technique and show how it extends very naturally to the LPV case.

[8] We point out that application of a transformation to the second order system in equation (7.1) gives nonlinear $\dot{\rho}$ dependence which could not be removed from the modal approximant in this way.

Consider introducing the frequency weights W_i and W_o at the plant input and output respectively.

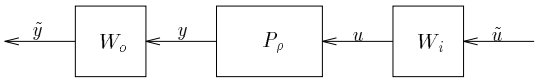

Figure 7.2 *Interconnection of the frequency weights.*

Assuming the following state-space realisations (there is no loss of generality by assuming P_ρ to be strictly proper)

$$P_\rho \stackrel{s}{=} \left[\begin{array}{c|c} A & B \\ \hline C & 0 \end{array}\right] \qquad W_i \stackrel{s}{=} \left[\begin{array}{c|c} A_i & B_i \\ \hline C_i & D_i \end{array}\right] \qquad \text{and} \qquad W_o \stackrel{s}{=} \left[\begin{array}{c|c} A_o & B_o \\ \hline C_o & D_o \end{array}\right],$$

where P_ρ is assumed to have n states, then a state-space realisation of the interconnection is given by

$$P_w \stackrel{s}{=} \left[\begin{array}{c|c} \bar{A} & \bar{B} \\ \hline C & 0 \end{array}\right] \tag{7.22}$$

$$P_w \stackrel{s}{=} \left[\begin{array}{ccc|c} A & 0 & BC_i & BD_i \\ B_oC & A_o & 0 & 0 \\ 0 & 0 & A_i & B_i \\ \hline D_oC & C_o & 0 & 0 \end{array}\right]. \tag{7.23}$$

Let $\bar{P}$ and $\bar{Q}$ be controllability and observability Gramians satisfying

$$\begin{aligned} -\dot{\bar{P}} + \bar{A}\bar{P} + \bar{P}\bar{A}^T + \bar{B}\bar{B}^T &< 0 \quad \forall\ \rho(t) \in F_\rho \\ \dot{\bar{Q}} + \bar{A}^T\bar{Q} + \bar{Q}\bar{A} + \bar{C}^T\bar{C} &< 0 \quad \forall\ \rho(t) \in F_\rho. \end{aligned}$$

The input-weighted controllability Gramian and the output-weighted observability Gramian are then defined as follows

$$P \stackrel{\triangle}{=} \left[\begin{array}{ccc} I_n & 0 & 0 \end{array}\right] \bar{P} \left[\begin{array}{c} I_n \\ 0 \\ 0 \end{array}\right] \qquad \text{and} \qquad Q \stackrel{\triangle}{=} \left[\begin{array}{ccc} I_n & 0 & 0 \end{array}\right] \bar{Q} \left[\begin{array}{c} I_n \\ 0 \\ 0 \end{array}\right].$$

Let $x(0) = [x_0 \ 0 \ 0]^T$ be partitioned in accordance with equation (7.23) with x_0 the initial state of P_ρ. Then the energy in the filtered output signal with $u(t) = 0$ for all $t \geq 0$ is bounded by

$$\|\tilde{y}\|_2^2 < x_0^T Q x_0.$$

Similarly with initial states given by $x(0) = [x_0 \ y_0 \ z_0]^T$ the energy required of a filtered input to reach this state is bounded by

$$\|u\|_2^2 > x_0^T P^{-1} x_0$$

for some y_0 and z_0. The intention is therefore to emphasis the frequency range of interest and effective results can be obtained. However, since the initial states are not matched in the above (i.e. in the inequality bounding the input energy the states of the weights are not constrained whereas in the inequality bounding the output energy the initial states of the weights are required to be zero) these singular values can be unreliable indicators of the frequency weighted error. Applying the balanced truncation technique using the weighted Gramians effectively removes any states that either do not contribute strongly to the input-output map or which only contribute strongly in a frequency range in which we have little interest.

The weighted approximation scheme is implemented by balancing the weighted controllability and weighted observability Gramians P and Q and then performing a standard balanced (naturally-balanced) truncation. That is, given $T(\rho)$ such that

$$T^{-1}(\rho)P(\rho)T^{-T}(\rho) = \mathrm{diag}(\sigma_1(\rho), \sigma_2(\rho)\ldots\sigma_n(\rho)) = T^T(\rho)Q(\rho)T(\rho),$$

partition the transformed system according to

$$P_\rho \stackrel{s}{=} \left[\begin{array}{c|c} T^{-1}AT - T^{-1}\dot{T} & T^{-1}B \\ \hline CT & 0 \end{array}\right] = \left[\begin{array}{cc|c} A_{11}(\rho,\dot{\rho}) & A_{12}(\rho,\dot{\rho}) & B_1(\rho) \\ A_{21}(\rho,\dot{\rho}) & A_{22}(\rho,\dot{\rho}) & B_2(\rho) \\ \hline C_1(\rho) & C_2(\rho) & 0 \end{array}\right].$$

Then the frequency-weighted model approximant is given by

$$\hat{P}_\rho \stackrel{s}{=} \left[\begin{array}{c|c} A_{11}(\rho,\dot{\rho}) & B_1(\rho) \\ \hline C_1(\rho) & D(\rho) \end{array}\right]. \tag{7.24}$$

Simple algebraic manipulations show that the controllability Gramian P satisfies

$$\left[\begin{array}{cc} -\dot{P} & -\dot{P}_{12} \\ -\dot{P}_{12}^T & -\dot{P}_{22} \end{array}\right] + \left[\begin{array}{cc} A & BC_i \\ 0 & A_i \end{array}\right]\left[\begin{array}{cc} P & P_{12} \\ P_{12}^T & P_{22} \end{array}\right] + \left[\begin{array}{cc} P & P_{12} \\ P_{12}^T & P_{22} \end{array}\right]\left[\begin{array}{cc} A & B_iC_i \\ 0 & A_i \end{array}\right]^T + \left[\begin{array}{c} BD_i \\ B_i \end{array}\right]\left[\begin{array}{cc} D_i^TB^T & B_i^T \end{array}\right] < 0,$$

while the observability Gramian Q satisfies

$$\left[\begin{array}{cc} \dot{Q} & \dot{Q}_{12} \\ \dot{Q}_{12}^T & \dot{Q}_{22} \end{array}\right] + \left[\begin{array}{cc} A & 0 \\ B_oC & A_o \end{array}\right]^T\left[\begin{array}{cc} Q & Q_{12} \\ Q_{12}^T & Q_{22} \end{array}\right] + \left[\begin{array}{cc} Q & Q_{12} \\ Q_{12}^T & Q_{22} \end{array}\right]\left[\begin{array}{cc} A & 0 \\ B_oC & A_o \end{array}\right]^T + \left[\begin{array}{c} C^TD_o^T \\ C_o^T \end{array}\right]\left[\begin{array}{cc} D_oC & C_o \end{array}\right] < 0.$$

In general neither $V = x^TP^{-1}(\rho)x$ nor $V = x^TQ(\rho)x$ is a Lyapunov function for the unweighted system P_ρ, and hence cannot be used to guarantee stability of the full-order model, let alone a reduced-order approximant. In the special case where unity input weighting ($W_i = I$) is used the controllability Gramian satisfies

$$-\dot{P} + AP + PA^T + BB^T < 0 \;\; \forall\, \rho(t) \in F_\rho.$$

Thus $V = x^T P^{-1} x$ is a Lyapunov function for the original parameter-varying system and on performing a balancing transformation it is easily shown that the $(1,1)$ block of the balanced controllability Gramian satisfies

$$-\dot{\Sigma} + A_{11}(\rho,\dot{\rho})\Sigma + \Sigma A_{11}^T(\rho,\dot{\rho}) + B_1 B_1^T < 0 \ \ \forall\ \rho(t) \in F_\rho,$$

where A_{11}, B_1 and C_1 are the state-space matrices of the output frequency-weighted model approximant (see equation 7.24). This shows that the frequency-weighted truncation scheme guarantees a stable model approximant with unity input weighting. A similar argument shows that the same stability result holds if unity output weighting ($W_o = I$) is used. For these two special cases we obtain stable approximants from stable systems when using frequency-weighted balanced truncation.

7.5 Approximation in the graph topology

A major drawback with the technique developed so far is the requirement of $\mathcal{Q}_e$ stability. If the system is not $\mathcal{Q}_e$ stable, or alternatively, if the parameter rates are not sufficiently restricted to give $\mathcal{Q}_e$ stability for all admissible parameter trajectories, then the system cannot be approximated using balanced truncation. The problem of extending the applicability of balanced truncation to unstable LTI systems by approximating the symbol of the system's graph has been studied by a number of authors ([38],[62],[65]). Our aim in this section is to extend some of the standard results on coprime factorisation of LTI systems to bounded-rate parameter-varying systems. In so doing we construct a symbol for the system's graph which can be approximated using the machinery already developed. Of course any coprime factorisation can be used to construct a symbol for the system's graph but we will concentrate on what we call a contractive coprime factorisation (ccf). This is analogous to the normalised coprime factorisation of LTI systems and its extension to LTV systems in [74]. For LPV systems we cannot satisfy a normalisation condition for all feasible parameter trajectories, hence the notion of a contractive coprime factorisation. It turns out that there is a nice duality between the Gramians of a ccf and the solutions of certain Riccati differential inequalities. This duality can be exploited to synthesise reduced-order LPV controllers, a topic we address in chapter 8.

Before we consider the fractional approach to model reduction of LPV systems we gather some relevant results on the factorisation of general linear time-varying (LTV) systems. These results are from Khargonekar et al [54] and Pascoal et al [68]. Let $\mathcal{M}$ denote the set of causal finite-dimensional LTV operators defined on $L_{2,e}^+$, and let $\mathcal{B}$ denote the corresponding subset of stable operators (ie: operators in $\mathcal{M}$ with finite induced norm). Denote by $\mathcal{B}^-$ the operators in $\mathcal{B}$ that admit causal, not necessarily stable, inverses in $\mathcal{M}$. The elements of $\mathcal{M}$ admit state-space realisations of the form

$$P \stackrel{s}{=} \left[\begin{array}{c|c} A(t) & B(t) \\ \hline C(t) & D(t) \end{array}\right],$$

as discussed in chapter 2. A realisation on an element P in $\mathcal{M}$ is said to be exponentially stable if its state transition matrix $\Phi(t,\tau)$ satisfies $\|\Phi(t,\tau)\| \leq \alpha e^{-\beta(t-\tau)}$ for some positive constants α

and β for all $t \geq \tau$. That is, the solution of the differential equation

$$\dot{x}(t) = A(t)x(t), \quad t \in \mathbb{R}^+$$

is uniformly asymptotically stable. A realisation is said to be stabilisable (respectively detectable) if there exists a bounded matrix function $F(t)$ (respectively $L(t)$) such that the system $dx/dt = (A(t) + B(t)F(t))x(t)$ (respectively $dx/dt = (A(t) + L(t)C(t))x(t)$) is exponentially stable.

Definition 7.5.1 *An operator $P \in M$ is said to admit a right (respectively left) coprime factorisation over $\mathcal{B}$, if there exist operators N, X, Y in $\mathcal{B}$ and M in $\mathcal{B}^-$ (respectively $\tilde{N}, \tilde{X}, \tilde{Y}$ in $\mathcal{B}$ and $\tilde{M}$ in $\mathcal{B}^-$) such that $P = NM^{-1}$ and $XN + YM = I$ (respectively, $P = \tilde{M}^{-1}\tilde{N}$ and $\tilde{N}\tilde{X} + \tilde{M}\tilde{Y} = I$). We denote right (respectively left) coprime factorisations by the ordered pair $[N, M]$ (respectively $[\tilde{N}, \tilde{M}]$).*

Right coprime factorisations are only unique up to right multiplication by a unit in $\mathcal{B}$ and similarly left factorisations are unique up to left multiplication by a unit in $\mathcal{B}$.

Theorem 7.5.2 *[54] Let P be a finite-dimensional LTV system which has a stabilisable and detectable realisation. Then P admits right and left coprime factorisations over $\mathcal{B}$.*

Having established the existence of coprime factorisations of general finite-dimensional LTV operators we can turn our attention to the subclass of finite-dimensional LPV operators. In the sequel we will replace the ring $\mathcal{B}$ with the subring of stable operators in $\mathcal{M}$ consisting of $\mathcal{Q}_e$ stable elements.

Definition 7.5.3 *Let $\mathcal{S}_F$ denote the ring of all causal, $\mathcal{Q}_e$ stable, finite-dimensional LPV systems defined on the underlying feasible parameter set F_ρ. Denote by $\mathcal{S}_F^-$ the elements in $\mathcal{S}_F$ that have causal inverses.*

Our objective is to obtain a coprime factorisation of the LPV system P_ρ over the ring $\mathcal{S}_F$. Such a factorisation can be obtained using the following lemma.

Lemma 7.5.4 *Let P_ρ have a continuous, $\mathcal{Q}_e$ stabilisable and $\mathcal{Q}_e$ detectable state-space realisation*

$$P_\rho \stackrel{s}{=} \left[\begin{array}{c|c} A(\rho) & B(\rho) \\ \hline C(\rho) & D(\rho) \end{array}\right].$$

Let $F(\rho)$ and $L(\rho)$ be continuous matrix functions such that $dx/dt = (A(\rho) + B(\rho)F(\rho))x(t)$ and $dx/dt = (A(\rho) + L(\rho)C(\rho))x(t)$ are $\mathcal{Q}_e$ stable for all $\rho \in F_\rho$, and define (dropping ρ dependence)

$$\left[\begin{array}{cc} N_\rho & \tilde{Y}_\rho \\ M_\rho & \tilde{X}_\rho \end{array}\right] \triangleq \left[\begin{array}{c|cc} A+BF & B & -L \\ \hline C+DF & D & I \\ F & I & 0 \end{array}\right]$$

$$\left[\begin{array}{cc} X_\rho & Y_\rho \\ \tilde{M}_\rho & -\tilde{N}_\rho \end{array}\right] \triangleq \left[\begin{array}{c|cc} A+LC & L & -(B+LD) \\ \hline F & 0 & I \\ C & I & -D \end{array}\right],$$

then

$$\begin{bmatrix} X_\rho & Y_\rho \\ \tilde{M}_\rho & -\tilde{N}_\rho \end{bmatrix} \begin{bmatrix} N_\rho & \tilde{Y}_\rho \\ M_\rho & \tilde{X}_\rho \end{bmatrix} = I.$$

Proof: The product has a state-space realisation given by

$$\begin{bmatrix} X_\rho & Y_\rho \\ \tilde{M}_\rho & -\tilde{N}_\rho \end{bmatrix} \begin{bmatrix} N_\rho & \tilde{Y}_\rho \\ M_\rho & \tilde{X}_\rho \end{bmatrix} \stackrel{s}{=} \left[\begin{array}{cc|cc} A+LC & LC-BF & -B & L \\ 0 & A+BF & B & -L \\ \hline F & F & I & 0 \\ C & C & 0 & I \end{array}\right].$$

Making use of the parameter-independent state transformation

$$T^{-1} = \begin{bmatrix} I & I \\ I & -I \end{bmatrix}, \qquad T = \begin{bmatrix} \frac{I}{2} & \frac{I}{2} \\ \frac{I}{2} & -\frac{I}{2} \end{bmatrix}, \qquad \text{gives}$$

$$\begin{bmatrix} X_\rho & Y_\rho \\ \tilde{M}_\rho & -\tilde{N}_\rho \end{bmatrix} \begin{bmatrix} N_\rho & \tilde{Y}_\rho \\ M_\rho & -\tilde{X}_\rho \end{bmatrix} \stackrel{s}{=} \left[\begin{array}{cc|cc} A+LC & 0 & 0 & 0 \\ LC-BF & A+BF & -2B & 2L \\ \hline F & 0 & I & 0 \\ C & 0 & 0 & I \end{array}\right]$$

which is unobservable and uncontrollable. ■

Definition 7.5.5 *Let $N_\rho \in \mathcal{S}_F$ and $M_\rho \in S_F^-$ have the same number of columns. The ordered pair $[N_\rho, M_\rho]$ represents a contractive right coprime factorisation (crcf) of P_ρ over the ring S_F, if*

i. $P_\rho = N_\rho M_\rho^{-1}$;

ii. there exist $X_\rho, Y_\rho \in \mathcal{S}_F$ *such that* $X_\rho N_\rho + Y_\rho M_\rho = I$;

iii. $[N_\rho^T \;\; M_\rho^T]^T$ *is a contraction in the following sense*

$$\sup_{\rho \in F_\rho} \sup_{\{u \in L_2^+ : \|u\|_2 \leq 1\}} \left\| \begin{bmatrix} N_\rho \\ M_\rho \end{bmatrix} u \right\| \leq 1.$$

Definition 7.5.6 *Define the contractive right graph symbol $\mathcal{G}_\rho : L_2^+ \mapsto L_2^+ \otimes L_2^+$ of an LPV system P_ρ as follows*

$$\mathcal{G}_\rho \stackrel{\triangle}{=} \begin{bmatrix} N_\rho \\ M_\rho \end{bmatrix},$$

where $[N_\rho, M_\rho]$ is a crcf of P_ρ.

It should be immediately obvious that $\mathcal{G}_\rho$ generates the set of all stable input-output pairs of the LPV system P_ρ by allowing $\mathcal{G}_\rho$ to act on the whole of L_2+.

Theorem 7.5.7 *Let P_ρ have a continuous, $\mathcal{Q}_e$ stabilisable and $\mathcal{Q}_e$ detectable realisation, then a contractive right graph symbol of P_ρ is given by*

$$\mathcal{G}_\rho \stackrel{\triangle}{=} \left[\begin{array}{c|c} A+BF & BS^{-\frac{1}{2}} \\ \hline C+DF & DS^{-\frac{1}{2}} \\ F & S^{-\frac{1}{2}} \end{array}\right], \tag{7.25}$$

where $F = -S^{-1}(B^TZ_1 + D^TC)$, $S = I + D^TD$, $R = I + DD^T$ and Z_1 is a solution of the generalised control Riccati inequality (GCRI)

$$\dot{Z}_1 + (A - BS^{-1}D^TC)^TZ_1 + Z_1(A - BS^{-1}D^TC) - Z_1BS^{-1}B^TZ_1 + C^TR^{-1}C < 0 \ \ \forall \rho(t) \in F_\rho. \tag{7.26}$$

Proof: We will use the quadratic dissipation function in definition 2.4.17 to show that the system is $\mathcal{Q}_e$ stable and a contraction. We reformulate the problem as follows

$$\begin{aligned}\inf\{\gamma : \dot{X} + X(A+BF) + (A+BF)^TX + (C+DF)^T(C+DF) + F^TF + \\ (XBS^{-\frac{1}{2}} + (C+DF)^TDS^{-\frac{1}{2}} + F^TS^{-\frac{1}{2}})(\gamma^2I - I)^{-1} \\ (XBS^{-\frac{1}{2}} + (C+DF)^TDS^{-\frac{1}{2}} + F^TS^{-\frac{1}{2}})^T < 0 \ \forall \rho(t) \in F_\rho.\}\end{aligned}$$

First observe that by taking $X(\rho) = Z_1(\rho)$, we have

$$XBS^{-\frac{1}{2}} + (C+DF)^TDS^{-\frac{1}{2}} + F^TS^{-\frac{1}{2}} = (Z_1B + C^TD + F^T(I + D^TD))S^{-\frac{1}{2}} = 0.$$

So we are left with the task of showing that the following inequality holds

$$\dot{Z}_1 + Z_1(A+BF) + (A+BF)^TZ_1 + (C+DF)^T(C+DF) + F^TF < 0 \quad \forall\, \rho(t) \in F_\rho. \tag{7.27}$$

Manipulating the left hand side of equation (7.27), it is easily shown to be equivalent to equation (7.26). This shows that the system is exponentially stable and has an induced norm which is bounded, from above, by $\gamma = 1 + \epsilon$ for arbitrary $\epsilon > 0$. Clearly $N_\rho \in \mathcal{S}_F$ and $M_\rho \in \mathcal{S}_F^-$. Finally, using the state-space formulas in lemma 7.5.4 and the detectability of P_ρ we can construct a left inverse for $\mathcal{G}_\rho$. ■

Remark 7.5.8 *The results as stated here are for right coprime factorisations; the dual results are easily obtained for left coprime factorisations.*

Lemma 7.5.9 *Let P_ρ have a continuous, $\mathcal{Q}_e$ stabilisable and a $\mathcal{Q}_e$ detectable realisation, and let the ordered pair $[N_\rho, M_\rho]$ represent the crcf of P_ρ given in equation (7.25). Then*

$$Q = Z_1 \quad \text{and} \quad P = (I + Z_2Z_1)^{-1}Z_2$$

are observability and controllability Gramians for the given realisation. Here Z_1 solves GCRI and Z_2 solves the generalised filtering Riccati inequality (GFRI) given by

$$-\dot{Z}_2 + (A - BD^TR^{-1}C)Z_2 + Z_2(A - BD^TR^{-1}C)^T - Z_2C^TR^{-1}CZ_2 + BS^{-1}B^T < 0 \ \ \forall \rho(t) \in F_\rho,$$

where $R = I + DD^T$ and $S = I + D^TD$.

Proof: Starting with GCRI and setting $Z_1 = Q$, some algebraic manipulations allow GCRI to be written as

$$\dot{Q} + (A+BF)^T Q + Q(A+BF) + (C+DF)^T(C+DF) + F^T F < 0 \ \ \forall \rho(t) \in F_\rho,$$

which is recognised as the observability inequality for the realisation in equation (7.25). To show that $P = (I + Z_2 Z_1)^{-1} Z_2$ is a controllability Gramian we need to show that

$$-\dot{P} + (A+BF)P + P(A+BF)^T + BS^{-1}B^T < 0 \ \ \forall \rho(t) \in F_\rho. \tag{7.28}$$

Substituting $P = (I + Z_2 Z_1)^{-1} Z_2$ into equation (7.28) and performing some lengthy manipulations gives

$$-\dot{P} + (A+BF)P + P(A+BF)^T + BS^{-1}B^T = \text{GFRI} + Z_2 \text{GCRI} Z_2 < 0 \ \ \forall \ \ \rho(t) \in F_\rho.$$

■

Definition 7.5.10 *Given the crcf of the n-state system P_ρ in equation (7.25), a controllability Gramian $P(\rho)$, an observability Gramian $Q(\rho)$, together with a parameter-dependent balancing (naturally-balancing) state transformation matrix $T(\rho)$ such that the transformed Gramians $\tilde{P}(\rho) = \tilde{Q}(\rho) = \Sigma(\rho)$ are diagonal, define a balanced (naturally-balanced) parameter-varying crcf of P_ρ as follows*

$$\begin{aligned}
\mathcal{G}_\rho &\stackrel{s}{=} \left[\begin{array}{c|c} \bar{A}(\rho,\dot{\rho}) + \bar{B}(\rho)\bar{F}(\rho) & \bar{B}(\rho)S^{-\frac{1}{2}}(\rho) \\ \hline \bar{C}(\rho) + D(\rho)\bar{F}(\rho) & D(\rho)S^{-\frac{1}{2}}(\rho) \\ \bar{F}(\rho) & S^{-\frac{1}{2}}(\rho) \end{array}\right], \\
\bar{A}(\rho,\dot{\rho}) &= T^{-1}(\rho)A(\rho)T(\rho) - T^{-1}(\rho)\dot{T}(\rho), \qquad \bar{B}(\rho) = T^{-1}(\rho)B(\rho) \\
\bar{C}(\rho) &= C(\rho)T(\rho), \qquad \bar{F}(\rho) = -S^{-1}(\rho)(\bar{B}^T(\rho)\Sigma(\rho) + D^T(\rho)\bar{C}(\rho)).
\end{aligned}$$

Definition 7.5.11 *Dropping ρ dependence, partition the balanced crcf of the n-state graph symbol in definition 7.5.10 according to*

$$\mathcal{G}_\rho \stackrel{s}{=} \left[\begin{array}{cc|c} \bar{A}_{11} + \bar{B}_1\bar{F}_1 & \bar{A}_{12} + \bar{B}_1\bar{F}_2 & \bar{B}_1 S^{\frac{-1}{2}} \\ \bar{A}_{21} + \bar{B}_2\bar{F}_1 & \bar{A}_{22} + \bar{B}_2\bar{F}_2 & \bar{B}_2 S^{\frac{-1}{2}} \\ \hline \bar{C}_1 + D\bar{F}_1 & \bar{C}_2 + D\bar{F}_2 & DS^{-\frac{1}{2}} \\ \bar{F}_1 & \bar{F}_2 & S^{-\frac{1}{2}} \end{array}\right], \tag{7.29}$$

where $\bar{A}_{11} \in \mathbb{R}^{r\times r}, \bar{A}_{12} \in \mathbb{R}^{r\times(n-r)}, \bar{A}_{21} \in \mathbb{R}^{(n-r)\times r}, \bar{A}_{22} \in \mathbb{R}^{(n-r)\times(n-r)}, \bar{B}_1 \in \mathbb{R}^{r\times m}, \bar{B}_2 \in \mathbb{R}^{(n-r)\times m}, \bar{C}_1 \in \mathbb{R}^{p\times r}, \bar{C}_2 \in \mathbb{R}^{p\times(n-r)}, \bar{F}_1 \in \mathbb{R}^{m\times r}$ and $\bar{F}_2 \in \mathbb{R}^{m\times(n-r)}$. Let $\hat{\mathcal{G}}_\rho$, of state-dimension r, be obtained by truncating $\mathcal{G}_\rho$ as follows

$$\hat{\mathcal{G}}_\rho \stackrel{s}{=} \left[\begin{array}{c|c} \bar{A}_{11} + \bar{B}_1\bar{F}_1 & \bar{B}_1 S^{-\frac{1}{2}} \\ \hline \bar{C}_1 + D\bar{F}_1 & DS^{-\frac{1}{2}} \\ \bar{F}_1 & S^{-\frac{1}{2}} \end{array}\right]. \tag{7.30}$$

We define $\hat{\mathcal{G}}_\rho$ to be a balanced fractional approximant of the system's graph symbol $\mathcal{G}_\rho$, and we associate with $\hat{\mathcal{G}}_\rho$ the following r-state model

$$\hat{P}_\rho = \left[\begin{array}{c|c} \bar{A}_{11} & \bar{B}_1 \\ \hline C_1 & D \end{array}\right].$$

Once again, balanced truncation of the system's graph symbol has an immediate physical interpretation. Essentially, we are removing those states which do not contribute strongly to the input-output mapping of $\mathcal{G}_\rho$. This implies that we are trying to keep the graph of $\hat{P}_\rho$ close to the graph of P_ρ, which is arguably the correct setting for approximation since the concept of the graph topology and the gap between systems is not restricted to LTI systems ([30],[74]). In fact, for time-varying systems it is shown in [68] that the graph topology is still the weakest topology in which feedback is a robust property in the sense of our earlier definitions.

Theorem 7.5.12 *Let $\mathcal{G}_\rho$, of state-dimension n, be balanced and let $\hat{\mathcal{G}}_\rho$, of state-dimension r, be obtained by truncating $\mathcal{G}_\rho$. Then $\hat{\mathcal{G}}_\rho$ is itself balanced and represents a crcf over $\mathcal{S}_F$ of the r-state model*

$$\hat{P}_\rho = \left[\begin{array}{c|c} \bar{A}_{11} & \bar{B}_1 \\ \hline C_1 & D \end{array}\right]. \tag{7.31}$$

Proof: The proof amounts to showing that $\hat{\mathcal{G}}_\rho$ is exponentially stable and a contraction. Showing that the factorisation is coprime requires a little more work and the results of lemma 7.5.13. Since we begin with a balanced crcf (equation (7.29)), the observability inequality is given by

$$\dot{\Sigma} + (\bar{A} + \bar{B}\bar{F})^T\Sigma + \Sigma(\bar{A} + \bar{B}\bar{F}) + (\bar{C} + \bar{D}\bar{F})^T(\bar{C} + \bar{D}\bar{F}) + \bar{F}^T\bar{F} < 0 \;\; \forall \rho(t) \in F_\rho,$$

and on extracting the $(1,1)$ block of this inequality we get

$$\dot{\Sigma}_1 + (\bar{A}_{11} + \bar{B}_1\bar{F}_1)^T\Sigma_1 + \Sigma_1(\bar{A}_{11} + \bar{B}_1\bar{F}_1) + (\bar{C}_1 + \bar{D}\bar{F}_1)^T(\bar{C}_1 + \bar{D}\bar{F}_1) + \bar{F}_1^T\bar{F}_1 < 0 \; \forall \rho(t) \in F_\rho. \tag{7.32}$$

Equation 7.32 shows that the balanced fractional approximant is exponentially stable and together with the $(1,1)$ block of the controllability inequality, balanced. Using the fact that $\bar{F}_1 = -S^{-1}(\bar{B}_1^T\Sigma_1 + D^T\bar{C}_1)$ equation (7.32) can be written as

$$\dot{\Sigma}_1 + (A_{11} - B_1S^{-1}D^TC_1)^T\Sigma_1 + \Sigma_1(A_{11} - B_1S^{-1}D^TC_1) - \Sigma_1B_1S^{-1}B_1^T\Sigma_1 + C_1^TR^{-1}C_1 < 0.$$

Recalling theorem 7.5.7, this shows that $\hat{\mathcal{G}}_\rho$ is a contractive factorisation of $\hat{P}_\rho$. ■

The following lemma is needed to prove that the realisation in equation (7.31) is detectable. It will also prove useful when we consider controller synthesis in chapter 8.

Lemma 7.5.13 *Given the LPV system*

$$P_\rho \stackrel{s}{=} \left[\begin{array}{c|c} A & B \\ \hline C & D \end{array}\right],$$

$Z_1(\rho)$ satisfying GCRI and a $Z_2(\rho)$ satisfying GFRI, then we have already shown (lemma 7.5.9) that $Q = Z_1$ and $P = (I + Z_2Z_1)^{-1}Z_2$ are observability and controllability Gramians for the realisation of the crcf given in equation (7.25). If the realisation in equation (7.25) is subsequently balanced and truncated to give the balanced fractional approximant in equation (7.30), then

$$\hat{Z}_1 = \Sigma_1 \qquad \textit{and} \qquad \hat{Z}_2 = (I - \Sigma_1^2)^{-1}\Sigma_1$$

satisfy GCRI and GFRI for the reduced-order model given by

$$\hat{P}_\rho = \left[\begin{array}{c|c} \bar{A}_{11} & \bar{B}_1 \\ \hline C_1 & D \end{array}\right]. \tag{7.33}$$

Proof: We need to show that the mappings $Q = Z_1$ and $P = (I + Z_2Z_1)^{-1}Z_2$ are invertible. The result is trivial in the LTI case where the inequalities can be replaced with equalities: we now show that the result is still true in the LPV case. First replace GCRI and GFRI with equalities as follows

$$\dot{Z}_1 + (A - BS^{-1}D^TC)^TZ_1 + Z_1(A - BS^{-1}D^TC) - Z_1BS^{-1}B^TZ_1 + C^TR^{-1}C + E_1(\rho,\dot{\rho}) = 0 \tag{7.34}$$

$$-\dot{Z}_2 + (A - BD^TR^{-1}C)Z_2 + Z_2(A - BD^TR^{-1}C)^T - Z_2C^TR^{-1}CZ_2 + BS^{-1}B^T + E_2(\rho,\dot{\rho}) = 0, \tag{7.35}$$

where $E_1(\rho,\dot{\rho}), E_2(\rho,\dot{\rho}) > 0 \ \ \forall\rho(t) \in F_\rho$. Putting $Z_1 = Q$ equation (7.34) is easily rearranged to give

$$\dot{Q} + (A + BF)^TQ + Q(A + BF) + (C + DF)^T(C + DF) + F^TF + E_1 = 0, \tag{7.36}$$

while left and right multiplying equation (7.34) by Z_2 and adding the result to equation (7.35) gives

$$-\dot{P} + (A + BF)P + P(A + BF)^T + BS^{-1}B^T + PE_1P + (I + Z_2Z_1)^{-1}E_2(I + Z_1Z_2)^{-1} = 0. \tag{7.37}$$

Let $T(\rho)$ be the balancing (naturally-balancing) transformation matrix such that $T^{-1}(\rho)P(\rho)T^{-T}(\rho) = \Sigma(\rho)$ and $T^T(\rho)Q(\rho)T(\rho) = \Sigma(\rho)$. Left multiplying equation (7.37) by T^{-1} and right multiplying by T^{-T} gives

$$-\dot{\Sigma} + (\bar{A} + \bar{B}\bar{F})\Sigma + \Sigma(\bar{A} + \bar{B}\bar{F})^T + \bar{B}S^{-1}\bar{B}^T + \Sigma T^TE_1T\Sigma + T^{-1}(I + Z_2Z_1)^{-1}E_2(I + Z_1Z_2)^{-1}T^{-T} = 0, \tag{7.38}$$

where $\bar{A}, \bar{B}, \bar{C}$ and $\bar{F}$ were defined in definition 7.5.10. Left multiplying equation (7.36) by T^T and right multiplying by T gives

$$\dot{\Sigma} + (\bar{A} + \bar{B}\bar{F})^T\Sigma + \Sigma(\bar{A} + \bar{B}\bar{F}) + (\bar{C} + D\bar{F})^T(\bar{C} + D\bar{F}) + \bar{F}^T\bar{F} + T^TE_1T = 0. \quad (7.39)$$

Putting $\Sigma = \bar{Z}_1$ allows equation (7.39) to be written as

$$\dot{\bar{Z}}_1 + (\bar{A} - \bar{B}S^{-1}D^T\bar{C})^T\bar{Z}_1 + \bar{Z}_1(\bar{A} - \bar{B}S^{-1}D^T\bar{C}) - \bar{Z}_1\bar{B}S^{-1}\bar{B}^T\bar{Z}_1 + \bar{C}^TR^{-1}\bar{C} + T^TE_1T = 0, \quad (7.40)$$

as desired. Finally, left and right multiplying equation (7.39) by Σ, subtracting the result from equation (7.38) and putting $\bar{Z}_2 = (I - \Sigma^2)^{-1}\Sigma$ gives

$$-\dot{\bar{Z}}_2 + (\bar{A} - \bar{B}D^TR^{-1}\bar{C})\bar{Z}_2 + \bar{Z}_2(\bar{A} - \bar{B}D^TR^{-1}\bar{C})^T - \bar{Z}_2\bar{C}^TR^{-1}\bar{C}\bar{Z}_2 + \bar{B}S^{-1}\bar{B}^T + T^{-1}(I + Z_2Z_1)^{-1}E_2(I + Z_1Z_2)^{-1}T^{-T} = 0. \quad (7.41)$$

Extracting the $(1,1)$ blocks of equation (7.40) and (7.41) shows that $\hat{Z}_1$ and $\hat{Z}_2$ have the stated properties. ■

Corollary 7.5.14 *The r-state model approximant*

$$\hat{P}_\rho = \left[\begin{array}{c|c} \bar{A}_{11} & \bar{B}_1 \\ \hline C_1 & D \end{array}\right]$$

is detectable and a stabilising output injection is given by $L = -(\bar{B}_1D^T + \hat{Z}_2\bar{C}_1^T)R^{-1}$.

7.6 Induced-norm error bounds for balanced truncation

The small gain theorem is the key result underpinning the development of robust control theory. For LTI systems it provides necessary and sufficient conditions for closed-loop stability when any specific operator in the feedback loop is subjected to a norm bounded LTI perturbation. For LPV systems the small gain theorem still gives sufficiency, making it important to have bounds on the size of any expected perturbations so that closed-loop stability can be assured. Model reduction can be viewed as subjecting a full-order operator to a predictable perturbation (this is depicted in Figure 7.3), so it is important to have have an idea of the size of this perturbation so that a sensible number of states can truncated. For LTI systems it is well known that if $P \in RH_\infty$ has McMillan degree n and $\hat{P} \in RH_\infty$ has McMillan degree k then

$$\inf_{\hat{P} \in RH_\infty} \|P - \hat{P}\|_\infty \geq \sigma_{k+1}(P),$$

where $\sigma_{k+1}(P)$ represents the $k+1$'th LTI Hankel singular value. Since the LTI case is typically (but not always) a special case for an LPV system we cannot do any better than this bound for any fixed $\rho \in F_\rho$. Our goal in this section is to determine under what conditions the known

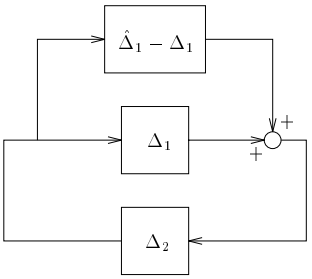

Figure 7.3 *Block diagram interpretation of approximation.*

upper bound on the approximation error resulting from balanced truncation of LTI systems can be extended to LPV systems. For LTI systems it has been shown ([28],[39]) that if $P \in RH_\infty$ has McMillan degree n, and $\hat{P} \in RH_\infty$ of McMillan degree r is obtained from balanced truncation of P, then

$$\|P - \hat{P}\|_\infty \leq 2 \sum_{i=r+1}^{n} \sigma_i(P),$$

where $\sigma_i(P)$ is the i'th LTI Hankel singular value.

We begin with a number of technical lemmas which we require in our efforts to obtain an induced-norm error bound for the proposed LPV balanced truncation technique. Explicit dependence on the parameter is not shown for clarity of presentation but is assumed throughout. First we will prove that the quadratic dissipation function given in definition 2.4.17 has the properties claimed therein.

Lemma 7.6.1 *Suppose $P_\rho : L_{2,e}^+ \mapsto L_{2,e}^+, u(t) \mapsto y(t)$ has a continuous, strictly proper state-space realisation given by*

$$P_\rho \stackrel{s}{=} \left[\begin{array}{c|c} A & B \\ \hline C & 0 \end{array}\right], \tag{7.42}$$

and let $\gamma > 0$ be a given constant. Then $\|P_\rho\| \leq \gamma$ if $\exists \quad X(\rho) = X^T(\rho) > 0$ such that

$$\dot{X} + A^T X + XA + C^T C + \gamma^{-2} XBB^T X < 0 \ \ \forall \rho(t) \in F_\rho. \tag{7.43}$$

Proof: First observe that equation (7.43) implies that the system is exponentially stable. Considering the solution of equation (7.42) with $u \in L_2^+$ and $x(0) = 0$, then

$$\begin{aligned} \frac{d}{dt}(x^T X x) &= \dot{x}^T X x + x^T \dot{X} x + x^T X \dot{x} \\ &= x^T (A^T X + XA + \dot{X}) x + u^T B^T X x + x^T X B u. \end{aligned}$$

Using equation (7.43) this can be written as

$$\frac{d}{dt}(x^T X x) < -x^T C^T C x + \gamma^2 u^T u - (\gamma^{-1} x^T X B - \gamma u^T)(\gamma^{-1} B^T X x - \gamma u).$$

Integrating from $t = 0$ to $t = \infty$ and using lemma 2.4.16, we get

$$\|y\|_2^2 < \gamma^2 \|u\|_2^2 - \|\gamma^{-1} B^T X x - \gamma u\|_2^2 \ \ \forall\ u \in L_2^+, \text{ as desired.}$$

■

Lemma 7.6.2 *Suppose $P_\rho : L_{2,e}^+ \mapsto L_{2,e}^+$ is an LPV system with $P_\rho : u(t) \mapsto y(t)$ defined by the following continuous state-space realisation*

$$P_\rho \stackrel{s}{=} \left[\begin{array}{c|c} A(\rho) & B(\rho) \\ \hline C(\rho) & D(\rho) \end{array}\right].$$

Suppose also that $\gamma^2 I - D^T D > 0$ and $\exists\ X(\rho) = X^T(\rho) > 0$ such that

$$\dot{X} + XA + A^T X + C^T C + (XB + C^T D)(\gamma^2 I - D^T D)^{-1}(B^T X + D^T C) < 0 \ \ \forall\ \rho(t) \in F_\rho. \quad (7.44)$$

Then P_ρ is exponentially stable and $\|P_\rho\| \leq \gamma$.

Proof: Define $\bar{P}_\rho$ according to the interconnection structure in Figure 7.4, where U is a unitary matrix given by

$$U \triangleq \left[\begin{array}{cc} \gamma^{-1} D^T & (I - \gamma^{-2} D^T D)^{\frac{1}{2}} \\ (I - \gamma^{-2} D D^T)^{\frac{1}{2}} & -\gamma^{-1} D \end{array}\right].$$

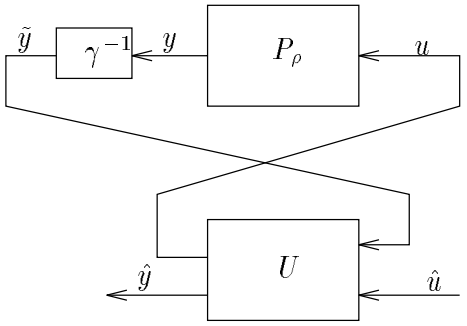

Figure 7.4 *Interconnection structure defining $\bar{P}_\rho$*

The operator $\bar{P}_\rho : L_{2,e}^+ \mapsto L_{2,e}^+$ defines an LPV system with a state-space realisation given by

$$\bar{P}_\rho = \left[\begin{array}{c|c} \bar{A} & \bar{B} \\ \hline \bar{C} & 0 \end{array}\right],$$

and it is easily shown that

$$\begin{aligned}\bar{A} &= A + B(\gamma^2 I - D^T D)^{-1} D^T C \\ \bar{B} &= \gamma B(\gamma^2 I - D^T D)^{-\frac{1}{2}} \\ \bar{C} &= (\gamma^2 I - DD^T)^{-\frac{1}{2}} C \\ \bar{D} &= 0. \end{aligned} \tag{7.45}$$

Define $\tilde{X} \stackrel{\Delta}{=} \gamma^{-2} X$ and rewrite equation (7.44) as

$$\dot{\tilde{X}} + \bar{A}^T \tilde{X} + \tilde{X}\bar{A} + \tilde{X}\bar{B}\bar{B}^T\tilde{X} + \bar{C}^T\bar{C} < 0.$$

Invoking lemma 7.6.1, we see that $\bar{P}_\rho$ is exponentially stable and satisfies $\|\bar{P}_\rho\| \leq 1$. Using the fact that the matrix U is unitary we can write

$$\hat{y}^T\hat{y} + u^T u = \tilde{y}^T\tilde{y} + \hat{u}^T\hat{u}.$$

So $\|\bar{P}_\rho\| \leq 1$ gives

$$\|\hat{y}\|_2 \leq \|\hat{u}\|_2 \Rightarrow \|\tilde{y}\|_2 \leq \|u\|_2.$$

To complete the proof we need to show that the range of $W : \hat{u} \mapsto u$ is all of L_2^+. But W^{-1} is given by

$$W^{-1} \stackrel{s}{=} \left[\begin{array}{c|c} A & B \\ \hline -\gamma^2(I - \gamma^{-2}D^T D)^{-\frac{1}{2}} D^T C & (I - \gamma^{-2}D^T D)^{\frac{1}{2}} \end{array}\right], \tag{7.46}$$

and since this is exponentially stable, $\hat{u}$ is uniquely determined as an element of L_2^+ for any given $u \in L_2^+$. ■

Lemma 7.6.3 *Given a continuous state-space realisation of an LPV system, then provided*

i. $\gamma^2 I - D^T D > 0$;

ii. $\exists\ X(\rho) = X^T(\rho) > 0$ *such that for all* $t \in [t_0, t_1]$

$$\begin{aligned}&\dot{X} + XA + A^T X + C^T C \\ &\qquad + (XB + C^T D)(\gamma^2 I - D^T D)^{-1}(B^T X + D^T C) < 0 \ \ \forall \rho(t) \in F_\rho,\end{aligned} \tag{7.47}$$

the following finite horizon bound holds

$$\|y\|^2_{2,[t_0,t_1]} < \gamma^2 \|u\|^2_{2,[t_0,t_1]} - x^T X x|_{t_0}^{t_1}.$$

Proof: Using the definitions in equation (7.45), equation (7.47) can be written as

$$\dot{\tilde{X}} + \bar{A}^T\tilde{X} + \tilde{X}\bar{A} + \bar{C}^T\bar{C} + \tilde{X}\bar{B}\bar{B}^T\tilde{X} < 0,$$

where $\tilde{X}$ is defined as

$$\tilde{X} \stackrel{\triangle}{=} \gamma^{-2}X.$$

Making use of the Lyapunov function $V = x^T\tilde{X}x$, completing the square as in lemma 7.6.1 and using lemma 7.6.2 the result follows readily. ■

Lemma 7.6.4 *Given a continuous state-space realisation of an LPV system, then provided*

i. $\gamma^2 I - D^T D > 0$;

ii. $\exists\ Y(\rho) = Y^T(\rho) > 0$ *such that for all* $t \in [t_0, t_1]$

$$-\dot{Y} + YA^T + AY + BB^T + (YC^T + BD^T)(\gamma^2 I - DD^T)^{-1}(CY + DB^T) < 0 \ \ \forall \rho(t) \in F_\rho, \quad (7.48)$$

the following finite horizon bound holds

$$\|y\|^2_{2,[t_0,t_1]} < \gamma^2\|u\|^2_{2,[t_0,t_1]} - \gamma^2 x^T Y^{-1}x\Big|_{t_0}^{t_1}.$$

Proof: This follows by defining

$$X \stackrel{\triangle}{=} \gamma^2 Y^{-1},$$

multiplying equation (7.48) on the left by $\gamma^2 Y^{-1}$, on the right by Y^{-1}, and by making use of lemma (7.6.3). ■

We are now in a position to examine the induced-norm error resulting from balanced (naturally-balanced) truncation. We will restrict attention to the case where only those states corresponding to one of the $\mathcal{Q}_e$ singular values are removed from the balanced (naturally-balanced) realisation[9]. The case where the states corresponding to more than one $\mathcal{Q}_e$ singular value are removed is easily obtained using the triangle inequality. Assume that P_ρ, of state-dimension n, is balanced (naturally-balanced) and that $\hat{P}_\rho$, of state-dimension r, is obtained from a balanced (naturally-balanced) truncation of P_ρ ($r < n$). Since P_ρ is balanced (naturally-balanced), there exist differentiable $P(\rho) = P^T(\rho) > 0$ and $Q(\rho) = Q^T(\rho) > 0$ which satisfy the Lyapunov inequalities

$$\begin{aligned} \dot{Q}(\rho) + A^T(\rho,\dot{\rho})Q(\rho) + Q(\rho)A(\rho,\dot{\rho}) + C^T(\rho)C(\rho) &< 0 \quad \forall \quad \rho(t) \in F_\rho \\ -\dot{P}(\rho) + A(\rho,\dot{\rho})P(\rho) + P(\rho)A^T(\rho,\dot{\rho}) + B(\rho)B^T(\rho) &< 0 \quad \forall \quad \rho(t) \in F_\rho, \end{aligned}$$

[9] We cannot rule out the possibility of a continuous degeneracy in the matrix $P(\rho)Q(\rho)$.

where

$$P(\rho) = Q(\rho) = \left[\begin{array}{cc} \Sigma(\rho) & 0 \\ 0 & \sigma(\rho)I \end{array}\right] > 0.$$

Conformally partitioning P_ρ such that

$$P_\rho \stackrel{s}{=} \left[\begin{array}{cc|c} A_{11}(\rho,\dot\rho) & A_{12}(\rho,\dot\rho) & B_1(\rho) \\ A_{21}(\rho,\dot\rho) & A_{22}(\rho,\dot\rho) & B_2(\rho) \\ \hline C_1(\rho) & C_2(\rho) & D \end{array}\right]$$

then $\hat{P}_\rho$ is given by

$$\hat{P}_\rho \stackrel{s}{=} \left[\begin{array}{c|c} A_{11}(\rho,\dot\rho) & B_1(\rho) \\ \hline C_1(\rho) & D \end{array}\right].$$

Now define the error operator $E_\rho : L_2^+ \mapsto L_2^+,\ u(t) \mapsto e(t)$ as follows

$$E_\rho \stackrel{s}{=} \left[\begin{array}{ccc|c} A_{11}(\rho,\dot\rho) & 0 & 0 & B_1(\rho) \\ 0 & A_{11}(\rho,\dot\rho) & A_{12}(\rho,\dot\rho) & B_1(\rho) \\ 0 & A_{21}(\rho,\dot\rho) & A_{22}(\rho,\dot\rho) & B_2(\rho) \\ \hline -C_1(\rho) & C_1(\rho) & C_2(\rho) & 0 \end{array}\right].$$

Lemma 7.6.5 *Let $[t_0, t_1]$ be any interval on which $\dot\sigma \le 0$, then*

$$\|e\|^2_{2,[t_0,t_1]} < 4\sigma^2_{\max}\|u\|^2_{2,[t_0,t_1]} - x^T T_1^{-T} X T_1^{-1} x\Big|_{t_0}^{t_1}, \tag{7.49}$$

where $\sigma_{\max} = \max_{\rho\in F_\rho}\sigma(\rho)$, and where the state of E_ρ is given by x, T_1 is a parameter-independent transformation matrix

$$T_1 = T_1^{-1} = \left[\begin{array}{ccc} -\frac{1}{\sqrt{2}}I & \frac{1}{\sqrt{2}}I & 0 \\ \frac{1}{\sqrt{2}}I & \frac{1}{\sqrt{2}}I & 0 \\ 0 & 0 & I \end{array}\right]$$

and X is the positive-definite matrix given by

$$X(\rho) = \left[\begin{array}{ccc} 2\Sigma(\rho) & 0 & 0 \\ 0 & 2\sigma^2(\rho)\Sigma^{-1}(\rho) & 0 \\ 0 & 0 & 2\sigma(\rho)I \end{array}\right].$$

Proof: Using the transformation matrix T_1 perform a state transformation on the operator E_ρ to obtain

$$E_\rho \stackrel{s}{=} \left[\begin{array}{ccc|c} A_{11}(\rho,\dot\rho) & 0 & \frac{1}{\sqrt{2}}A_{12}(\rho,\dot\rho) & 0 \\ 0 & A_{11}(\rho,\dot\rho) & \frac{1}{\sqrt{2}}A_{12}(\rho,\dot\rho) & \sqrt{2}B_1(\rho) \\ \frac{1}{\sqrt{2}}A_{21}(\rho,\dot\rho) & \frac{1}{\sqrt{2}}A_{21}(\rho,\dot\rho) & A_{22}(\rho,\dot\rho) & B_2(\rho) \\ \hline \sqrt{2}C_1(\rho) & 0 & C_2(\rho) & 0 \end{array}\right].$$

Now dilate the operator to get $E_{d_1} : L_2^+ \otimes L_2^+ \mapsto L_2^+ \otimes L_2^+, u_{d_1}(t) \mapsto e_{d_1}(t)$ by introducing an additional input and an additional output as follows:

$$E_{d_1} \stackrel{s}{=} \left[\begin{array}{c|c} A_{d_1} & B_{d_1} \\ \hline C_{d_1} & D_d \end{array}\right]$$

$$E_{d_1} \stackrel{s}{=} \left[\begin{array}{ccc|cc} A_{11}(\rho,\dot\rho) & 0 & \frac{1}{\sqrt{2}}A_{12}(\rho,\dot\rho) & 0 & -\sqrt{2}\sigma(\rho)\Sigma^{-1}(\rho)C_1^T(\rho) \\ 0 & A_{11}(\rho,\dot\rho) & \frac{1}{\sqrt{2}}A_{12}(\rho,\dot\rho) & \sqrt{2}B_1(\rho) & 0 \\ \frac{1}{\sqrt{2}}A_{21}(\rho,\dot\rho) & \frac{1}{\sqrt{2}}A_{21}(\rho,\dot\rho) & A_{22}(\rho,\dot\rho) & B_2(\rho) & -C_2^T(\rho) \\ \hline \sqrt{2}C_1(\rho) & 0 & C_2(\rho) & 0 & 2\sigma(\rho)I \\ 0 & -\sqrt{2}\sigma(\rho)B_1^T(\rho)\Sigma^{-1}(\rho) & -B_2^T(\rho) & 2\sigma(\rho)I & 0 \end{array}\right].$$

This dilation has been chosen to ensure that

i. $(2\sigma_{\max} + \epsilon)^2 I - D_d^T D_d > 0$ for any $\epsilon > 0$;

ii. $XB_{d_1} + C_{d_1}^T D_d = 0$.

We will now show that X satisfies equation (7.47) on the interval $[t_0, t_1]$ and as a consequence of lemma (7.6.3) the dilated operator E_{d_1} satisfies

$$\|e_{d_1}\|_{2,[t_0,t_1]}^2 < 4\sigma_{\max}^2 \|u_{d_1}\|_{2,[t_0,t_1]}^2 - x^T T_1^{-T} X T_1^{-1} x|_{t_0}^{t_1},$$

where e_{d_1} is the output of E_{d_1} and u_{d_1} is the input to E_{d_1}. Substituting X and the dilated operator state-space matrices into equation (7.47), the following inequality must hold

$$\left[\begin{array}{ccc} \sqrt{2}I & 0 & 0 \\ 0 & \sqrt{2}\sigma\Sigma^{-1} & 0 \\ 0 & 0 & I \end{array}\right] \left\{ \left[\begin{array}{ccc} \dot\Sigma & 0 & 0 \\ 0 & \frac{2\dot\sigma}{\sigma}\Sigma - \dot\Sigma & 0 \\ 0 & 0 & 2\dot\sigma I \end{array}\right] + \left[\begin{array}{ccc} C_1^T C_1 & 0 & C_1^T C_2 \\ 0 & B_1 B_1^T & B_1 B_2^T \\ C_2^T C_1 & B_2 B_1^T & C_2^T C_2 + B_2 B_2^T \end{array}\right] + \left[\begin{array}{ccc} \Sigma A_{11} + A_{11}^T \Sigma & 0 & \Sigma A_{12} + \sigma A_{21}^T \\ 0 & A_{11}\Sigma + \Sigma A_{11}^T & \sigma A_{12} + \Sigma A_{21}^T \\ \sigma A_{21} + A_{21}^T \Sigma & A_{21}\Sigma + \sigma A_{12}^T & 2\sigma A_{22} + 2\sigma A_{22}^T \end{array}\right] \right\} \left[\begin{array}{ccc} \sqrt{2}I & 0 & 0 \\ 0 & \sqrt{2}\sigma\Sigma^{-1} & 0 \\ 0 & 0 & I \end{array}\right] < 0. \quad (7.50)$$

This is equivalent to

$$\left[\begin{array}{cc} 0 & 0 \\ I & 0 \\ 0 & I \end{array}\right] \left\{ \left[\begin{array}{cc} -\dot\Sigma & 0 \\ 0 & -\dot\sigma I \end{array}\right] + A \left[\begin{array}{cc} \Sigma & 0 \\ 0 & \sigma I \end{array}\right] + \left[\begin{array}{cc} \Sigma & 0 \\ 0 & \sigma I \end{array}\right] A^T + BB^T + \left[\begin{array}{cc} 2\frac{\dot\sigma}{\sigma}\Sigma & 0 \\ 0 & 2\dot\sigma I \end{array}\right] \right\} \left[\begin{array}{ccc} 0 & I & 0 \\ 0 & 0 & I \end{array}\right] +$$

$$\left[\begin{array}{cc} I & 0 \\ 0 & 0 \\ 0 & I \end{array}\right] \left\{ \left[\begin{array}{cc} \dot\Sigma & 0 \\ 0 & \dot\sigma I \end{array}\right] + A^T \left[\begin{array}{cc} \Sigma & 0 \\ 0 & \sigma I \end{array}\right] + \left[\begin{array}{cc} \Sigma & 0 \\ 0 & \sigma I \end{array}\right] A + C^T C \right\} \left[\begin{array}{ccc} I & 0 & 0 \\ 0 & 0 & I \end{array}\right] < 0.$$

This shows that equation (7.47) is satisfied on the specified time interval. Finally, we can use the fact that E_ρ is a contraction of E_{d_1} to obtain equation (7.49). ■

Lemma 7.6.6 *Let $[t_0, t_1]$ be any interval on which $\dot{\sigma} \geq 0$, then*

$$\|e\|^2_{2,[t_0,t_1]} < 4\sigma^2_{\max}\|u\|^2_{2,[t_0,t_1]} - 4\sigma^2_{\max} x^T T_2^{-T} Y^{-1} T_2^{-1} x|_{t_0}^{t_1}, \tag{7.51}$$

where again $\sigma_{\max} = \max_{\rho \in F_\rho} \sigma(\rho)$. The state of E_ρ is given by x, T_2 is a parameter-independent state transform matrix

$$T_2 = \begin{bmatrix} I & -I & 0 \\ I & I & 0 \\ 0 & 0 & I \end{bmatrix} \qquad \textit{and} \qquad T_2^{-1} = \begin{bmatrix} \frac{I}{2} & \frac{I}{2} & 0 \\ -\frac{I}{2} & \frac{I}{2} & 0 \\ 0 & 0 & I \end{bmatrix}$$

and Y is the positive-definite matrix given by

$$Y(\rho) = \begin{bmatrix} \Sigma(\rho) & 0 & 0 \\ 0 & \sigma^2(\rho)\Sigma^{-1}(\rho) & 0 \\ 0 & 0 & 2\sigma(\rho)I \end{bmatrix}.$$

Proof: Using the transform matrix T_2 perform a state transformation on the operator E_ρ to obtain

$$E_\rho \stackrel{s}{=} \left[\begin{array}{ccc|c} A_{11}(\rho,\dot{\rho}) & 0 & \frac{1}{2}A_{12}(\rho,\dot{\rho}) & B_1(\rho) \\ 0 & A_{11}(\rho,\dot{\rho}) & \frac{1}{2}A_{12}(\rho,\dot{\rho}) & 0 \\ A_{21}(\rho,\dot{\rho}) & A_{21}(\rho,\dot{\rho}) & A_{22}(\rho,\dot{\rho}) & B_2(\rho) \\ \hline 0 & 2C_1(\rho) & C_2(\rho) & 0 \end{array}\right].$$

Dilate this operator by introducing an additional input and an additional output to get $E_{d_2} : L_2^+ \otimes L_2^+ \mapsto L_2^+ \otimes L_2^+, u_{d_2}(t) \mapsto e_{d_2}(t)$ as follows

$$E_{d_2} \stackrel{s}{=} \left[\begin{array}{c|c} A_{d_2} & B_{d_2} \\ \hline C_{d_2} & D_d \end{array}\right] \tag{7.52}$$

$$E_{d_2} \stackrel{s}{=} \left[\begin{array}{ccc|cc} A_{11}(\rho,\dot{\rho}) & 0 & \frac{1}{2}A_{12}(\rho,\dot{\rho}) & B_1(\rho) & 0 \\ 0 & A_{11}(\rho,\dot{\rho}) & \frac{1}{2}A_{12}(\rho,\dot{\rho}) & 0 & -\sigma(\rho)\Sigma^{-1}(\rho)C_1^T(\rho) \\ A_{21}(\rho,\dot{\rho}) & A_{21}(\rho,\dot{\rho}) & A_{22}(\rho,\dot{\rho}) & B_2(\rho) & -C_2^T(\rho) \\ \hline 0 & 2C_1(\rho) & C_2(\rho) & 0 & 2\sigma(\rho)I \\ -2\sigma(\rho)B_1^T(\rho)\Sigma^{-1} & 0 & -B_2^T(\rho) & 2\sigma(\rho)I & 0 \end{array}\right] \tag{7.53}$$

The dilation has been chosen to give

1. $(2\sigma_{\max} + \epsilon)^2 I - D_d^T D_d > 0$ for any $\epsilon > 0$;
2. $YC_{d_2}^T + B_{d_2} D_d = 0$.

We will now show that Y satisfies equation (7.48) on the interval $[t_0, t_1]$. Substituting Y and the dilated operator state-space matrices into equation (7.48), the following inequality must hold

$$\begin{bmatrix} I & 0 & 0 \\ 0 & \sigma\Sigma^{-1} & 0 \\ 0 & 0 & I \end{bmatrix} \left\{ \begin{bmatrix} -\dot{\Sigma} & 0 & 0 \\ 0 & \dot{\Sigma} - \frac{2\dot{\sigma}}{\sigma}\Sigma & 0 \\ 0 & 0 & -2\dot{\sigma}I \end{bmatrix} + \begin{bmatrix} A_{11}\Sigma + \Sigma A_{11}^T & 0 & \sigma A_{12} + \Sigma A_{21} \\ 0 & \Sigma A_{11} + A_{11}^T\Sigma & \Sigma A_{12} + \sigma A_{21}^T \\ A_{21}\Sigma + \sigma A_{21}^T & A_{21}\sigma + A_{12}^T\Sigma & 2\sigma A_{22} + 2\sigma A_{22}^T \end{bmatrix} + \begin{bmatrix} B_1B_1^T & 0 & B_1B_2^T \\ 0 & C_1^TC_1 & C_1^TC_1 \\ B_2B_1^T & C_2^TC_1 & C_2^TC_2 + B_2B_2^T \end{bmatrix} \right\} \begin{bmatrix} I & 0 & 0 \\ 0 & \sigma\Sigma^{-1} & 0 \\ 0 & 0 & I \end{bmatrix} < 0. \quad (7.54)$$

This is equivalent to

$$\begin{bmatrix} I & 0 \\ 0 & 0 \\ 0 & I \end{bmatrix} \left\{ \begin{bmatrix} -\dot{\Sigma} & 0 \\ 0 & -\dot{\sigma}I \end{bmatrix} + A \begin{bmatrix} \Sigma & 0 \\ 0 & \sigma I \end{bmatrix} + \begin{bmatrix} \Sigma & 0 \\ 0 & \sigma I \end{bmatrix} A^T + BB^T \right\} \begin{bmatrix} I & 0 & 0 \\ 0 & 0 & I \end{bmatrix} + \begin{bmatrix} 0 & 0 \\ I & 0 \\ 0 & I \end{bmatrix} \left\{ \begin{bmatrix} \dot{\Sigma} & 0 \\ 0 & \dot{\sigma}I \end{bmatrix} + A^T \begin{bmatrix} \Sigma & 0 \\ 0 & \sigma I \end{bmatrix} + \begin{bmatrix} \Sigma & 0 \\ 0 & \sigma I \end{bmatrix} A + C^TC + \begin{bmatrix} -2\frac{\dot{\sigma}}{\sigma}\Sigma & 0 \\ 0 & -2\dot{\sigma}I \end{bmatrix} \right\} \begin{bmatrix} 0 & I & 0 \\ 0 & 0 & I \end{bmatrix} < 0. \quad (7.55)$$

This shows that equation (7.48) is satisfied on the specified interval. Finally, use the fact that E_ρ is a contraction of E_{d_2} to obtain equation (7.51). ■

Remark 7.6.7 *Either lemma 7.6.5 or lemma 7.6.6 shows that the $\mathcal{Q}_e$ singular values bound the truncation error for each fixed $\rho \in F_\rho$, that is*

$$\|P_\rho - \hat{P}_\rho\|_\infty \leq 2 \sum_{i=r+1}^{n} \sigma_i(\rho), \ \forall\, \rho \in F_\rho : \dot{\rho} = 0.$$

Alternatively, if the rate of parameter variation is assumed to be unbounded then both Gramians must necessarily become constant. In this case the $\mathcal{Q}_e$ singular values also give an upper bound on the truncation error.

We now give a computable upper bound on the worst case error resulting from balanced truncation of a single state for a given LPV system. This bound depends on the path traced out by the parameter $\rho(t)$ in the parameter space and is limited to trajectories that only change on a finite time horizon.

Theorem 7.6.8 *Given any finite-horizon parameter trajectory $\rho(t) \in F_\rho$, then it is possible to bound the induced norm of the error resulting from the truncation of a single state of a balanced realisation according to*

$$\|e\|_2 \leq 2\sigma_{\max} \left(\frac{\sigma_{\max}}{\sigma_{\min}} \right)^N \|u\|_2. \quad (7.56)$$

The integer N represents the number of times $\dot{\sigma}$ undergoes a transition from $\dot{\sigma} < 0$ to $\dot{\sigma} > 0$ within the finite horizon.

Proof: We include a proof in Appendix B. ■

It is interesting to observe that an adjustment to the controllability and observability inequalities can be used to generalise the LTI error bound. This adjustment can be interpreted as providing a measure of the degree of stability of the given LPV system. Unfortunately, it is not possible to determine the necessary adjustment apriori so these results are of theoretical interest only. Given a balanced (naturally-balanced) realisation of an LPV system P_ρ of state-dimension n, let $\hat{P}_\rho$, of state-dimension r, be obtained by truncation of P_ρ, then the LTI error bound can be made to hold for the following subset of the feasible parameter space

$$F_u \triangleq \left\{ \rho(t) \in F_\rho : \frac{|\dot{\sigma}_i|}{\sigma_i} < \alpha(\rho), \ \forall\, i = r+1, r+2, \ldots n \right\}.$$

The term $\alpha(\rho) > 0$ is a measure of the degree of stability of the parameter-varying system. That is, provided the system is sufficiently stable (in a sense which will be made precise shortly), it is possible to reproduce the LTI upper bound with the machinery already developed. We relate $\alpha(\rho)$ to the decay rate of an LPV system which we define as follows

Definition 7.6.9 *Given a $\mathcal{Q}_e$ stable LPV system we define the decay rate α as follows*

$$\alpha = \inf_{\rho(t) \in F_\rho} \sup_{\gamma > 0} \{\gamma : \lim_{t \to \infty} e^{\gamma t} \|x(t)\| = 0\}.$$

For stable LTI systems the decay rate is the negated real part of the eigenvalue closest to the imaginary axis which has the intuitive appeal of representing a stability measure.

Proposition 7.6.10 *A lower bound on the decay rate can be obtained if we can find a quadratic function $V = x^T P(\rho) x > 0$ and a positive constant $\alpha > 0$ such that*

$$\frac{dV}{dt} \leq -2\alpha V.$$

Proof:

$$\begin{aligned}
&\frac{dV}{dt} \leq -2\alpha V \\
&\Rightarrow V(t) \leq e^{-2\alpha t} V(0) \\
&\Rightarrow x^T P(\rho) x \leq e^{-2\alpha t} x_0 P(\rho_0) x_0 \\
&\Rightarrow \underline{\lambda}(P(\rho)) x^T x \leq \bar{\lambda}(P(\rho_0)) e^{-2\alpha t} x_0^T x_0 \\
&\Rightarrow \|x\| \leq \kappa^{\frac{1}{2}}(P) e^{-\alpha t} \|x_0\|
\end{aligned}$$

where

$$\kappa(P) = \max_\rho \frac{\bar{\lambda}(P(\rho))}{\underline{\lambda}(P(\rho))}.$$

■

Now consider the following modified Lyapunov inequalities

$$-\dot{P} + AP + PA^T + BB^T + \alpha(\rho)P < 0 \ \forall \ \rho(t) \in F_\rho \tag{7.57}$$
$$\dot{Q} + A^TQ + QA + C^TC + \alpha(\rho)Q < 0 \ \forall \ \rho(t) \in F_\rho. \tag{7.58}$$

If we can find a $P(\rho)$ satisfying equation (7.57) or a $Q(\rho)$ satisfying equation (7.58) then the system is $\mathcal{Q}_e$ stable and has a decay rate of at least $\min_{\rho \in F_\rho} \alpha(\rho)/2$. More importantly, if we satisfy both of these inequalities then it is still possible to balance the Gramians[10] in which case the following inequalities hold

$$-\frac{d}{dt}(\sigma^{-1}P) + A(\sigma^{-1}P) + (\sigma^{-1}P)A^T + \sigma^{-1}BB^T < 0 \quad \forall \ \rho(t) \in F_u$$
$$\frac{d}{dt}(\sigma^{-1}Q) + A^T(\sigma^{-1}Q) + (\sigma^{-1}Q)A + \sigma^{-1}C^TC < 0 \quad \forall \ \rho(t) \in F_u.$$

The additional terms allow us to scale the Gramians by scaling the plant at the input and at the output, hence

$$\hat{P} = \sigma^{-1}P = \begin{bmatrix} \hat{\Sigma} & 0 \\ 0 & I \end{bmatrix} \quad \text{and} \quad \hat{Q} = \sigma^{-1}Q = \begin{bmatrix} \hat{\Sigma} & 0 \\ 0 & I \end{bmatrix}$$

are controllability and observability Gramians for the scaled system with the following state-space realisation

$$P_s \stackrel{s}{=} \left[\begin{array}{c|c} A & \frac{1}{\sqrt{\sigma}}B \\ \hline \frac{1}{\sqrt{\sigma}}C & 0 \end{array}\right].$$

This system is depicted in Figure 7.5.

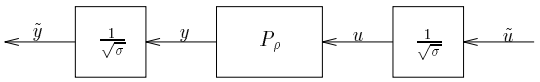

Figure 7.5 *Scaled system.*

Partitioning P_s conformally with $\hat{P}$ and $\hat{Q}$ gives

$$P_s \stackrel{s}{=} \left[\begin{array}{cc|c} A_{11} & A_{12} & \frac{1}{\sqrt{\sigma}}B_1 \\ A_{21} & A_{22} & \frac{1}{\sqrt{\sigma}}B_2 \\ \hline \frac{1}{\sqrt{\sigma}}C_1 & \frac{1}{\sqrt{\sigma}}C_2 & 0 \end{array}\right].$$

If we take the truncated model approximant as

$$\hat{P}_s \stackrel{s}{=} \left[\begin{array}{c|c} A_{11} & \frac{1}{\sqrt{\sigma}}B_1 \\ \hline \frac{1}{\sqrt{\sigma}}C_1 & 0 \end{array}\right],$$

[10] It is easily shown that if a state transformation is introduced then the formulas given for the transformed Gramians in lemma 7.3.5 still hold.

then the scaled error operator $E_s : L_2^+ \mapsto L_2^+,\ \tilde{u}(t) \mapsto \tilde{y}(t)$ has the following state-space realisation

$$E_s \stackrel{s}{=} \left[\begin{array}{ccc|c} A_{11} & 0 & 0 & \frac{1}{\sqrt{\sigma}}B_1 \\ 0 & A_{11} & A_{12} & \frac{1}{\sqrt{\sigma}}B_2 \\ 0 & A_{21} & A_{22} & \frac{1}{\sqrt{\sigma}}B_2 \\ \hline -\frac{1}{\sqrt{\sigma}}C_1 & \frac{1}{\sqrt{\sigma}}C_1 & \frac{1}{\sqrt{\sigma}}C_2 & 0 \end{array}\right].$$

Either lemma 7.6.5 or lemma 7.6.6 can now be used to show that removing the state corresponding to the constant $\mathcal{Q}_e$ singular value of the scaled system gives

$$\|E_s\| \leq 2 \Longleftrightarrow \|\tilde{y}\|_2 \leq 2\|\tilde{u}\|_2$$

and using the relations

$$\tilde{y} = \frac{1}{\sqrt{\sigma}}y \quad \text{and} \quad u = \frac{1}{\sqrt{\sigma}}\tilde{u},$$

it is a simple matter to show that

$$\frac{1}{\sqrt{\sigma_{\max}}}\|y\|_2 \leq 2\sqrt{\sigma_{\max}}\|u\|_2.$$

That is, removing the state corresponding to the smallest $\mathcal{Q}_e$ singular value of the original system gives

$$\|y\|_2 \leq 2\sigma_{\max}\|u\|_2.$$

Unfortunately, it is not possible to determine $\alpha(\rho)$ prior to the computation of the Gramians so from a practical perspective this does not help us much when we want guaranteed error bounds. A conservative approach to bounding the error would be to choose $\alpha > 0$ to be a positive constant and then explicitly calculate the set F_u for which the guaranteed bound holds. A better approach would be to use the upper bound on the approximation error given by the $\mathcal{Q}_e$ singular values when $\dot{\rho} \to 0$ to determine which states should be truncated from the model and then explicitly compute a quadratic dissipation function to bound the approximation error in the general case.

7.7 Computational issues

In this section we outline a computational procedure for finding a controllability Gramian and an observability Gramian for a given parameter-dependent system. The objective of making the $\mathcal{Q}_e$ singular values small will be shown to result in an optimisation problem that involves convex constraints and a non-convex penalty function. In order to deal with the lack of convexity in the penalty function we will show how the LPV Gramians can be viewed as perturbations of the LTI Gramians, with the latter being used as weights in a weighted optimisation which is locally convex. Let P_ρ have the continuous state-space realisation

$$P_\rho \stackrel{s}{=} \left[\begin{array}{c|c} A(\rho) & B(\rho) \\ \hline C(\rho) & D(\rho) \end{array}\right].$$

We are required to find a solution to two linear matrix inequalities while satisfying an infinite number of constraints. In other words, we are dealing with an convex programming problem with infinitely many constraints. The approach we take is to satisfy the inequalities on a suitably dense grid covering the parameter space, which then allows us to exploit the continuity properties of the plant matrices to ensure that the inequalities are satisfied everywhere. Given bounds on the rate at which the parameter can vary we need to find a differentiable $P(\rho) = P^T(\rho) > 0$ and a differentiable $Q(\rho) = Q^T(\rho) > 0$ satisfying

$$\dot{\rho}\frac{dQ}{d\rho} + A^T(\rho)Q(\rho) + Q(\rho)A(\rho) + C^T(\rho)C(\rho) < -\delta^2 I \;\; \forall \rho(t) \in F_\rho \tag{7.59}$$

$$-\dot{\rho}\frac{dP}{d\rho} + A(\rho)P(\rho) + P(\rho)A^T(\rho) + B(\rho)B^T(\rho) < -\delta^2 I \;\; \forall \rho(t) \in F_\rho, \tag{7.60}$$

for some $\delta^2 > 0$. The small constant δ allows the feasibility of the solutions at the grid points to be extended to the entire parameter space. One approach to this problem involves choosing any set of suitable basis functions, denoted $\phi_i(\rho)$, and searching for feasible solutions to the above equations among the set of trial functions given by

$$P(\rho) = \sum_{i=1}^{n} \phi_i(\rho) P_i > 0$$

$$Q(\rho) = \sum_{i=1}^{n} \phi_i(\rho) Q_i > 0,$$

$$P_i = P_i^T, \quad Q_i = Q_i^T \quad i = 1, 2 \ldots n.$$

There is a lot of freedom in the choice of basis functions from which the set of trial functions can be constructed. From a computational perspective a highly convenient choice of basis functions is the set of cubic splines. A similar gridding procedure to that taken here can be found in [75] where cubic spline interpolation techniques are used to obtain suboptimal controllers for certain classes of nonlinear systems. Their work also discusses the use of product splines which could be of use on LPV systems having multiple parameter dependence. Partition the interval $[\rho_{\min}, \rho_{\max}]$ into m equal intervals and define the associated knot points

$$\rho_{j+1} - \rho_j = h = (\rho_{\max} - \rho_{\min})/m, \quad j = 0, 1, \ldots m-1.$$

It is well known that any continuous function can be approximated arbitrarily closely on a closed interval by a cubic spline which interpolates that function at a set of sufficiently close knot points [70]. This property, together with the ability to evaluate the splines at points other than the knot points without incurring significant roundoff error proves advantageous in the sequel[11]. Next we define the usual B-spline basis for the linear space of cubic splines as follows

$$\phi_i(\rho) = \frac{1}{4h^3}[(\rho - \rho_{i-2})_+^3 - 4(\rho - \rho_{i-1})_+^3 + 6(\rho - \rho_i)_+^3 - 4(\rho - \rho_{i+1})_+^3 + (\rho - \rho_{i+2})_+^3] \quad i = -1, 0, \ldots, m+1,$$

$$\text{where} \quad (\rho)_+ = \begin{cases} \rho, & \rho \geq 0 \\ 0, & \rho < 0. \end{cases} \tag{7.61}$$

Each basis function $\phi_i(\rho)$ has compact support on the interval $[\rho_{i-2}, \rho_{i+2}]$ and satisfies $\phi_i(\rho) \in C^2$. The basis function $\phi_i(\rho)$ is shown in Figure 7.6.

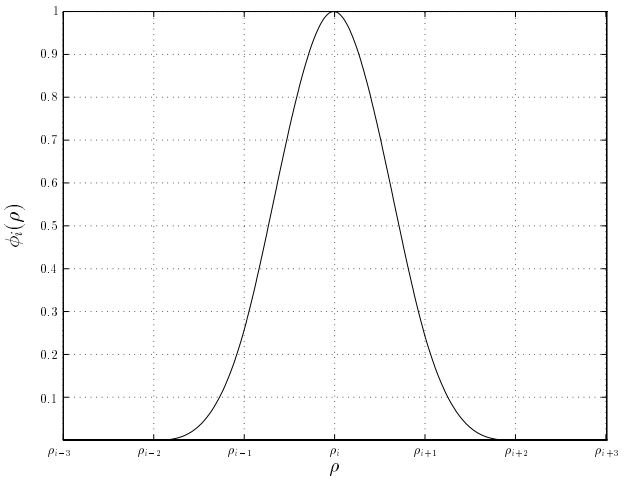

Figure 7.6 *Basis function $\phi_i(\rho)$ for cubic interpolation.*

With this (or any other) choice of basis functions, solution of equation (7.59) and equation (7.60) at a set of grid points becomes a convex feasibility problem for which there exist powerful numerical techniques [12] that are guaranteed to find a feasible solution in polynomial time when one exists. Furthermore, since the inequalities are affine in the rate parameter it is only necessary to satisfy them at the upper rate bound and the lower rate bound of the closed interval defining the set of feasible parameter rates. This ensures that they are satisfied for all possible rates of parameter variation as set out in the problem definition. An example of a system having only single parameter dependence and uniformly spaced knot points is shown in Figure 7.7. The dark dots are the knot points and these extend beyond the feasible parameter range to ensure that a sufficient number of functions are available to form a basis for the linear space of cubic

[11] Observe that cubic splines are not analytic.

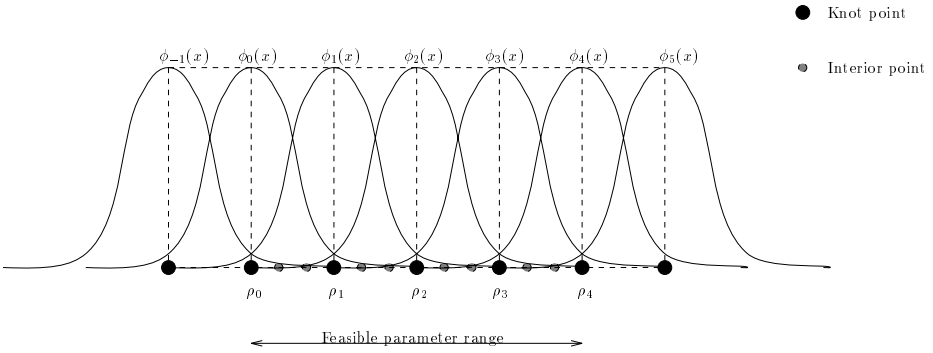

Figure 7.7 *Gridding of the parameter space.*

splines. The matrix inequalities are satisfied at the knot points lying on the feasible parameter space and possibly at additional interior points which are depicted by light dots in Figure 7.7. We refer to the totality of knot and interior points as grid points. Forcing the inequalities to be satisfied at points other than the knot points it is possible to increase the grid density without increasing the number of basis functions in the trial solution. This proves to be a particularly useful feature when attempting to satisfy the inequalities for all parameter values rather than just at the grid points. Actually, there is no reason why the interior points need to be uniformly spaced and if there is a particular region in the parameter space where the system dynamics vary rapidly it might prove useful to use a denser grid over that region.

From a model-reduction perspective we want to do rather more than just find solutions to the Lyapunov inequalities. What we really want is to find solutions to equation (7.59) and equation (7.60) and simultaneously minimise

$$\max_{\rho} \lambda_i(P(\rho)Q(\rho)),$$

for each eigenvalue $\lambda_i(P(\rho)Q(\rho))$. If we restrict attention to a specified set of grid points this is equivalent to minimising

$$J = \sum_k \text{trace}(P(\rho_k)Q(\rho_k)), \tag{7.62}$$

where each ρ_k is a grid point. Minimising equation (7.62) subject to the constraints given by equation (7.59) and equation (7.60) constitutes a constrained optimisation with convex constraints but with a non-convex penalty function. As an alternative we suggest the following iterative scheme.

Procedure 7.7.1 .

i. Find $Q_1(\rho)$ which satisfies equation (7.59) and minimises

$$J_1 = \sum_k \mathit{trace}(Q_1(\rho_k)P_0(\rho_k)),$$

where $P_0(\rho_k)$ represents the LTI controllability Gramian at the grid point ρ_k.

ii. Solve for $P_1(\rho)$ which satisfies equation (7.60) and minimises

$$J_2 = \sum_k trace(P_1(\rho_k)Q_1(\rho_k)).$$

iii. Solve for $Q_2(\rho)$ which satisfied equation (7.59) and minimises

$$J_3 = \sum_k trace(Q_2(\rho_k)P_1(\rho_k)).$$

iv. Repeat steps ii. and iii. until the decrease in the cost function satisfies an appropriate convergence criterion.

For certain systems it may help to invert the LMIs so that instead of solving for $P(\rho)$ and $Q(\rho)$ we solve for their inverses, which satisfy

$$\begin{bmatrix} -\dot{Q}^{-1}(\rho) + Q^{-1}(\rho)A^T(\rho) + A(\rho)Q^{-1}(\rho) & \delta Q^{-1} & Q^{-1}(\rho)C(\rho)^T \\ \delta Q^{-1} & -I & 0 \\ C(\rho)Q^{-1}(\rho) & 0 & -I \end{bmatrix} < 0 \qquad (7.63)$$

$$\begin{bmatrix} \dot{P}^{-1}(\rho) + P^{-1}(\rho)A(\rho) + A^T(\rho)P^{-1}(\rho) & \delta P^{-1} & P^{-1}(\rho)B(\rho) \\ \delta P^{-1} & -I & 0 \\ B^T(\rho)P^{-1}(\rho) & 0 & -I \end{bmatrix} < 0. \qquad (7.64)$$

The reason for doing this is to ensure that the smallest $\mathcal{Q}_e$ singular values contribute most to the cost function, which is now given by

$$J = -\sum_k \text{trace}(P^{-1}(\rho_k)Q^{-1}(\rho_k)).$$

For systems where the $\mathcal{Q}_e$ singular values vary over several orders of magnitude it is possible for the contribution made by the smallest singular values to be completely dominated by numerical errors. By inverting the Gramians this situation is avoided because the smallest singular values now make the largest contribution to the cost function. This ensures that the numerical procedure is consistent with the objective of producing the tightest upper bound on the truncation error. Observe that in the first step of the iteration the cost function is weighted using the LTI controllability Gramian. So in a sense we are looking for Gramians that satisfy the LPV Lyapunov inequalities and are close the the LTI Gramians. This can be regarded as posing balanced model reduction of LPV systems as a perturbation of the same technique for LTI systems. Computational experience has shown that this greatly increases the speed of convergence and furthermore, when the rate limit is set to zero, the solutions computed using this procedure approximate the LTI Gramians very accurately[12]. At worst, the procedure can be viewed as

[12] Of course this is only true if the trial functions are constructed from a sufficiently rich basis set.

skewing the Gramians to give better accuracy for slow rates of parameter variation. The optimisation is locally convex (but not globally convex) so it is possible to find a global minimum at each step in the iteration before moving to the next step in the procedure. However, we cannot guarantee that the procedure will find the global minimum of the non-convex cost function.

Having found solutions which satisfy the inequalities at the grid points it is possible to guarantee that they are satisfied everywhere by making use of the following well known matrix inequality.

Lemma 7.7.2 *Given two real symmetric matrices $A, B \in \mathbb{R}^{n\times n}$, then*

$$|\bar{\lambda}(A) - \bar{\lambda}(B)| \leq \bar{\sigma}(A - B) \leq \|A - B\|_F, \tag{7.65}$$

where $\|.\|_F$ denotes the Frobenius norm.

Also define

$$\begin{aligned} h_k &\triangleq (\rho_{k+1} - \rho_k) \\ \hat{\rho} &\triangleq \max\{|\dot{\rho}_{\min}|, |\dot{\rho}_{\max}|\}, \end{aligned}$$

where h_k will only be equal to h when no points other than the knot points are used in the analysis. Assuming that the plant matrices have continuous derivatives with respect to the parameter the following result is easily proved.

Theorem 7.7.3 *Given parameter-varying observability and controllability Gramians satisfying equation (7.59) and equation (7.60) on a specified set of grid points, denoted $\rho_0, \rho_1 \ldots \rho_m$, then equation (7.59) and equation (7.60) are satisfied on the entire parameter space, provided*

$$\begin{aligned} h_k . \max \Bigg\{ & \max_{\rho}(\hat{\rho}\sum_i \|\frac{d^2}{d\rho^2}\phi_i(\rho)Q_i\|_F + 2\sum_i \|Q_i\frac{d}{d\rho}(\phi_i(\rho)A(\rho))\|_F + \|\frac{d}{d\rho}(C^T(\rho)C(\rho))\|_F) \,, \\ & \max_{\rho}(\hat{\rho}\sum_i \|\frac{d^2}{d\rho^2}\phi_i(\rho)P_i\|_F + 2\sum_i \|\frac{d}{d\rho}(\phi_i(\rho)A(\rho))P_i\|_F + \|\frac{d}{d\rho}(C^T(\rho)C(\rho))\|_F) \Bigg\} \leq \delta^2 \end{aligned}$$

for all $k = 0, 1 \ldots m-1$.

Proof: We prove the result for the observability Gramian, the proof for the controllability Gramian being essentially the same. For any point $\rho_k \leq \rho \leq \rho_{k+1}$ define

$$\begin{aligned} E_k \triangleq & \left(\dot{\rho}\sum_i \frac{d}{d\rho}\phi_i(\rho)Q_i + A^T(\rho)\sum_i \phi_i(\rho)Q_i + \sum_i \phi_i(\rho)Q_iA(\rho) + C^T(\rho)C(\rho) \right) - \\ & \left(\dot{\rho}\sum_i \frac{d}{d\rho}\phi_i(\rho_k)Q_i + A^T(\rho_k)\sum_i \phi_i(\rho_k)Q_i + \sum_i \phi_i(\rho_k)Q_iA(\rho_k) + C^T(\rho_k)C(\rho_k) \right) \end{aligned}$$

from which it follows that

$$\|E_k\|_F \leq \hat{\rho} \sum_i \|(\phi_i'(\rho) - \phi_i'(\rho_k))Q_i\|_F + 2\sum_i \|Q_i(\phi_i(\rho)A(\rho) - \phi_i(\rho_k)A(\rho_k)\|_F + \|C^T(\rho)C(\rho) - C^T(\rho_k)C(\rho_k)\|_F.$$

Making use of Taylor's theorem this can be written as

$$\|E_k\|_F \leq \hat{\rho}.h_k \sum_i \|\frac{d^2}{d\rho^2}(\phi_i(\rho))|_{\epsilon_{i1}} Q_i\|_F + 2h_k \sum_i Q_i \frac{d}{d\rho}(\phi_i(\rho)A(\rho))|_{\epsilon_{i2}}\|_F + h_k\|\frac{d}{d\rho}(C^T(\rho)C(\rho))|_{\epsilon_{i3}}\|_F,$$

for some $\epsilon_{i1}, \epsilon_{i2}, \epsilon_{i3} \in [\rho_k, \rho_{k+1}]$. ■

In practice it is often far less conservative to compute the inequalities over a very dense grid and verify that they are not violated on the much denser grid.

7.8 Existence and continuity properties of the state transformation matrix

In this section we assume that a controllability Gramian and an observability Gramian have been found and we examine the continuity properties of the balancing state transformation matrix. This is an important issue since continuity of the transformation matrix determines whether the system can be balanced directly or whether the natural-balancing transformation matrix must be computed. We begin with a number of preliminary results that will be needed later.

Theorem 7.8.1 *Let $T(\rho) \in \mathbb{R}^{n\times n}$ be a positive-definite matrix function for all $\rho \in I$. If the elements of $T(\rho)$ are analytic in the domain $\mathcal{D}$ such that $I \subset \mathcal{D}$, then the unique upper-triangular Cholesky factor of $T(\rho)$*

$$T(\rho) = R^T(\rho)R(\rho),$$

is analytic for all $\rho \in I$.

Proof: The proof is inductive. Let $T(\rho) \in \mathbb{R}^{2\times 2}$ be an analytic matrix function with

$$T(\rho) = \begin{bmatrix} a(\rho) & b(\rho) \\ b(\rho) & c(\rho) \end{bmatrix} = \begin{bmatrix} d(\rho) & 0 \\ e(\rho) & f(\rho) \end{bmatrix} \begin{bmatrix} d(\rho) & e(\rho) \\ 0 & f(\rho) \end{bmatrix},$$

representing the unique Cholesky factorisation of $T(\rho)$. It follows that

$$\begin{aligned} a(\rho) = d^2(\rho) &\Rightarrow d(\rho) = \sqrt{a(\rho)} \\ b(\rho) = d(\rho)e(\rho) &\Rightarrow e(\rho) = \frac{b(\rho)}{\sqrt{a(\rho)}} \\ c(\rho) = e^2(\rho) + f^2(\rho) &\Rightarrow 2f(\rho)\frac{df(\rho)}{d\rho} + 2e(\rho)\frac{de(\rho)}{d\rho} = \frac{dc(\rho)}{d\rho} \end{aligned}$$

By positive definiteness of $T(\rho)$, $a(\rho) > 0$ so both $d(\rho)$ and $e(\rho)$ are analytic for all $\rho \in I$. Since $f(\rho) > 0$, $f(\rho)$ is also analytic on the specified interval. Next consider $T_1(\rho) \in \mathbb{R}^{(n-1)\times(n-1)}$ which is assumed to be analytic with the Cholesky factorisation

$$T_1(\rho) = R_1^T(\rho)R_1(\rho).$$

Let $T(\rho) \in \mathbb{R}^{n\times n}$ be obtained by bordering $T_1(\rho)$ as follows

$$T(\rho) = \begin{bmatrix} & & a_1(\rho) \\ & T_1(\rho) & a_2(\rho) \\ & & \vdots \\ a_1(\rho) & a_2(\rho) \quad \ldots & a_n(\rho) \end{bmatrix}.$$

The Cholesky factorisation of $T(\rho)$ is easily verified as being

$$T(\rho) = \begin{bmatrix} & R_1^T(\rho) & & 0 \\ & & & \\ s_1(\rho) & s_2(\rho) & \ldots & \sqrt{a_n(\rho) - s(\rho)} \end{bmatrix} \begin{bmatrix} & s_1(\rho) \\ R_1(\rho) & s_2(\rho) \\ & \vdots \\ 0 & \sqrt{a_n(\rho) - s(\rho)} \end{bmatrix}$$

where

$$\begin{aligned} s_1(\rho) &= \frac{a_1(\rho)}{R_1(1,1)} \\ s_2(\rho) &= \frac{a_2(\rho)}{R_1(2,2)} - \frac{a_1(\rho)R_1(1,2)}{R_1(1,1)R_1(2,2)} \\ &\vdots \\ s(\rho) &= s_1^2(\rho) + s_2^2(\rho) + \ldots s_{n-1}^2(\rho). \end{aligned}$$

It then follows from the assumption that $R_1(\rho)$ is analytic and positive definite (ie: $R_1(i,i) > 0$), that all of the elements in the above factorisation are analytic. ■

Corollary 7.8.2 *If $T(\rho) \in \mathbb{R}^{n\times n}$ is differentiable, but not analytic, then the Cholesky factors of $T(\rho)$ are differentiable.*

In the sequel we will require the derivatives of the singular values and singular vectors of a real, symmetric, parameter-dependent matrix $T(\rho)$ which has analytic elements for all $\rho \in I$. A number of very strong results exist for this class of matrices (particularly when the matrix is analytic).

Lemma 7.8.3 *([53],[73])*
Let $T(\rho) \in \mathbb{R}^{n\times n}$ be a (real) positive-definite analytic matrix function on the open interval $I \subset \mathbb{R}$. Then there exists an analytic diagonal matrix function $\tilde{\Sigma}(\rho) = diag(\tilde{\sigma}_1(\rho), \tilde{\sigma}_2(\rho) \ldots \tilde{\sigma}_n(\rho)) \in$

$\mathbb{R}^{n\times n}$ *and analytic orthonormal matrix functions* $\tilde{U} = [\tilde{u}_1(\rho)\ldots\tilde{u}_n(\rho)] \in \mathbb{R}^{n\times n}$ *and* $\tilde{V}(\rho) = [\tilde{v}_1(\rho)\ldots\tilde{v}_n(\rho)] \in \mathbb{R}^{n\times n}$, *defined on* I, *such that*

$$\tilde{\Sigma}(\rho) = \tilde{U}^T(\rho)T(\rho)\tilde{V}(\rho).$$

Remark 7.8.4 *Although* $\{\tilde{\sigma}_i(\rho)\}$ *is the set of singular values of the matrix* $T(\rho)$, *the* $\tilde{\sigma}_i(\rho)$*'s are not in any particular order. By permuting the rows and columns of* $\tilde{U}(\rho)$ *and* $\tilde{V}(\rho)$ *to get* $U(\rho)$ *and* $V(\rho)$ *it is possible to rearrange the* $\tilde{\sigma}_i(\rho)$*'s to give the ordered singular values* $\sigma_i(\rho)$. *While each* $\tilde{\sigma}_i(\rho)$ *is analytic, the ordered singular values are generally not. The same is true of the columns of* $\tilde{V}(\rho)$ *and* $\tilde{U}(\rho)$ *which are analytic while those of* $V(\rho)$ *and* $U(\rho)$ *are generally not. At worst, the* $\sigma_i(\rho)$*'s are piecewise analytic, as are* $V(\rho)$ *and* $U(\rho)$.

The reason why we have insisted that the matrix function $T(\rho)$ should be analytic, as opposed to satisfying the weaker condition of being differentiable, can be found in the following lemma.

Lemma 7.8.5 *[53]*
Let $T(\rho) \in \mathbb{R}^{n\times n}$ *be a (real) positive-definite differentiable matrix function on the open interval* $I \subset \mathbb{R}$. *Then there exists a differentiable diagonal matrix function* $\tilde{\Sigma}(\rho) = diag(\tilde{\sigma}_1(\rho), \tilde{\sigma}_2(\rho)\ldots\tilde{\sigma}_n(\rho))$ *and piecewise differentiable orthonormal matrix functions* $\tilde{U} = [\tilde{u}_1(\rho)\ldots\tilde{u}_n(\rho)] \in \mathbb{R}^{n\times n}$ *and* $\tilde{V}(\rho) = [\tilde{v}_1(\rho)\ldots\tilde{v}_n(\rho)] \in \mathbb{R}^{n\times n}$, *defined on* I, *such that*

$$\tilde{\Sigma}(\rho) = \tilde{U}^T(\rho)T(\rho)\tilde{V}(\rho).$$

The effect of replacing analyticity by differentiability is demonstrated by the following example [53]. Assume that we are looking for the left singular vectors of $T(\rho)$ with

$$T(\rho)T^T(\rho) = I + e^{-\rho^{-2}}\begin{bmatrix} \cos\frac{2}{\rho} & \sin\frac{2}{\rho} \\ \sin\frac{2}{\rho} & -\cos\frac{2}{\rho} \end{bmatrix}, \quad T(0)T^T(0) = I.$$

$T(\rho)T^T(\rho)$ is continuous and infinitely differentiable for all $\rho \in \mathbb{R}$. So are the eigenvalues of $T(\rho)T^T(\rho)$ which are given by $\lambda = 1 + \pm e^{-\frac{1}{\rho^2}}$ for all $\rho \neq 0$ and one for $\rho = 0$. While the eigenvalues are continuous and differentiable it is impossible to find a nonzero eigenvector which is even continuous at $\rho = 0$. Of course these difficulties are exacerbated somewhat when it is considered that the ordering forced by the balancing algorithm

$$\sigma_1(\rho) \geq \sigma_2(\rho)\ldots\sigma_n(\rho) > 0$$

may result in the differentiability of the $\tilde{\sigma}_i(\rho)$ being replaced by piecewise differentiability of the ordered singular values $\sigma_i(\rho)$. The importance of this is that if two or more of the $\mathcal{Q}_e$ singular values cross at specific points in the parameter space then it is not enough that the Gramians be differentiable if we wish to compute a valid transformation matrix to diagonalise them.

Let $P(\rho) = P^T(\rho) > 0$ and $Q(\rho) = Q^T(\rho) > 0$ be given as analytic matrix functions[13]. Obtain the unique Cholesky factors as follows

$$\begin{aligned} Q(\rho) &= R_q^T(\rho)R_q(\rho) \qquad & R_q(\rho) \text{ upper triangular} \\ P(\rho) &= R_p(\rho)R_p^T(\rho) \qquad & R_p(\rho) \text{ lower triangular.} \end{aligned} \tag{7.66}$$

From theorem 7.8.1 we know that the Cholesky factors are analytic. Next perform a singular value decomposition on the product $R_q(\rho)R_p(\rho)$ to get

$$U(\rho)S(\rho)V^T(\rho) = R_q(\rho)R_p(\rho),$$

where $U(\rho)$ and $V(\rho)$ are unique up to the sign of corresponding columns and $S(\rho)$ has the $\mathcal{Q}_e$ singular values $\sigma_i(\rho)$ in descending order along its main diagonal. If none of the $\mathcal{Q}_e$ singular values cross each other then by lemma 7.8.3 $S(\rho), U(\rho)$ and $V(\rho)$ can all be chosen to be analytic matrix functions in which case we define the balancing state transformation matrix as follows

$$\begin{aligned} T^{-1}(\rho) &\stackrel{\triangle}{=} S^{-\frac{1}{2}}(\rho)U^T(\rho)R_q(\rho) \\ T(\rho) &\stackrel{\triangle}{=} R_p(\rho)V(\rho)(\rho)S^{-\frac{1}{2}}(\rho). \end{aligned} \tag{7.67}$$

It is easily verified that $T(\rho)$ has the required properties. The derivative of the transformation matrix can be computed using perturbation methods. We start with

$$\frac{dT}{d\rho} = \frac{dR_p}{d\rho}VS^{-\frac{1}{2}} + R_p(\frac{dV}{d\rho}S^{-\frac{1}{2}} - \frac{1}{2}VS^{-\frac{3}{2}}\frac{dS}{d\rho}). \tag{7.68}$$

Equation (7.68) shows that we will need an explicit formula for the derivative of the Cholesky factor R_p. This can be computed as the unique lower triangular solution of the following Lyapunov equation

$$\frac{dP}{d\rho} = \frac{dR_p}{d\rho}R_p^T + R_p\frac{dR_p}{d\rho}^T. \tag{7.69}$$

Define

$$Z_{p_1}(\rho) \stackrel{\triangle}{=} R_p^T(\rho)R_q^T(\rho)R_q(\rho)R_p(\rho). \tag{7.70}$$

$S^2(\rho)$ has the eigenvalues of $Z_{p_1}(\rho)$ along its main diagonal arranged in descending order and $V(\rho)$ is the matrix of corresponding normalised eigenvectors. Define $Z_{p_2}(\rho)$ as

$$Z_{p_2} \stackrel{\triangle}{=} (\frac{dR_p^T}{d\rho}R_q^TR_pR_q) + (R_p^T\frac{dR_q}{d\rho}^TR_qR_p) + (\frac{dR_p^T}{d\rho}R_q^TR_pR_q)^T + (R_p^T\frac{dR_q}{d\rho}^TR_qR_p)^T,$$

[13] This is not a strong assumption since we can always choose the basis functions from which the Gramians are constructed to comply with this.

with $\frac{dR_q}{d\rho}$ computed in a similar fashion to $\frac{dR_p}{d\rho}$. Using perturbation expansions [48] it is easily shown that

$$\frac{d\sigma_i}{d\rho} = \frac{v_i^T Z_{p_2} v_i}{2\sigma_i},$$

where v_i is the i'th column of V corresponding to the i'th $\mathcal{Q}_e$ singular value σ_i. Similarly

$$\frac{dv_k}{d\rho_i} = \sum_{j \neq k} \left(\frac{v_j^T Z_{p_2} v_k}{(\sigma_k^2 - \sigma_j^2)} \right) v_j,$$

which completes the calculation of the balancing state transformation matrix and its derivative.

For problems where two or more of the $\mathcal{Q}_e$ singular values cross[14] it is possible to reorder the columns of the singular vectors in such a way as to make them differentiable. In many cases this is not a trivial problem as it is possible for the singular values to cross in close proximity to each other or for more than two singular values to cross at a single point. Since a singular value decomposition of an analytic matrix function requires the computation of the eigenvalues and eigenvectors of two semi-simple matrix functions we will first show how to compute an analytic transformation matrix to diagonalise a real, symmetric, analytic matrix function. Once we have shown how this can be done it is a straightforward matter to compute the natural-balancing transformation matrix using the procedure outline above. Let $Z(\rho)$ be a real, symmetric, analytic matrix function defined on some open interval I. Let us assume that there is at least one point $\rho \in I$ where at least two of the continuous curves representing the eigenvalues of $Z(\rho)$ cross each other. Using the notation in Kato [53] we can separate the eigenvalues of $Z(\rho)$ into distinct λ groups. Any two (or possibly more) eigenvalues that cross each other are sorted into the same λ group while eigenvalues that are everywhere distinct form their own λ group. In general the eigenprojections onto the invariant subspaces spanned by the eigenvectors of $Z(\rho)$ are not analytic, but it can be shown [53] that the total projection (ie: the sum of the eigenprojections) onto each λ group is analytic. Associate with the matrix $Z(\rho)$ the unique analytic eigenprojection $\mathcal{P}_i(\rho)$ onto the total lambda group λ_i. Define

$$Q(\rho) \triangleq \sum_i \frac{dP_i}{d\rho} \mathcal{P}_i(\rho),$$

where $\frac{d\mathcal{P}_i}{d\rho}$ can be computed using standard perturbation formulae [48]. Let $X(\rho)$ be the unique orthonormal matrix function solving

$$\frac{dX}{d\rho} = Q(\rho)X(\rho), \qquad X(\rho_{\min}) = I.$$

Then $T(\rho)$ is given by

$$T(\rho) = X(\rho)T_{\min},$$

[14] There can only be a finite number of these points in any compact set [53].

and $T_{\min}$ is the matrix of eigenvectors satisfying

$$T_{\min}^T Z(\rho_{\min}) T_{\min} = \mathrm{diag}(\lambda_i(\rho_{\min})).$$

The ordering of the eigenvalues $\lambda_i(\rho_{\min})$ is essentially arbitrary, but it must be borne in mind that this ordering will determine the ordering of $\lambda(\rho)$ for all ρ. This completes the computation of the analytic matrix function $T(\rho)$. By way of example, consider the following matrix function

$$Z(\rho) = \begin{bmatrix} 1 + \sin^2 \rho & \rho \\ \rho & 1 \end{bmatrix}, \qquad \rho \in [-1, 1].$$

This matrix has a single degeneracy at $\rho = 0$. Using the above procedure we may compute the analytic matrix function $T(\rho)$ such that $Z(\rho)$ is diagonalised by $T(\rho)$ over the given interval. We also compute the matrix function $T_d(\rho)$ by computing the normalised eigenvectors of $Z(\rho)$ at each point in the closed interval and ordering them such that $T_d^T Z(\rho) T_d(\rho) = \mathrm{diag}(\lambda_i(\rho))$ with $\lambda_1(\rho) \geq \lambda_2(\rho)$. Figure 7.8 shows the continuous curves representing the diagonal elements of $T^T(\rho)Z(\rho)T(\rho)$ and $T_d^T(\rho)Z(\rho)T_d(\rho)$ respectively. While the elements of the former are differentiable for all $\rho \in [-1, 1]$, the elements of the latter are not differentiable at $\rho = 0$. Figure 7.9 allows all four elements of $T(\rho)$ to be compared to the corresponding elements of $T_d(\rho)$. Discontinuities in two of the elements of $T_d(\rho)$ are clearly evident. It should also be apparent that the computational algorithm used to compute $T(\rho)$ has simply swapped the first and second columns of $T_d(\rho)$ subsequent to ρ becoming greater than zero.

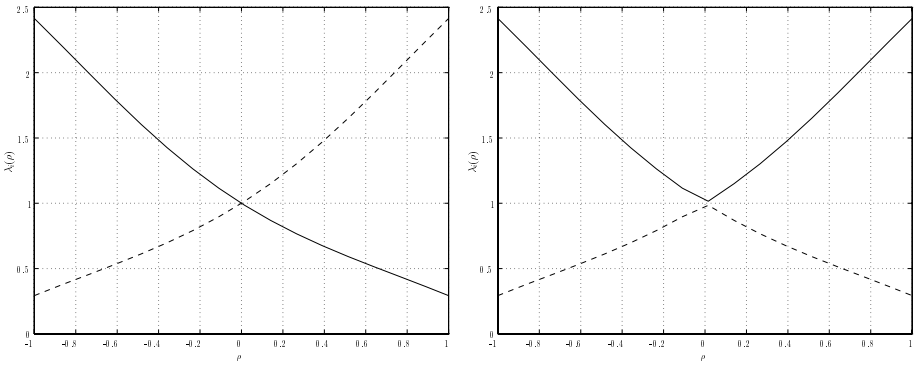

Figure 7.8 *Diagonal elements of* $T^T(\rho)Z(\rho)T(\rho)$ *and* $T_d^T(\rho)Z(\rho)T_d(\rho)$ *respectively.*

To compute the natural-balancing transformation matrix we begin with the Cholesky factorisations in equation 7.66 which is assumed to be analytic (based on the analyticity of $P(\rho)$ and $Q(\rho)$). We first show how to compute the natural singular value decomposition

$$\tilde{U}(\rho)\tilde{S}(\rho)\tilde{V}^T(\rho) = R_q(\rho)R_p(\rho),$$

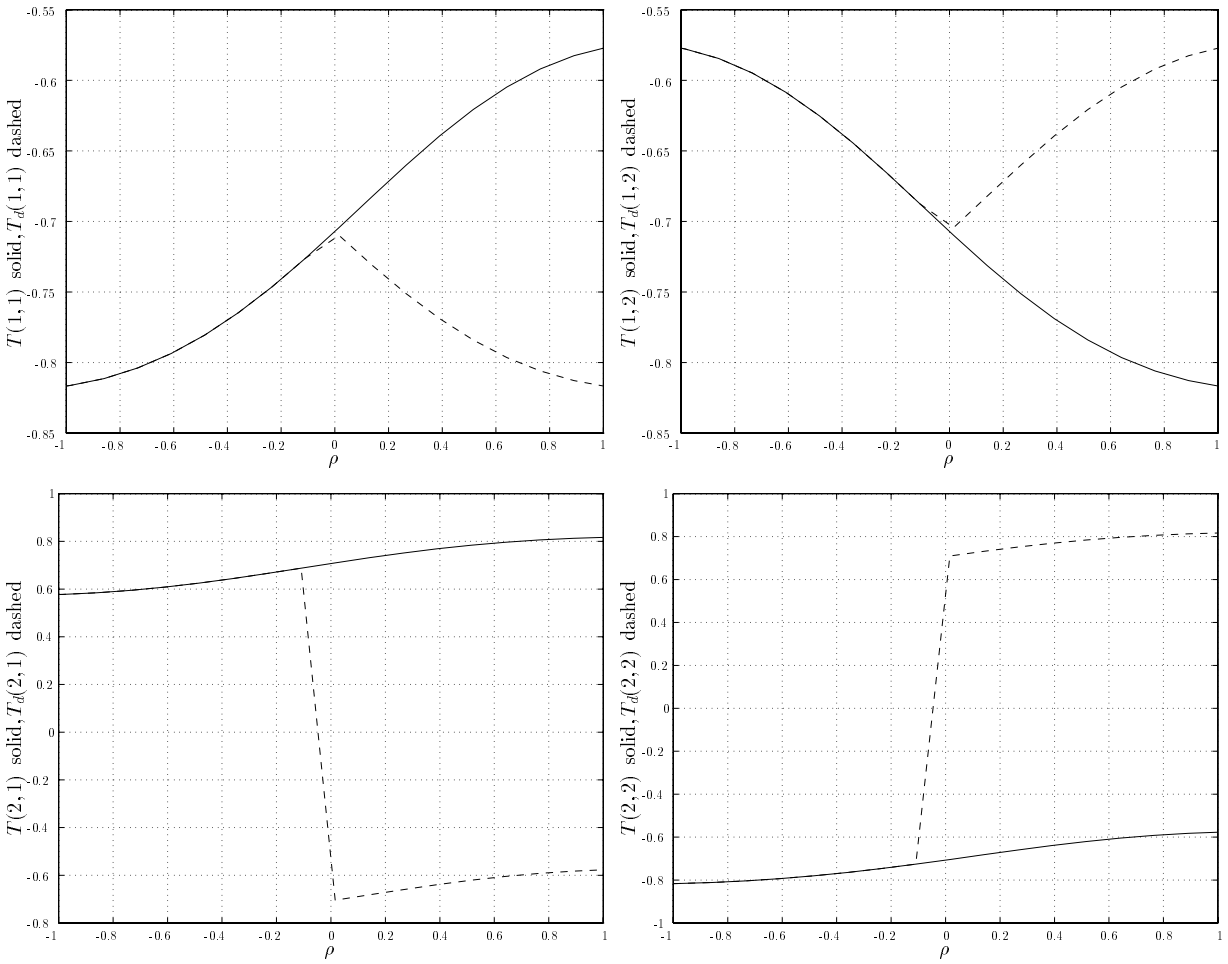

Figure 7.9 *Elements of* $T(\rho)$ *and* $T_d(\rho)$.

with $\tilde{U}(\rho), \tilde{V}(\rho)$ and $\tilde{S}(\rho)$ all analytic. To obtain the orthonormal matrix function $\tilde{V}(\rho)$ define Z_{p_1} as in equation 7.70. Associate with this matrix the unique analytic projections $\mathcal{P}_i(\rho)$ onto the total lambda groups $\lambda_i(\rho)$. Define

$$Q(\rho) \stackrel{\triangle}{=} \sum_i \frac{d\mathcal{P}_i}{d\rho}\mathcal{P}_i(\rho)$$

where $\frac{d\mathcal{P}_i}{d\rho}$ can be computed using standard perturbation formulae. Define $X(\rho)$ to be the unique orthonormal matrix function solving

$$\frac{dX}{d\rho} = Q(\rho)X(\rho), \quad X(\rho_{\min}) = I.$$

Then $\tilde{V}(\rho)$ is given by

$$\tilde{V}(\rho) \quad = \quad X(\rho)V(\rho_{\min}),$$

where $V(\rho_{\min})$ is the matrix of ordered right singular vectors satisfying

$$U(\rho_{\min})S(\rho_{\min})V^T(\rho_{\min}) \quad = \quad R_q(\rho_{\min})R_p(\rho_{\min}).$$

The orthonormal matrix function $\tilde{U}(\rho)$ is computed analogously (except we use the eigenvalues and eigenprojections of $R_q(\rho)R_p(\rho)R_p^T(\rho)R_q^T(\rho)$). Once the natural singular value decomposition has been found it is possible to use the formulae given in equation (7.67) to obtain the natural balancing state transformation matrix. By defining $\tilde{V}(\rho_{\min}) = V(\rho_{\min})$ and $\tilde{U}(\rho_{\min}) = U(\rho_{\min})$ we are implicitly defining a sorting of the natural singular values which is certainly decreasing at $\rho_{\min}$ but may not be decreasing for all ρ.

We now consider a number of computational examples which have been chosen to demonstrate the theory developed in the previous sections. The LMI's which arise in these examples were all solved using the interior-point methods implemented in [34][15].

7.9 Examples

7.9.1 Example 1

The first example is very simple, but demonstrates that bounding the rate of parameter variation does not always reduce conservatism. Consider the following state-space realisation of a second-order system

$$P_\rho \stackrel{s}{=} \left[\begin{array}{cc|c} -\rho & 0 & \sqrt{\rho} \\ 0 & -(1-\rho) & \sqrt{1-\rho} \\ \hline \sqrt{\rho} & \sqrt{1-\rho} & 0 \end{array}\right],$$

[15] We are grateful to the authors for making an early version of this software available to us.

where for fixed ρ the transfer function is given by

$$P_\rho(s) = \frac{\rho}{s+\rho} + \frac{(1-\rho)}{s+(1-\rho)}.$$

We consider this system over the range $\rho \in [0.25, 0.75]$. First we compute the frozen parameter Hankel singular values and plot them in Figure 7.10. These indicate that one of the states contributes very little to the input-output map and if removed by balanced truncation it is possible to bound the resulting error according to $\max_{\rho \in F_\rho} \|P_\rho(s) - \hat{P}_\rho(s)\|_\infty \leq 0.1340$.

Next we allow the parameter to be time varying with no rate bound, which makes it necessary to search for constant solutions to the controllability and observability inequalities. Even with constant candidate functions and linear parameter dependence in $A(\rho)$[16], the irrational parameter dependence in $B(\rho)$ and $C(\rho)$ makes it necessary to use the gridding procedure outlined in section 7.7. To this end, satisfying the inequalities at 15 equally spaced grid points proved to be sufficient to ensure that they were satisfied on the whole interval. Using the LTI controllability Gramian as a weight to start procedure 7.7.1, only one iteration resulted in the $\mathcal{Q}_e$ singular values superimposed on the Hankel singular values in Figure 7.10. From these we can conclude that the system is stable for arbitrary rates of variation and if we subsequently balance and truncate the system to one state, we can bound the error according to $\|P_\rho - \hat{P}_\rho\| \leq 0.1459$. Since the LPV and LTI upper bounds on the approximation error are so close, there is little to be gained (except an increase in the computational complexity) by bounding the rate of parameter variation.

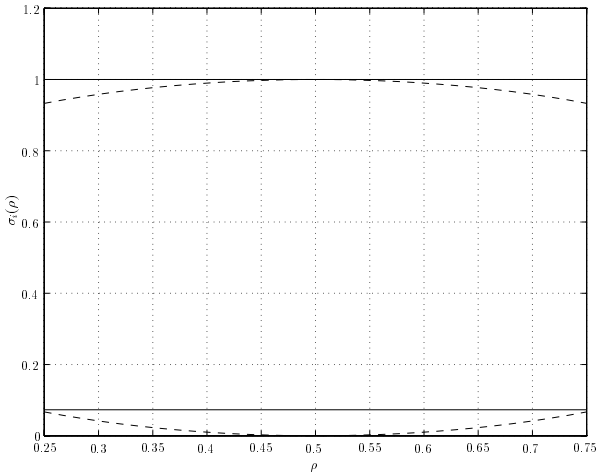

Figure 7.10 *LTI Hankel singular values (dashed), LPV $\mathcal{Q}_e$ singular values (solid).*

[16] If both $B(\rho)$ and $C(\rho)$ were constant we would only need to satisfy the inequalities at the vertices $\rho = 0.25$ and $\rho = 0.75$.

Figure 7.11 shows a comparison between the frozen-parameter frequency responses of the two state model and the single state balanced approximant obtained from the LPV Gramians (no rate bound) at $\rho = 0.25$ (this position corresponds to the worst case LTI error).

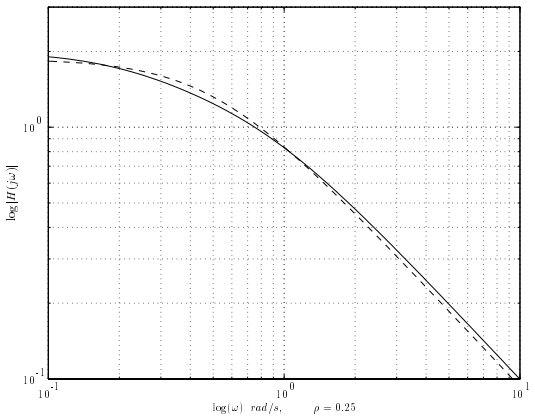

Figure 7.11 *Two state model (solid), single state model (dashed).*

7.9.2 Example 2

The second example comes from the flexible beam studied in the previous chapters. We include this for two reasons: firstly, if we do not bound the rate of parameter variation in the analysis then it turns out that we cannot find solutions to the controllability and observability inequalities (for any realistic contact range), and secondly, the $\mathcal{Q}_e$ singular values of this system do actually cross each other. One drawback with this model stems from the fact that it exhibits strong parameter dependence and the more modes we retain in the model, the more severe this parameter dependence becomes (a glance at the eigenfunctions in chapter 3 clearly indicates why this is the case). This means that a very dense grid is necessary when satisfying the Lyapunov inequalities that arise in the balancing procedure. For this reason the elastic deformation of the beam will be approximated by retaining only two vibration modes in the modal expansion in our LPV model. While not giving an accurate representation of the physical system, this gives a three degree of freedom approximation (see Figure 7.12) which has all of the complexities associated with higher order models and for which the Gramians can be computed in a reasonable length of time (typically 17 hours on a SPARC-10). In this example we examine the physical interval $0.6 \leq \rho/l \leq 0.75$.

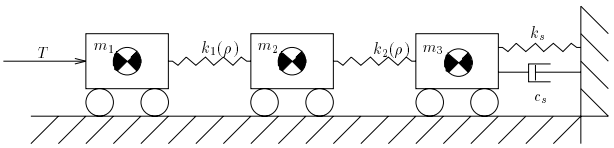

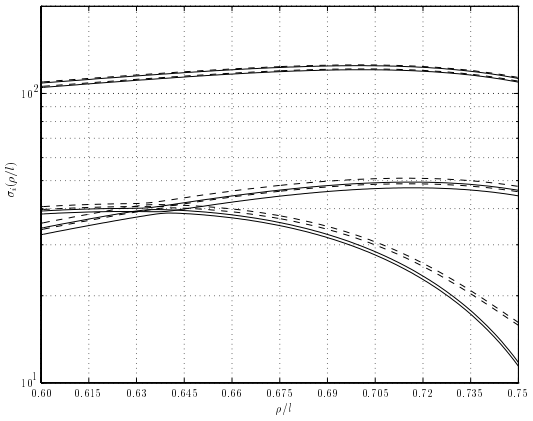

Figure 7.13 *LTI Hankel singular values (solid), $\mathcal{Q}_e$ singular values (dashed).*

Figure 7.12 *Simple physical model of the constrained beam with three vibration modes.*

The highest vibration frequency in the three mode model results from approximating the rigid constraint by a stiff spring and represents an artificial "bouncing mode" where the beam remains approximately rigid and oscillates about its pivot. Ideally, we would like to remove this mode since it has no physical significance. We begin by computing the Hankel singular values of the LTI system obtained by freezing the value of the parameter. These are plotted in Figure 7.13. Superimposed on Figure 7.13 are the $\mathcal{Q}_e$ singular values computed using 15 B-splines (315 decision variables) and 40 uniformly spaced grid points with the rate limit set to zero[17]. Satisfying the inequalities at fewer grid points resulted in them being violated at intermediate parameter values. It can be seen that both the Hankel and the $\mathcal{Q}_e$ singular values can be grouped into pairs, each pair being associated with one vibration mode. Observe that the $\mathcal{Q}_e$ singular values cross at a number of points in the physical region shown, hence it will be necessary to make use of the natural-balancing transformation matrix to balance this system. Having established a suitable dimension for the basis set, we compute the $\mathcal{Q}_e$ singular values with rate limits of $|\dot{\rho}| \leq 1\ cm/s$, $|\dot{\rho}| \leq 2.5\ cm/s$, $|\dot{\rho}| \leq 5\ cm/s$ and $|\dot{\rho}| \leq 10\ cm/s$. Figure 7.14 has been included to demonstrate how sensitive the $\mathcal{Q}_e$ singular values are to changes in the rate limit, indicating why, at least for this system, it is so important to use realistic rate bounds in the analysis. Unfortunately, because balanced truncation does no emphasis low frequency approximation simply truncating this system is likely to give a poor approximant. This is confirmed in Figure 7.15 which shows the frozen-parameter frequency response of the 6-state model and a 4-state balanced approximant which was obtained from the Gramians computed with a rate bound of 2.5 cm/s. The results correspond to $\rho/l = 0.6$. To demonstrate how useful the frequency weighting procedure in section 7.4 can be, we introduce the following weight at

[17] Since we have not inverted the Gramians the large singular values are approximated better than the small singular values.

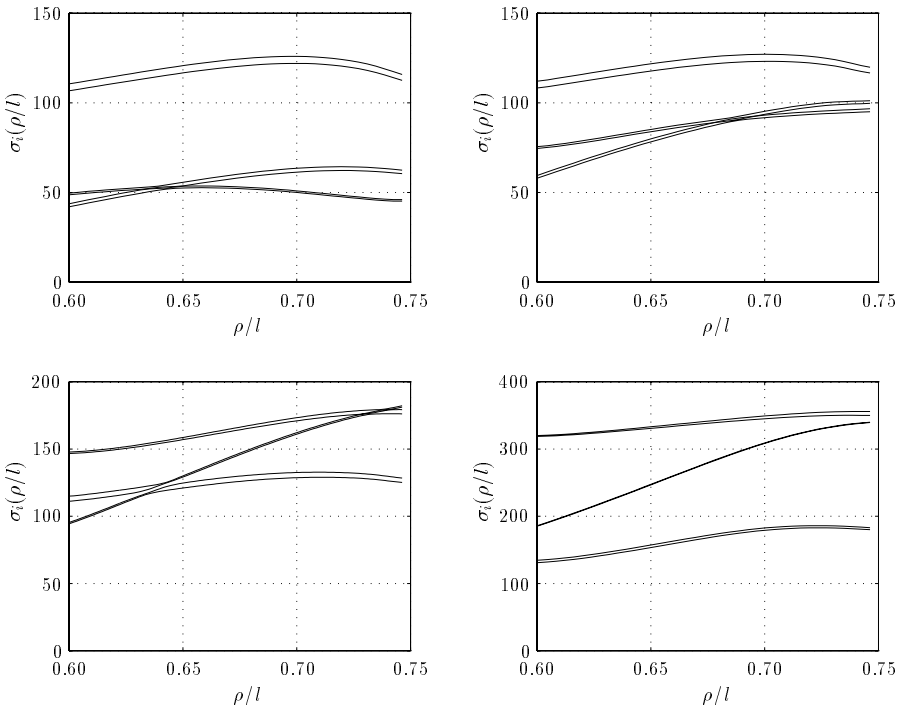

Figure 7.14 $\mathcal{Q}_e$ *singular values computed with the rate limits of* $|\dot{\rho}| \leq 1$ *cm/s,* $|\dot{\rho}| \leq 2.5$ *cm/s,* $|\dot{\rho}| \leq 5$ *cm/s and* $|\dot{\rho}| \leq 10$ *cm/s, respectively.*

the plant input

$$W(s) = \frac{10}{s+1}.$$

Computing the frequency-weighted Gramians (with a rate bound of $|\dot{\rho}| \leq 2.5$ *cm/s*) using the procedure given in section 7.4, two interesting observations emerge. Firstly, the frequency-weighted $\mathcal{Q}_e$ singular values do not cross at any points in the given interval. This makes computation of the frequency-weighted balancing transformation matrix much easier. Secondly, the approximant is much improved at low and intermediate frequencies. This is confirmed by including the frequency response of the 4-state rate-bounded frequency-weighted balanced approximant at $\rho/l = 0.60$ in Figure 7.15.

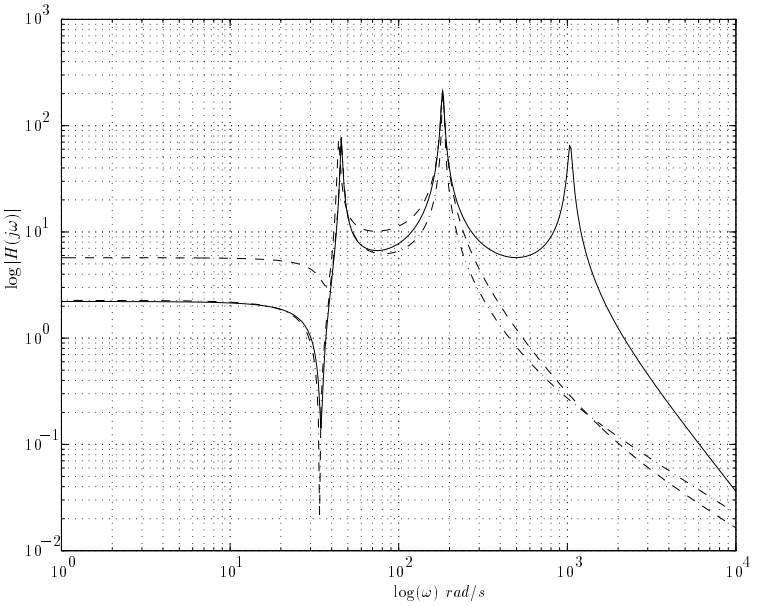

Figure 7.15 *Frequency response of the 6-state model (solid), 4-state balanced approximant (dashed), and 4-state frequency-weighted balanced approximant (dot-dashed). Responses computed at* $\rho/l = 0.60$.

7.9.3 Example 3

Our final example is a realistic model-reduction example which makes use of the factorisation theory developed for unstable systems. Helicopter rotor blades are susceptible to high vibratory loads, aeromechanical instabilities and high dynamic stresses. To reduce the dynamics loads experienced by the rotor blade much research is being expended on the development of actuators whereby control forces can be introduced to dissipate the vibration energy[18] [16]. Figure 7.16 shows a hypothetical example of such a system.

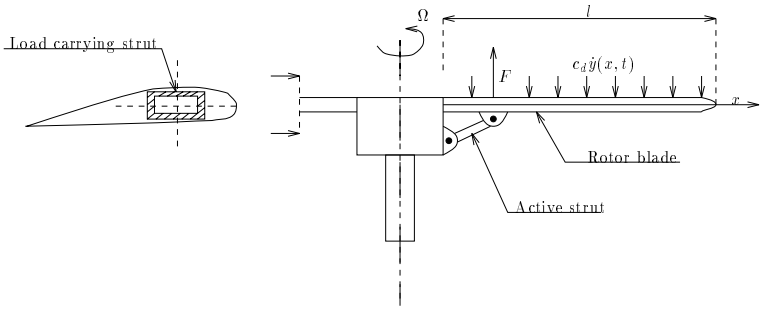

Figure 7.16 *Rotor blade control system.*

[18] Popular techniques involve embedding piezoceramic materials into the blade itself so that an internal bending moment can be applied to the blade.

The load-carrying strut is modelled as an Euler beam of length l, clamped at one end and free at the other. Assume that an active strut allows a vertical force to be applied to the blade at $x = l/6$, and strain gauge sensors located at $x = l/15$ are used to measure the bending moment at the root of the blade. The effective stiffness of this system exhibits strong dependence on the angular velocity Ω, which is assumed to vary about a nominal value of 1500 rpm between the limits of 1250 rpm and 1750 rpm. The equation governing the transverse vibration of the beam is easily derived as being

$$\frac{\partial^2 y}{\partial t^2} - \frac{1}{2}\Omega^2 l^2 \frac{\partial}{\partial x}((1 - \frac{x^2}{l^2})\frac{\partial y}{\partial x}) + \frac{c_d}{m}\frac{\partial y}{\partial t} + \frac{EI}{m}\frac{\partial^4 y}{\partial x^4} = \frac{F}{m}\delta(x - l/6), \tag{7.71}$$

where l is the length of the beam, E Young's modulus, I the second moment of area and m the mass per unit length. Taking a beam of unit length, the system is normalised so that when the beam is not rotating its first natural frequency is 1 Hz. Using the clamped-free eigenfunctions derived in chapter 3 the following expansion

$$y(x,t) = \sum_{i=1}^{N} a_i(t)\phi_i(x),$$

generates a finite-dimensional model of the form

$$I\ddot{a}(t) + \alpha I\dot{a}(t) + K(\Omega^2(t))a(t) = \Phi F.$$

The simple physical damping model results in the small proportional damping factor α which is chosen to give 1% damping in the first vibration mode when the blade is rotating at 1500 rpm. The stiffness matrix is a linear function of the parameter Ω^2 and can be computed from

$$k_{ij} = w_i^2\delta_{i,j} + \frac{\Omega^2}{2}\int_0^l (1 - \frac{x^2}{l^2})\phi_i'(x)\phi_j'(x)dx,$$

where $\delta_{i,j}$ is the Kronecker delta.

Assume, for the purpose of control, that it is desired to reject deviations in the mean bending moment due to aerodynamic disturbances having frequencies below 25 Hz. To capture the dynamics of the beam sufficiently accurately in this frequency range four modes are retained in the modal expansion of $y(x,t)$. Frequency weighting is introduced in order to apply a gain-scheduled equivalent of the H_∞ loop-shaping design procedure (this will be developed in chapter 8). In this example a third-order parameter-dependent weight

$$W(s) = \frac{\Omega^3}{s}\frac{150^2}{(s^2 + 90s + 150^2)},$$

gives sufficiently fast roll-off above crossover to prevent strong interaction with high frequency modes, and integral action at low frequency to meet the performance objective. Figure 7.17 shows the loop shapes of the 11-state weighted model with $\Omega = 1250$ rpm, $\Omega = 1500$ rpm and $\Omega = 1750$ rpm and gives an idea of the sensitivity of the system to variations in the rotation rate.

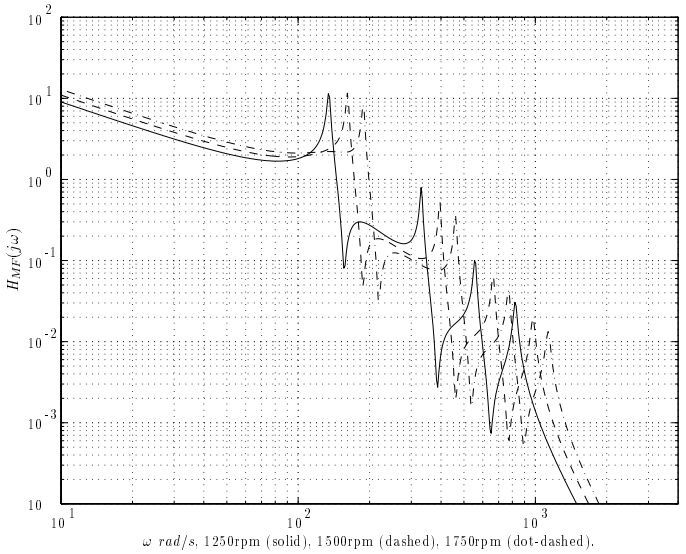

Figure 7.17 *Frequency response from the control force to the bending moment.*

We treat the weighted system as an unstable LPV operator (since the weight contains an integrator) and attempt to model-reduce it by approximating the symbol of its graph. We begin by determining the number of B-splines and grid points required in the computation of GCRI and GFRI. To this end we set $\dot{\Omega} = 0$ and solve GCRI and GFRI on a specified grid. We can then check whether the LMI's are satisfied on a much denser grid covering the feasible parameter range and also compare the $\mathcal{Q}_e$ singular values of the contractive graph symbol $\mathcal{G}_\rho$ to the Hankel singular values of the normalised graph symbol obtained by computing a normalised coprime factorisation of the plant at the grid points. In the limit $\dot{\Omega} \to 0$, the $\mathcal{Q}_e$ singular values of $\mathcal{G}_\rho$ should coincide with the Hankel singular values if a sufficient number of B-splines are used in the approximation of GCRI and GFRI. It was found that 8 B-splines (528 decision variables) and 30 grid points were sufficient to accurately reproduce the LTI Hankel singular values and ensure that GCRI and GFRI were satisfied for all feasible values of Ω. Figure 7.18 allows the Hankel singular values of the normalised graph symbol to be compared to the $\mathcal{Q}_e$ singular values of the contractive graph symbol. Examining the frozen-parameter $\mathcal{Q}_e$ singular values over the given parameter range we obtain Table 7.1.

	$i=1$	$i=2$	$i=3$	$i=4$	$i=5$	i=6
$\max_{\rho\in F_\rho} \sigma_i(\rho)$	0.9370	0.8044	0.6200	0.3529	0.3420	0.2060
	$i=7$	$i=8$	$i=9$	$i=10$	$i=11$	-
$\max_{\rho\in F_\rho} \sigma_i(\rho)$	0.1068	0.0533	0.0523	0.0158	0.0154	-

Table 7.1 *Bounds on the $\mathcal{Q}_e$ singular values.*

Table 7.1 indicates that the last four states contribute little to the input-output map of the contractive graph symbol $\mathcal{G}_\rho$. Truncating these states, Figure 7.19 allows the frequency responses

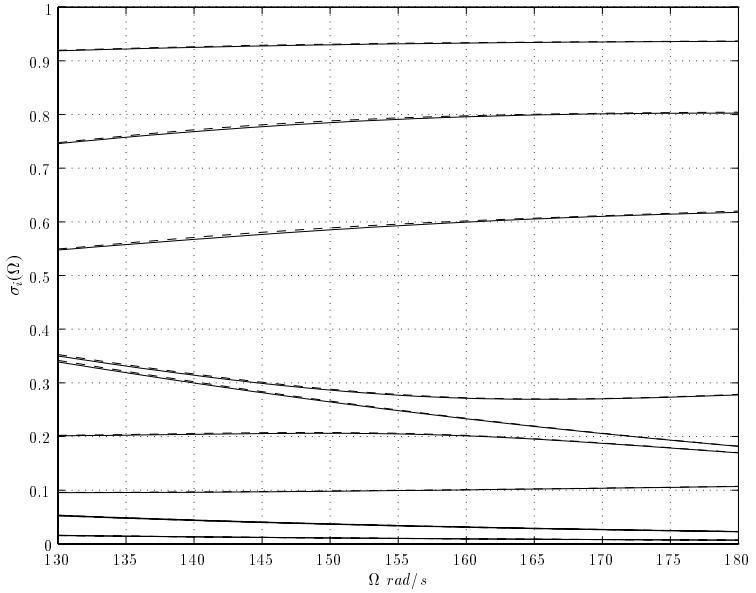

Figure 7.18 *LTI Hankel singular values (solid) and LPV $\mathcal{Q}_e$ singular values (dashed).*

of the 11-state model and the 7-state approximant to be compared at the three rotation speeds $\Omega = 1250\ rpm$, $\Omega = 1500\ rpm$ and $\Omega = 1750\ rpm$. As desired, the 7-state approximant captures the dynamics of the 11-state model over the chosen frequency range, effectively truncating the high frequency vibration modes while preserving the low frequency behaviour.

With the same number of B-splines and grid points we re-compute[19] solutions to GCRI and GFRI with rate bounds of $|\dot{\Omega}| \leq 5\ rad/s^2$, $|\dot{\Omega}| \leq 10\ rad/s^2$, $|\dot{\Omega}| \leq 15\ rad/s^2$, and $|\dot{\Omega}| \leq 20\ rad/s^2$. The variation in the $\mathcal{Q}_e$ singular values as a function of $\dot{\Omega}$ is shown in Figure 7.20. This indicates that the four smallest $\mathcal{Q}_e$ singular values continue to contribute little to the input-output map of $\mathcal{G}_\rho$ even when $\dot{\Omega}$ is allowed to vary as rapidly as $20\ rad/s^2$. Observe that the other singular values are much more sensitive to the bound on $\dot{\Omega}$. Of particular interest is the sensitivity exhibited by the largest singular value which will be shown, in chapter 8, to bound the achieved stability margin in a generalisation of the four-block synthesis setup considered in chapter 4. In fact it is the sensitivity of the largest singular value which highlights the importance of using realistic rate bounds. With the rate bound set at $|\dot{\Omega}| \leq 20\ rad/s^2$ we extract a 7-state model approximant using balanced truncation[20]. In Figure 7.21 we plot the frozen-parameter frequency responses of the 11-state model and the 7-state balanced approximant computed using the rate-bounded Gramians. Again, the balanced approximant captures the dominant dynamics very nicely. Unfortunately, attempts to compute a quadratic dissipation function to bound the

[19]Each computation took approximately 24 hours on a SPARC-10.

[20]Observe that none of the $\mathcal{Q}_e$ singular values cross each other so we can use the standard algorithm to extract the balancing transformation matrix.

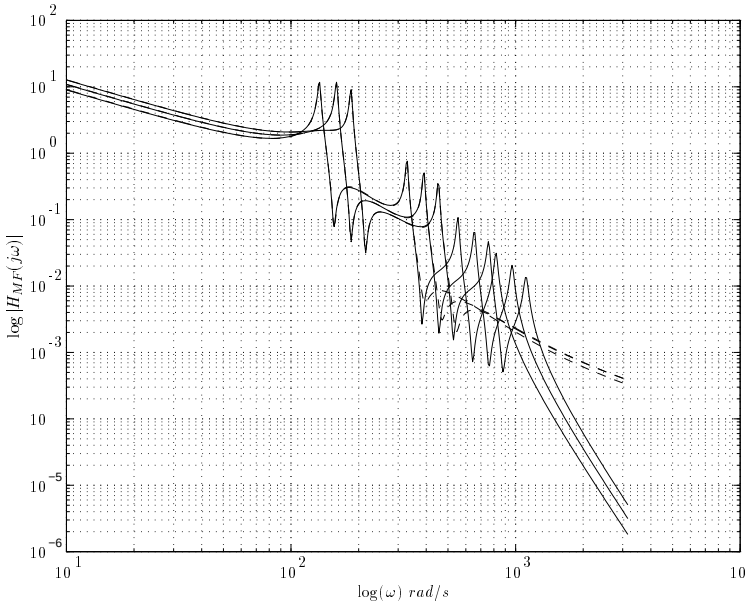

Figure 7.19 *Frequency response* $1250rpm \leq \Omega \leq 1750rpm$*, 11-state model (solid), 7-state model (dashed).*

error between $\mathcal{G}_\rho$ and $\hat{\mathcal{G}}_\rho$ proved to be unsuccessful. This was a consequence of the fact that the error operator had 18 states, which made the size of the problem too large for the available hardware.

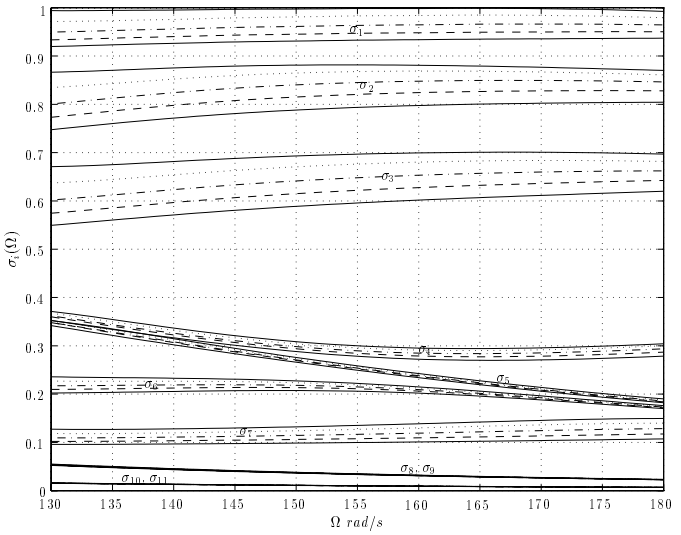

Figure 7.20 $\dot{\Omega} = 0$ *(solid),* $|\dot{\Omega}| \leq 5 rad/s^2$ *(dashed),* $|\dot{\Omega}| \leq 10 rad/s^2$ *(dot-dash),* $|\dot{\Omega}| \leq 15 rad/s^2$ *(dot-dot) and* $|\dot{\Omega}| \leq 20 rad/s^2$ *(solid).*

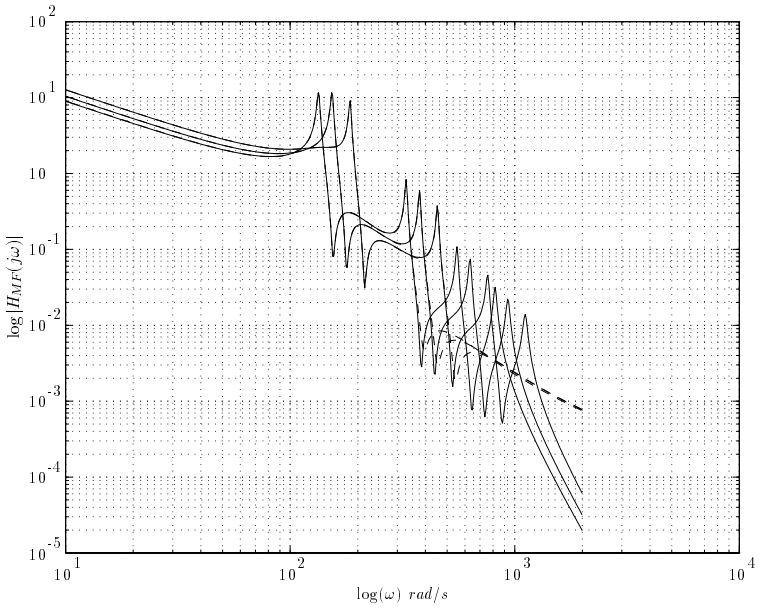

Figure 7.21 *Frozen parameter frequency responses, 11-state model (solid), 7-state balanced approximant (dashed),* $|\dot{\Omega}| \leq 20$.

7.10 Summary

In this chapter we have extended the technique of balanced truncation of LTI systems to bounded-rate LPV systems. For stable systems our approach was based upon the solution of two parameter-dependent Lyapunov differential inequalities, whereas for unstable systems it was based upon the solution of two parameter-dependent Riccati differential inequalities which were used to obtain a factorisation of the unstable system over a specified ring of stable systems. In both cases, upper bounds on the truncation error which are known to hold for balanced truncation of LTI systems have been shown to carry over to the LPV setting when there is no rate bound. We have not been able to reproduce the upper bound for finite rate bounds, but have obtained some insight in the general case and have shown that provided the system is sufficiently stable, then the bound carries over. Special care has been paid to the continuity properties of the balancing transformation matrix and we have shown that in some situations this may fail to be continuous. For systems which exhibit this phenomenon we have introduced an alternative to the balancing transformation which we called the natural-balancing transformation. This allows the system to be truncated in the usual manner, but more care is required in the interpretation. We have also introduced a method for computing solutions to the differential inequalities which arise in the analysis. This is based upon a gridding procedure and continuity properties in order to make it tractable. Finally, we have presented some examples which demonstrate a number of the interesting issues that arise in the analysis. Although the computations required to compute the balancing transformation matrix are intensive, we feel that this technique has much to offer, particularly for the purpose of reduced-order controller synthesis. This will be demonstrated in chapter 8.

8

Synthesis of Parameter-Dependent Controllers for Parameter-Dependent Dynamical Systems

8.1 Introduction

The explicit state-space procedures for computing suboptimal H_∞ controllers presented in [24] represent a major milestone in the development of H_∞ control theory, effectively opening the way for its application to a much wider class of problems. By expressing the existence of suboptimal controllers in terms of the existence of solutions to two algebraic Riccati equations, it became straightforward to reliably compute controllers having a state dimension equal to that of the generalised plant. The original solution to the H_∞ control problem relied heavily on the results of operator theory, being obtained through the Youla parametrisation of all internally stabilising controllers to obtain the set of all stable closed-loop transfer functions, spectral factorisations to reduce this to a 2-block general distance problem, reduction to a Nehari problem and solution by the methods of Glover [39]. Not only was this original solution procedure more complicated computationally, but it also tended to produce high order controllers.

The state-space results were later extended to the class of linear time-varying systems in [55] where the existence of suboptimal controllers bounding the closed-loop L_2 gain of a given time-varying system was expressed in terms of the existence of solutions to two Riccati differential equations, one of which must be integrated over all future time. Of course the basic underlying assumption leading to time-varying systems, that the time dependence is known exactly for all future time, means that there is no conceptual difficulty with having to solve these differential equations. Unfortunately, many systems fail to satisfy this assumption, as is the case with any system whose dynamics depend causally (but not predictably) on some measurable parameter. Important developments toward being able to deal with the latter class of systems came through the restatement of the conditions for the existence of suboptimal controllers for LTI plants in terms of the existence of solutions to two Riccati inequalities ([33],[77],[78]. Using affine matrix inequalities these can be reformulated as convex constraints on the space of real symmetric positive-definite matrices, and allow some of the assumptions made in [24] to be relaxed [33].

The inequality approach was adapted by Packard [67] to synthesise linear parameter-dependent controllers for parameter-dependent plants. By expressing both the plant and the controller as an LFT in the unknown parameter(s) he made use of the optimally scaled small gain theorem to

pose the problem of existence in a small gain framework. Using this formulation the existence of a parameter-dependent controller which meets the closed-loop objectives can be converted into a convex feasibility problem involving LMI's. Unfortunately, the LFT approach does have drawbacks: in particular, the optimally scaled small gain theorem does not exploit the fact that the parameter is real (as opposed to being complex) and allows for arbitrary rates of parameter variation. Allowing the parameter to be complex generally makes this formulation more conservative than using a single quadratic Lyapunov function to bound the induced L_2 gain, although the latter approach typically leads to a convex feasibility problem with infinitely many constraints.

The application of a single quadratic function[1] to establish stability and to bound the induced norm of an LPV system has led to the notion of quadratic stability and quadratic performance. The existence of linear parameter-dependent controllers which quadratically stabilise various classes of LPV systems has been studied in, amongst others ([9],[12],[101]). Necessary and sufficient conditions for the existence of output feedback parameter-dependent controllers which quadratically stabilise an LPV plant and which achieve a specified bound on the closed-loop L_2 gain have been obtained in ([7],[8]). These are expressed in terms of the existence of constant solutions to two parameter-dependent Riccati inequalities which are easily reformulated as convex feasibility conditions involving LMI's. For certain classes of LPV systems which exhibit linear parameter dependence, Becker [7] has shown that the LMI's can be solved as a finite-dimensional linear programming problem, although, in the general case, a gridding procedure similar to that used in chapter 7 must be used. Unfortunately, the quadratic performance formulation is also conservative, effectively allowing for arbitrary rates of parameter variation.

In this chapter we develop a very natural extension of the quadratic performance methods developed by Becker by making use of parameter-dependent Lyapunov functions to bound the closed-loop induced L_2 gain, explicitly constraining the rate of parameter variation in the process. These bounded-rate synthesis results are based upon an extension of the early results of Sampei et al [77] and have been obtained independently using a slightly different formulation by Wu et al [93]. We will show that the existence of a controller achieving a $\mathcal{Q}_\gamma$ performance bound can be expressed in terms of the existence of solutions to two parameter-dependent Riccati differential inequalities subject to a spectral radius coupling constraint. Once again, the existence of solutions to the Riccati inequalities can be posed as a convex feasibility problem involving LMI's and solved using a gridding procedure similar to that outlined in chapter 7. We will take this problem a step further and consider the problem of synthesising reduced-order controllers for bounded-rate LPV systems, developing a framework based upon the four-block problem studied in chapter 4 which is very natural for this purpose. In general, the Riccati differential inequalities arising in the controller synthesis problem must be solved simultaneously because they are required to satisfy a spectral radius coupling condition. This implies that the problem of finding the tightest bound on the closed-loop L_2 gain requires an iteration and this can be

[1] By a single quadratic Lyapunov function we mean a parameter-independent Lyapunov function of the form $V(x) = x^T P x$ where $P = P^T > 0$ is a constant matrix.

very expensive computationally. For the four-block problem we will show how the LMI's can be separated and the problem reformulated as a quasi-convex optimisation problem that does away with the requirement for iteration. This is reminiscent of the LTI solution of the four-block problem which can be stated exactly in terms of the solutions of two algebraic Riccati equations [59].

8.2 General output feedback synthesis

The problem is posed in the standard framework (Figure 8.1) where we consider the interconnection of a causal finite-dimensional LPV plant $P_\rho : L^+_{2,e} \otimes L^+_{2,e} \mapsto L^+_{2,e} \otimes L^+_{2,e}$ and a causal finite-dimensional LPV controller $C_\rho : L^+_{2,e} \mapsto L^+_{2,e}$.

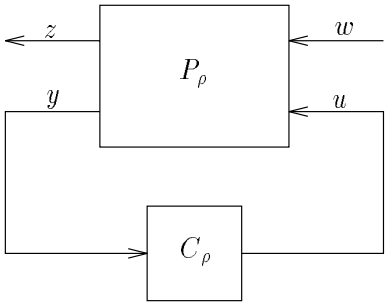

Figure 8.1 *Synthesis setup.*

It is assumed that the generalised plant P_ρ contains all loop-shaping weights, disturbance weights and performance filters. The vector $z \in \mathbb{R}^{z\times 1}$ is the vector of controlled outputs, $w \in \mathbb{R}^{w\times 1}$ is the vector of disturbance signals, $y \in \mathbb{R}^{p\times 1}$ is the vector of measured outputs and $u \in \mathbb{R}^{m\times 1}$ is the vector of manipulated inputs. If we partition the operator P_ρ conformally with the dimensions of its inputs and its outputs

$$P_\rho = \begin{bmatrix} P_{11_\rho} & P_{12_\rho} \\ P_{21_\rho} & P_{22_\rho} \end{bmatrix},$$

it is possible to write the closed-loop operator $\mathcal{F}_l(P_\rho, C_\rho) : L^+_{2,e} \mapsto L^+_{2,e}$, $w(t) \mapsto z(t)$ as follows

$$\mathcal{F}_l(P_\rho, C_\rho) = P_{11_\rho} + P_{12_\rho} C_\rho (I - P_{22_\rho} C_\rho)^{-1} P_{21_\rho}.$$

Given a stabilisable and detectable state-space realisation of P_ρ, our objective is to find a causal LPV controller C_ρ which makes the closed loop exponentially stable and which also bounds the induced norm from w to z such that $\|\mathcal{F}_l(P_\rho, C_\rho)\| \leq \gamma$ for all $\rho(t) \in F_\rho$. Our approach is to make use of the stronger notion of performance defined in chapter 2. That is, we look for a controller which exponentially stabilises the closed loop and which achieves a specified $\mathcal{Q}_\gamma$ performance level (which is of course sufficient to ensure that $\|\mathcal{F}_l(P_\rho, C_\rho)\| \leq \gamma$).

We assume that the generalised plant has a continuous state-space realisation given by

$$P_\rho \stackrel{s}{=} \left[\begin{array}{c|cc} A(\rho(t)) & B_1(\rho(t)) & B_2(\rho(t)) \\ \hline C_1(\rho(t)) & D_{11}(\rho(t)) & D_{12}(\rho(t)) \\ C_2(\rho(t)) & D_{21}(\rho(t)) & 0 \end{array}\right]. \tag{8.1}$$

The assumption that $D_{22} = 0$ results in no loss of generality since any direct throughput term can be absorbed into the controller. We initially restrict the controller C_ρ to be strictly proper and assume that it has a state-space realisation given by

$$C_\rho \stackrel{s}{=} \left[\begin{array}{c|c} \hat{A}(\rho(t)) & \hat{B}(\rho(t)) \\ \hline \hat{C}(\rho(t)) & 0 \end{array}\right]. \tag{8.2}$$

It follows that a state-space realisation of the closed-loop operator $\mathcal{F}_l(P_\rho, C_\rho)$ is given by

$$\mathcal{F}_l(P_\rho, C_\rho) \stackrel{s}{=} \left[\begin{array}{c|c} A_c(\rho(t)) & B_c(\rho(t)) \\ \hline C_c(\rho(t)) & D_c(\rho(t)) \end{array}\right], \tag{8.3}$$

$$\mathcal{F}_l(P_\rho, C_\rho) \stackrel{s}{=} \left[\begin{array}{cc|c} A(\rho(t)) & B_2(\rho(t))\hat{C}(\rho(t)) & B_1(\rho(t)) \\ \hat{B}(\rho(t))C_2(\rho(t)) & \hat{A}(\rho(t)) & \hat{B}(\rho(t))D_{21}(\rho(t)) \\ \hline C_1(\rho(t)) & D_{12}(\rho(t))\hat{C}(\rho(t)) & D_{11}(\rho(t)) \end{array}\right]. \tag{8.4}$$

The following lemma will be required in the proof of the main result

Lemma 8.2.1 *Given a positive constant $\gamma > 0$, and a differentiable $P(\rho) = P^T(\rho) > 0$ which satisfies*

$$\dot{P} + PA + A^TP + C^TC + (PB + C^TD)(\gamma^2 I - D^TD)^{-1}(B^TP + D^TC) < 0 \;\; \forall \rho(t) \in F_\rho, \tag{8.5}$$

then $Q(\rho) \stackrel{\triangle}{=} \gamma^2 P^{-1}(\rho)$ satisfies

$$-\dot{Q} + AQ + QA^T + BB^T + (QC^T + BD^T)(\gamma^2 I - DD^T)^{-1}(CQ + DB^T) < 0 \;\; \forall \rho(t) \in F_\rho. \tag{8.6}$$

Proof: This follows from multiplying equation (8.5) on the left by $\gamma^2 P^{-1}$, on the right by P^{-1} and some algebraic manipulation to get equation (8.6). ■

The following theorem states necessary and sufficient conditions for the existence of a controller achieving a specified level of $\mathcal{Q}_\gamma$ performance. For clarity of presentation the ρ dependence of the state matrices is suppressed.

Theorem 8.2.2 *There exists a strictly proper controller which satisfies a chosen $\mathcal{Q}_\gamma$ performance level if, and only if:*

i. $\gamma^2 I - D_{11}^T D_{11} > 0$;

ii. there exists a differentiable $P(\rho) = P^T(\rho) > 0$ *and a differentiable* $Q(\rho) = Q^T(\rho) > 0$ *such that*

a. there exists an $F(\rho)$ *such that*

$$\dot{P} + P\tilde{A} + \tilde{A}^T P + \tilde{C}^T\tilde{C} + (PB_1 + \tilde{C}^T D_{11})(\gamma^2 I - D_{11}^T D_{11})^{-1}(B_1^T P + D_{11}^T\tilde{C}) < 0 \ \ \forall \rho(t) \in F_\rho, \quad (8.7)$$

where $\tilde{A} = A + B_2 F$ *and* $\tilde{C} = C_1 + D_{12}F$;

b. there exists an $K(\rho)$ *such that*

$$-\dot{Q} + Q\bar{A}^T + \bar{A}Q + \bar{B}\bar{B}^T + (QC_1^T + \bar{B}D_{11}^T)(\gamma^2 I - D_{11}D_{11}^T)^{-1}(C_1 Q + D_{11}\bar{B}^T) < 0 \ \ \forall \rho(t) \in F_\rho, \quad (8.8)$$

where $\bar{A} = A + KC_2$ *and* $\bar{B} = B_1 + KD_{21}$;

c. $\gamma^2 I > PQ$.

Given that conditions (i.), (ii.) are satisfied, then one such controller that achieves the specified level of $\mathcal{Q}_\gamma$ *performance is given by*

$$\hat{A} = -\hat{B}C_2 + A + B_2\hat{C} - Q(\gamma^2 I - PQ)^{-1}M^T \quad (8.9)$$

$$\hat{B} = -\gamma^2(\gamma^2 I - QP)^{-1}K \quad (8.10)$$

$$\hat{C} = F \quad (8.11)$$

where

$$M = PB_2F - H + (C_1 + D_{12}F)^T D_{12}F + (PB_1 + C_1^T D_{11} + F^T D_{12}^T D_{11}) (\gamma^2 I - D_{11}^T D_{11})^{-1}(D_{11}^T D_{12}F + (D_{21}^T\hat{B}^T - B_1^T)(\gamma^2 Q^{-1} - P)) \quad (8.12)$$

$$H = \dot{P} + P(A + B_2F) + (A + B_2F)^T P + (C_1 + D_{12}F)^T(C_1 + D_{12}F) + (PB_1 + (C_1 + D_{12}F)^T D_{11})(\gamma^2 I - D_{11}^T D_{11})^{-1}(B_1^T P + D_{11}^T(C_1 + D_{12}F)). \quad (8.13)$$

Proof: The proof is relatively long and extends the results of Sampei et al [77] where the solution of the LTI problem was stated in terms of two algebraic Riccati inequalities subject to a coupling constraint. If there exists a strictly proper controller C_ρ achieving the specified $\mathcal{Q}_\gamma$ performance level, then by assumption

1. $\gamma^2 I - D_{11}^T D_{11} > 0$.

2. $\exists\ P_c(\rho) = P_c^T(\rho) > 0$ such that

$$\dot{P}_c + P_c A_c + A_c^T P_c + C_c^T C_c + (P_c B_c + C_c^T D_c)(\gamma^2 I - D_c^T D_c)^{-1}(B_c^T P_c + D_c^T C_c) < 0 \ \ \forall\ \ \rho(t) \in F_\rho. \quad (8.14)$$

Partition P_c conformally with A_c to get

$$P_c = \begin{bmatrix} P_{11} & P_{12} \\ P_{12}^T & P_{22} \end{bmatrix}.$$

Now introduce the parameter-varying transformation matrix

$$\tilde{T}(\rho) \stackrel{\triangle}{=} \begin{bmatrix} I & 0 \\ -P_{22}^{-1}P_{12}^T & I \end{bmatrix} \qquad \tilde{T}^{-1}(\rho) = \begin{bmatrix} I & 0 \\ P_{22}^{-1}P_{12}^T & I \end{bmatrix},$$

which can be used to transform P_c, A_c, B_c and C_c as follows

$$\begin{aligned}
\tilde{P}_c &\stackrel{\triangle}{=} \tilde{T}^T P_c \tilde{T} = \begin{bmatrix} P_{11} - P_{12}P_{22}^{-1}P_{12}^T & 0 \\ 0 & P_{22} \end{bmatrix} \\
\tilde{A}_c &\stackrel{\triangle}{=} \tilde{T}^{-1} A_c \tilde{T} = \begin{bmatrix} A + B_2\hat{C}\tilde{E} & \bullet \\ \bullet & \bullet \end{bmatrix} \\
\tilde{B}_c &\stackrel{\triangle}{=} \tilde{T}^{-1} B_c = \begin{bmatrix} B_1 \\ \bullet \end{bmatrix} \\
\tilde{C}_c &\stackrel{\triangle}{=} C_c \tilde{T} = \begin{bmatrix} C_1 + D_{12}\hat{C}\tilde{E} & \bullet \end{bmatrix},
\end{aligned}$$

where $\tilde{E} = -P_{22}^{-1}P_{12}$ and the bullet $\bullet$ is used for blocks that are of no interest. Multiplying equation (8.14) on the left by $\tilde{T}^T$ and on the right by $\tilde{T}$ gives

$$\tilde{T}^T\dot{P}_c\tilde{T} + \tilde{P}_c\tilde{A}_c + \tilde{A}_c^T\tilde{P}_c + \tilde{C}_c^T\tilde{C}_c + (\tilde{P}_c\tilde{B}_c + \tilde{C}_c^T D_c)(\gamma^2 I - D_c^T D_c)^{-1}(\tilde{B}_c^T\tilde{P}_c + D_c^T\tilde{C}_c) < 0.$$

The $(1,1)$ block of $\tilde{T}^T\dot{P}_c\tilde{T}$ commutes under differentiation, that is

$$(\tilde{T}^T\dot{P}_c\tilde{T})_{(1,1)} = \dot{P}_{11} - \dot{P}_{12}P_{22}^{-1}P_{12}^T - P_{12}P_{22}^{-1}(\dot{P}_{12}^T - \dot{P}_{22}P_{22}^{-1}P_{12}^T) = \frac{d}{dt}(\tilde{T}^T P_c \tilde{T})_{(1,1)}. \quad (8.15)$$

Define the matrix P_z as follows

$$P_z \stackrel{\triangle}{=} P_{11} - P_{12}P_{22}^{-1}P_{12}^T,$$

and use P_z to write the $(1,1)$ block of equation (8.15) as

$$\dot{P}_z + P_z\tilde{A} + \tilde{A}^T P_z + \tilde{C}^T\tilde{C} + (P_z B_1 + \tilde{C}^T D_{11})(\gamma^2 I - D_{11}^T D_{11})^{-1}(B_1^T P_z + D_{11}^T\tilde{C}) < 0,$$

where $\tilde{A} = A + B_2\hat{C}\tilde{E}$ and $\tilde{C} = C_1 + D_{12}\hat{C}\tilde{E}$. Putting $\tilde{F} = \hat{C}\tilde{E}$ gives condition (ii.a.). If we go a step further and define $P \stackrel{\triangle}{=} (1-\epsilon)P_z$, then condition (ii.a.) is satisfied by P for sufficiently

small $\epsilon > 0$ (by continuity) and $P < P_z \ \forall \ \epsilon > 0$. To complete the proof of necessity define $\bar{T}$ according to

$$\bar{T}(\rho) \stackrel{\triangle}{=} \begin{bmatrix} I & -P_{11}^{-1}P_{12} \\ 0 & I \end{bmatrix} \qquad \bar{T}^{-1}(\rho) = \begin{bmatrix} I & P_{11}^{-1}P_{12} \\ 0 & I \end{bmatrix}.$$

The matrix $\bar{T}(\rho)$ can be used to transform P_c, A_c, B_c and C_c as follows

$$\begin{aligned} \bar{P}_c &= \bar{T}^T P_c \bar{T} = \begin{bmatrix} P_{11} & 0 \\ 0 & \bullet \end{bmatrix} \\ \bar{A}_c &= \bar{T}^{-1} A_c \bar{T} = \begin{bmatrix} A + \bar{E}\hat{B}C_2 & \bullet \\ \bullet & \bullet \end{bmatrix} \\ \bar{B}_c &= \bar{T}^{-1} B_c = \begin{bmatrix} B_1 + \bar{E}\hat{B}D_{21} \\ \bullet \end{bmatrix} \\ \bar{C}_c &= C_c \bar{T} = [\ C_1 \quad \bullet\ ], \end{aligned}$$

where $\bar{E} = P_{11}^{-1}P_{12}$. Again it can be shown that

$$\frac{d}{dt}(\bar{T}^T P_c \bar{T})_{(1,1)} = (\bar{T}^T \dot{P}_c \bar{T})_{(1,1)}. \tag{8.16}$$

Multiplying equation (8.14) on the left by $\bar{T}^T$ and on the right by $\bar{T}$ gives

$$\bar{T}^T \dot{P}_c \bar{T} + \bar{P}_c \bar{A}_c + \bar{A}_c^T \bar{P}_c + \bar{C}_c^T \bar{C}_c + (\bar{P}_c \bar{B}_c + \bar{C}_c^T D_c)(\gamma^2 I - D_c^T D_c)^{-1}(\bar{B}_c^T \bar{P}_c + D_c^T \bar{C}_c) < 0. \tag{8.17}$$

Now define $\bar{Q}_c \stackrel{\triangle}{=} \gamma^2 \bar{P}_c^{-1}$, multiply equation (8.17) on the left by $\gamma^2 \bar{P}_c^{-1}$, on the right by $\bar{P}_c^{-1}$ and use lemma 8.2.1 to get

$$\gamma^2 \bar{P}_c^{-1}\bar{T}^T \dot{P}_c \bar{T}\bar{P}_c^{-1} + \bar{Q}_c \bar{A}_c^T + \bar{A}_c \bar{Q}_c + \bar{B}_c \bar{B}_c^T + (\bar{Q}_c \bar{C}_c^T + \bar{B}_c D_c^T)(\gamma^2 I - D_c D_c^T)^{-1}(\bar{C}_c \bar{Q}_c + D_C \bar{B}_c^T) < 0.$$

Equation (8.16) allows us to write

$$\begin{aligned} &\gamma^2 \begin{bmatrix} P_{11}^{-1}\dot{P}_{11}P_{11}^{-1} & \bullet \\ \bullet & \bullet \end{bmatrix} + \gamma^2 \begin{bmatrix} P_{11}^{-1} & 0 \\ 0 & \bullet \end{bmatrix} \begin{bmatrix} (A + \bar{E}\hat{B}C_2)^T & \bullet \\ \bullet & \bullet \end{bmatrix} + \begin{bmatrix} (A + \bar{E}\hat{B}C_2) & \bullet \\ \bullet & \bullet \end{bmatrix} \begin{bmatrix} \gamma^2 P_{11}^{-1} & 0 \\ 0 & \bullet \end{bmatrix} + \\ &\begin{bmatrix} (B_1 + \bar{E}\hat{B}D_{21}) \\ \bullet \end{bmatrix} [\ (B_1 + \bar{E}\hat{B}D_{21})^T \quad \bullet\ ] + \left(\begin{bmatrix} \gamma^2 P_{11}^{-1} C_1^T \\ \bullet \end{bmatrix} + \begin{bmatrix} B_1 D_{11}^T + \bar{E}\hat{B}D_{21}D_{11}^T \\ \bullet \end{bmatrix} \right) \\ &\qquad (\gamma^2 I - D_{11}D_{11}^T)^{-1} \left([\ \gamma^2 C_1 P_{11}^{-1} \quad \bullet\ ] + [\ (B_1 D_{11}^T + \bar{E}\hat{B}D_{21}D_{11}^T)^T \quad \bullet\ ] \right) < 0, \end{aligned}$$

the $(1,1)$ block of which gives

$$-\dot{Q} + Q\bar{A}^T + \bar{A}Q + \bar{B}\bar{B}^T + (QC_1^T + \bar{B}D_{11}^T)(\gamma^2 I - D_{11}D_{11}^T)^{-1}(C_1 Q + D_{11}\bar{B}^T) < 0, \tag{8.18}$$

where $\bar{A} = A + \bar{E}\hat{B}C_2$, $\bar{B} = B_1 + \bar{E}\hat{B}D_{21}$ and $Q = \gamma^2 P_{11}^{-1}$. So setting $K = \bar{E}\hat{B}$ gives condition (ii.b.). Finally, recall that

$$\begin{aligned} P &= (1-\epsilon)(P_{11} - P_{12}P_{22}^{-1}P_{12}^T) \\ \Rightarrow \gamma^2 Q^{-1} &= P_{11} > P \\ \Rightarrow \gamma^2 I &> PQ. \end{aligned}$$

This gives condition (ii.c.) and completes the proof of necessity.

In order to prove sufficiency we need to show that given a differentiable $P(\rho) = P^T(\rho) > 0$ and a differentiable $Q(\rho) = Q^T(\rho) > 0$ such that there exists an $F(\rho)$ and a $K(\rho)$ satisfying conditions (i.) and (ii.) of theorem 8.2.2, then we can construct a strictly proper controller C_ρ and a positive definite matrix $P_c = P_c^T > 0$ such that

$$\dot{P}_c + P_c A_c + A_c^T P_c + C_c^T C_c + (P_c B_c + C_c^T D_c)(\gamma^2 I - D_c^T D_c)^{-1}(B_c^T P_c + D_c^T C_c) < 0 \; \forall \rho \in F_\rho . \quad (8.19)$$

Consider the following positive definite matrix

$$P_c \triangleq \begin{bmatrix} \gamma^2 Q^{-1} & -(\gamma^2 Q^{-1} - P) \\ -(\gamma^2 Q^{-1} - P) & (\gamma^2 Q^{-1} - P) \end{bmatrix}. \quad (8.20)$$

The state transformation matrices

$$\tilde{T} \triangleq \begin{bmatrix} I & 0 \\ I & I \end{bmatrix} \qquad \tilde{T}^{-1} = \begin{bmatrix} I & 0 \\ -I & I \end{bmatrix}$$

$$\bar{T} \triangleq \begin{bmatrix} I & \gamma^{-2} Q(\gamma^2 Q^{-1} - P) \\ 0 & I \end{bmatrix} \qquad \bar{T}^{-1} = \begin{bmatrix} I & -\gamma^{-2} Q(\gamma^2 Q^{-1} - P) \\ 0 & I \end{bmatrix},$$

will be used to transform P_c into a block diagonal form as follows

$$\tilde{P}_c \triangleq \tilde{T}^T P_c \tilde{T} = \begin{bmatrix} P & 0 \\ 0 & \gamma^2 Q^{-1} - P \end{bmatrix}$$

$$\bar{P}_c \triangleq \bar{T}^T P_c \bar{T} = \begin{bmatrix} \gamma^2 Q^{-1} & 0 \\ 0 & \bullet \end{bmatrix}.$$

Multiplying equation (8.19) on the left by $\tilde{T}^T$ and on the right by $\tilde{T}$ gives

$$\tilde{S} \triangleq \dot{\tilde{P}}_c + \tilde{P}_c \tilde{A}_c + \tilde{A}_c^T \tilde{P}_c + \tilde{C}_c^T \tilde{C}_c + (\tilde{P}_c \tilde{B}_c + \tilde{C}_c^T D_c)(\gamma^2 I - D_c^T D_c)^{-1}(\tilde{B}_c^T \tilde{P}_c + D_c^T \tilde{C}_c), \quad (8.21)$$

where

$$\tilde{A}_c = \tilde{T}^{-1} A_c \tilde{T} = \begin{bmatrix} A + B_2 \hat{C} & B_2 \hat{C} \\ \hat{A} + \hat{B} C_2 - A - B_2 \hat{C} & \hat{A} - B_2 \hat{C} \end{bmatrix}$$

$$\tilde{B}_c = \tilde{T}^{-1} B_c = \begin{bmatrix} B_1 \\ \hat{B} D_{21} - B_1 \end{bmatrix}$$

$$\tilde{C}_c = C_c \tilde{T} = \begin{bmatrix} C_1 + D_{12} \hat{C} & D_{12} \hat{C} \end{bmatrix}.$$

Extracting the $(1,1)$ and $(1,2)$ blocks of equation (8.21) gives

$$\tilde{S}_{(1,1)} = \dot{P} + P(A + B_2 \hat{C}) + (A + B_2 \hat{C})^T P + (C_1 + D_{12} \hat{C})^T (C_1 + D_{12} \hat{C}) + (P B_1 + (C_1 + D_{12} \hat{C})^T D_{11})(\gamma^2 - D_{11}^T D_{11})^{-1}(B_1^T P + D_{11}^T (C_1^T + \hat{C}^T D_{12}^T))$$

$$\tilde{S}_{(1,2)} = PB_2\hat{C} + (\hat{A} + \hat{B}C_2 - A - B_2\hat{C})^T(\gamma^2 Q^{-1} - P) + (C_1 + D_{12}\hat{C})^T D_{12}\hat{C} + (PB_1 + (C_1 + D_{12}\hat{C})^T D_{11})(\gamma^2 I - D_{11}^T D_{11})^{-1}((\hat{B}D_{21} - B_1)^T(\gamma^2 Q^{-1} - P) + D_{11}^T D_{12}\hat{C}).$$

Now put $\hat{C} = F$ and $\hat{A} = -\hat{B}C_2 + A + B_2\hat{C} - (\gamma^2 Q^{-1} - P)^{-1}M^T$, where

$$M = PB_2\hat{C} - H + (C_1 + D_{12}\hat{C})^T D_{12}\hat{C} + (PB_1 + C_1^T D_{11} + \hat{C}^T D_{12}^T D_{11})(\gamma^2 I - D_{11}^T D_{11})^{-1} (D_{11}^T D_{12}\hat{C} + (D_{21}^T\hat{B}^T - B_1^T)(\gamma^2 Q^{-1} - P))$$

and

$$H = \dot{P} + P(A + B_2F) + (A + B_2F)^T P + (C_1 + D_{12}F)^T(C_1 + D_{12}F) + (PB_1 + (C_1 + D_{12}F)^T D_{11})(\gamma^2 I - D_{11}^T D_{11})^{-1}(B_1^T P + D_{11}^T(C_1 + D_{12}F)). \quad (8.22)$$

This gives $\tilde{S}_{(1,1)} = \tilde{S}_{(1,2)} = H < 0$ for all $\rho(t) \in F_\rho$.

Now use the transformation $\bar{T}$ and define

$$\bar{A}_c \triangleq \bar{T}^{-1}A_c\bar{T} = \begin{bmatrix} A - \gamma^{-2}Q(\gamma^2 Q^{-1} - P)\hat{B}C_2 & \bullet \\ \bullet & \bullet \end{bmatrix} \quad (8.23)$$

$$\bar{B}_c \triangleq \bar{T}^{-1}B_c = \begin{bmatrix} B_1 - \gamma^{-2}Q(\gamma^2 Q^{-1} - P)\hat{B}D_{21} \\ \hat{B}D_{21} \end{bmatrix} \quad (8.24)$$

$$\bar{C}_c \triangleq C_c\bar{T} = \begin{bmatrix} C_1 & \gamma^{-2}C_1Q(\gamma^2 Q^{-1} - P) + D_{12}\hat{C} \end{bmatrix} \quad (8.25)$$

Multiplying equation (8.19) on the left by $\bar{T}^T$ and on the right by $\bar{T}$ gives

$$\bar{S} \triangleq \bar{T}^T\dot{P}_c\bar{T} + \bar{P}_c\bar{A}_c + \bar{A}_c^T\bar{P}_c + \bar{C}_c^T\bar{C}_c + (\bar{P}_c\bar{B}_c + \bar{C}_c^T D_c)(\gamma^2 I - D_c^T D_c)^{-1}(\bar{B}_c^T\bar{P}_c + \bar{D}_c^T\bar{C}_c).$$

Once again we have

$$\bar{T}^T\dot{P}_c\bar{T}_{(1,1)} = \frac{d}{dt}(\bar{T}^T P_c\bar{T})_{(1,1)}.$$

This allows us to write

$$\bar{S}_{11} = \gamma^2 Q^{-1}\Big\{-\dot{Q} + (A - \gamma^{-2}Q(\gamma^2 Q^{-1} - P)\hat{B}C_2)Q + Q(A - \gamma^{-2}Q(\gamma^2 Q^{-1} - P)\hat{B}C_2)^T + (B_1 - \gamma^{-2}Q(\gamma^2 Q^{-1} - P)\hat{B}D_{21})(B_1 - \gamma^{-2}Q(\gamma^2 Q^{-1} - P)\hat{B}D_{21})^T + (QC_1^T + (B_1 - \gamma^{-2}Q(\gamma^2 Q^{-1} - P)\hat{B}D_{21})D_{11}^T)(\gamma^2 I - D_{11}D_{11}^T)^{-1} (QC_1^T + (B_1 - \gamma^{-2}Q(\gamma^2 Q^{-1} - P)\hat{B}D_{21})D_{11}^T)^T\Big\} Q^{-1}.$$

Finally putting

$$\hat{B} = -\gamma^2(\gamma^2 Q^{-1} - P)^{-1}Q^{-1}K$$

gives

$$\bar{S}_{11} = \gamma^2 Q^{-1}\left\{-\dot{Q} + Q\bar{A}^T + \bar{A}Q + \bar{B}\bar{B}^T + (QC_1^T + \bar{B}D_{11}^T)(\gamma^2 I - D_{11}D_{11}^T)^{-1}(C_1 Q + D_{11}\bar{B}^T)\right\}Q^{-1} < 0$$

Now

$$\tilde{S}_{22} = \bar{S}_{11} - \tilde{S}_{11} + \tilde{S}_{12} + \tilde{S}_{12}^T < 0$$

which gives

$$\tilde{S} = \begin{bmatrix} H & H \\ H^T & \bar{S}_{11} + H \end{bmatrix} < 0 \ \ \forall \rho(t) \in F_\rho.$$

■

Remark 8.2.3 *In order to prove sufficiency we have explicitly constructed a single controller which achieves a specified $\mathcal{Q}_\gamma$ performance level. This lacks the generality of the results obtained in [24] for LTI plants where the set of all controllers achieving a specified H_∞ norm bound is parametrised and shown to be homeomorphic to the unit ball in RH_∞. An additional drawback with the formulae is the explicit dependence on the rate of parameter variation (equation 8.22). This complicates the controller, making it necessary to have measurements of the parameter and its rate of change.*

Remark 8.2.4 *When $D_{11} = 0$, the solution technique developed by Scherer [78] for LTI systems can be used to show that there is no loss in generality by assuming that the controller is strictly proper. That is, if $D_{11} = 0$, then if there exists a proper controller satisfying a specified $\mathcal{Q}_\gamma$ performance level, there exists a strictly proper controller which satisfies the same performance level. Similarly, when $D_{11} \neq 0$ then provided D_{12} has full column rank and D_{21} has full row rank the solution technique developed by Becker [7] for quadratic performance problems can be extended to show that there is no loss in generality when it is assumed that the controller is strictly proper.*

Remark 8.2.5 *Since the rate dependence enters affinely into the controllers state equations, it is possible to make use of a Lyapunov transformation to remove the rate term. This will give a state-space realisation of the controller which does not require explicit measurement of the rate of parameter variation, but it is not clear whether this will make the controller sensitive to measurement noise.*

Conditions (ii.a) and (ii.b) of theorem 8.2.2 can be formulated as LMI problems directly. Consider condition (ii.a), multiply equation 8.7 on the left by $\gamma^2 P^{-1}$ and on the right by P^{-1}, define $P_1 \stackrel{\triangle}{=} \gamma^2 P^{-1}$ and $P_2 \stackrel{\triangle}{=} FP_1$ and use lemma 8.2.1 to get

$$\begin{bmatrix} -\dot{P}_1 + AP_1 + P_1A^T + B_2P_2 + P_2^TB_2^T + B_1B_1^T & (P_1C_1^T + P_2^TD_{12}^T + B_1D_{11}^T) \\ (C_1P_1 + D_{12}P_2 + D_{11}B_1^T) & -(\gamma^2 I - D_{11}D_{11}^T) \end{bmatrix} < 0.$$

This is affine in the unknown variables P_1 and P_2. An identical procedure can be used on equation (8.8) as follows. Define $Q_1 \stackrel{\triangle}{=} \gamma^2 Q^{-1}$ and $Q_2 \stackrel{\triangle}{=} Q_1 K$ which can be used to write equation (8.8) as

$$\begin{bmatrix} \dot{Q}_1 + A^T Q_1 + Q_1 A + C_2^T Q_2^T + Q_2 C_2 + C_1^T C_1 & (Q_1 B_1 + Q_2 D_{21} + C_1^T D_{11}) \\ (B_1^T Q_1 + D_{21}^T Q_2^T + C_1^T D_{11}) & -(\gamma^2 I - D_{11}^T D_{11}) \end{bmatrix} < 0,$$

which, again, is affine in the unknown variables Q_1 and Q_2. In terms of these definitions the spectral radius coupling condition becomes

$$\begin{bmatrix} P_1 & \gamma I \\ \gamma I & Q_1 \end{bmatrix} > 0.$$

This constitutes a system of three LMI in terms of the unknown variables P_1, P_2, Q_1 and Q_2 and for fixed γ can be solved as a convex feasibility problem using similar methods to those discussed in chapter 7. Unfortunately, this offers little insight into the nature of the solution and the resulting controller formulae. Finding the optimal γ bound also requires an iteration, which is of course standard in most H_∞ control problems, but for LPV systems can be very expensive computationally. In the next section we make use of the methodology developed by Becker ([7],[8]) to solve the quadratic-performance output-feedback problem to remove $F(\rho)$ from equation (8.7) and $K(\rho)$ from equation (8.8). Not only does this lead to a simplification of the formulae, but, as will be shown, for the four-block scheduling problem it reproduces Hyde's scheduling framework [50] with the requisite modifications for guaranteed performance and stability.

8.3 Simplifying the controller formulation

Conditions (i.) and (ii.a) of theorem 8.2.2 are exactly the conditions that would arise when trying to find a parameter-dependent state feedback $F(\rho)$ to achieve a specified level of $\mathcal{Q}_\gamma$ performance for the bounded-rate LPV system depicted in Figure 8.2.

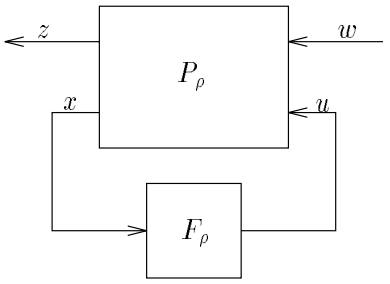

Figure 8.2 *State feedback problem*

where

$$P_\rho \stackrel{s}{=} \left[\begin{array}{c|cc} A & B_1 & B_2 \\ \hline C_1 & D_{11} & D_{12} \\ I & 0 & 0 \end{array}\right]. \tag{8.26}$$

This suggests that a careful examination of the state feedback problem could simplify the formulation in the output feedback case by removing $F(\rho)$ from condition (ii.a). This was first carried out using the notion of quadratic performance by Becker ([7],[8]), where no bound was placed on the rate of parameter variation. A similar approach will be adopted here. Conditions (i.) and (ii.b) of theorem 8.2.2 are the conditions that would arise when trying to find a parameter-dependent output injection that achieves a specified level of $\mathcal{Q}_\gamma$ performance for the bounded-rate LPV system shown in Figure 8.3,

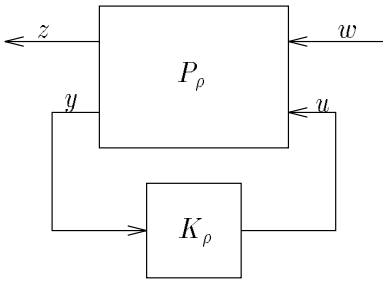

Figure 8.3 *Output injection problem*

where

$$P_\rho \stackrel{s}{=} \left[\begin{array}{c|cc} A & B_1 & I \\ \hline C_1 & D_{11} & 0 \\ C_2 & D_{21} & 0 \end{array}\right]. \tag{8.27}$$

Again, a careful examination of the output injection problem should make it possible to remove $K(\rho)$ from condition (ii.b). Our aim is to convert conditions (ii.a),(ii.b) and (ii.c) into a convex feasibility problem involving P and Q only. We begin with some standard assumptions [24].

Assumptions 8.3.1 .

1. *D_{12} has full column rank and $D_{12} = [0 \;\; I]^T$.*
2. *D_{21} has full row rank and $D_{21} = [0 \;\; I]$.*
3. *$D_{22} = 0$.*

The rank assumptions on the D_{12} and D_{21} matrices are standard, and if relaxed result in singular control problems. If they are not satisfied then the formulae developed in the previous section are applicable, although it can be argued that any sensible problem formulation will always impose some penalty on control effort (full column rank of D_{12}) and all measurements will be influenced by noise (full row rank of D_{21}). The normalisation condition can be achieved through unitary scaling ([7],[40]). The assumption that $D_{22} = 0$ results in no loss of generality [40] and can be achieved by introducing a simple loop transformation. With these assumptions we can write a state-space representation of the generalised plant as follows

$$P_\rho \stackrel{s}{=} \left[\begin{array}{c|ccc} A & B_{11} & B_{12} & B_2 \\ \hline C_{11} & D_{1111} & D_{1112} & 0 \\ C_{12} & D_{1121} & D_{1122} & I \\ C_2 & 0 & I & 0 \end{array}\right]. \tag{8.28}$$

We also use the standard notation,

$$D_{111\bullet} \stackrel{\triangle}{=} [D_{1111} \;\; D_{1112}] \qquad D_{11\bullet 1} \stackrel{\triangle}{=} \left[\begin{array}{c} D_{1111} \\ D_{1121} \end{array}\right]$$
$$D_{112\bullet} \stackrel{\triangle}{=} [D_{1121} \;\; D_{1122}] \qquad D_{11\bullet 2} \stackrel{\triangle}{=} \left[\begin{array}{c} D_{1112} \\ D_{1122} \end{array}\right].$$

Theorem 8.3.2 *Given a continuous state-space realisation of an LPV system $P_\rho : L^+_{2,e} \otimes L^+_{2,e} \mapsto L^+_{2,e} \otimes L^+_{2,e}$, partitioned in accordance with equation (8.28), then condition (ii.a) of theorem 8.2.2 holds if, and only if:*

i. $\gamma^2 I - D_{11}^T D_{11} > 0$.

ii. $\exists \; Y(\rho) = Y^T(\rho) > 0$ *such that*

$$\left[\begin{array}{ccc} -\dot{Y} + Y\check{A}^T + \check{A}Y - B_2 B_2^T & \check{B} & YC_{11}^T \\ \check{B}^T & -\gamma^2 I & D_{111\bullet}^T \\ C_{11}Y & D_{111\bullet} & -I \end{array}\right] < 0, \tag{8.29}$$

where $\check{A} = A - B_2 C_{12}$, $\check{B} = B_1 - B_2 D_{112\bullet}$ and $Y = P^{-1}$. One such F satisfying condition (ii.a) in theorem 8.2.2 is given by

$$\begin{aligned} F &= -(\bar{D}^T\bar{D})^{-1}(\bar{B}^T Y^{-1} + \bar{D}^T\bar{C}) \\ \bar{B} &= B_2 + B_1(\gamma^2 I - D_{11}^T D_{11})^{-1} D_{11}^T D_{12} \\ \bar{C} &= (I + D_{11}(\gamma^2 I - D_{11}^T D_{11})^{-1} D_{11}^T)^{\frac{1}{2}} C_1 \\ \bar{D} &= (I + D_{11}(\gamma^2 I - D_{11}^T D_{11})^{-1} D_{11}^T)^{\frac{1}{2}} D_{12}. \end{aligned}$$

Proof: Using the Shur-complement, condition (ii.a) in theorem 8.2.2 is easily shown to be equivalent to

$$\begin{bmatrix} \dot{P}+P\tilde{A}+\tilde{A}^TP & PB_1 & \tilde{C}^T \\ B_1^TP & -\gamma^2 I & D_{11}^T \\ \tilde{C} & D_{11} & -I \end{bmatrix} < 0$$

$$\Longleftrightarrow \begin{bmatrix} \dot{P}+PA+A^TP & PB_1 & C_1^T \\ B_1^TP & -\gamma^2 I & D_{11}^T \\ C_1 & D_{11} & -I \end{bmatrix} + \begin{bmatrix} PB_2 \\ 0 \\ D_{12} \end{bmatrix} \begin{bmatrix} F & 0 & 0 \end{bmatrix} + \begin{bmatrix} F^T \\ 0 \\ 0 \end{bmatrix} \begin{bmatrix} B_2^TP & 0 & D_{12}^T \end{bmatrix} < 0$$

$$\Longleftrightarrow \underbrace{\begin{bmatrix} \dot{P}+A^TP+PA & PB_1 & C_{11}^T & C_{12}^T \\ B_1^TP & -\gamma^2 I & D_{111\bullet}^T & D_{112\bullet}^T \\ C_{11} & D_{111\bullet} & -I & 0 \\ C_{12} & D_{112\bullet} & 0 & -I \end{bmatrix}}_{\bar{R}} + \underbrace{\begin{bmatrix} PB_2 \\ 0 \\ 0 \\ I \end{bmatrix}}_{\bar{U}} \underbrace{\begin{bmatrix} F & 0 & 0 & 0 \end{bmatrix}}_{\bar{F}} +$$

$$\begin{bmatrix} F^T \\ 0 \\ 0 \\ 0 \end{bmatrix} \begin{bmatrix} B_2^TP & 0 & 0 & I \end{bmatrix} < 0.$$

This is equivalent to

$$\bar{R} + \bar{U}\bar{F} + \bar{F}^T\bar{U}^T < 0.$$

Define the orthogonal completion of $\bar{U}$ as follows

$$\bar{U}_\perp \triangleq \begin{bmatrix} P^{-1} & 0 & 0 \\ 0 & I & 0 \\ 0 & 0 & I \\ -B_2^T & 0 & 0 \end{bmatrix}.$$

This can be used to obtain

$$\bar{U}_\perp^T(\bar{R} + \bar{U}\bar{F} + \bar{F}^T\bar{U}^T)\bar{U}_\perp = \bar{U}_\perp^T\bar{R}\bar{U}_\perp,$$

which shows that condition (ii.a) of theorem 8.2.2 implies that

$$\bar{U}_\perp^T\bar{R}\bar{U}_\perp < 0.$$

This is easily rearranged to give

$$\begin{bmatrix} -\dot{Y}+Y\check{A}^T+\check{A}Y-B_2B_2^T & \check{B} & YC_{11}^T \\ \check{B}^T & -\gamma^2 I & D_{111\bullet}^T \\ C_{11}Y & D_{111\bullet} & -I \end{bmatrix} < 0,$$

where $Y = P^{-1}$.

To prove the converse we need to show that given a $Y(\rho) = Y^T(\rho) > 0$ satisfying equation (8.29) we can construct a $P(\rho) = P^T(\rho) > 0$ and an $F(\rho)$ such that condition (ii.a) of theorem 8.2.2 is satisfied. Expanding the latter gives

$$\dot{P} + P(\tilde{A} + B_1(\gamma^2 I - D_{11}^T D_{11})^{-1} D_{11}^T \tilde{C}) + (\tilde{A}^T + \tilde{C}^T D_{11}(\gamma^2 I - D_{11}^T D_{11})^{-1} B_1^T)P + \tilde{C}^T(I + D_{11}(\gamma^2 I - D_{11}^T D_{11})^{-1} D_{11}^T)\tilde{C} + PB_1(\gamma^2 I - D_{11}^T D_{11})^{-1} B_1^T P < 0.$$

Now defining

$$\begin{aligned} \bar{A} &\triangleq A + B_1(\gamma^2 I - D_{11}^T D_{11})^{-1} D_{11}^T C_1 \\ \bar{B} &\triangleq B_2 + B_1(\gamma^2 I - D_{11}^T D_{11})^{-1} D_{11}^T D_{12} \\ \bar{C} &\triangleq ((I + D_{11}(\gamma^2 I - D_{11}^T D_{11})^{-1} D_{11}^T)^{\frac{1}{2}} C_1 \\ \bar{D} &\triangleq ((I + D_{11}(\gamma^2 I - D_{11}^T D_{11})^{-1} D_{11}^T)^{\frac{1}{2}} D_{12} \end{aligned}$$

allows condition (ii.a) to be written as

$$\dot{P} + P\bar{A} + \bar{A}^T P + P\bar{B}F + F^T \bar{B}^T P + \bar{C}^T \bar{C} + \bar{C}^T \bar{D} F + F^T \bar{D}^T \bar{C} + F^T \bar{D}^T \bar{D} F + PB_1(\gamma^2 I - D_{11}^T D_{11})^{-1} B_1^T P < 0.$$

Completing the square with respect to F gives

$$\dot{P} + P\bar{A} + \bar{A}^T P + PB_1(\gamma^2 I - D_{11}^T D_{11})^{-1} B_1^T P + \bar{C}^T \bar{C} + (\bar{D}F + \bar{D}(\bar{D}^T\bar{D})^{-1}\bar{B}^T P + \bar{C})^T(\bar{D}F + \bar{D}(\bar{D}^T\bar{D})^{-1}\bar{B}^T P + \bar{C}) - (\bar{C} + \bar{D}(\bar{D}^T\bar{D})^{-1}\bar{B}^T P)^T(\bar{C} + \bar{D}(\bar{D}^T\bar{D})^{-1}\bar{B}^T P) < 0.$$

Setting

$$F = -(\bar{D}^T\bar{D})^{-1}(\bar{B}^T P + \bar{D}^T\bar{C})$$

gives

$$\dot{P} + P\bar{A} + \bar{A}^T P + PB_1(\gamma^2 I - D_{11}^T D_{11})^{-1} B_1^T P - \bar{C}^T\bar{D}(\bar{D}^T\bar{D})^{-1}\bar{B}^T P - P\bar{B}(\bar{D}^T\bar{D})^{-1}\bar{D}^T\bar{C} - P\bar{B}(\bar{D}^T\bar{D})^{-1}\bar{B}^T P < 0. \quad (8.30)$$

The following expressions follow from the definitions

$$\begin{aligned} \bar{D}^T\bar{D} &= \gamma^2 D_{12}^T(\gamma^2 I - D_{11}D_{11}^T)^{-1} D_{12} && (8.31) \\ \bar{C}^T\bar{C} &= \gamma^2 C_1^T(\gamma^2 I - D_{11}D_{11}^T)^{-1} C_1 && (8.32) \\ \bar{D}^T\bar{C} &= \gamma^2 D_{12}^T(\gamma^2 I - D_{11}D_{11}^T)^{-1} C_1 && (8.33) \end{aligned}$$

and making use of the matrix inversion lemma [49],

$$\begin{bmatrix} A & B \\ B^T & C \end{bmatrix}^{-1} = \begin{bmatrix} (A - BC^{-1}B^T)^{-1} & A^{-1}B(B^TA^{-1}B - C)^{-1} \\ (B^TA^{-1}B - C)^{-1}B^TA^{-1} & (C - B^TA^{-1}B)^{-1} \end{bmatrix},$$

we can write

$$(\gamma^2 I - D_{11}D_{11}^T)^{-1} = \begin{bmatrix} \gamma^2 I - D_{111\bullet}D_{111\bullet}^T & -D_{111\bullet}D_{112\bullet}^T \\ -D_{112\bullet}D_{111\bullet}^T & \gamma^2 I - D_{112\bullet}D_{112\bullet}^T \end{bmatrix}^{-1}$$

to give

$$\bar{D}^T\bar{D} = (I - D_{112\bullet}(\gamma^2 I - D_{111\bullet}^T D_{111\bullet})^{-1}D_{112\bullet}^T)^{-1}. \tag{8.34}$$

Left and right multiplying equation (8.30) by P^{-1} gives

$$-\dot{Y} + Y\bar{A}^T + \bar{A}Y + B_1(\gamma^2 I - D_{11}^T D_{11})^{-1}B_1^T + Y\bar{C}^T\bar{C}Y - (\bar{B}^T + \bar{D}^T\bar{C}Y)^T(\bar{D}^T\bar{D})^{-1}(\bar{B}^T + \bar{D}^T\bar{C}Y) < 0.$$

Using equations (8.32), (8.33) and equation (8.34) gives equation (8.29). ■

Theorem 8.3.3 *Given a continuous state-space realisation of an LPV system $P_\rho : L_{2,e}^+ \otimes L_{2,e}^+ \mapsto L_{2,e}^+ \otimes L_{2,e}^+$, partitioned in accordance with equation (8.28), then condition (ii.b) of theorem 8.2.2 holds if, and only if:*

i. $\gamma^2 I - D_{11}D_{11}^T > 0$.

ii. $\exists\ Z(\rho) = Z^T(\rho) > 0$ *such that*

$$\begin{bmatrix} \dot{Z} + \breve{A}^T Z + Z\breve{A} - C_2^T C_2 & \breve{C}^T & ZB_{11} \\ \breve{C} & -\gamma^2 I & D_{11\bullet 1} \\ B_{11}^T Z & D_{11\bullet 1}^T & -I \end{bmatrix} < 0, \tag{8.35}$$

where $\breve{A} = A - B_{12}C_2$, $\breve{C} = C_1 - D_{11\bullet 2}C_2$ and $Z = Q^{-1}$. One such $K(\rho)$ that satisfies condition (ii.b) in theorem 8.2.2 is given by

$$\begin{aligned} K &= -(Q\grave{B}^T + \grave{C}\grave{D}^T)(\grave{D}\grave{D}^T)^{-1} \\ \grave{B} &= C_2 + D_{21}D_{11}^T(\gamma^2 I - D_{11}D_{11}^T)^{-1}C_1 \\ \grave{C} &= B_1(I + D_{11}^T(\gamma^2 I - D_{11}D_{11}^T)^{-1}D_{11})^{\frac{1}{2}} \\ \grave{D} &= D_{21}(I + D_{11}^T(\gamma^2 I - D_{11}D_{11}^T)^{-1}D_{11})^{\frac{1}{2}} \end{aligned}$$

Proof: Using the Shur-complement, condition (ii.b) in theorem 8.2.2 can be written as

$$\begin{bmatrix} -\dot{Q}+Q(A+KC_2)^T+(A+KC_2)Q & QC_1^T & B_1+KD_{21} \\ C_1Q & -\gamma^2 I & D_{11} \\ (B_1+KD_{21})^T & D_{11}^T & -I \end{bmatrix} < 0$$

$$\iff \underbrace{\begin{bmatrix} -\dot{Q}+QA^T+AQ & QC_1^T & B_{11} & B_{12} \\ C_1Q & -\gamma^2 I & D_{11\bullet 1} & D_{11\bullet 2} \\ B_{11}^T & D_{11\bullet 1}^T & -I & 0 \\ B_{12}^T & D_{11\bullet 2}^T & 0 & -I \end{bmatrix}}_{\underline{R}} + \underbrace{\begin{bmatrix} K \\ 0 \\ 0 \\ 0 \end{bmatrix}}_{\underline{K}} \underbrace{\begin{bmatrix} C_2Q & 0 & 0 & I \end{bmatrix}}_{\underline{H}} +$$

$$\begin{bmatrix} QC_2^T \\ 0 \\ 0 \\ I \end{bmatrix} \begin{bmatrix} K^T & 0 & 0 & 0 \end{bmatrix} < 0.$$

This is equivalent to

$$\underline{R} + \underline{K}\,\underline{H} + \underline{H}^T\underline{K}^T < 0.$$

Defining the orthogonal completion of H as

$$\underline{H}_\perp \stackrel{\triangle}{=} \begin{bmatrix} Q^{-1} & 0 & 0 & -C_2^T \\ 0 & I & 0 & 0 \\ 0 & 0 & I & 0 \end{bmatrix}$$

we get

$$\underline{H}_\perp(\underline{R} + \underline{K}\,\underline{H} + \underline{H}^T\,\underline{K}^T)\underline{H}_\perp^T < 0 \Longrightarrow \underline{H}_\perp\,\underline{R}\,\underline{H}_\perp^T < 0$$

which on expanding shows that condition (ii.b) of theorem 8.2.2 implies the following

$$\begin{bmatrix} \dot{Z}+\breve{A}^TZ+Z\breve{A}-C_2^TC_2 & \breve{C}^T & ZB_{11} \\ \breve{C} & -\gamma^2 I & D_{11\bullet 1} \\ B_{11}^TZ & D_{11\bullet 1}^T & -I \end{bmatrix} < 0,$$

with $Z = Q^{-1}$.

Conversely, given a $Z(\rho) = Z(\rho)^T > 0$ satisfying equation (8.35), we need to show that it is possible to construct a $K(\rho)$ and a $Q(\rho) = Q^T(\rho) > 0$ satisfying condition (ii.b) in theorem 8.2.2. As before, expanding condition (ii.b) gives

$$-\dot{Q} + Q(A^T + C_2^TK^T) + (A+KC_2)Q + (B_1+KD_{21})(B_1+KD_{21})^T + (QC_1^T + (B_1+KD_{21})D_{11}^T)(\gamma^2 I - D_{11}D_{11}^T)^{-1}(C_1Q + D_{11}(B_1+KD_2)^T) < 0$$

which can be written as

$$-\dot{Q} + Q(A^T + C_2^T K^T + C_1^T(\gamma^2 I - D_{11}D_{11}^T)^{-1}D_{11}(B_1 + KD_{21})^T) + (A + KC_2 + (B_1 + KD_{21})$$
$$D_{11}^T(\gamma^2 I - D_{11}D_{11}^T)^{-1})C_1)Q + (B_1 + KD_{21})(I + D_{11}^T(\gamma^2 I - D_{11}D_{11}^T)^{-1})D_{11})(B_1 + KD_{21})^T +$$
$$QC_1^T(\gamma^2 I - D_{11}D_{11}^T)^{-1}C_1Q < 0. \quad (8.36)$$

Now define

$$\begin{aligned}
\grave{A} &\triangleq A + B_1 D_{11}^T(\gamma^2 I - D_{11}D_{11}^T)^{-1}C_1 \\
\grave{B} &\triangleq C_2 + D_{21}D_{11}^T(\gamma^2 I - D_{11}D_{11}^T)^{-1}C_1 \\
\grave{C} &\triangleq B_1(I + D_{11}^T(\gamma^2 I - D_{11}D_{11}^T)^{-1}D_{11})^{\frac{1}{2}} \\
\grave{D} &\triangleq D_{21}(I + D_{11}^T(\gamma^2 I - D_{11}D_{11}^T)^{-1}D_{11})^{\frac{1}{2}}
\end{aligned}$$

which allows equation (8.36) to be written as

$$-\dot{Q} + Q\grave{A}^T + \grave{A}Q + Q\grave{B}^T K^T + K\grave{B}Q + K\grave{D}\grave{D}^T K^T +$$
$$K\grave{D}\grave{C}^T + \grave{C}\grave{D}^T K^T + \grave{C}\grave{C}^T + QC_1(\gamma^2 I - D_{11}D_{11}^T)^{-1}C_1Q < 0.$$

Completing the square with respect to K gives

$$-\dot{Q} + Q\grave{A}^T + \grave{A}Q + QC_1^T(\gamma^2 I - D_{11}D_{11}^T)^{-1}C_1Q + \grave{C}\grave{C}^T +$$
$$(\grave{D}^T K^T + \grave{D}^T(\grave{D}\grave{D}^T)^{-1}\grave{B}Q + \grave{C}^T)^T(\grave{D}^T K^T + \grave{D}^T(\grave{D}\grave{D}^T)^{-1}\grave{B}Q + \grave{C}^T) -$$
$$(\grave{D}^T(\grave{D}\grave{D}^T)^{-1}\grave{B}Q + \grave{C}^T)^T(\grave{D}^T(\grave{D}\grave{D}^T)^{-1}\grave{B}Q + \grave{C}^T) < 0$$

and putting

$$K = -(Q\grave{B}^T + \grave{C}\grave{D}^T)(\grave{D}\grave{D}^T)^{-1}$$

gives

$$-\dot{Q} + Q\grave{A}^T + \grave{A}Q + QC_1^T(\gamma^2 I - D_{11}D_{11}^T)^{-1}C_1Q + \grave{C}\grave{C}^T -$$
$$(\grave{D}^T(\grave{D}\grave{D}^T)^{-1}\grave{B}Q + \grave{C}^T)^T(\grave{D}^T(\grave{D}\grave{D}^T)^{-1}\grave{B}Q + \grave{C}^T) < 0.$$

Again, this can be shown to be equivalent to equation (8.35). ■

8.4 Explicit formulas for the four-block problem

In this section we return to the four-block problem studied in chapter 4. The essential difference between the problem considered here and the problem considered previously stems from the fact that we have replaced the LTI model of the plant with an LPV model and we no longer assume the controller to be LTI but allow it to be a causal LPV operator.

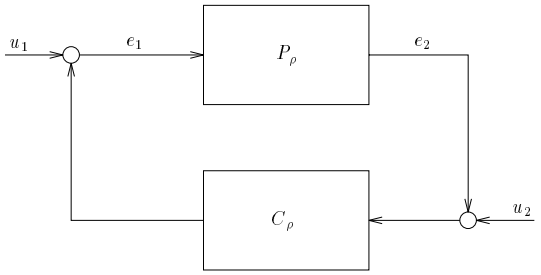

Figure 8.4 *Four-block setup*

For the setup in Figure 8.4 we define the generalised stability margin b_{P_ρ,C_ρ} as follows.

Definition 8.4.1 *For the feedback pair (P_ρ, C_ρ) define the generalised stability margin b_{P_ρ,C_ρ} as*

$$b_{P_\rho,C_\rho} \triangleq \begin{cases} \left\| \begin{bmatrix} P_\rho \\ I \end{bmatrix} (I - C_\rho P_\rho)^{-1} [C_\rho \;\; I] \right\|^{-1}, & \text{if } (P_\rho, C_\rho) \quad \text{is stable} \\ 0 & \text{otherwise.} \end{cases}$$

In the LTI case, it is well known that the central H_∞ controller generated by the setup in Figure 8.4 has an explicit observer structure. This fact was exploited by Hyde [50] to schedule H_∞ controllers on a generic VSTOL aircraft. Unfortunately, scheduling controllers designed using frozen-parameter models does not guarantee that the controller will perform adequately when the plant is really time varying. Indeed, this was Hyde's motivation for scheduling controllers that achieved a specified level of robustness for all frozen-parameter values, thereby treating the time variations as perturbations to be covered by the stability margin. In this section we re-examine the four-block scheduling setup in greater detail. The aim is to find a scheduled controller that is guaranteed to be stable and to satisfy certain performance bounds for all parameter values. We also examine the cost associated with these guarantees, both in terms of the computational effort required to compute the controller, and in terms of the complexity of the resulting controller. We will show that the four-block setup can lead to a substantial reduction in the computational effort required to compute the controller because a reformulation of the problem allows the LMI's to be solved independently of each other. In the reformulated version of this problem the spectral radius coupling condition is used to obtain the optimal stability margin in terms of the computed solutions to two differential Riccati inequalities.

It is assumed that we have a plant P_s which has been weighted to achieve nominal performance/robustness tradeoffs in the sense of MacFarlane and Glover [59]. Typically, this can be achieved by introducing weights which give a sensible loop shape for all frozen-parameter values, thereby fixing the performance objectives in the frequency domain. It also allows us to make performance/robustness tradeoffs using classical loop-shaping concepts allowing, for example, controller effort to be frequency limited to avoid exciting unmodelled dynamics. Suppressing ρ dependence and assuming that the weighted plant P_s has a continuous strictly proper state-space realisation given by

$$P_s = \left[\begin{array}{c|c} A & B \\ \hline C & 0 \end{array}\right],$$

the generalised plant in the four-block problem is easily shown to have the following realisation

$$P_\rho \stackrel{s}{=} \left[\begin{array}{c|ccc} A & B & 0 & B \\ \hline C & 0 & 0 & 0 \\ 0 & I & 0 & I \\ C & 0 & I & 0 \end{array}\right].$$

Note that the assumptions made in section 8.3 are automatically satisfied by this setup, obviating the need for unitary scaling to get $D_{12}^T = [0,\ I]^T$ and $D_{21} = [0,\ I]$. For the four-block problem the feasibility conditions in theorems 8.3.2 and 8.3.3 can be used to obtain the following result.

Proposition 8.4.2 *Given a continuous, strictly proper, $\mathcal{Q}_e$ stabilisable and $\mathcal{Q}_e$ detectable state-space realisation of an LPV system P_ρ, there exists a parameter-dependent controller C_ρ such that the feedback pair (P_ρ, C_ρ) is internally stable and $b_{P_\rho,C_\rho} \geq \frac{1}{\gamma}$ if there exist positive definite matrix functions $Z(\rho)$ and $Y(\rho)$ such that:*

i.
$$\gamma^2 I - D_{11}^T D_{11} > 0;$$

ii.
$$\left[\begin{array}{cc} -\dot{Y} + AY + YA^T - BB^T & YC^T \\ CY & -I \end{array}\right] < 0; \tag{8.37}$$

iii.
$$\left[\begin{array}{cccc} \dot{Z} + A^T Z + ZA - C^T C & C^T & 0 & ZB \\ C & -\gamma^2 I & 0 & 0 \\ 0 & 0 & -\gamma^2 I & I \\ B^T Z & 0 & I & -I \end{array}\right] < 0; \tag{8.38}$$

iv.
$$\left[\begin{array}{cc} Z & \gamma^{-1} I \\ \gamma^{-1} & Y \end{array}\right] > 0. \tag{8.39}$$

For each fixed value of the parameter, equations (8.37) and (8.38) are affine in the unknown variables Y and Z. Furthermore, if we fix γ, then equation (8.39) represents a convex constraint. This implies that we can go about computing suboptimal controllers using similar techniques to those used in the model reduction problem considered in chapter 7. In other words, we can select a set of suitable basis functions from which a set of trial functions can be constructed. From the set of trial functions we can search for elements which satisfy equations (8.37), (8.38) and (8.39) at a specified set of grid points, use continuity arguments to infer that the inequalities are satisfied everywhere, and then explicitly construct a suboptimal scheduled controller from the computed solutions using theorem 8.2.2. Finding the optimal stability margin would, of course, require an iteration and the above procedure would have to be repeated in its entirety during each step of the iteration. Given that all three inequalities must be satisfied simultaneously at the grid points this can involve some intensive computations, so any technique that allows the computational complexity to be relaxed is worthy of investigation. In the next section we will outline a solution procedure that is quasi-convex, that does away with the coupling constraint and represents a significant computational saving over the procedure just described. We feel that the loss of convexity is justified by the computational savings that result.

8.5 Computational solution of the four-block problem

Expanding equations (8.37), (8.38) and (8.39) we obtain the following conditions

$$-\dot{Y} + AY + YA^T - BB^T + YC^TCY < 0 \tag{8.40}$$

$$\dot{Z} + A^TZ + ZA + \gamma^2(\gamma^2-1)^{-1}ZBB^TZ + \gamma^{-2}(1-\gamma^2)C^TC < 0 \tag{8.41}$$

$$ZY > \gamma^{-2}I. \tag{8.42}$$

The first of these is related to the generalised control Riccati inequality (GCRI) and is clearly independent of γ. We will now show that a solution to the four-block problem can be constructed directly from the generalised filtering Riccati inequality (GFRI) and GCRI, the solutions of which are independent of γ. The spectral radius coupling condition can then be used to give the optimal stability margin in terms of the computed solutions. Our motivation for this is twofold, namely:

1. Since the solutions of GCRI and GFRI are independent of γ, no iteration is required when searching for the optimal stability margin [2]. Memory requirements are also reduced since we no longer need to satisfy all three LMI's simultaneously.

2. GCRI and GFRI provide a connection between the model reduction theory developed in chapter 7 and the controller synthesis problem being considered here. In fact we will show that we can construct reduced-order controllers directly from GCRI and GFRI without having to satisfy any other inequalities.

Defining

$$\tilde{Y} \triangleq Y^{-1} \qquad \text{and} \qquad \tilde{Z} \triangleq \frac{(\gamma^2-1)}{\gamma^2}Z^{-1},$$

[2] Actually, it will be seen that the optimal stability margin depends explicitly on the computed solutions, and since these are not unique we will need to take some care to ensure that we obtain a sensible result.

we obtain the following result.

Proposition 8.5.1 *Given a continuous, strictly proper, $\mathcal{Q}_e$ stabilisable and $\mathcal{Q}_e$ detectable state-space realisation of an LPV system P_ρ, there exists a parameter-dependent controller C_ρ such that the feedback pair (P_ρ, C_ρ) is internally stable and $b_{P_\rho,C_\rho} \geq \frac{1}{\gamma}$ if there exist positive definite matrix functions $\tilde{Y}(\rho)$ and $\tilde{Z}(\rho)$ such that:*

i. $$\dot{\tilde{Y}} + \tilde{Y}A + A^T\tilde{Y} - \tilde{Y}BB^T\tilde{Y} + C^TC < 0 \ \forall \ \rho(t) \in F_\rho;$$

ii. $$-\dot{\tilde{Z}} + \tilde{Z}A^T + A\tilde{Z} - \tilde{Z}C^TC\tilde{Z} + BB^T < 0 \ \forall \ \rho(t) \in F_\rho;$$

iii. $$\gamma^2 > \max_{\rho \in F_\rho} \bar{\lambda}(\tilde{Z}\tilde{Y}) + 1.$$

One such suboptimal controller is given by

$$\begin{aligned} C_\rho &\stackrel{s}{=} \left[\begin{array}{c|c} A + BF + LC - ((1-\gamma^2)I + \tilde{Z}\tilde{Y})^{-1}\tilde{Z}H & -L \\ \hline F & 0 \end{array}\right] \\ F &= -B^T\tilde{Y} \\ L &= \gamma^2((1-\gamma^2)I + \tilde{Z}\tilde{Y})^{-1}\tilde{Z}C^T \\ H &= \dot{\tilde{Y}} + \tilde{Y}A + A^T\tilde{Y} + C^TC - \tilde{Y}BB^T\tilde{Y}. \end{aligned}$$

Proof: The result follows by rewriting equations (8.40), (8.41) and (8.42) in terms of $\tilde{Y}$ and $\tilde{Z}$ and by direct application of theorems 8.2.2, 8.3.2 and 8.3.3.

■

Remark 8.5.2 *Setting $\dot{\rho}$ to zero and replacing GCRI and GCRI with the corresponding algebraic Riccati equations we recover the observer structure of the LTI controller solving the frozen parameter version of this problem.*

The structure of the controller in proposition 8.5.1 is ideal for scheduling. It is constructed from the model's state matrices $A(\rho), B(\rho)$ and $C(\rho)$, the state and observer gains $F(\rho)$ and $L(\rho)$, and one additional term through which the rate dependence enters into the controller. Again, the rate dependence can be removed by computing a Lyapunov transformation as demonstrated in chapter 7.

We are now in a position to investigate the numerical issues that arise in the solution of the four-block problem. We modify the problem slightly and attempt to satisfy the following two Riccati differential inequalities

$$\begin{aligned} \dot{\tilde{Y}} + \tilde{Y}A + A^T\tilde{Y} - \tilde{Y}BB^T\tilde{Y} + C^TC &< -\delta^2 I \\ -\dot{\tilde{Z}} + \tilde{Z}A^T + A\tilde{Z} - \tilde{Z}C^TC\tilde{Z} + BB^T &< -\delta^2 I. \end{aligned}$$

The small positive constant $\delta^2 > 0$ has been introduced so as to allow the feasibility of the LMI's at the grid points which cover the parameter space to be extended, through continuity arguments, to the whole parameter space. These inequalities are easily written as LMI's with the unknown variables entering affinely as follows

$$\begin{bmatrix} -\frac{d}{dt}(\tilde{Y}^{-1}) + A\tilde{Y}^{-1} + \tilde{Y}^{-1}A^T - BB^T & \tilde{Y}^{-1}C^T & \delta\tilde{Y}^{-1} \\ C\tilde{Y}^{-1} & -I & 0 \\ \delta\tilde{Y}^{-1} & 0 & -I \end{bmatrix} < 0 \tag{8.43}$$

$$\begin{bmatrix} \frac{d}{dt}(\tilde{Z}^{-1}) + A^T\tilde{Z}^{-1} + \tilde{Z}^{-1}A - C^TC & \tilde{Z}^{-1}B & \delta\tilde{Z}^{-1} \\ B^T\tilde{Z}^{-1} & -I & 0 \\ \delta\tilde{Z}^{-1} & 0 & -I \end{bmatrix} < 0. \tag{8.44}$$

Choosing any set of suitable basis functions $\phi_i(\rho)$ we can search for feasible solutions among the following set of trial functions

$$\begin{aligned} \tilde{Y}^{-1}(\rho) &= \sum_{i=1}^{n} \phi_i(\rho) Y_i > 0 \\ \tilde{Z}^{-1}(\rho) &= \sum_{i=1}^{n} \phi_i(\rho) Z_i > 0 \\ Y_i = Y_i^T, \quad Z_i &= Z_i^T, \ \ i = 1, 2 \ldots n. \end{aligned}$$

Choosing the B-spline basis used in chapter 7, this problem is entirely analogous to the model reduction problem considered there. Again, we need to take care when solving the Riccati inequalities to ensure that we extract a sensible solution (ie: one which is consistent with the objective of obtaining the best stability margin). Ideally we would like to minimise the penalty function

$$J = -\sum_j \text{trace}(\tilde{Z}^{-1}(\rho_j)\tilde{Y}^{-1}(\rho_j)),$$

thereby minimising each of the eigenvalues $\lambda_i(\tilde{Z}(\rho_j)\tilde{Y}(\rho_j))$ at the grid points ρ_j. In view of the fact that this penalty function is not convex we suggest the following procedure instead.

Procedure 8.5.3 .

i. Find $\tilde{Y}^{-1} > 0$ satisfying equation (8.43) and minimise the following cost function

$$J_1 = -\sum_j trace(\tilde{Y}^{-1}(\rho_j)\tilde{Z}_0^{-1}(\rho_j)),$$

where $\tilde{Z}_0(\rho_j)$ is the solution of the generalised filtering algebraic Riccati equation

$$\tilde{Z}_0 A^T + A\tilde{Z}_0 - \tilde{Z}_0 C^T C \tilde{Z}_0 + BB^T = 0$$

at the grid point ρ_j.

ii. Find $\tilde{Z}^{-1} > 0$ *satisfying equation (8.44) and minimise the following cost function*

$$J_2 = -\sum_j trace(\tilde{Z}^{-1}(\rho_j)\tilde{Y}^{-1}(\rho_j)),$$

where $\tilde{Y}(\rho_j)$ *is the solution generated in the first step.*

This procedure could be repeated with the most recent solutions of $\tilde{Y}$ and $\tilde{Z}$ being used as weights, but computational experience indicates that this often yields only modest improvement. Observe that in the first step of this procedure we use the solution of the frozen-parameter algebraic Riccati equation as a weight in the cost function. So as with the model reduction setup of chapter 7, we are looking for a controller that is close to the frozen-parameter controller at each grid point but with guarantees on stability and performance when the parameter is truly time varying.

Difficulties with this approach could arise if the frozen-parameter solution of the generalised filtering algebraic Riccati equation $Z_0(\rho_j)$ is not invertible (ie: if (A,B) has stable uncontrollable modes) at any of the grid points. If this is the case then it may be necessary to reverse the order of the iteration and use $Y_0(\rho_j)$, the solution of the generalised control algebraic Riccati equation, as the LTI weight instead (presuming that (C, A) has no stable unobservable modes). If neither of the algebraic Riccati equations generates invertible solutions at the grid points then the full set of three inequalities must be solved simultaneously. Another valid criticism is that the cost function does not emphasise minimisation of $\bar{\lambda}(\tilde{Y}\tilde{Z})$ and as such is not consistent with the objective of maximising the achieved stability margin. In fact this could easily lead to difficulties with this procedure if there are states in the plant that are only weakly controllable or weakly observable (since these would tend to dominate the cost function). In this case it is possible to force the solution to bound b_{P_ρ,C_ρ} by using the following modification. Replace the constraints $\tilde{Z}^{-1} > 0$ and $\tilde{Y}^{-1} > 0$ with $\tilde{Y}^{-1} > (\gamma_{\max}^2 - 1)^{-1}\tilde{Z}$ and $\tilde{Z}^{-1} > (\gamma_{\max}^2 - 1)^{-1}\tilde{Y}$. This introduces no additional computational cost since we require $\tilde{Z} > 0$ and $\tilde{Y} > 0$ anyway. This modification gives a controller which is guaranteed to satisfy $b_{P_\rho,C_\rho} \geq \frac{1}{\gamma_{\max}}$ (if one exists).

8.6 Reduced-order controller synthesis

In this section we turn to an important problem, that of synthesising reduced-order controllers for LPV systems. We have already demonstrated that it is possible to synthesise controllers which give guaranteed levels of performance and robustness for a set of bounded-rate parameter trajectories. Since the state matrices of these controllers are parameter-dependent, implementation will require real-time updates of both the state vector and the controller matrices. This makes the task of reducing the complexity of these controllers all the more important from an implementation perspective. In this section we consider an approach to reducing the state complexity based on the balanced truncation techniques developed in chapter 7.

One approach to synthesising a reduced-order controller would be to balance the full-order model of the plant, reduce the plant using balanced truncation, then synthesise a controller using the reduced-order approximant. That the balanced approximant is dependent on the parameter and its derivative does not complicate the synthesis step since the parameter rate enters into the approximant in an affine manner. The alternative would be to synthesise a high-order controller, balance the resulting controller (which also has affine rate dependence) and truncate those states which do not contribute strongly to the controller's input-output map. Since neither procedure is based on closed-loop considerations we cannot guarantee that the reduced-order controller will result in a satisfactory closed loop, and the only way to check this is by explicitly computing a quadratic dissipation function to bound the closed-loop L_2 gain. This approach to synthesising reduced-order controllers could easily result in difficulties if the plant or controller is unstable, and both approaches require us to compute solutions to two separate systems of LMI's, one set for the model reduction problem, and one set for the controller synthesis problem. In this regard the four-block setup has much to offer, allowing us to synthesise reduced-order controllers by solving GCRI and GFRI, irrespective of the stability properties of the plant. We now outline a procedure for computing reduced-order controllers using the four-block setup.

Procedure 8.6.1 *Given a continuous, strictly proper, n-state $\mathcal{Q}_e$ stabilisable and $\mathcal{Q}_e$ detectable realisation of an LPV system P_ρ, let $\tilde{Y}(\rho) > 0$ and $\tilde{Z}(\rho) > 0$ satisfy GCRI and GFRI*

$$\begin{aligned}\dot{\tilde{Y}} + \tilde{Y}A + A^T\tilde{Y} - \tilde{Y}BB^T\tilde{Y} + C^TC < 0 \ \ \forall \ \ \rho(t) \in F_\rho \\ -\dot{\tilde{Z}} + \tilde{Z}A^T + A\tilde{Z} - \tilde{Z}C^TC\tilde{Z} + BB^T < 0 \ \ \forall \ \ \rho(t) \in F_\rho.\end{aligned}$$

Define $Q \triangleq \tilde{Y}$ and $P \triangleq (I + \tilde{Z}\tilde{Y})^{-1}\tilde{Z}$, and let $T(\rho)$ be a balancing (alternatively, naturally-balancing) transformation matrix such that $T^TQT = T^{-1}PT^{-T} = \Sigma$, where Σ is a diagonal matrix with the $\mathcal{Q}_e$ singular values of the contractive graph symbol of P_ρ (see chapter 7) along the diagonal[3]*. Use $T(\rho)$ to transform P_ρ as follows*

$$P_\rho \stackrel{s}{=} \left[\begin{array}{c|c} T^{-1}(\rho)A(\rho)T(\rho) - T^{-1}(\rho)\dot{T}(\rho) & T^{-1}(\rho)B(\rho) \\ \hline C(\rho)T(\rho) & 0 \end{array}\right].$$

Pick a number $r < n$ and partition Σ according to

$$\Sigma = \left[\begin{array}{cc} \Sigma_1 & 0 \\ 0 & \Sigma_2 \end{array}\right]$$

where $\Sigma_1 = diag(\sigma_1, \sigma_2, \ldots, \sigma_r)$ and $\Sigma_2 = diag(\sigma_{r+1}, \sigma_{r+2}, \ldots, \sigma_n)$. Partition A, B and C conformally with the partition of Σ:

$$P_\rho \stackrel{s}{=} \left[\begin{array}{cc|c} A_{11}(\rho,\dot{\rho}) & A_{12}(\rho,\dot{\rho}) & B_1(\rho) \\ A_{21}(\rho,\dot{\rho}) & A_{22}(\rho,\dot{\rho}) & B_2(\rho) \\ \hline C_1(\rho) & C_2(\rho) & 0 \end{array}\right].$$

[3] Typically these will be in descending order unless we make use of the natural balancing state transformation.

For any γ satisfying

$$\gamma^2 > \max_{\rho \in F_\rho} \bar{\lambda}(\tilde{Z}\tilde{Y}) + 1,$$

define the r-state reduced-order controller for the n-state LPV system P_ρ as follows:

$$\begin{aligned}
C_\rho &\stackrel{s}{=} \left[\begin{array}{c|c} A_{11} + B_1 F + LC_1 - ((1-\gamma^2)I + Z_1\Sigma_1)^{-1} Z_1 H & -L \\ \hline F & 0 \end{array}\right] \\
F &= -B_1^T \Sigma_1 \\
L &= \gamma^2((1-\gamma^2)I + Z_1\Sigma_1)^{-1} Z_1 C_1^T \\
H &= \dot{\Sigma}_1 + \Sigma_1 A_{11} + A_{11}^T \Sigma_1 + C_1^T C_1 - \Sigma_1 B_1 B_1^T \Sigma_1 \\
Z_1 &= (I - \Sigma_1^2)^{-1} \Sigma_1.
\end{aligned}$$

Remark 8.6.2 *The reduced-order controller given in procedure 8.6.1 is the full-order controller for the reduced-order plant that results from balanced truncation of the contractive graph symbol of P_ρ as detailed in chapter 7.*

8.7 Example

The following example demonstrates the generality of the techniques developed in this and the previous chapter. The increasingly high levels of performance being achieved by modern tactical aircraft necessitate a commensurate improvement in missile technology. The large and rapidly-varying acceleration demands generated by the guidance systems of future high-performance missiles will have to be met by the autopilot system. This is true even when the missile is operating at high, and possibly rapidly-varying, angles of attack. Standard gain scheduling design procedures, based on interpolating controllers designed from frozen-parameter linearisations, cannot deliver guaranteed performance when the scheduling parameter varies rapidly. This motivates an application of the procedures developed in this chapter to a generic missile autopilot design.

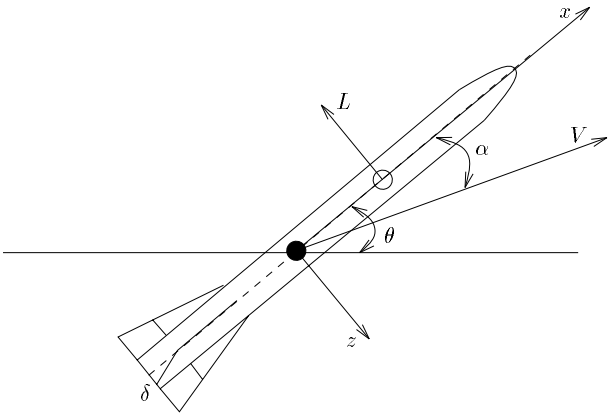

Figure 8.5 *Schematic view of a missile*

The model is taken from Shamma and Cloutier [80] and is representative of a missile travelling at Mach 3 at an altitude of 20,000 ft. The control objective is to control normal acceleration, expressed in g, (see Figure 8.5) using tail fin deflections. The longitudinal dynamics of the missile are nonlinear and have the following form:

$$\frac{d}{dt}\begin{bmatrix} \alpha \\ q \end{bmatrix} = \begin{bmatrix} \frac{fgQS\cos(\alpha/f)\phi_z(\alpha)}{WV} \\ \frac{fQSd\phi_m(\alpha)}{I_{yy}} \end{bmatrix} + \begin{bmatrix} 0 & 1 \\ 0 & 0 \end{bmatrix}\begin{bmatrix} \alpha \\ q \end{bmatrix} + \begin{bmatrix} \frac{fgQS\cos(\alpha/f)b_z}{WV} \\ \frac{fQSdb_m}{I_{yy}} \end{bmatrix}\delta,$$

where

$$\begin{aligned}
d &= \text{reference diameter, } 0.75\ ft \\
f &= \text{radians-to-degrees, } 180/\pi \\
g &= \text{acceleration of gravity, } 32.2\ ft/s^2 \\
I_{yy} &= \text{pitch moment of inertia, } 182.5\ slug - ft^2 \\
m &= C_mQSd \text{ pitch moment, } ft - lb \\
Q &= \text{dynamic pressure, } 6132.8\ lb - ft^2 \\
q &= \text{pitch rate, } deg/s \\
S &= \text{reference area, } 0.44\ ft^2 \\
V &= \text{speed, } 3109.3\ ft/s \\
W &= \text{weight, } 450\ lb \\
Z &= C_zQS \text{ normal force, } lb \\
\alpha &= \text{angle of attack, } deg.
\end{aligned}$$

The normal force and pitch moment aerodynamic coefficients are approximated by

$$\begin{aligned}
C_z &= \phi_z(\alpha) + b_z\delta \\
C_m &= \phi_m(\alpha) + b_m\delta,
\end{aligned}$$

where

$$\begin{aligned} b_m &= -0.206 \\ b_z &= -0.034 \\ \delta &= \text{fin deflection}, \quad deg \\ \phi_m(\alpha) &= 0.000215\alpha^3 - 0.0195\alpha|\alpha| + 0.051\alpha \\ \phi_z(\alpha) &= 0.000103\alpha^3 - 0.00945\alpha|\alpha| - 0.170\alpha. \end{aligned}$$

The missile tail-fin actuator is modelled as a second-order system with the following transfer function:

$$\delta(s) = \frac{w_a^2}{s^2 + 1.4w_a s + w_a^2}\delta_c(s),$$

where δ_c is the command deflection and $w_a = 150\ rad/s$ is the actuator bandwidth. Observe that there exists a family of equilibrium states $q_{eq}(\alpha)$ and $\delta_{eq}(\alpha)$ such that

$$0 = \begin{bmatrix} \frac{fgQS\cos(\alpha/f)\phi_z(\alpha)}{WV} \\ \frac{fQSd\phi_m(\alpha)}{I_{yy}} \end{bmatrix} + \begin{bmatrix} 0 & 1 \\ 0 & 0 \end{bmatrix} \begin{bmatrix} \alpha \\ q_{eq}(\alpha) \end{bmatrix} + \begin{bmatrix} \frac{fgQS\cos(\alpha/f)b_z}{WV} \\ \frac{fQSdb_m}{I_{yy}} \end{bmatrix} \delta_{eq}(\alpha).$$

Shamma and Cloutier [80] demonstrate how this system can be converted into a quasi-LPV form using a nonlinear state transformation:

$$\frac{d}{dt}\begin{bmatrix} \alpha \\ q - q_{eq}(\alpha) \\ \delta - \delta_{eq}(\alpha) \end{bmatrix} = \begin{bmatrix} 0 & 1 & \frac{fgQS\cos(\alpha/f)b_z}{WV} \\ 0 & -\frac{dq_{eq}(\alpha)}{dt} & \frac{fQSdb_m}{I_{yy}} - \frac{dq_{eq}(\alpha)}{dt}\frac{fgQS\cos(\alpha/f)b_z}{WV} \\ 0 & -\frac{d\delta_{eq}(\alpha)}{dt} & -\frac{d\delta_{eq}(\alpha)}{dt}\frac{fgQS\cos(\alpha/f)b_z}{WV} \end{bmatrix} \begin{bmatrix} \alpha \\ q - q_{eq}(\alpha) \\ \delta - \delta_{eq}(\alpha) \end{bmatrix} + \begin{bmatrix} 0 \\ 0 \\ 1 \end{bmatrix} v, \tag{8.45}$$

where

$$\delta = \int v$$

This representation of the nonlinear dynamics does not involve any pointwise linearisations, and as such remains exact even when the scheduling parameter undergoes rapid time variations. By appending an integrator to the input of the plant, this realisation also does away with the need for an inner trim loop. The requirement for an inner trim loop, as would arise if pointwise linearisation of the nonlinear dynamics had been performed, can destroy the robustness properties of an inherently robust controller by exciting high frequency dynamics (for example the first bending mode of the missile). The representation of the system dynamics given by

equation (8.45) is often referred to as being quasi-LPV in as much as the exogenous scheduling variable is actually an internal state. The measured plant outputs are pitch rate q (rate gyro), angle of attack (estimated) and the normal acceleration (accelerometer) which is given by

$$n = \frac{QS}{W}\left(\phi_z(\alpha) - \frac{b_z}{b_m}\phi_m(\alpha)\right) + \frac{QSb_z}{W}\left(\delta - \delta_{eq}(\alpha)\right).$$

The general performance objective is to track acceleration step commands with a steady-state tracking error of less than 0.5% and a time constant of $0.2s$. Loop-shaping is achieved by adding weights at the plant outputs, which are given by $q - q_{eq}(\alpha)$ and n, as shown in Figure 8.6.

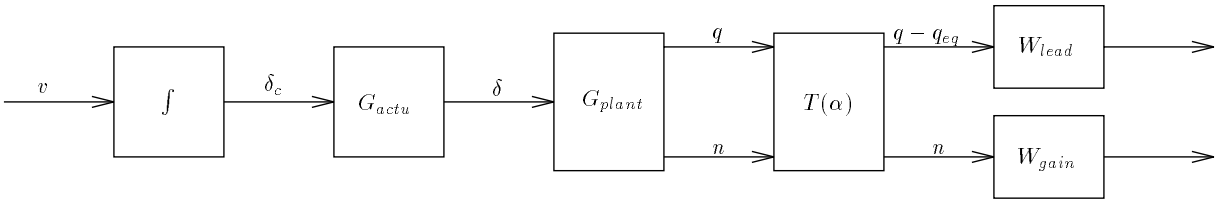

Figure 8.6 *Weighted plant*

The pitch rate measurement is used to increase closed-loop damping and to set the high frequency roll-off characteristics. The acceleration loop is used to meet the low frequency tracking objective and to set the effective closed-loop bandwidth. It is rolled off at a lower frequency than the pitch-rate loop because the accelerometer is more sensitive to high frequency noise/unmodelled dynamics. After appending the actuator dynamics to the input, a simple lead filter

$$W_{lead} = \frac{40s + 400}{s + 100},$$

was used to give a satisfactory loop shape for the rate loop over a 30 deg angle of attack flight envelope. The integrator at the input makes it possible to meet the low frequency tracking objective simply by scaling the normal acceleration loop to give the required crossover frequency. Figure 8.7 shows the loop shapes of the weighted plant at the two extremes of the flight envelope. The crossover frequencies have been set so as to avoid exciting the first bending mode of the missile's airframe which is typically around 150 rad/s.

Having introduced suitable frequency weighting, the four-block synthesis problem can now be solved. Our first objective is to determine the total number of B-splines and grid points necessary in the solution of the Riccati inequalities. As in the model reduction setup, we set $\dot{\alpha}$ to zero and solve the equivalent frozen-parameter problem. This allows us to compare the closed-loop induced L_2 gain at each of the grid points obtained from the LMI formulation, to the optimal frozen parameter H_∞ norm at the same grid points. It was found that a total of 12 B-splines (252 decision variables) together with 25 grid points over the 30 deg envelope was sufficient to reproduce the frozen parameter H_∞ norm at the grid points, and to ensure that the Riccati

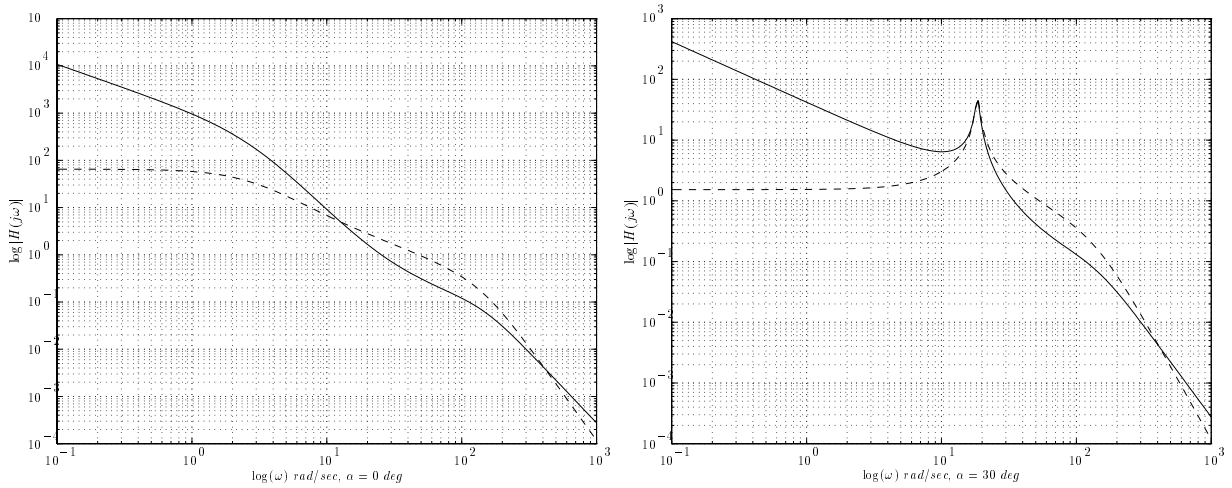

Figure 8.7 *Loop shapes of the weighted plant, acceleration loop-solid, rate-rate loop-dashed.*

differential inequalities were negative for all feasible values of α. Having established a suitable number of basis functions we recompute the solution to the four-block problem with the following rate limits: $|\dot{\alpha}| \leq 100\ deg/s$, $|\dot{\alpha}| \leq 150\ deg/s$ and $|\dot{\alpha}| \leq \infty$. These rate limits were determined from nonlinear simulations, where it was found that $150\ deg/s$ was just sufficient to cover a $40g$ acceleration demand. In each case the achieved closed-loop L_2 gain can be determined by examining Figure 8.8. A plot of the $\mathcal{Q}_e$ singular values of the contractive graph symbol of the missile model has been included in Figure 8.9 in order to determine whether any states can be truncated to generate reduced-order controllers.

The effect of constraining the parameter rate is clearly discernible in Figure 8.8. For unbounded rates the achieved stability margin is given by $b_{P_\rho,C_\rho} = 0.23$, with a rate bound of $150\ deg/s$ the stability margin is more satisfactory at $b_{P_\rho,C_\rho} = 0.26$, for $100\ deg/s$ slightly better at $b_{P_\rho,C_\rho} = 0.28$, and the worst case frozen-parameter bound is given by $b_{P_\rho,C_\rho} = 0.31$. Figure 8.9 indicates that one state, possibly even two states, could be truncated from the controller using procedure 8.6.1. However, for the controller computed with no bound on the rate of parameter variation it is unlikely that further degradation in the stability margin would be acceptable. The picture is somewhat different with the bounded-rate controllers and for these it might well be possible to reduce their state dimension for implementation purposes.

To demonstrate this point procedure 8.6.1 was employed to obtain reduced-order controllers $\hat{C}_\rho$ for each of the given rate bounds (the balancing transformation matrices and their derivatives were computed using the results of chapter 7). Having computed reduced-order controllers, the resulting degradation in the achieved stability margin was explicitly computed. In each case a quadratic dissipation function was computed (using the same rate limits that were used when synthesising the controllers) in order to bound $b_{P_\rho,\hat{C}_\rho}$. This involved finding an

$X(\alpha) = X^T(\alpha) > 0$ satisfying the following differential inequality

$$\dot{X} + A_{cl}^T X + X A_{cl} + C_{cl}^T C_{cl} + (X B_{cl} + C_{cl}^T D_c)(\gamma^2 I - D_{cl}^T D_{cl})^{-1}(B_{cl}^T X + D_{cl}^T C_{cl}) < 0 \ \ \forall \ \ \alpha(t) \in F_\alpha$$

where A_{cl}, B_{cl}, C_{cl} and D_{cl} are the closed-loop state matrices corresponding to the feedback loop in Figure 8.4. The results are listed in Table 8.1.

$\dot{\alpha}$	$\hat{C}_\rho$	$b_{P_\rho,\hat{C}_\rho}$	$\dot{\alpha}$	$\hat{C}_\rho$	$b_{P_\rho,\hat{C}_\rho}$	$\dot{\alpha}$	$\hat{C}_\rho$	$b_{P_\rho,\hat{C}_\rho}$
∞	6-states	1/4.40	150 deg/s	6-states	1/3.80	100 deg/s	6-states	1/3.60
∞	5-states	1/4.60	150 deg/s	5-states	1/3.90	100 deg/s	5-states	1/3.70
∞	4-states	1/6.50	150 deg/s	4-states	1/5.40	100 deg/s	4-states	1/5.20

Table 8.1 *Stability margins for the full-order and reduced-order controllers*

For all three rate limits, truncating a single state does not result in a significant degradation in the achieved stability margin. However, the reduction in stability margin that results when two states are truncated from any of the controllers is not acceptable. In the final analysis we can obtain a 5-state reduced-order controller which, with a realistic rate bound of 150 deg/s, satisfies $b_{P_\rho,\hat{C}_\rho} = 1/3.90$, whereas with no rate limit the best we can do with a 6-state controller is $b_{P_\rho,C_\rho} = 1/4.40$.

We conclude with nonlinear simulations of the closed loop step response to $20g$, $30g$ and $40g$ demand signals[4] for the full-order and the reduced-order controllers for each of the three rate bounds. These can be found in Figures 8.10 through 8.12. Also included is a plot of $\dot{\alpha}$ which can be used to determine the appropriateness of the chosen rate bounds. It can be seen that the 5-state controller gives a very satisfactory response, in all cases meeting the rise time specification with no steady tracking error.

[4]Except for the controller computed with a rate limit of 100 deg/s where a $40g$ step violates the rate bound quite considerably.

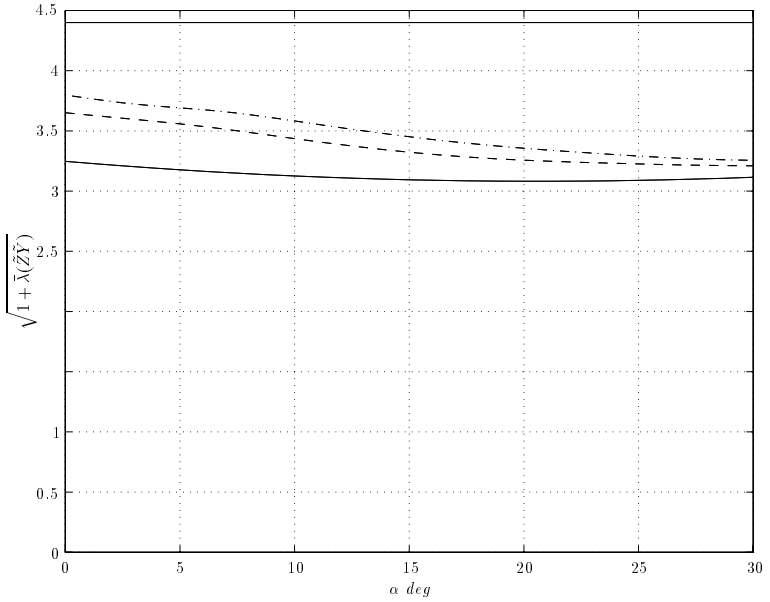

Figure 8.8 $b^{-1}_{P_\rho, C_\rho} = \max_{\alpha \in F_\alpha} \sqrt{1+\bar{\lambda}(\tilde{Z}\tilde{Y})}$, $\dot{\alpha} = 0$ *(solid)*, $|\dot{\alpha}| \leq 100$ *deg/s (dashed)*, $|\dot{\alpha}| \leq 150$ *deg/s (dot-dashed)*, $|\dot{\alpha}| \leq \infty$ *(solid)*.

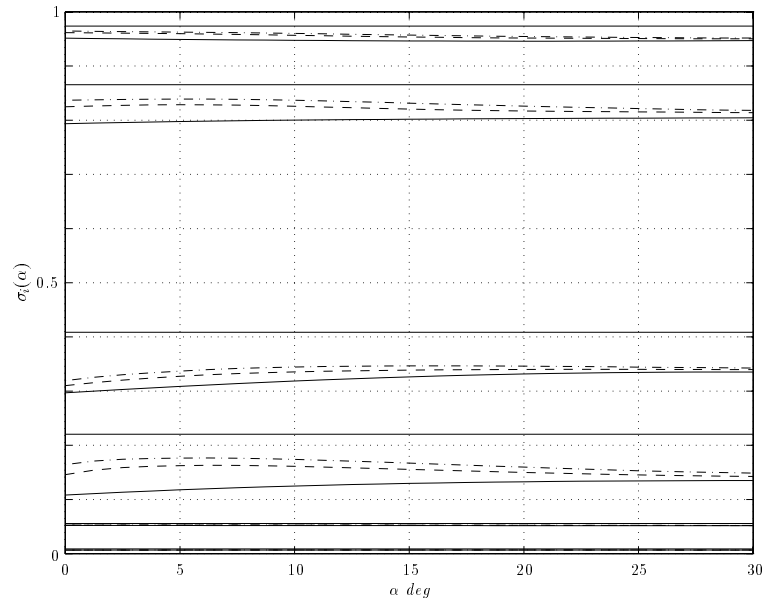

Figure 8.9 $\mathcal{Q}_e$ *singular values of the contractive graph symbol,* $\dot{\alpha} = 0$ *(solid)*, $|\dot{\alpha}| \leq 100$ *deg/s (dashed)*, $|\dot{\alpha}| \leq 150$ *deg/s (dot-dashed)*, $|\dot{\alpha}| \leq \infty$ *(solid)*.

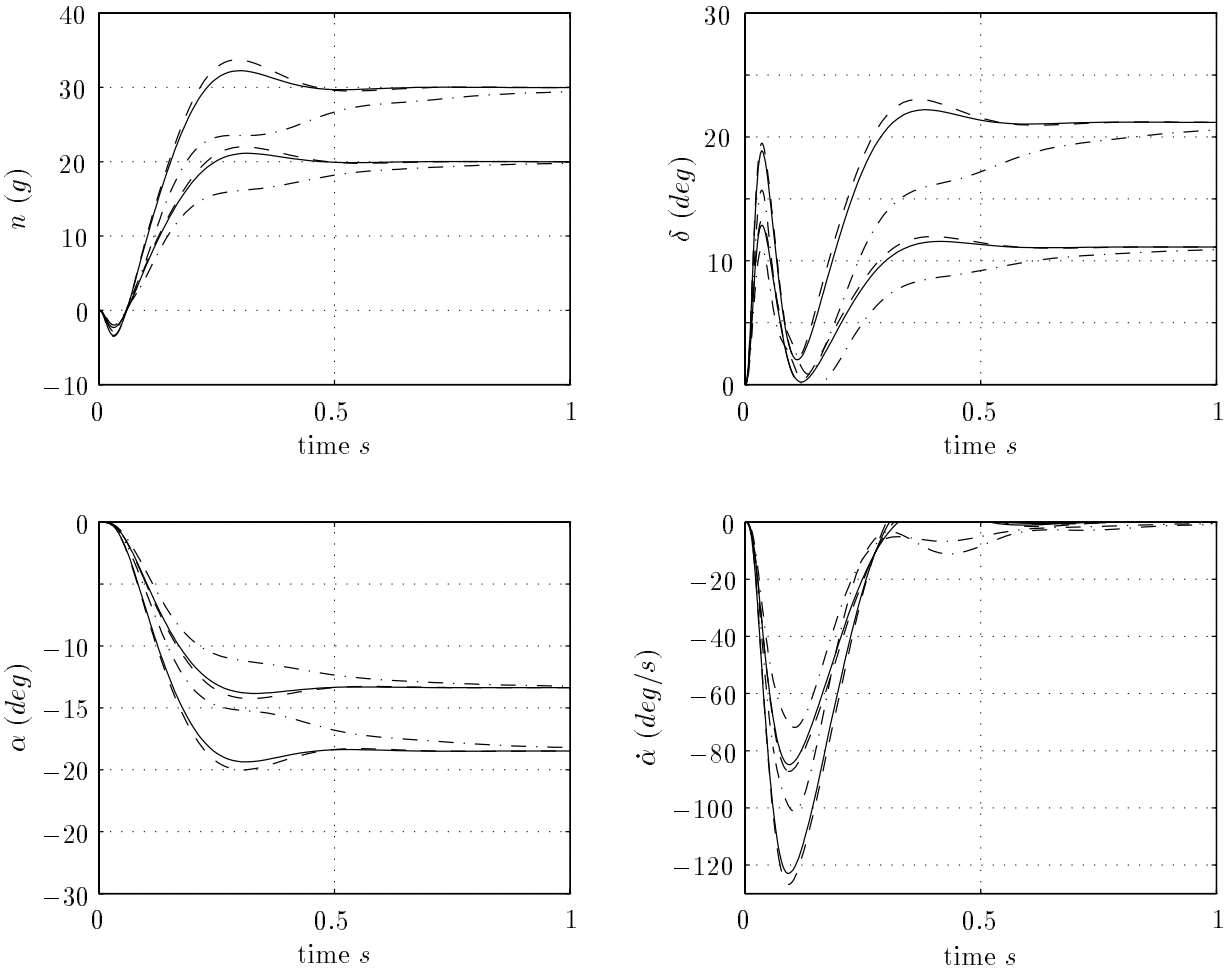

Figure 8.10 *Nonlinear simulation, controller computed with rate bound of* 100 *deg/s, solid lines are with* 6*-state controller, dashed lines are with* 5*-state controller, and dot-dashed lines are with* 4*-state controller.*

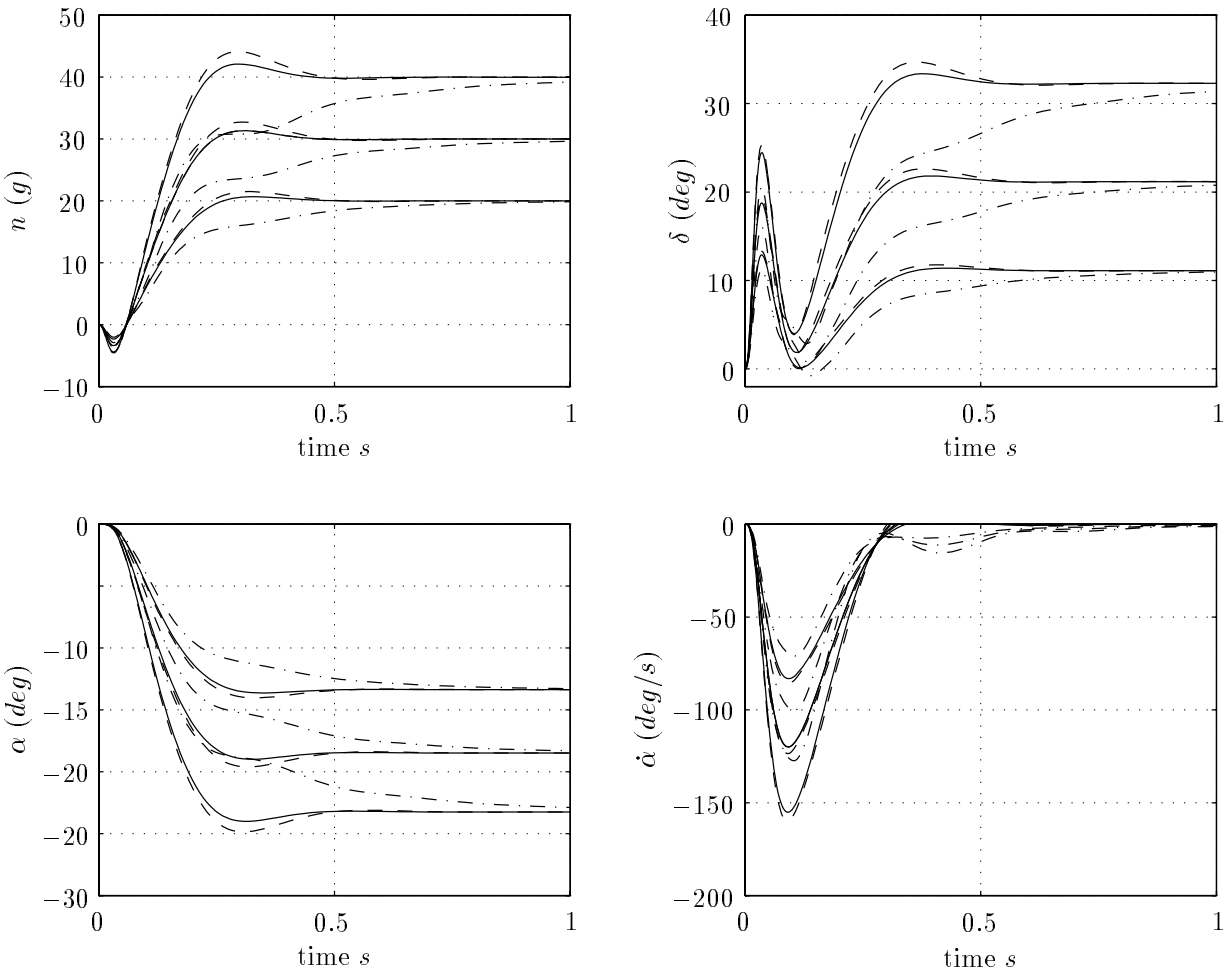

Figure 8.11 *Nonlinear simulation, controller computed with rate bound of* 150 *deg/s, solid lines are with* 6*-state controller, dashed lines are with* 5*-state controller, and dot-dashed lines are with* 4*-state controller.*

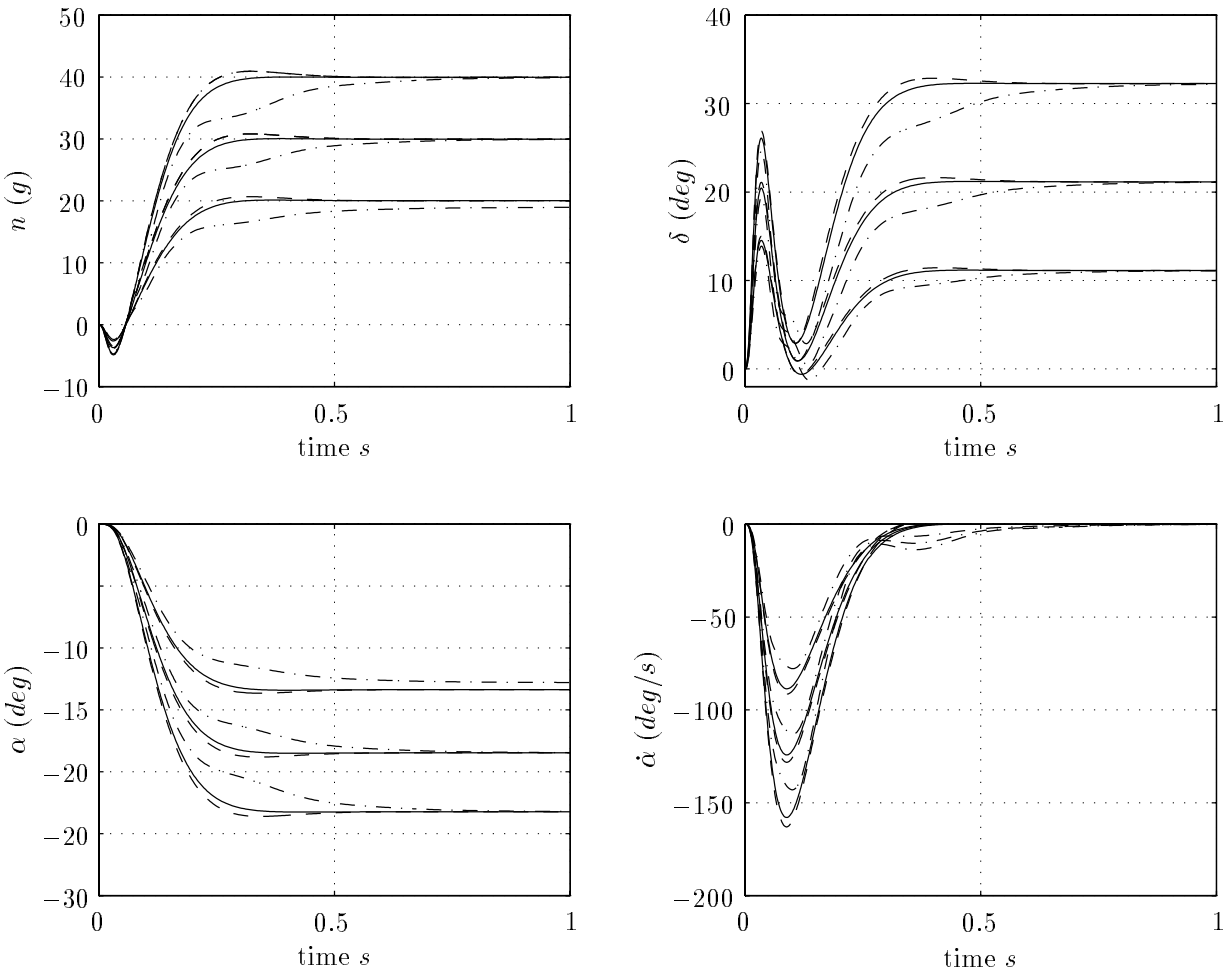

Figure 8.12 *Nonlinear simulation, unbounded rate controller, solid lines are with* 6*-state controller, dashed lines are with* 5*-state controller, and dot-dashed lines are with* 4*-state controller.*

8.8 Summary

In this chapter we have considered the problem of synthesising parameter-dependent controllers for bounded-rate parameter-dependent systems. This was done in order to relax the conservatism that appears in the quadratic-performance output feedback problem which allows for unbounded rates of parameter variation. Our solution uses an extension of the earlier LTI results of Sampei et al [77] and is expressed in terms of the solutions to two parameter-dependent Riccati differential inequalities. We have made use of the techniques developed by Becker [7] to simplify the formulation and have shown that the four-block setup considered in chapter 4 leads to a very elegant solution. Finally, we have made a connection between the synthesis results in this chapter and the model reduction results in the previous chapter, giving a direct and explicit procedure for synthesising reduced-order controllers in the four-block setup. Computational procedures similar to those used in the previous chapter find direct application to the synthesis problem and we have demonstrated the generality of these techniques on a challenging missile control problem, with very satisfactory results.

9

Concluding Remarks

We conclude this thesis with a summary of what we perceive to be the main contributions and give suggestions for possible future research.

9.1 Contributions

- Motivated by the violin bowing problem a mathematical model of a geometrically simple parameter-dependent structure has been developed. This was used to highlight a number of unusual properties possessed by this class of mechanical systems. These include: pole-zero cancellations (frozen-parameter case), continuity properties of modal transformation matrices and related model reduction issues, and shortcomings associated with commonly-used damping models (parameter-varying case).

- A novel application of H_∞ loop-shaping to parameter-dependent flexible structures has been undertaken. Difficulties that can arise when controlling this class of systems have been highlighted and various new robustness measures have been shown to provide a way of overcoming these difficulties. These allow a clear tradeoff to be made between performance, robustness and sensitivity to parameter variation.

- Switching techniques that allow for large parameter variations have been shown to be effective in the H_∞ loop-shaping context. Careful attention to the issues of reference signal injection and bumpless transfer indicate that switching can be effective on systems that are very sensitive to sudden transients and that it provides a viable approach to dealing with large parameter variations.

- An experimental facility has been developed and used in a thorough experimental evaluation of SISO and MISO controllers. The importance of adequate robustness/performance tradeoffs has been demonstrated, as has the effectiveness of the proposed switching technique. The controllers have been shown to give satisfactory performance to a wide range of time-varying parameter trajectories.

- Complexity issues have led to the development of a balanced model-reduction technique for bounded-rate LPV systems. The applicability of this technique depends on recently

developed convex optimisation methods to solve the Lyapunov and Riccati differential inequalities which are central to the balancing technique. Known error bounds for a related LTI model reduction technique have been shown to generalise to the new procedure under certain conditions and important insights have been obtained in the general case. A detailed study has been made of the continuity properties of the model approximant and procedures for computing the balancing transformation matrix have been developed. A number of examples have been used to demonstrate the application of this technique.

- Synthesis techniques for LPV systems have been extended by allowing for the incorporation of rate bounds to reduce conservatism. The so-called four-block problem has been shown to lead to a particularly elegant solution and it has been shown that it also leads to a reduction in the computational complexity of the synthesis procedure. Direct techniques that allow for the synthesis of reduced-order bounded-rate controllers have been developed for the four-block problem. It has been shown that this can be achieved in a very efficient manner using the newly-developed balanced model-reduction technique to approximate the symbol of the system's graph. A challenging example has been used to demonstrate the applicability of these techniques.

9.2 Suggestions for future research

- Application of the techniques in chapter 4 to a structure that is geometrically more complicated would be of interest. In this regard, experimental equipment is already being developed to build a violin bowing machine that will have a number of inputs and possibly multiple outputs.

- For the violin bowing problem it is not possible to measure the bow-pressure directly. This raises some interesting filtering problems for parameter-dependent systems of this type.

- Complexity issues associated with the extended H_∞ loop-shaping control technique need more careful consideration. The applicability of recent results on the synthesis of bounded-complexity controllers [89] would be worthy of investigation. These techniques produce controllers that are less sensitive to parameter variations.

- The error bounds for the bounded-rate balanced model reduction procedure need further investigation. Since the computations required to bound the error in the LPV case are much more intensive than in the LTI case, tight error bounds are seen as being of particular importance.

- For the bounded-rate LPV synthesis technique we have remarked that the rate term entering into the controller equations can be removed by computing a Lyapunov transformation. Whether this makes the controller sensitive to measurement noise is not clear. A careful examination of this technique with L_∞ bounds on parameter measurement noise represents an interesting, but very challenging problem.

- The application of the LPV synthesis techniques to nonlinear systems is of interest. Methods for obtaining LPV or quasi-LPV models of nonlinear systems in such a manner as to preserve the robustness properties of the LPV controller when applied to the original nonlinear system would be worthy of investigation.

A

Appendix

For the flexible beam considered in chapter 3 we show that modelling the constraint as if it were rigid leads to a model with ρ, $\dot{\rho}$ and $\ddot{\rho}$ dependence. Differentiating the constraint equation (3.14) twice gives

$$\ddot{\rho}(t)\theta(t) + (\rho(t)+r)\ddot{\theta}(t) + 2\dot{\rho}(t)\dot{\theta}(t) + \sum_j \ddot{a_j}(t)\phi_j(\rho(t)) + 2\sum_j \dot{a_j}(t)\dot{\rho}(t)\phi_j'(\rho(t)) + \sum_j a_j(t)\ddot{\rho}(t)\phi_j'(\rho(t)) + \sum_j a_j(t)\dot{\rho}^2(t)\phi_j''(\rho(t)) = 0,$$

where $'$ denotes differentiation with respect to x. Using a similar procedure to that used in section 3.2, it is possible to eliminate the constraint force using the following relation

$$\frac{F_1(t)}{m}\sum_j \phi_j^2(\rho(t)) = \left(\frac{\ddot{\rho}(t)}{\rho(t)+r} - 2\left(\frac{\dot{\rho}(t)}{\rho(t)+r}\right)^2\right)\sum_j a_j(t)(\phi_j(\rho(t)) - (\rho(t)+r)\phi_j'(\rho(t))) + 2\frac{\dot{\rho}(t)}{\rho(t)+r}\sum_j \dot{a}_j(t)(\phi_j(\rho(t)) - (\rho(t)+r)\phi_j'(\rho(t))) + \sum_j a_j(t)(\lambda_j^2\phi_j(\rho(t)) - \dot{\rho}(t)^2\phi_j''(\rho(t))).$$

Using the series expansion $w(x,t) = \sum_i a_i(t)\phi_i(x)$ for the elastic deformation of the beam, the forced response of the beam is given by

$$\ddot{a_i}(t) + \lambda_i^2 a_i(t) + \frac{m\gamma_i}{I_h}\sum_j \gamma_j\lambda_j^2 a_j(t) - \frac{\phi_i(\rho(t))}{\sum_k \phi_k^2(\rho(t))}\left\{\left(\frac{\ddot{\rho}(t)}{\rho(t)+r} - 2\left(\frac{\dot{\rho}(t)+r}{\rho(t)}\right)^2\right)\sum_j \left(\phi_j(\rho(t)) - (\rho(t)+r)\phi_j'(\rho(t))\right)a_j(t) + \sum_j \left(\lambda_j^2\phi_j(\rho(t)) - \dot{\rho}(t)^2\phi_j''(\rho(t))\right)a_j(t) + 2\frac{\dot{\rho}(t)}{\rho(t)+r}\sum_j(\phi_j(\rho(t)) - (\rho(t)+r)\phi_j'(\rho(t)))\dot{a_j}(t)\right\} = -\frac{\gamma_i}{I_h}T.$$

A gain-scheduled controller for this system, synthesised using the methods developed in chapter 8, will have the same parameter complexity.

B

Appendix

In this Appendix we provide a proof of theorem 7.6.8. The results of lemma 7.6.5 and lemma 7.6.6 give the following:

i. if $\dot{\sigma} \geq 0 \ \forall \ t \in [t_0, t_1]$, then

$$\|e\|^2_{2,[t_0,t_1]} \leq 4\sigma^2_{\max}\|u\|^2_{2,[t_0,t_1]} - 4\sigma^2_{\max}x^T T_2^{-T} Y^{-1} T_2^{-1} x|_{t_0}^{t_1};$$

ii. if $\dot{\sigma} \leq 0 \ \forall \ [t_2, t_3]$, then

$$\|e\|^2_{2,[t_2,t_3]} \leq 4\sigma^2_{\max}\|u\|^2_{2,[t_2,t_3]} - x^T T_1^{-T} X T_1^{-1} x|_{t_2}^{t_3},$$

where X, Y, T_1 and T_2 were defined in lemma 7.6.5 and lemma 7.6.6. Now suppose that $t_0 < t_1 < t_2$ and that $x(t_0) = x(t_2) = 0$. Furthermore, assume that $\dot{\sigma} \geq 0 \ \forall \ [t_0, t_1]$ and that $\dot{\sigma} \leq 0 \ \forall \ [t_1, t_2]$. It follows that

$$\|e\|^2_{2,[t_0,t_2]} \leq 4\sigma^2_{\max}\|u\|^2_{2,[t_0,t_2]} + x(t_1)^T(T_1^{-T}X(\rho(t_1))T_1^{-1} - 4\sigma^2_{\max}T_2^{-T}Y^{-1}(\rho(t_1))T_2^{-1})x(t_1).$$

Using the definitions of X, Y, T_1 and T_2 it is easily shown that

$$T_1^T(T_1^{-T}X(\rho(t_1))T_1^{-1} - 4\sigma^2_{\max}T_2^{-T}Y^{-1}(\rho(t_1))T_2^{-1})T_1 =$$
$$\begin{bmatrix} 2(1-\frac{\sigma^2_{\max}}{\sigma^2(\rho(t_1))})\Sigma(\rho(t_1)) & 0 & 0 \\ 0 & 2\sigma^2(\rho(t_1))(1-\frac{\sigma^2_{\max}}{\sigma^2(\rho(t_1))})\Sigma^{-1}(\rho(t_1)) & 0 \\ 0 & 0 & 2\sigma(\rho(t_1))(1-\frac{\sigma^2_{\max}}{\sigma^2(\rho(t_1))}) \end{bmatrix}. \tag{B.1}$$

So it is clear that if $x(t_0) = x(t_2) = 0$, then

$$\|e\|^2_{2,[t_0,t_2]} \leq 4\sigma^2_{\max}\|u\|^2_{2,[t_0,t_2]}.$$

It should also be clear that this argument would not have held had we assumed that $\dot{\sigma} \leq 0 \ \forall \ [t_0, t_1]$ and that $\dot{\sigma} \geq 0 \ \forall \ [t_1, t_2]$. Now partition the time axis in accordance with Figure B.1.

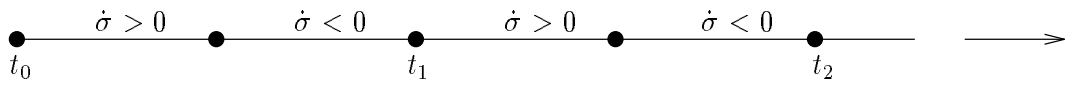

Figure B.1 *Partition of the time axis.*

With $x(t_0) = 0$ we can now write the following finite-horizon bounds

$$\begin{aligned}
\|e\|^2_{2,[t_0,t_1]} &\leq 4\sigma^2_{\max}\|u\|^2_{2,[t_0,t_1]} - x^T(t_1)T_1^{-T}X(\rho(t_1))T_1^{-1}x(t_1) \\
\|e\|^2_{2,[t_1,t_2]} &\leq 4\sigma^2_{\max}\|u\|^2_{2,[t_1,t_2]} + 4\sigma^2_{\max}x^T(t_1)T_2^{-T}Y^{-1}(\rho(t_1))x(t_1) - x^T(t_2)T_1^{-T}X(\rho(t_2))T_1^{-1}x(t_2) \\
\|e\|^2_{2,[t_2,t_3]} &\leq 4\sigma^2_{\max}\|u\|^2_{2,[t_2,t_3]} + 4\sigma^2_{\max}x^T(t_2)T_2^{-T}Y^{-1}(\rho(t_2))x(t_2) - x^T(t_3)T_1^{-T}X(\rho(t_3))T_1^{-1}x(t_3), \text{ etc}
\end{aligned}$$

Multiplying the second of these equations by $\sigma^2_{\min}/\sigma^2_{\max}$ and adding the result to the first equation gives

$$\begin{aligned}
\|e\|^2_{2,[t_0,t_1]} + \frac{\sigma^2_{\min}}{\sigma^2_{\max}}\|e\|^2_{2,[t_1,t_2]} \leq 4\sigma^2_{\max}\|u\|^2_{2,[t_0,t_1]} + 4\sigma^2_{\min}\|u\|^2_{2,[t_1,t_2]} + 4\sigma^2_{\min}x^T(t_1)T_2^{-T}Y^{-1}(\rho(t_1))T_2^{-1}x(t_1) - \\
x^T(t_1)T_1^{-T}X(\rho(t_1))T_1^{-1}x(t_1) - \frac{\sigma^2_{\min}}{\sigma^2_{\max}}x^T(t_2)T_1^{-T}X(\rho(t_2))T_1^{-1}x(t_2).
\end{aligned}$$

Making use of equation (B.1), this can be rearranged to give

$$\|e\|^2_{2,[t_0,t_2]} \leq 4\sigma^2_{\max}\frac{\sigma^2_{\max}}{\sigma^2_{\min}}\|u\|^2_{2,[t_0,t_2]} - x^T(t_2)T_1^{-T}X(\rho(t_2))T_1^{-1}x(t_2).$$

If we repeat this procedure, it is not difficult to see that Theorem 7.6.8 follows inductively. ■

It should be apparent that for multiple transitions from $\dot{\sigma} \leq 0$ to $\dot{\sigma} \geq 0$ there must be an equal number of transitions from $\dot{\sigma} \geq 0$ to $\dot{\sigma} \leq 0$. So the statement of theorem 7.6.8 could just have easily been phrased in terms of the number of transitions from $\dot{\sigma} \geq 0$ to $\dot{\sigma} \leq 0$. The indication is that it is periodic parameter trajectories that prevent us from generalising the LTI error bound.

Bibliography

[1] B.D.O. Anderson and Yi. Liu, *Controller Reduction: Concepts and Approaches*, IEEE. Trans. Automat. Control, Vol.34, No.8, pp 802-812, 1989.

[2] B.D.O Anderson and J.B. Moore, *Optimal Control - Linear Quadratic Methods*, Prentice Hall, 1989.

[3] K.J. Astrom and L. Rundqwist, *Integrator Windup and How to Avoid It*, In the Proceedings of the 1989 American Control Conference, pp 1693-1698, 1989.

[4] G. Balas, *Robust Control of Flexible Structures: Theory and Experiment*, Phd dissertation, Caltech, 1990.

[5] B.R. Barmish and H.I. Kang, *A Survey of Extreme Point Results for Robustness of Control Systems*, Automatica, Vol.29, No.1, pp 13-35, 1993.

[6] K.J. Bathe, *Finite Element Procedures in Engineering Analysis*, Prentice-Hall, Englewood Cliffs, N.J, 1982.

[7] G.S. Becker, *Quadratic Stability and Performance of Linear Parameter Dependent Systems*, Phd dissertation, University of California at Berkeley, 1993.

[8] G. Becker and A. Packard, *Robust Performance of Linear Parametrically Varying Systems Using Parametrically-Dependent Linear Feedback*, Systems and Control Letter, Vol. 23, 1994.

[9] J. Bernussou, P.L.D Peres, and J.C. Geromel, *A Linear Programming Oriented Procedure for Quadratic Stabilisation of Uncertain Systems*, Systems and Control Letters, Vol.13, pp 65-72, 1989.

[10] J.S. Bendat and A.G. Piersol, *Random Data: Analysis and Measurement Procedures*, John Wiley, N.Y, 1986.

[11] S.Boyd and Q. Yang, *Structured and Simultaneous Lyapunov Functions for System Stability Problems*, Int. J. Control, Vol.49, No.6, pp 2215-2240, 1989.

[12] S. Boyd, L. El Ghaoui, E. Feron and V. Balakrishnan, *Linear Matrix Inequalities in System and Control Theory*, SIAM Studies in Applied Mathematics, 1994.

[13] F.M. Callier and C.A. Desoer, *Linear System Theory*, Springer Verlag, N.Y, 1991.

[14] P.J. Campo, *Studies in Robust Control of Systems Subject to Constraints*, Phd dissertation, Caltech, 1990.

[15] C.T. Chen, *Linear Systems Theory and Design*, Holt, Rinehart and Winston, 1984.

[16] I. Chopra, *Design and Analysis Trends of Helicopter Rotor Systems*, Centre for Rotorcraft Education and Research, Dept of Aerospace Engineering, Maryland, 1991.

[17] M. Corless, *Control of Uncertain Nonlinear Systems*, ASME Jour. of Dyn. Sys. Meas. and Control, 50th Anniversary issue, pp 362-372, 1993.

[18] R.A. Davis, *Model Validation for Robust Control*, Phd dissertation, Cambridge University, 1995.

[19] J.C. Doyle, *Guaranteed Margins for LQG Regulators*, IEEE. Trans. Automat. Control, Vol.23, No.4, pp 756-757, 1978.

[20] J.C. Doyle and G. Stein, *Multivariable Feedback Design: Concepts for a Classical/Modern Synthesis*, IEEE. Trans. Automat. Control, Vol.26, pp 4-16, 1981.

[21] J.C. Doyle, *Analysis of Feedback Systems with Structured Uncertainty*, IEE Proceedings, Part D, Vol.129, pp 242-250, 1982.

[22] J.C. Doyle, *Structured Uncertainty in Control System Design*, In the Proceedings of the 24'th CDC, Ft. Lauderdale, 1985.

[23] J.C. Doyle, R.S. Smith and D.F. Enns, *Control of Plants with Input Saturation Nonlinearities*, In the Proceedings of the 1987 American Control Conference, pp 1034-1039, 1987.

[24] J.C. Doyle, K. Glover, P.P. Khargonekar and B.A. Francis, *State Space Solutions to Standard H_2 and H_∞ Control Problems*, IEEE. Trans. Automat. Control, Vol.34, No.8, pp 831-847, 1989.

[25] J.C. Doyle, B.A. Francis and A.R. Tannenbaum, *Feedback Control Theory*, Maxwell MacMillan 1992.

[26] A. El-Sakkary, *The Gap Metric: Robustness of Stabilisation of Feedback Systems*, IEEE. Trans. Automat. Control, Vol.30, pp 240-247, 1985.

[27] M.J. Engelhard and M.C. Smith, *A Four-Block Problem for H_∞ Design: Properties and Applications*, Automatica, Vol.27, No.5, pp 811-818, 1991.

[28] D. Enns, *Model Reduction for Control Systems Design*, Phd dissertation, Stanford University, 1984.

[29] D.J. Ewins, *Modal Testing: Theory and Practice*, Research Studies Press, Letchworth and Wiley, N.Y, 1984.

[30] A. Feintuch, *The Gap Metric for Time-Varying Systems*, Systems and Control Letters, Vol. 16, pp 277-279, 1991.

[31] B.A. Francis and G. Zames, *On H_∞ Optimal Sensitivity Theory for SISO Feedback Systems*, IEEE. Trans. Automat. Control, Vol.29, No.1, pp 9-16, 1984.

[32] B.A. Francis, *A Course In H_∞ Control Theory*, Springer Verlag, N.Y, 1987.

[33] P. Gahinet and P. Apkarian, *A Linear Matrix Inequality Approach to H_∞ Control*, International Journal of Robust and Nonlinear Control, Vol.4, pp 421-448, 1994.

[34] P. Gahinet, A. Nemirovskii, A.J. Laub and M. Chilali, *The LMI Control Toolbox*, Beta-Release Version, The Mathworks Inc. Mass., November 1994.

[35] P. Gahinet, P. Apkarian and M. Chilali, *Affine Parameter-Dependent Lyapunov Functions for Real Parametric Uncertainty*, In the Proceedings of the 33'rd CDC, Florida, December, 1994.

[36] T.T. Georgiou, *On the Computation of the Gap Metric*, Systems and Control Letters, Vol.11, pp 253-257, 1988.

[37] T.T. Georgiou and M.C. Smith, *Optimal Robustness in the Gap Metric*, IEEE. Trans. Automat. Control, Vol.35, No.6, pp 673-687, 1990.

[38] T.T. Georgiou and M.C. Smith, *Upper and Lower Bounds for Approximation in the Gap Metric*, IEEE. Trans. Automat. Control, Vol.38, pp 946-951, 1993.

[39] K. Glover, *All Optimal Hankel Norm Approximations of Linear Multivariable Systems and their L_∞ Error Bounds*, Int. J. Control, Vol.39, pp 1115-1193, 1984.

[40] K. Glover, D.J.N. Limebeer, J.C. Doyle, E.M. Kasenally and M.G. Safanov, *A Characterisation of all Solutions to the Four-Block General Distance Problem*, SIAM Journal of Control and Optimisation, Vol.29, No.2, pp 283-324, 1991.

[41] K. Glover and D.C. MacFarlane, *Stabilisation of Normalised Coprime Factor Plant Descriptions with H_∞ Bounded Uncertainty*, IEEE. Trans. Automat. Control, Vol.34, No.8, pp 821-830, 1989.

[42] P.J. Goddard, *Performance-Preserving Frequency Weighted Controller Approximation*, Phd dissertation, Cambridge University, 1995.

[43] H. Goldstein, *Classical Mechanics*, Addison Wesley, 1980.

[44] M. Green, *A Relative Error Bound for Balanced Stochastic Truncation*, IEEE. Trans. Automat. Control, Vol.33, No.10, pp 961-965, 1988.

[45] M. Green and D.J.N. Limebeer, *Linear Robust Control*, Prentice Hall, 1995.

[46] R. Hanus, M. Kinnaert, and J.L. Henrotte, *Conditioning Technique, a General Anti-Windup and Bumpless Transfer Method*, Automatica, Vol.23, No.6, pp 729-739, 1987.

[47] G.C. Heise and M.G. Safanov, *Conservatism of the Gap Metric*, In the Proceedings of the 30'th CDC, Brighton, England, 1991.

[48] E.J. Hinch, *Perturbation Methods*, Cambridge University Press, 1991.

[49] R.A. Horn and C.R. Johnson, *Matrix Analysis*, Cambridge University Press, 1985.

[50] R.A. Hyde, *The Application of Robust Control to VSTOL Aircraft*, Phd dissertation, Cambridge University, 1991.

[51] R.A. Hyde and K. Glover, *The Application of Scheduled H_∞ Controllers to a VSTOL Aircraft*, IEEE. Trans. Automat. Control, Vol.38, No.7, pp 1021-1039, 1993.

[52] T. Kailath, *Linear Systems*, Prentice Hall, N.J, 1980.

[53] T. Kato, *Perturbation Theory for Linear Operators*, Springer Verlag, N.Y., 1966.

[54] P.P. Khargonekar and M.A. Rotea, *Coprime Factorisation for Linear Time-Varying Systems*, In the Proceedings of the American Control Conference, Atlanta, pp 848-851, 1988.

[55] P.P. Khargonekar, R. Ravi and K.M. Nagpal, *H_∞ Control of Linear Time Varying Systems: A State Space Approach*, SIAM Journal of Control and Optimisation, Vol.29, No.6, pp 1394-1413, November 1991.

[56] M.V. Kothare, P.J. Campo and M. Morari, *A Unified Framework for the Study of Anti-Windup Designs*, Chemical Engineering, Report 210-41, Caltech, 1993.

[57] E. Kreyszig, *Introductory Functional Analysis*, Wiley Classics, 1989.

[58] Yi. Liu, B.D.O. Anderson and Uy-Loi Ly, *Coprime Factorisation Controller Reduction with Bezout Identity Induced Frequency Weighting*, Automatica, Vol.26, No.2, pp 233-249, 1990.

[59] D.C. MacFarlane and K. Glover, *Robust Controller Design Using Normalised Coprime Factor Plant Descriptions*, Springer Verlag, Lecture Notes in Control and Information Sciences, 1990.

[60] J.M. Maciejowski, *Multivariable Feedback Design*, Wokingham, Addison Wesley, 1989.

[61] L. Meirovitch, *Analytical Methods in Vibrations*, Macmillan, N.Y, 1967.

[62] D.G. Meyer, *Fractional Balanced Reduction: Model Reduction via Fractional Representations*, IEEE. Trans. Automat. Control, Vol.35, pp 1341-1345.

[63] B.C. Moore, *Principal Components Analysis in Linear Systems*, IEEE. Trans. Automat. Control, Vol.26, pp 17-32, 1981.

[64] D.E. Newland, *Mechanical Vibration Analysis and Computation*, Longman Scientific and Technical, 1989.

[65] R.J. Ober and D.C. MacFarlane, *Balanced Canonical Forms for Minimal Systems: a Normalised Coprime Factor Approach*, Linear Algebra and its Applications, 122-124: 23-64, 1989.

[66] A.K. Packard and J.C. Doyle, *The Complex Structured Singular Value*, Automatica, Vol.29, pp 71-109, 1993.

[67] A. Packard, *Gain Scheduling via Linear Fractional Transformations*, Systems and Control Letters, Vol.22, pp 79-92, 1994.

[68] A.M. Pascoal, R. Ravi and P.P. Khargonekar, *The Graph Topology for Linear Plants with Application to Nonlinear Robust Stabilisation*, IEEE. Trans. Automat. Control, Vol. 38, No. 2, 1993.

[69] K. Poolla, P. Khargonekar, A. Tikku, J. Krause and K. Nagpal, *A Time-Domain Approach to Model Validation*, IEEE. Trans. Automat. Control, Vol. 39, No. 5, 1994.

[70] M.J.D. Powell, *Approximation Theory and Methods*, Cambridge University Press, 1991.

[71] K. Qui and E.J. Davison, *Feedback Stability under Simultaneous Gap Metric Uncertainties in Plant and Controller*, Systems and Control Letters, Vol.18, pp 9-22, 1992.

[72] K. Qui and E.J. Davison, *Pointwise Gap Metrics and Transfer Matrices*, IEEE. Trans. Automat. Control, Vol.37, No.6, pp 770-780, 1992.

[73] Li. Qui, B.Bernhardson, A. Rantzer, E.J. Davison, P.M. Young and J.C. Doyle, *A Formula for Computation of the Real Stability Radius*, Automatica, Vol.31, No.6, pp 879-890.

[74] R. Ravi, A.M. Pascoal and P.P. Khargonekar, *Normalised Coprime Factorisations for Linear Time Varying Systems*, Systems and Control Letters, Vol 18, pp 455-465, 1992.

[75] V. Rehbock, K.L. Teo and L.S. Jennings, *Suboptimal Feedback Control for a Class of Nonlinear Systems using Spline Interpolation*, Preprint, Department of Mathematics, University of Western Australia, 1995.

[76] B.G. Romanchuck and M.C. Smith, *Incremental Gain Analysis of Linear Systems with Bounded Controls and its Application to the Anti-Windup Problem*, In preparation, Cambridge University, 1995.

[77] M. Sampei, T. Mita and M. Nakamichi, *An Algebraic Approach to H_∞ Feedback Problems*, Systems and Control Letters, Vol 14, pp 13-24, 1990.

[78] C. Scherer, *H_∞ Optimisation Without Assumptions on Finite or Infinite Zeros*, SIAM Journal of Control and Optimisation, Vol. 30, No.1, pp 143-166, 1992.

[79] J.A. Sefton and K. Glover, *Pole/Zero Cancellations in the General H_∞ Problem with Reference to a Two Block Design*, Systems and Control Letters, No.14, pp 295-306, 1990.

[80] J.S. Shamma and J.R. Cloutier, *Gain-Scheduled Missile Autopilot Design Using Linear Parameter Varying Transformations*, Journal of Guidance, Control and Dynamics, Vol.16, No.2, 1993.

[81] S. Skogestad, M. Morari and J.C. Doyle, *Robust Control of Ill-Conditioned Plants: High Purity Distillation*, IEEE. Trans. Automat. Control, Vol.33, No.12, pp 1092-1105, 1988.

[82] M. Vidyasagar and B.A. Francis, *Algebraic and Topological Aspects of the Regulator Problem for Lumped Linear Systems*, Automatica, Vol.19, No.1, pp 87-90, 1983.

[83] M. Vidyasagar, *The Graph Metric for Unstable Plants and Robustness Estimates for Feedback Stability*, IEEE. Trans. Automat. Control, Vol.29, No.5, pp 403-417, 1984.

[84] M. Vidyasagar, *Control System Synthesis: A Factorisation Approach*, MIT Press, Cambridge, MA, 1985.

[85] M. Vidyasagar and H. Kimura, *Robust Controllers for Uncertain Linear Multivariable Systems*, Automatica, Vol.22, pp 85-94, 1986.

[86] M. Vidyasagar, *Nonlinear Systems Analysis*, Prentice Hall, 1993.

[87] G. Vinnicombe, *Measuring the Robustness of Feedback Systems*, Phd dissertation, Cambridge University, 1993.

[88] G. Vinnicombe, *Frequency Domain Uncertainty and the Graph Topology*, IEEE. Trans. Automat. Control, Vol.38, No.9, pp 1371-1383, 1993.

[89] G. Vinnicombe, *The Robustness of Feedback Systems with Bounded Complexity Controllers*, Submitted to IEEE. Trans. Automat. Control, Nov 1994.

[90] J. Woodhouse, *On the Playability of Violins, Part 1: Reflection Functions*, Acustica, Vol.78, pp 125-136, 1993.

[91] J. Woodhouse, *On the Playability of Violins, Part 2: Minimum Bow Force and Transients*, Acustica, Vol.78, pp 137-153, 1993.

[92] P.M.R. Wortleboer, *Frequency-Weighted Balanced Reduction of Closed-loop Mechanical Systems*, Phd dissertation, Delft University of Technology, 1994.

[93] F. Wu, X. Yang, A. Packard and G. Becker, *Induced L_2-Norm Control of LPV System with Bounded Parameter Variation Rates*, Submitted to the International Journal of Nonlinear and Robust Control, December, 1994.

[94] N. Young, *An Introduction to Hilbert Space*, Cambridge University Press, 1988.

[95] P.M. Young, *Robustness with Parametric and Dynamic Uncertainty*, Phd dissertation, Caltech, 1993.

[96] P.M. Young, *Controller Design with Real Parametric Uncertainty*, Report no 116-81, Caltech, 1994.

[97] G. Zames and A.K. El-Sakkary, *Unstable Systems and Feedback: The Gap Metric*, Proc. Allerton. Conf, pp 380-385.

[98] G. Zames, *On the Input-Output Stability of Time Varying Nonlinear Feedback Systems, Part I, Conditions Using Concepts of Loop Gain, Conicity and Positivity*, IEEE. Trans. Automat. Control, Vol.11, No.2, pp 228-238, 1966.

[99] G. Zames, *Feedback and Optimal Sensitivity: Model Reference Transformations, Multiplicative Seminorms, and Approximate Inverses*, IEEE. Trans. Automat. Control, Vol.26, pp 301-320, 1981.

[100] G. Zames and B.A. Francis, *Feedback, Minimax Sensitivity and Optimal Robustness*, IEEE. Trans. Automat. Control, Vol.28, No.5, pp 585-600, 1983.

[101] K. Zhou and P. Khargonekar, *Robust Stabilisation of Linear Systems with Norm-bounded Time-varying Uncertainty*, Systems and Control Letters, Vol.10 , pp 17-20, 1988.

[102] K. Zhou, C. D'Souza and J.R. Cloutier, *Structurally Balanced Controller Order Reduction with Guaranteed Closed Loop Performance*, Systems and Control Letters, Vol.24, No.4, pp 235-242, 1995.

[103] K.Zhou with J.C. Doyle and K. Glover, *Robust and Optimal Control*, Book in preparation, 1995.

[104] S.Q. Zhu, *Graph Topology and Gap Topology for Unstable Systems*, IEEE. Trans. Automat. Control, Vol.34, No.8, pp 348-355, 1989.